Study of Synthesis, Reactions and Enantiomerization of C_α- Chiral Grignard Reagents

Neeraj Narendra Patwardhan

Dissertation submitted to the faculty of the Virginia Polytechnic Institute and State University in partial fulfillment of the requirements for the degree of

Doctor of Philosophy
In
Chemistry

Paul R. Carlier, (Chairman)
David G. I. Kingston
James M. Tanko
Webster L. Santos

May 2nd 2012
Blacksburg, VA

Keywords: enantiomerization, kinetics, chiral Grignard reagents, solvent effects, reaction order, ion-pair separation, entropy of activation, electrostriction, DFT calculations

Study of Synthesis, Reactions and Enantiomerization of C_α- Chiral Grignard Reagents

Neeraj Narendra Patwardhan

ABSTRACT

The development of chiral organometallics for asymmetric synthesis is a topic of significant research in the recent past. The most studied in this class are the chiral organolithium reagents with many reported examples. The primary focus of our research is the development of C_α-chiral Grignard reagents, where the metal bearing α-carbon is the sole source of chirality. Examples of such Grignard reagents are rare owing to the problems associated with their synthesis, and their low configurational stability. We have studied these problems in three different modules of this project.

Reactions of 1-magnesio-2,2-diphenyl-cyclopropylcarbonitrile with carbon electrophiles are first attempted in order to expand the utility of this configurationally stable C_α-chiral Grignard reagent in asymmetric synthesis. This reagent has been shown to be non-reactive towards carbon electrophiles at low temperatures. Consequently, we attempt to enhance the reactivity of this compound through two different approaches, Lewis-base activation and the "ate-complex" generation. The Magnesium/Halogen (Mg/X) exchange reactions have been shown to be extremely useful in the synthesis of complex Aryl, alkenyl (sp^2) and alkynyl (sp) Grignard reagents. Examples of Mg/X exchange reactions of Alkyl (sp^3) halides are, however, rare. Even more rare are such examples with secondary and tertiary alkyl halides, justifying the relative paucity of chiral Grignard reagents. In this module of our project, we study the Mg/X exchange reactions on secondary alkyl halides possessing a γ-hydroxyl group, as an internal activator for such Mg/X exchange reactions.

Enantiomerization pathways of chiral organolithium compounds have been widely studied. However, few such studies have been performed on chiral Grignard reagents. In this module of the project, we studied the solvent assisted enantiomerization mechanism of the C_α-chiral 1-magnesio-2,2-diphenyl-cyclopropylcarbonitrile. Rate constant for the enantiomerization of this compound was measured in three different ethereal solvents to study the effect of solvent on the configurational stability. Finally, the order of the enantiomerization process with respect to [Et_2O] was studied in order to predict the mechanism of this process in Et_2O solvent.

Our kinetic studies on the enantiomerization process provided us with a definitive picture for the enantiomerization of the C_α-chiral 1-magnesio-2,2-diphenyl-cyclopropylcarbonitrile, where solvation of the Grignard reagent preceded an ion-pair separation step which eventually lead to enantiomerization of the Grignard species. However, the precise structure of all the involved solvated intermediates could not be determined as kinetics was not able to distinguish between these intermediates. We next performed computational calculations to study the effect of solvation on the analogous 1-magnesio-cyclopropylcarbonitrile in order to address the unanswered questions from our kinetic studies.

Acknowledgements

I would like to begin by expressing my heartfelt gratitude towards my adviser Dr. Paul R. Carlier. I was extremely fortunate to receive his tutelage in the long, often exasperating duration of the graduate program. I am deeply inspired by his zealous attitude towards science along with his disciplined, and at the same time skeptical approach towards tackling any scientific problem. Connecting the dots on this highly scattered picture of my project would not have been possible for me without his guidance. I will always be thankful for the way he patiently helped me overcome the pessimism that arose within me from working on a challenging project. I would also like to thank the members of my advisory committee, Dr. Kingston, Dr. Tanko and Dr. Santos, for all their help and guidance. A special note of thanks is due to Dr. Tanko, for all the helpful discussions on chemical kinetics, which led me to a far better understanding of my project.

I would like to thank my colleagues in the Carlier group, Dr. Dawn Wong, Dr. Larry Williams, Dr. Ming Ma, Dr. Nipa Deora, Dr. Josh Harstel, Dr. Chris Monceaux, Dr. Qiao Hong Chen, Dr. Ming Gao, Dr. Derek Craft, Mr. Jimit Mehta, Ms. Stephanie Bryson, Ms. Astha, Mr. Max Hockenbury and Mr. Eugene Camerino, for all the help that they offered to me over all these years. I would like to acknowledge all the help from Dr. Ming Gao who was my partner on a major part of this project. Also, discussions on synthetic chemistry with Dr. Qiao Hong Chen, Dr. Derek Craft, Dr. Chris Monceaux and computational chemistry discussions with Dr. Nipa Deora were extremely helpful.

The support I received from my family: my mother Nayana, my lovely wife Shraddha, my younger brother Ninad, his wife Ela, and Shraddha's parents Prof. V.G.

Patil and Dr. Mrs. Rekha Patil, was extremely crucial in this phase of my life.

I am deeply indebted to my Mother Nayana, for all the success I have managed to achieve in life. The idea of an average person like me writing a doctoral dissertation in life would not have been possible had she not inculcated the constant desire of achieving greater heights in me. I will never be able to thank her enough for the great pains she took in order to provide me with all possible opportunities and amenities in life.

Coming to a small town like Blacksburg from a fairly large city in India is a unique experience in itself. My close friends Jimit, Abhijit, Asif, Sujit, Keyur and Nipa made this experience extremely enjoyable. The time we spent together will always be in my memory as the most enjoyable time I ever had in life.

Finally and most importantly, I would like to express my gratitude to my beloved wife Shraddha. I would not have been able to maintain my sanity through this exhausting experience if I didn't have her constant encouragement and support. I am thankful for the patience with which she supported me during all this time. Her ability to support me without expecting anything from me in return is a testimony of her unwavering love, which is the biggest achievement and joy of my life.

Dedication

To my mother Nayana and wife Shraddha for their constant love and encouragement

Table of Contents

Chapter 1: Synthesis and Reactions of C_α-Chiral Organomagnesium Reagents. 1

1.1 Introduction……...…..……...……...……....1
1.1.1 Metalated nitriles……..……1
1.1.1.1 Structural properties of metalated nitriles…….....2
1.1.1.2 Synthesis of Metalated nitriles via the metal-halogen exchange reaction……..……4
1.1.2 Enantiopure metalated cyclopropylnitriles…….……...7
1.1.3 Enhancement of reactivity of Grignard reagents at low temperatures……12
1.1.3.1 Ate complexes…….……12
1.1.3.2 Reactivity of ate complexes…..……...13
1.1.3.3 Magnesate complexes in Mg/X exchange reactions……..16
1.1.4 Mg/X exchange routes to secondary sp^3 Grignards – potential method for the synthesis of chiral Grignards…….….26
1.1.4.1 Magnesium –Halogen (Mg/X) exchange reactions on aryl and alkenyl (sp^2) halides…….……27
1.1.4.2 Magnesium –Halogen (Mg/X) exchange reactions on alkyl (sp^3) halides…….28
1.1.5 Appropriately placed activators to assist Mg/X exchange reactions…….…32
1.2 Results and Discussion: Reactions of 1-magnesio-2,2-diphenyl cyclopropylcarbonitrile **1-21** with electrophiles - Reactivity studies……..36
1.2.1 Development of magnesio cyclopropylnitrile reagents bearing smaller substituents and study of their Mg/X exchange reactions….……36
1.2.2 In-situ activation of 1-magnesio-2,2-diphenyl cyclopropylnitrile **1-21**…….42
1.2.3 Exploration of anionic magnesates formed from bromonitrile **1-20**……...……..45
1.2.4 Conclusions for attempted Lewis base activation of cyclopropyl Grignard reagents……..……..49
1.3 Results and Discussion: Towards γ-hydroxyl directed Mg/X exchange reactions on secondary alkyl halides –A potential method for synthesizing chiral Grignard reagents…….……..50
1.3.1 Synthesis and Mg/X exchange reactions of certain γ-hydroxyl group containing alkyl halides……...51
1.3.2 Conclusions for section 1.3……...……...57
1.4 References for Chapter 1…….58

Chapter 2: Solvent assisted enantiomerization of C_α-chiral 1-magnesio-2,2 diphenyl cyclopropylcarbonitrile……...……62

2.1 Introduction.....63
2.1.1: Common methods used to study configurational stability of chiral organolithium compounds……..…… 63

2.1.2 Configurational stability of chiral organolithium compounds……..…..66
2.1.2.1 Solvent effects on configurational stability of chiral organolithium compounds. ……67
2.1.3: Configurational Stability of organomagnesium compounds……...71
2.2 Investigation of configurational stability of 1-magnesio-2,2-diphenyl-cyclopropylcarbonitrile **2-40**……..……..76
2.3 Reinvestigation of the configurational stability of **2-40** – a new and improved protocol…..……..79
2.3.1 Derivation of expression used to calculate enantiomerization rate constant k_{enant}……..80
2.3.2 Experimental Details of the new protocol to study enantiomerization…….82
2.4 Measurement of enantiomerization rates and corresponding activation parameters……84
2.4.1 Studies in Diethyl Ether (Et_2O) ……..……84
2.4.2 Studies in 2-methyl tetrahydrofuran (2-MeTHF) and tetrahydrofuran (THF) ……..85
2.4.3 Calculation of Activation parameters in three solvents...……88
2.5 Measurement of reaction orders to determine enantiomerization pathway involved……91
2.5.1 Measurement of reaction order with respect to Grignard reagent **2-40**……..…91
2.5.2 Measurement of reaction order with respect to [Et_2O]……...…….94
2.6 Determination of stoichiometry of Mg/X exchange-trapping reaction of **2-39**……..99
2.7 Derivation of expression to relate k_{enant} to [Et_2O]……..101
2.8 Solvent electrostriction as the probable cause of large negative entropy of activation……..……..103
2.9 Plausible mechanism for enantiomerization of **2-40**…….104
2.10 Conclusions……107
2.11 References for Chapter 2……..…….109

Chapter 3: DFT studies on solvation and ion-pair separation of Grignard reagents……...113

3.1 Introduction and motivation……..114
3.1.1 Experimental studies on Grignard reagent structure…….112
3.1.2 Computational studies on Grignard reagent structure in solution……...…..119
3.2 Computational Methods……122
3.3 DFT studies on the solvation of methylmagnesium chloride (MeMgCl)…..124
3.3.1 Solvation of MeMgCl monomers……..124
3.3.2 Solvation of MeMgCl dimers……...…….130
3.4 DFT studies on the solvation/ion-pair separation of 1-magnesio cyclopropylcarbonitrile……..……140
3.4.1 Introduction and motivation……...……..140
3.4.2 Different unsolvated heterodimeric structures studied…...……..141

3.4.3 Solvation of heterodimers by Me_2O and Et_2O..……144
3.4.3.1 Mono-solvates of heterodimers **3-27** – **3-29**……..……144
3.4.3.2 Disolvates of heterodimers……..……..147
3.4.3.3 Trisolvates of μ-Cl-μ(1,3)-cyclopropylnitrile heterodimers……..……151
3.4.4 Thermodynamics of solvation of μ-Cl-μ(1,3)-cyclopropylnitrile heterodimers……...153
3.4.5 Ion-pair separation from trisolvate species **3-29•$(Et_2O)_3$-B** in Et_2O……..….156
3.4.6 Two atypical structures observed in the process……162
3.5 Conclusions……164
3.6 References for Chapter 3……...166

Chapter 4: Experimental……...170

4.1 Experimental procedures for Chapter 1……171
4.1.1 Synthetic procedures towards synthesis of 1-bromo cyclopropylcarbonitrile compounds (±) **1-76**……..……171
4.1.2 Synthesis of (*S*)-1-bromo-2,2-diphenylcyclopropanecarbonitrile (*S*)-**1-20**……...176
4.1.3 Mg/Br exchange/ electrophilic trapping reactions of 1-bromo-cyclopropylcarbonitrile **1-20** and **1-76**……..……178
4.1.3.1 Typical procedure for Mg/Br exchange/ electrophilic quench reactions with 2.2 equiv *i*-PrMgCl..……...……...178
4.1.3.2 Typical procedure for Mg/Br exchange reactions with 2.2 equiv *i*-PrMgCl at 195 K and electrophilic quench reactions at elevated temperatures…….179
4.1.3.3 Typical procedure for Mg/Br exchange reactions with 2.2 equiv *i*-PrMgCl and in-situ activation of the resulting Grignard species 1-20 using an appropriate Lewis base at 195 K……...……180
4.1.3.4 Typical procedure for Mg/Br exchange reactions with 1. 5 equiv of the ate-complex *i*-$PrBu_2MgLi$ at 195 K…….……181
4.1.3.5 Typical procedure for Mg/Br exchange reactions with in situ formation of ate complex 1-87 at 195 K……..…….182
4.1.3.6 Analytical Data for the electrophilic quench products……..183
4.1.4 Procedures for synthesis various γ–hydroxyl group containing alkyl halides…….……...184
4.1.4.1 NMR data as additional proof for structure for compounds 1-93, 1-101 and 1-112……...199
4.1.5 Mg/X exchange/ electrophilic trapping reactions of γ–hydroxyl group containing alkyl halides……204
4.1.5.1 Mg/X exchange reactions with 3.0 equiv of Grignard reagent (*i*-PrMgCl) in Et_2O at 195 K…….…204
4.1.5.2 Mg/X exchange reactions with in-situ formation of ate complex……..204
4.1.5.3 Mg/X exchange reactions with above protocols at elevated temperatures…205
4.1.5.4 Analytical data for the new products obtained after Mg/X exchange/ electrophilic trapping reactions of γ–hydroxyl group containing alkyl halides……...…….206

4.2 Experimental procedures for Chapter 2…….207
4.2.1 Procedures for Mg/Br exchange/D-OCH_3 trapping experiments…..…….207
4.2.1.1 General Procedure for Mg/Br exchange/D-OCH_3 trapping experiments at $[Mg]_{total}$ = 0.034 M…….207
4.2.1.2 Mg/Br exchange/D-OCH_3 trapping experiments at varying $[Mg]_{total}$ in Et_2O……208
4.2.1.3 Mg/Br exchange/D-OCH_3 trapping experiments at varying $[Et_2O]$……..208
4.2.2 Analysis of Deuterio product $[D_1]$-2-41 using ^{1}HNMR and HPLC……..210
4.2.2.1 Determination of %Conversion and %Deuterium incorporation by ^{1}H NMR Spectroscopy……..210
4.2.2.2 Determination of enantiomer ratio using CSP-HPLC analysis…..…….212
4.2.3 Kinetic data and plots……...…….…….217
4.2.3.1 Error estimation method……217
4.2.3.2 Raw data for determination of k_{enant} in 3 solvents…….……217
4.2.3.3 Determination of activation parameters using standard Eyring analysis…...219
4.2.3.4 Kinetic plots and rate constants as $[Mg]_{total}$ is varied in Et_2O at 195 K…….220
4.2.3.5 Kinetic plots and rate constants as $[Et_2O]$ is varied in toluene at two temperatures……..…….221
4.3 Experimental data for Chapter 3……...…….223
4.3.1 Tabulation of energies of all structures studied in chapter 3…….223
4.3.2 XYZ Coordinates for B3LYP/6-31G* optimized structures studied...…….230
4.4 References for Chapter 4……...274

List of Schemes

Scheme 1-1: Valence-bond isomerization and ionization of metalated nitriles.....2
Scheme 1-2: Fleming and Knochel's Mg/X & Li/X exchange route to metalated nitriles. 5
Scheme 1-3: Fleming and Knochel's Mg/X & Li/X exchange route to metalated nitriles.....6
Scheme 1-4: Free anions of nitriles studied for inversion barrier. 8
Scheme 1-5: Walborsky's deprotonation/deuteration of acyclic nitriles and cyclopropylcarbonitriles.....9
Scheme 1-6: Mg/Br exchange/D_2O trapping reactions reported by Carlier *et al*.....10
Scheme 1-7: The equilibrium operative in ate complex solutions.....16
Scheme 1-8: Oshima's titanium mediated self-coupling reactions of magnesates.....20
Scheme 1-9: Xu's magnesations of hydroxyl group containing aryl halides.....23
Scheme 1-10: Xu's magnesate/halogen exchange reactions on indolyl iodides.....23
Scheme 1-11: Oshima's magnesate exchange of cyclopropyl bromide.....25
Scheme 1-12: Mg/X exchange reactions of various polyfunctional aryl halides studied by Knochel.....28
Scheme 1-13: Negishi's exchange/trapping reactions of alkyl iodides using *t*-BuLi.....29
Scheme 1-14: Knochel's Mg/X exchange reaction with cyclcopropyliodoester.....30
Scheme 1-15: Hoffmann's Mg/X exchange reactions of α–halo alkyl halides.....30
Scheme 1-16: Sulfoxide/Mg exchange reactions toward secondary Grignard reagents...31
Scheme 1-17: Directed I/Mg exchange reactions of γ and δ–hydroxyl group containing primary sp^3 alkyl halides. 32
Scheme 1-18: Mg/X exchange reactions of alkyl halides bearing γ–activator groups. 34
Scheme 1-19: Fleming's diastereoselective metalated nitrile formation by 1-3 induction/deprotonation. 35
Scheme 1-20: Synthesis of (±)-1-bromospiro[2.5]octane-1-carbonitrile - (±)-**1-76**. 37
Scheme 1-21: Published (a) and attempted (b, c) resolutions of bromo acid **1-74**.....40
Scheme 1-22: Lewis base activation of Grignard reagents.....42
Scheme 1-23: Proposed formation of highly nucleophilic lithium magnesate reagents and their trapping reactions. 45
Scheme 1-24: Equilibrium thought to exist in Mg/X exchange reactions of **1-76** with magnesates.....48
Scheme 1-25: Synthesis of 3-halo-5-phenylpentan-1-ol substrates **1-94** and **1-95**.....52
Scheme 1-26: Synthesis of 2,2 dimethyl 3-halo-5-phenylpentan-1-ol substrates **1-102**...54
Scheme 1-27: Synthesis of substrate **1-113**.....56
Scheme 2-1: Example for measurement of configurational stability by kinetic methods. 64
Scheme 2-2: Enantiomerization barrier for 1-phenylseleno-2-phenyl-ethyllithium **2-3**...66

Scheme 2-3: Enantiomerization of organolithium by a dissociative pathway.....67
Scheme 2-4: Configurationally stable organolithium species **2-5**. 68
Scheme 2-5: Deprotonation/alkylation by allyl chloride of **2-9**.....68
Scheme 2-6: Stereochemical outcome of [2, 3] Wittig rearrangement reactions of (*S*,*E*)-[3-(Allyloxy)prop-1-ene-1,3-diyl]dibenzene **2-11**. 69
Scheme 2-7: Enantiomerization of *N*-Boc-2-lithiopiperidine (*S*)-**2-14**.....70
Scheme 2-8: Enantiomerization of a chiral organolithium by an associative pathway....70
Scheme 2-9: Enantiomerization of 1-lithio-3, 5-diphenylcyclohexane **2-17**.....71
Scheme 2-10: Examples of configurationally stable Grignards **2-17** and **2-19**.....72
Scheme 2-11: Jensen's NMR analysis of norbornyl Grignard **2-23**.....73
Scheme 2-12: Hoffmann's investigations into the synthesis and configurational stability of Grignard reagent **2-29.**.....74
Scheme 2-13: Configurationally stable Grignard reagent **2-35**.....75
Scheme 2-14: Mg/Br exchange/D_2O trapping reactions reported by Carlier *et al*.....76
Scheme 2-15: Conducted tour pathway for enantiomerization of lithio-2,2-diphenyl cyclopropylnitrile **2-42**.....78
Scheme 2-16: Solvent assisted ion pair separation mechanism for enantiomerization.....79
Scheme 2-17: Dimerization of Grignard **2-40**.....90
Scheme 2-18: Proposed scenario for Mg/Br exchange reaction of **2-39**.....100
Scheme 2-19: Ionogenic reactions showing large negative values for $\Delta S^{\ddagger}$.....103
Scheme 2-20: Proposed mechanism of enantiomerization of heterodimer **2-51** in Et_2O solvent.....105
Scheme 2-21: Possible structures for resting solution species and higher solvated species. 106
Scheme 2-22: Ionogenic conducted tour mechanism towards enantiomerization of **2-58** and **2-61**.....107
Scheme 3-1: Disproportionating equilibrium proposed in THF solutions.....117
Scheme 3-2: Resting solvation structure *trans*-**3-29•$(Et_2O)_2$** and postulated higher solvated species **3-29•$(Et_2O)_3$-B**.....156
Scheme 3-3: Possible ion-pair separation/ enantiomerization through μ-Cl-μ(1,1)-cyclopropylnitrile structure **3-35•$(Et_2O)_3$** and relative energies at B3LYP/6-31G*.....164
Scheme 4-1: Synthesis of *S*-(+)-1-bromo-2,2-diphenylcyclopropanecarbonitrile (*S*)-**1-20**.. 178

List of Figures

Figure 1-1: X-ray crystal structures of 1-lithio phenylacetonitrile **1-5**, and lithio cyclopropylnitrile **1-6**.....3
Figure 1-2: Representations of nitrile anion keteniminate structures. 4
Figure 1-3: Common charged complexes observed in organometallic chemistry.....13
Figure 1-4: Non-oxidative charge cancellation process (ligand transfer) 14
Figure 1-5: Examples of magnesates bearing different ligands for understanding ligand transfer aptitude. 15
Figure 1-6: Ionic Mechanism for Mg/X exchange between Ar-X and RMgCl.....27
Figure 1-7: Postulated mechanism for sulfoxide/Mg exchange reaction. 31
Figure 1-8: Suggested mechanism of directed Mg/X exchange reaction. 33
Figure 1-9: Possible reason for no-reaction observed in case of Mg/I exchange of **1-102**.....56
Figure 2-1: Plot of ln ((%*ee*([D_1]-**2-41**))/100) vs delay time *t* (s) in Et_2O at 173 K. Data replicated from the published article by Carlier et al.....77
Figure 2-2: Plausible stereochemical pathway involved in synthesis and quench of **2-40** (Structure **2-40** does not imply any particular solvation or aggregation state) 78
Figure 2-3: Plot of ln (|2X_R([D_1]-**2-41**)-1|) vs delay time *t* for reactions in Et_2O.....85
Figure 2-4: Plot of ln (|2X_R([D_1]-**2-41**)-1|) vs delay time *t* for reactions in 2-MeTHF.....86
Figure 2-5: Plot of ln (|2X_R([D_1]-**2-41**)-1|) vs delay time *t* for reactions in THF.....87
Figure 2-6: Plot of calculated $\Delta G^{\ddagger}$ values versus temperature T and activation parameters for the enantiomerization of **2-40** calculated using the Eyring equation.....88
Figure 2-7: Negative activation entropies reported for racemization of chiral organolithiums **2-46** – **2-49**.....89
Figure 2-8: Plot of ln(2X_R([D_1]-**2-41**)-1) vs delay time *t* at different $[Mg]_{total}$.....93
Figure 2-9: Plot of ln(2X_R([D_1]-**2-41**)-1) vs delay time *t* in varying [Et_2O] at 195K.....95
Figure 2-10: Plot of ln(2X_R([D_1]-**2-41**)-1) vs delay time *t* in varying [Et_2O] at 212K.....96
Fig 2-11: Plot of k_{enant} versus [Et_2O] in toluene co-solvent at 195 K at $[Mg]_{total}$ = 0.006 M 97
Fig 2-12: Plot of k_{enant} versus [Et_2O] in toluene co-solvent at 212 K at $[Mg]_{total}$ = 0.006 M 98
Figure 2-13: Solvent electrostriction – cartoon representation.....103
Figure 3-1: The Schlenk and dimerization equilibriums prevalent in Grignard solutions.....113
Figure 3-2: Representations of observed X-ray crystal structures of EtMgBr•$(OEt_2)_2$, PhMgBr•$(OEt_2)_2$, and $(Ph)_3CMgBr•(OEt_2)_2$. 115
Figure 3-3: Representations of observed structures of organomagnesium chlorides by X-ray crystallography…….....116

Figure 3-4: X-ray crystal structures observed for various THF solvates of Grignard compounds. 117
Figure 3-5: μ_2–Chlorodimer species **3-17** and open linear dimer species **3-19** studied by Mori and co-workers.....121
Figure 3-6: B3LYP/6-31G* optimized geometries and relative energies of mono-solvated monomers of MeMgCl possessing different conformations of solvent Et_2O. Selected bond lengths in Å.....123
Figure 3-7: B3LYP/6-31G* optimized geometries for unsolvated and mono-solvated structures of MeMgCl monomers. Selected bond lengths in Å.....125
Figure 3-8: B3LYP/6-31G* optimized geometries for disolvated structures of MeMgCl monomers. Selected bond lengths in Å.....126
Figure 3-9: B3LYP/6-31G* optimized geometries for disolvated structures of MeMgCl monomers. Selected bond lengths in Å.....127
Figure 3-10: B3LYP/6-31G* optimized geometries for unsolvated and mono-solvated structures of MeMgCl bis (μ_2–Cl) dimer **3-25**. Selected bond lengths in Å, signed quantities are the Mulliken charges.....131
Figure 3-11: B3LYP/6-31G* optimized geometries and relative energies for four disolvated structures of MeMgCl bis (μ_2–Cl) dimer **3-25**. Selected bond lengths in Å, signed quantities are the Mulliken charges.....132
Figure 3-12: B3LYP/6-31G* optimized geometries and relative energies for four disolvated structures of MeMgCl bis (μ_2–Cl) dimer **3-25**. Selected bond lengths in Å, signed quantities are the Mulliken charges. 133
Figure 3-13: B3LYP/6-31G* optimized geometries of trisolvated open dimers. Selected bond lengths in Å, signed quantities are the Mulliken charges.....136
Figure 3-14: Comparison of energies of trisolvated open dimer with respect to the closed trisolvated dimer and disolvated dimer similar to those reported by Mori et. al.....138
Figure 3-15: 1-Magnesio cyclopropylcarbonitrile species analogous to **2-40**.....140
Figure 3-16: Different unsolvated heterodimeric structures modeled at B3LYP/6-31G*.....141
Figure 3-17: B3LYP/6-31G* optimized geometries of unsolvated heterodimers. Selected bond lengths in Å, signed quantities are the Mulliken charges.....142
Figure 3-18: Mono-solvated heterodimers **3-27 – 3-29**.....144
Figure 3-19: B3LYP/6-31G* optimized geometries and relative energies of mono-solvated heterodimers. Selected bond lengths in Å, signed quantities are the Mulliken charges.....145
Figure 3-20: Disolvates of heterodimers **3-27** and **3-29**.....147
Figure 3-21: B3LYP/6-31G* optimized geometries of Me_2O-disolvates of heterodimers of **3-27** and **3-29**. 148
Figure 3-22: B3LYP/6-31G* optimized geometries of Et_2O-disolvates of heterodimers of **3-27** and **3-29**.....149

Figure 3-23: Trisolvates of μ-Cl-μ(1,3)-cyclopropylnitrile heterodimer **3-29**.....151
Figure 3-24: B3LYP/6-31G* optimized geometries of trisolvated heterodimers **3-29**..151
Figure 3-25: B3LYP/6-31G* Optimized geometries for the ground state trisolvate structure **3-29•$(Et_2O)_3$-B**, IPS transition structure **3-32•$(Et_2O)_3$** and SIP species **3-33•$(Et_2O)_3$**. NIMAG = number of imaginary frequencies calculated.....157
Figure 3-26: Reaction coordinate for ion-pair separation from **3-29•$(Et_2O)_3$** calculated at B3LYP/6-31G*. E= electronic energies of the calculated structures.....160
Figure 3-27: Optimized geometry for the tetrasolvated species **3-29•$(Et_2O)_4$** at B3LYP/6-31G* and thermodynamics of the fourth solvation of **3-29**.....161
Figure 3-28: Two atypical heterodimeric structures observed at B3LYP/6-31G*.....162
Figure 4-1: Comparison of the chemical shifts of alkyl protons in the ^{1}H NMR spectra of compounds **1-92** and **1-93**……199
Figure 4-2: Comparison of the chemical shifts of alkyl carbons in the ^{13}C spectra of compounds **1-92** and **1-93**……200
Figure 4-3: Comparison of the chemical shifts of alkyl protons in the ^{1}H NMR spectra of compounds **1-100** and **1-101**……201
Figure 4-4: Comparison of the chemical shifts of alkyl carbons in the ^{13}C spectra of compounds **1-100** and **1-101**……201
Figure 4-5: Comparison of the chemical shifts of alkyl protons in the ^{1}H NMR spectra of compounds **1-111** and **1-112**……202
Figure 4-6: Comparison of the chemical shifts of alkyl protons in the ^{13}C NMR spectra of compounds **1-111** and **1-112**……..203
Figure 4-7: Overlay of the alkyl regions of the ^{1}H NMR spectra of pure samples of **[D_1]-2-41**, **2-41**, and (*S*)-**2-39**.....211
Figure 4-8. ^{1}H NMR Spectrum of a typical Mg/Br exchange/trapping reaction mixture (Et_2O, 195 K, *t* = 5 min) 211
Figure 4-9:HPLC Chromatogram (OD-H) of mixture of (*S*)- and (*R*)-**2-39** (72:28 er) 213
Figure 4-10: HPLC Chromatogram (OD-H) of enantiopure (*S*)-**2-39**.....214
Figure 4-11: HPLC Chromatogram (AD-H) of (±)-**[D_1]-2-41**.....215
Figure 4-12: HPLC Chromatogram (AD-H) of enantioenriched **[D_1]-2-41** ((*R*) : (*S*) = 90 :
10).....216
Figure 4-13: Traditional Eyring Plot to determine the activation parameters of the enantiomerization process in 3 solvents at $[Mg]_{total}$ = 0.0342 M.....219

List of Tables

Table 1-1: Reactions of 1-magnesio-2,2 diphenyl-cyclopropylnitrile **1-21** with carbon electrophiles.....11
Table 1-2: Oshima's magnesates/halogen exchange with aryl halides and quenching with electrophile.....17
Table 1-3: Oshima's magnesate/halogen exchange reactions of alkenyl iodides and subsequent electrophilic quench.....19
Table 1-4: Oshima's magnesate/halogen exchange of heteroaryl halides.....21
Table 1-5: Iida's formylation reactions of aryl-heteroaryl dibromides via magnesate intermediates.....22
Table 1-6: Fukuhara's magnesate exchange reactions of 1,4 di-iodo alkadienes. 24
Table 1-7: Mg/X exchange/trapping reactions of (±)-**1-76**.....38
Table 1-8: Reaction of **1-77** with BnBr at elevated temperatures. 39
Table 1-9: Effect of temperature on reactivity of **1-21**.....41
Table 1-10: Reactions of **1-21** with different electrophiles and attempted reactions for activation of **1-21** using different Lewis bases.....44
Table 1-11: Reactions of (±)-1-bromospiro[2.5]octane-1-carbonitrile (±)-**1-76** with magnesate reagents.....46
Table 1-12: Reactions of enantiopure 1-bromo-2,2-diphenyl cyclopropylnitrile (*S*)-**1-20** with magnesate reagents.....48
Table 1-13: Mg/X exchange, trapping reactions of 3-iodo-5-phenylpentan-1-ol **1-94**.....53
Table 1-14: Mg/X exchange, trapping reactions of 3-iodo-2,2-dimethyl-5-phenylpentan-1-ol **1-98**.....54
Table 1-15: Mg/X exchange-trapping reactions of **1-114** and **1-115**.....57
Table 2-1: Enantiomerization rate constants and activation free energies at four temperatures in Et_2O.....85
Table 2-2: Enantiomerization rate constants and activation free energies at three temperatures in 2-MeTHF.....86
Table 2-3: Enantiomerization rate constants and activation free energies at three temperatures in THF.....87
Table 2-4: Measurement of first order enantiomerization rate constants k_{enant} at different $[Mg]_{total}$ at 195 K.....93
Table 2-5: Et_2O/Toluene mixture compositions and resulting $[Et_2O]$ used.....94
Table 2-6: Dependence of k_{enant} and extrapolated t = 0 er of **2-40** on $[Et_2O]$ at 195 K.....96
Table 2-7: Dependence of k_{enant} and extrapolated t = 0 er of **2-40** on $[Et_2O]$ at 212K.....97
Table 2-8: Studies towards determining reaction stoichiometry.....99
Table 3-1: Ehlers et al's B-VWN-P DFT studies towards solvation and dimerization of organomagnesium chlorides.....120

Table 3-2: Tabulation of the bond lengths of the significant bonds in B3LYP/6-31G* optimized structures of monomers **3-24 - 3-24•$(Et_2O)_3$ – B**.....128
Table 3-3: Thermodynamics of solvation of MeMgCl monomers with Me_2O and Et_2O.....129
Table 3-4: Tabulation of the bond lengths of the significant bonds in B3LYP/6-31G* optimized structures of monomers **3-25 - 3-25•$(Et_2O)_3$ – C**.....134
Table 3-5: Thermodynamics of solvation of MeMgCl dimers with Me_2O and Et_2O.....135
Table 3-6: Relative energies of open and closed trisolvated dimers.....137
Table 3-8: Tabulation of the bond lengths of the significant bonds in B3LYP/6-31G* optimized structures of heterodimers **3-27 - 3-29**.....142
Table 3-9: Relative electronic energies of unsolvated heterodimers **3-27-3-29** calculated at B3LYP/6-31G*.....143
Table 3-10: Tabulation of the lengths of the significant bonds in B3LYP/6-31G* optimized structures of mono-solvated heterodimers.....146
Table 3-11: Relative energies of mono-solvated heterodimers **3-27•Me_2O -3-29•Et_2O**.....146
Table 3-12: Tabulation of the bond lengths of the significant bonds in B3LYP/6-31G* optimized structures of disolvated heterodimers.....149
Table 3-13: Relative energies of disolvated heterodimers **3-27-3-29**.....150
Table 3-14: Tabulation of the bond lengths of the significant bonds in B3LYP/6-31G* optimized structures of disolvated heterodimers.....152
Table 3-15: Relative electronic energies of trisolvated heterodimers.....153
Table 3-16: Thermodynamics of sequential solvation of μ-Cl-μ(1,3)-cyclopropylnitrile heterodimer **3-29**.....154
Table 3-17: Tabulation of the bond lengths of the significant bonds in B3LYP/6-31G* optimized structures of disolvated heterodimers.....157
Table 3-18: Comparison of the electronic energies of all trisolvate species calculated at B3LYP/6-31G*.....163
Table 4-1: Preparation of 0.25 M stock solutions of *i*-PrMgCl. 209
Table 4-2: Volumes of added solvent and final [Et_2O] 210
Table 4-3: HPLC analysis conditions and retention times.....212
Table 4-4: Enantiomer ratios in diethyl ether (Et_2O) at $[Mg]_{total}$ = 0.0342 M.....217
Table 4-5: Enantiomer ratios in diethyl ether (2-MeTHF) at $[Mg]_{total}$ = 0.0342 M.....218
Table 4-6: Enantiomer ratios in diethyl ether (THF) at $[Mg]_{total}$ = 0.0342 M.....218
Table 4-7: Activation parameters from the Eyring analysis.....219
Table 4-8: Enantiomer ratios at four different $[Mg]_{total}$ at a constant temp of 195 K....220
Table 4-9: Enantiomer ratios at varying concentrations of Et_2O solvent at 195 K.....221
Table 4-10: Enantiomer ratios at varying concentrations of Et_2O solvent at 212 K. 221
Table 4-11: Electronic Energies, ZPVE at 298.15 K and 1 atm, all at B3LYP/6-31G* for MeMgCl monomers (**3-24**) and dimers (**3-25**).....223

Table 4-12: MP2/6-31G* Single-point electronic energies on B3LYP/6-31G* optimized geometries of selected (lowest energy conformer) solvates of MeMgCl monomers (**3-24**) and dimers (**3-25**)…….224
Table 4-13: Free energies at 195 K calculated at B3LYP/6-31G* for selected (lowest energy conformer) solvates of MeMgCl monomers (**3-24**) and dimers (**3-25**)……...225
Table 4-14: Free energies at 195 K calculated at MP2/6-31G*//B3LYP/6-31G* using G_{corr} values obtained at B3LYP/6-31G* for selected (lowest energy conformers) solvates of MeMgCl monomers (**3-24**) and dimers (**3-25**)……226
Table 4-15: Electronic Energies, ZPVE at 298.15 K and 1 atm, all at B3LYP/6-31G* for heterodimers **3-27**, **3-28**, and **3-29** of magnesiated cyclopropylnitrile/*i*-PrMgCl……...227
Table 4-16: MP2/6-31G* Single-point electronic energies on B3LYP/6-31G* optimized geometries of selected (lowest energy conformer) solvates of heterodimer **3-29** of magnesiated cyclopropylnitrile/*i*-PrMgCl……...228
Table 4-17: Free energies at 195 K calculated at B3LYP/6-31G* for selected (lowest energy conformer) solvates of heterodimer **3-29** of magnesiated cyclopropylnitrile/*i*-PrMgCl……228
Table 4-18: Free energies at 195 K calculated at MP2/6-31G*//B3LYP/6-31G* using G_{corr} values obtained at B3LYP/6-31G* for selected (lowest energy conformer) solvates of heterodimer **3-29** of magnesiated cyclopropylnitrile/*i*-PrMgCl……..229

Chapter 1: Synthesis and Reactions of C_α-Chiral Organomagnesium Reagents

1.1 Introduction

The development of C_α-chiral organometallics, where the metal bearing carbon is the sole source of chirality has been a topic of significant amount of research in the past.[1-4] The potential of synthesizing different chiral compounds in a single electrophilic quench reaction is the reason for the interest in their development. Traditionally, the strategy of employing chiral electrophiles in reactions with achiral/chiral-stereolabile organometallics has been successfully employed in asymmetric synthesis.[5] However, the development of chiral organometallics is still lagging behind because of various problems involved with their synthesis, configurational stability, and the stereochemical course of their reactions with electrophiles. In this chapter we will discuss our studies on the synthesis and reactions of C_α-chiral Grignard reagents, which involved two separate projects. First, we will describe our study of reactions of 1-magnesio-2,2-diphenyl cyclopropylnitrile **1-21**. Second we will describe our attempts to achieve Mg/X exchange reactions at secondary sp^3 carbon centers – a strategy which has been heretofore unsuccessful owing to the lower reactivity of secondary halides in such reactions, and thus rarely explored for synthesizing chiral Grignard reagents.

1.1.1 Metalated nitriles

The utility of nitrile-containing compounds in medicinal chemistry and the recent discovery of novel nitrile-containing natural products has prompted interest in the synthesis of such compounds.[6] Metalated nitriles have long been hailed as powerful nucleophiles in organic synthesis.[7-9] The nitrile group is a very favorable substituent on a nucleophile, as it does not sterically interfere in electrophilic substitution reactions.

Similarly its potential to be transformed into a large number of functional groups makes metalated nitriles important synthetic intermediates.

1.1.1.1: Structural properties of metalated nitriles

Although their applications are widely popular in the literature, the exact structure of metalated nitriles is complicated owing to a large number of interplaying factors. Before we enter the discussion on synthesis and reactions of metalated nitriles, we first discuss the structural features of these compounds. The biggest structural complexity in metalated nitriles arises from the α–nitrile group. Scheme 1-1 shows the two commonly accepted structural representations arising from the polarization of the carbon-metal bond and delocalization into the nitrile group. Structure **1-1** is commonly referred as the C-metalated nitrile and **1-2** as the N-metalated nitrile or the keteniminate species.

Scheme 1-1: Valence-bond isomerization and ionization of metalated nitriles

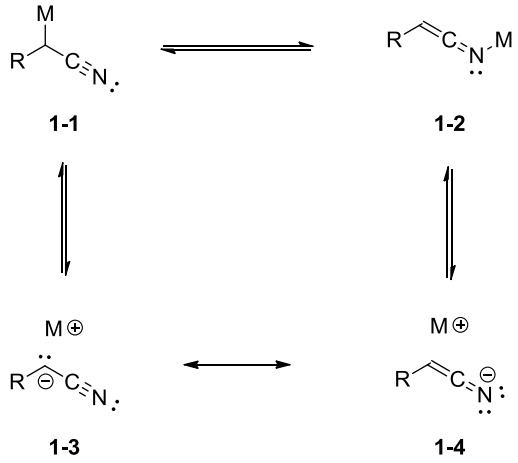

X-ray crystallography has been successfully used to study structure of metalated nitriles. Figure 1-1 shows the structures of two important metalated nitriles observed by X-ray crystallography.

Figure 1-1: X-ray crystal structures of 1-lithio phenylacetonitrile **1-5** and lithio cyclopropylnitrile **1-6**.

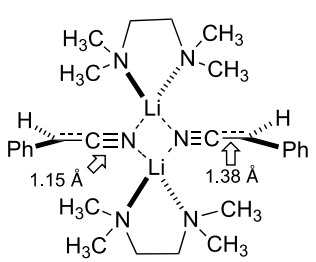

1-5

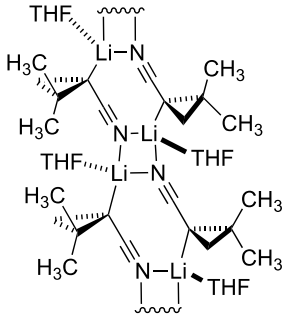

1-6

N-metalated species have been observed by X-ray crystallography on various metalated nitriles.[10] Structure **1-5** shows the *N*-metalated nitrile structure in the crystals of 1-lithio phenylacetonitrile. Even though keteniminate like structures **1-5** are observed, close observation of the C-N bond lengths in these structures show a complex scenario.[11,12] The CN bonds in **1-5** were found to be slightly elongated as compared to the standard nitrile bond distance of 1.14 Å.[11,12] On the other hand, the C-CN bond length was found to be diminished to a length similar to that of the C=C double bond.[11,12] This observation implied that the delocalization of the electrons into the cyano group happens minimally in this case. If delocalization were to be prominent, the CN triple bond would be significantly elongated to match a C=N double bond. Thus, whatever stabilization is provided by the cyano group comes from the inductive effect than its capacity to delocalize the formal negative charge. Similar types of structural features are observed in crystals of a few other metalated nitriles.[8,9]

On the other hand, C-Metalated species have only been observed in the case of 1-lithio cyclopropylcarbonitrile **1-6**.[13] X-ray crystal structure of 1-lithio, 2,2-dimethyl

cyclopropylnitrile **1-6** observed by Boche et. al [12] revealed that the lithium bearing carbon was pyramidalized and not planar as observed in keteniminate type crystal structures of metalated nitriles such as 1-lithio phenylacetonitrile **1-13** (Figure 1-2). Interestingly, both Li-N and Li-C contacts are observed in **1-6**.

Fleming concluded from these observed structural features in keteniminate species like **1-5** that the structure **1-2b** where there is significant charge localization on the nitrile bearing carbon may be a better representation of the keteniminate species (Figure 1-2).[8] Because of this localized negative charge density on the carbon bearing the nitrile, it has been observed that metalated nitriles prefer to react with electrophiles at the Carbon rather than the Nitrogen. Apart from this, identity of the metal, identity of the solvent, the presence of additives and aggregation state are other factors that have been found to influence structure of metalated nitriles.

Figure 1-2: Representations of nitrile anion keteniminate structures.

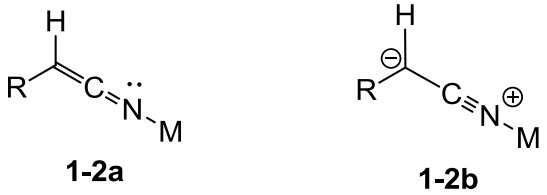

1.1.1.2: Synthesis of Metalated nitriles via the metal-halogen exchange reaction

Traditionally, deprotonation of corresponding carbonitriles has been the most successful strategy towards synthesis of metalated nitriles (nitrile anions).[9] Typically strong bases such as LDA and HMDS are employed for deprotonation of un-activated aliphatic nitriles, while weaker bases such as Et_3N, KOH, NaOH etc. have been used to deprotonate the more acidic aryl acetonitrile compounds.[14] However, this strategy

imposes several restrictions on the substrate compatibility owing to the conditions required. For substrates where stronger bases are required, substituent functional group compatibility is an issue that needs to be addressed. Metal-halogen exchange routes have been typically used to solve this problem.[15] Better substrate compatibility of such reactions and the possibility of in-situ generation of the desired organometallic are the key advantages of such reactions. We will present a detailed discussion on the topic of magnesium - halogen (Mg/X) exchange reactions in section 1.1.3.

The use of the metal-halogen exchange route towards the synthesis of metalated nitriles was first suggested by Fleming and Knochel. [16,17] As suggested by the name, this method involves treatment of the corresponding α–halo nitriles **1-7,** with organolithium or organomagnesium reagents leading to the corresponding metalated nitrile **1-8** (Scheme 1-2). The resulting magnesio and lithio nitrile compounds were then trapped using various electrophiles leading to different substitution products **1-9** (Scheme 1-3).

Scheme 1-2: Fleming and Knochel's Mg/X & Li/X exchange route to metalated nitriles.[16]

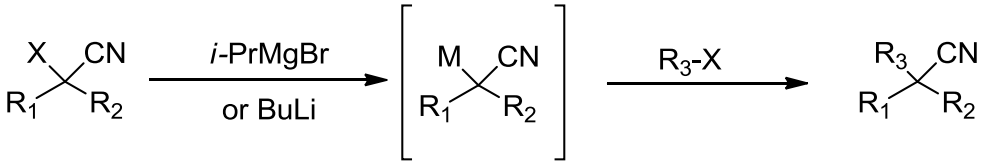

1-7 **1-8** **1-9**

X= Cl, Br, I

All the generated metalated nitriles react efficiently to yield good isolated yields of the corresponding electrophilic substitution products. Acyclic, cyclic and activated halo-nitriles all reacted well in the suggested reaction conditions which include a sequential metalation – alkylation protocol as well as an in-situ protocol where the

electrophile and halo-nitrile were combined before addition of the organometallic for exchange reaction.

Scheme 1-3: Fleming and Knochel's Mg/X & Li/X exchange route to metalated nitriles.[17]

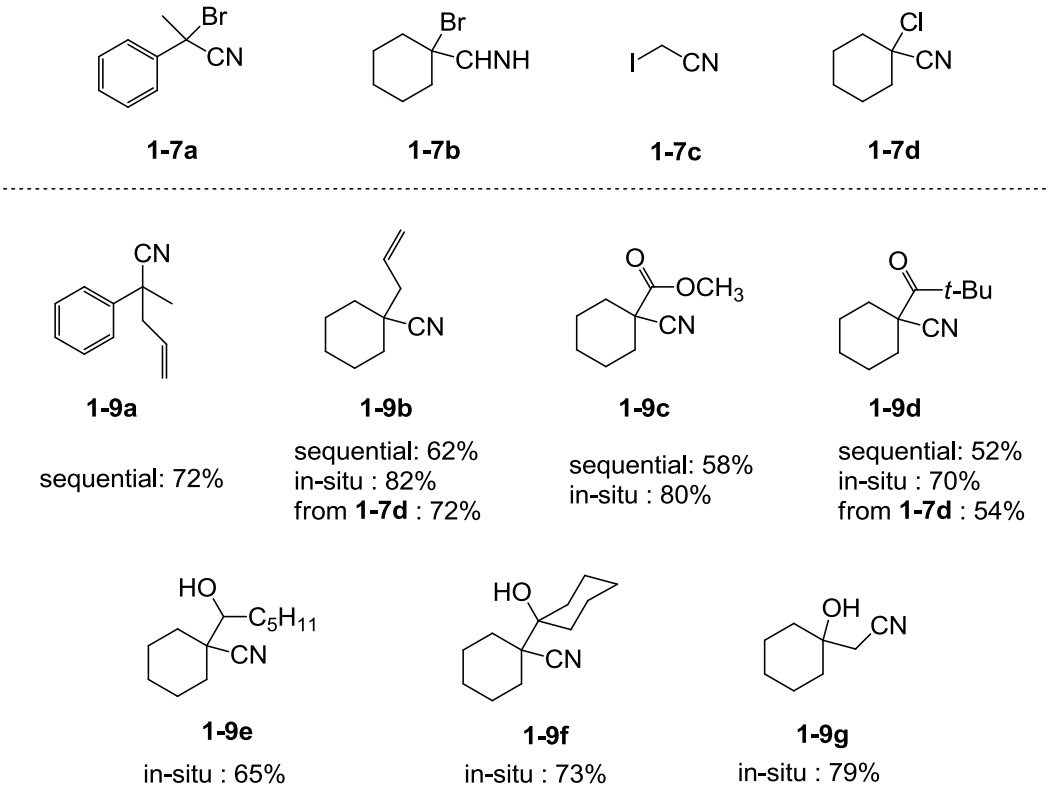

While the bromo and iodonitrile compounds **1-7a-c** undergo facile Mg/X exchange reaction under both conditions with the organomagnesium reagent (*i*-PrMgCl) generating the corresponding magnesio nitrile reagents **1-8a-c**, the less reactive chloro-nitrile compounds **1-7d** reacted well with the organolithium reagent (*n*-BuLi) under the sequential protocol generating the corresponding lithio nitrile reagent **1-7d**. This result confirmed the comparatively higher reactivity of organolithiums in halogen exchange reactions. This non-deprotonative method of synthesizing metalated nitriles was appealing since it provided a method to synthesize magnesionitrile compounds that could

not be synthesized using traditional metal insertion reactions.

1.1.2: Enantiopure metalated cyclopropylnitriles

Versatile nucleophiles like metalated nitriles would be even more useful if they could be synthesized as enantiopure reagents.[7] However, metalated nitriles bearing macroscopic configurational stability are rare. One reason behind this scarcity is the low barrier of inversion possessed by nitrile anions and the ability of metalated nitriles to form free carbanions through ion pair separation and other pathways (configurational stability of chiral organometallic compounds will be discussed in some detail in chapter 2).[18] In this section we will discuss enantiopure metalated cyclopropylnitriles and how they are potentially chiral nucleophiles for asymmetric synthesis.

Cyclopropylcarbonitrile carbanions have been computationally shown to possess higher barriers of inversion than their acyclic analogs. Carlier studied the transformation of carbanions **1-10** and **1-11** to the corresponding inversion transition structures **1-12** and **1-13** at the B3LYP/6-31+G* level (Scheme 1-4).[18] While the acetonitrile anion **1-10** was found to possess a very small inversion barrier (0.3 kcal/mol), the cyclopropylcarbonitrile anion **1-11** had a significantly larger inversion barrier (5.2 kcal/mol). The higher barrier for inversion in case of cyclopropyl carbanions was attributed to the higher angle strain in **1-11** as compared to **1-10**. Also, it is important to again note that the X-ray crystal structure analysis by Boche on 1-lithio-2,2-dimethyl cyclopropylcarbonitrile **1-6** (Figure 1-1) showed that the lithium bearing carbon was pyramidalized and not planar as with ketenaminates **1-5**. This suggests that cyclopropyl carbanions may have a higher barrier for inversion than other alkyl carbanions.

Scheme 1-4: Free anions of nitriles studied for inversion barrier.[18]

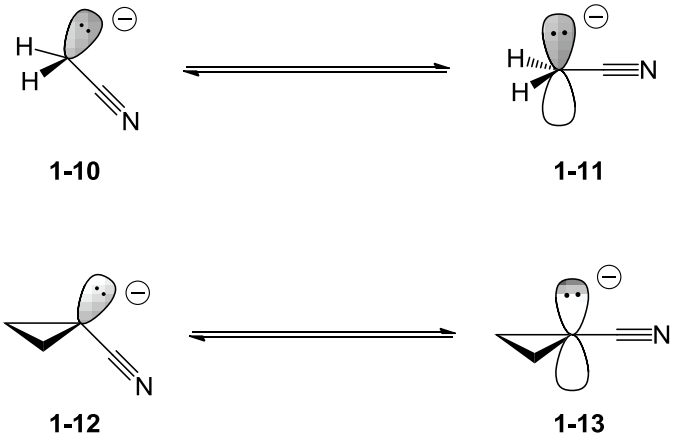

The development of metalated cyclopropyl carbanions has been studied by several authors in order to exploit this higher inversion barrier and generate enantiopure organometallics.[19-24] Similarly development of enantiopure metalated cyclopropylcarbonitriles has also been attempted. Walborsky studied the deprotonation/deuteration of enantiopure (*R*)-2,2-diphenyl cyclopropylcarbonitrile **1-14** using sodium methoxide as a base in methanol (Scheme 1-5a).[25] The deuteration was found to give highly retentive product at 50 ^{o}C. However, in contrast the acyclic analogue **1-16** under similar conditions yielded the corresponding racemic product [D_1]-**1-16** (Scheme 1-5b). The corresponding sodiated cyclopropylcarbonitrile **1-15** was concluded to possess microscopic configurational stability – sufficient enough to undergo fast retentive deuteration under the reaction conditions. On the other hand, the acyclic sodiated nitrile **1-16** is configurationally unstable, where the rate of racemization was even faster than deuteration reaction. This result clearly proved the higher configurational stability of cyclopropyl carbanions over acyclic carbanions.

Scheme 1-5: Walborsky's deprotonation/deuteration of acyclic and cyclopropylcarbonitriles. [25]

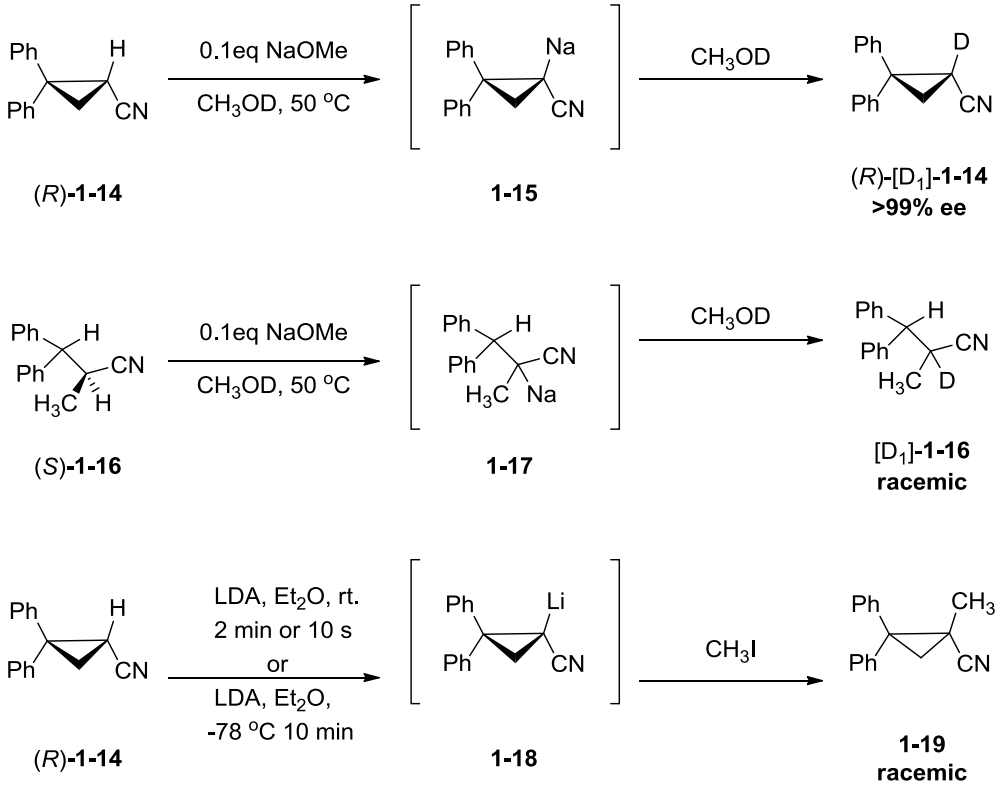

Similarly, Walborsky attempted the same deprotonation strategy to obtain metalated nitrile followed by electrophilic quench using lithium diisopropyl amide (LDA) as the base under sequential conditions.[26] Under all the attempted conditions including the very low temperatures of dry-ice acetone mixtures (195 K) the putative lithio cyclopropylcarbonitrile **1-18** intermediate yielded the racemic electrophilic methylation product **1-19**.[27] Carlier and Zhang re-investigated Walborsky's results with a variety of different bases like LDA, LiHMDS, KHMDS.[7] Regardless of the identity of the base used, identity of the solvent (THF, Et_2O, Me_2O) or the electrophile (MeI, BnBr, D_2O), racemic products were obtained. Even under in-situ conditions, where the electrophile (MeI, BnBr) is present in solution while deprotonation is taking place, or extremely low

temperatures of -136 ^{o}C, racemic products were obtained. These results suggested that the rate of racemization of lithiated cyclopropylnitrile **1-18** was extremely fast as compared to the rate of its electrophilic quenching reaction.

The first example of an enantioenriched metalated cyclopropylnitrile possessing macroscopic configurational stability was reported in by Carlier and Zhang,[7] where 1-magnesio, 2,2 diphenyl-cyclopropylcarbonitrile **1-21** was synthesized using a Mg/Br exchange reaction from the corresponding enantiopure bromonitrile **1-20**. It was demonstrated that 2.2 equivalents of the reactant isopropyl magnesium chloride (*i*-PrMgCl) was needed for an efficient exchange reaction at the very low reaction temperature of 173 K. The Grignard reagent was subsequently quenched using D_2O giving very high yields of the deuteriated nitrile **1-14** (Scheme 1-6) which was found to be highly enantioenriched using CSP-HPLC analysis.

Scheme 1-6: Mg/Br exchange/D_2O trapping reactions reported by Carlier *et al*.[7]

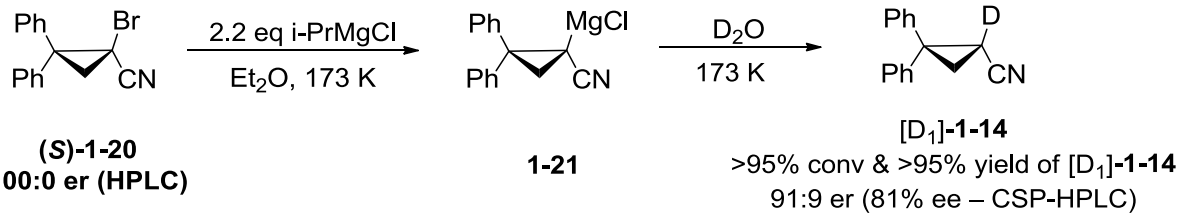

This study demonstrated the utility of Mg/X exchange reaction as a useful method to synthesize a chiral metalated nitrile. The deuterium quench of this magnesiated nitrile **1-21** resulted in the corresponding deutero compound **1-14** in >95% conversion and 81% ee, suggesting that 81% of **1-21** stayed in the same configuration till the electrophilic quench was performed. Unfortunately, this metalated nitrile reagent was not reactive towards carbon electrophiles (Table 1-1).

Table 1-1: Reactions of 1-magnesio-2,2 diphenyl-cyclopropylnitrile **1-21** with carbon electrophiles

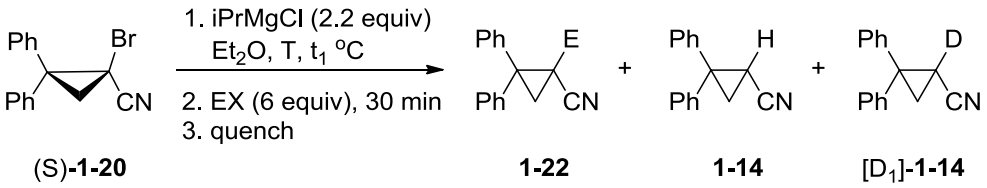

(S)-**1-20** **1-22** **1-14** [D_1]-**1-14**

Entry	E-X	Temp T (^{o}C)	t_1 (min)	quench	1-20 mol%	1-22 mol% (% ee)	1-14,[D_1]-1-14 mol% (% ee)
1	CH_3I	-78	1	NH_4Cl	1	0	99,0 (NR)
2	BnBr	-78	1	NH_4Cl	3	0	97,0 (NR)
3	CH_3OTf	-78	1	NH_4Cl	19	0	81,0 (NR)
4	CH_3OTf	-42	2	D_2O	2	8 (6)	18,72 (41)

In all attempted reactions, no significant alkylation product was formed. Electrophiles CH_3I, BnBr and even the highly reactive CH_3OTf (Entry 1, 2 & 3) did not yield any electrophilic substitution product **1-22**. Even at elevated temperatures of -42 ^{o}C and using the most reactive electrophile (Entry 4) only 8% of methyl product **1-22** was obtained. Along with the low reactivity, severe depletion of the enantiomeric excess of both alkylation product **1-22** and deuterium quench product [D_1]-**1-14** was observed. The configurational stability of **1-21** was also investigated; details of these studies will be discussed in chapter 2 where we will also demonstrate our studies towards understanding this configurational stability. The observed non-reactivity of **1-21** towards carbon electrophiles was either due to the steric hindrance of the 2, 2 diphenyl substituents, or simply due to lower nucleophilicity of **1-21** at low temperatures.

1.1.3 Enhancement of reactivity of Grignard reagents at low temperatures

The low reactivity of **1-21** at low temperatures was an intriguing problem. As seen in Table 1-1-Entry 4 at elevated temperature of -42 ^{o}C, severe depletion of the enantiomeric excess of both **1-22** and **1-14** was observed, thus increasing temperature to achieve alkylation was not a viable option to get a successful enantioselective C-C bond formation. However if the reactivity of **1-21** at low temperatures was enhanced using some method, a successful reaction with some electrophile could be envisioned. Activation of Lewis acidic compounds using Lewis basic compounds is a fundamental concept in catalysis and activation.[28] In case of Grignard reagent activation, it can be postulated that on association of a Lewis base to this Grignard reagent may cause increase in electron density on the metal, affording a Lewis base·RMgX complex that can be thought to possess enhanced nucleophilicity. In section 1.2 we will discuss our attempts at activation of magnesio cyclopropylnitrile **1-21**. Another approach of enhancing the reactivity of Grignard reagents based on the same Lewis base activation principle is the 'ate' complex methodology.

1.1.3.1 Ate complexes

Ate complexes can be defined as the combination compounds of Lewis acids and Lewis bases, where the central atom attains a high electron density by expansion of the valance shell. For example - dimethylmagnesium (Lewis Acid) and methyllithium (Lewis Base) react to form the ate compound Me_3Mg^- Li^+ or lithium trimethylmagnesate. A formal negative charge lies on the central metal atom and this peculiar feature of these compounds is proposed to impart their characteristic reactivity. Numerous important review articles have been reported concerning ate complexes and their reactions.[29-31]

These articles are important guidelines for this section and provide necessary insight into the early studies and conceptual understanding of ate chemistry. Any referrals to the above mentioned review articles are duly cited and referenced. Structural features of Ate complexes have been discussed by various authors in the past and will not be discussed in this section.[32-35] In this section, we will discuss the reactivity and synthetic applications of magnesate –ate complexes generated from Grignard reagents and diorganomagnesium compounds and some higher basic organometallic like organolithium.

1.1.3.2 Reactivity of Ate complexes

The structure of ate complexes is considered to have an electron rich metal center with various ligands present on it. These ligands are nucleophilic with the electron rich center oriented directly towards the central metal atom. The central atom thus has excess electrons on it and the most plausible reaction pathway for this species will be towards quenching of this extra-accumulated charge. As a result, these species can now react in various ways depending on their charge cancellation processes.

Figure 1-3: Common charged complexes observed in organometallic chemistry

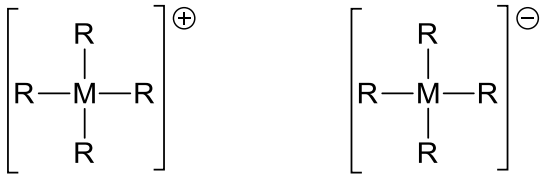

Onium Complex Ate Complex

If a comparison is made between the two opposite charged species, the onium and ate complexes (Figure 1-3), it can be observed that in both cases the formal charge on the central atom is the driving force for their reactivity.[31] The onium complex induces electron deficiency in its attached ligands by the inductive effect exerted by the

electronegative center and thus encourages the loss of these ligands, leaving their pair of electrons on the central atom. Conversely, the ate complex induces electron abundance on the attached ligands due to the electropositive center and thus, the charge cancellation of these species happens through a non-oxidative process by ejecting one of its ligands (Figure 1-4).

Figure 1-4: Non-oxidative charge cancellation process (ligand transfer)

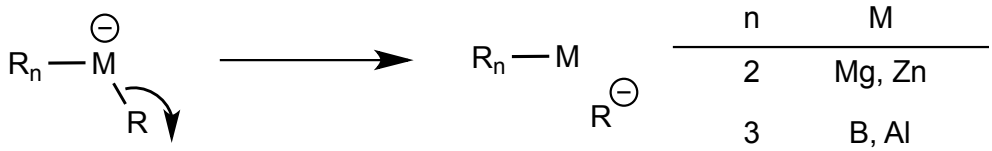

In the most interesting cases, the reactivity and/or selectivity of this hetero-bimetallic complex cannot be replicated by either of its homo-metallic components; therefore, we can say that the behavior of ate complexes is neither conventional alkali-metal like, nor like the conventional organomagnesium, but completely unique.[29,30] These unique set of compounds thus exhibit a very distinct reactivity towards various reaction conditions. The ligand transfer is the major charge cancellation process and the most interesting consequence of this is the high nucleophilicity of the ligands as compared to their basicity, which helps in nullifying a major drawback observed in case of conventional organometallic reagents like Grignard reagents and organolithiums.[32,36]

Another important factor governing the reactions in ate complexes is the transfer aptitude of the ligands. If the magnesates are homoleptic (all identical ligands) then the ligand transfer aptitude does not matter and we have only one type of anion generated from these complexes. But if heteroleptic complexes (at least one ligand different from others) are considered, then the ligand transfer aptitude does make a difference and we

get preferential transfer depending on various factors.[30] Although no model has been proposed to explain the transfer aptitude of ligands in ate complexes, we make an attempt to understand this by looking at four examples of heteroleptic magnesate complexes in Figure 1-5. In complex **1-23** and **1-24**, the most basic ligand – the isopropyl ligand- is transferred, while in case of **1-25**, the least basic phenyl ligand is transferred. Similarly in case of **1-26**, the least basic tetramethylpiperidino ligand is transferred. Whenever there is a competition between sp^2 and sp^3 ligands, we find that the sp^2 carbon bearing ligands transfers preferentially. This can be attributed to the lower basicity of the phenyl anion over the butyl anion. The reason for the preferential transfer of the most basic ligand in **1-23** and **1-24,** however, can be attributed to the relief of steric strain. Thus, the branched isopropyl ligand is transferred in preference as compared to the linear *n*-butyl ligand. Thus we can conclude that in case of competition between sp^3 heteroleptic ligands the steric factor becomes important and the group with bulkier center near the central metal will be transferred first.

Figure 1-5: Examples of magnesates bearing different ligands for understanding ligand transfer aptitude.

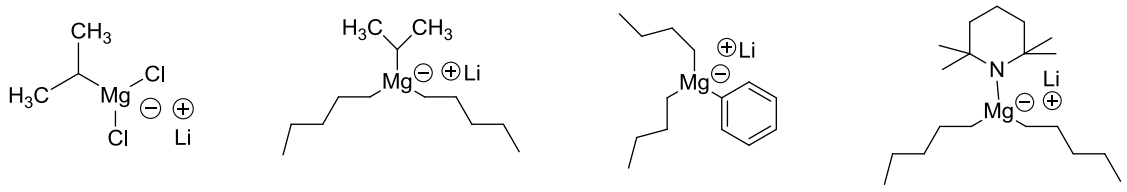

1-23 **1-24** **1-25** **1-26**

Besides the steric argument, an electronic argument can be presented for the aryl ate complexes like **1-25** where the least basic ligand transfers to the electrophile. Complexes like **1-25** are typically synthesized from an Mg/X exchange reaction from the corresponding aryl halide (Scheme 1-7). Although the ate species **1-25** could be

generated, an equilibrium in such organometallic solutions can be thought to exist, which can generate the corresponding aryl organolithium species in solution. The formation of this organolithium species will be favorable since it will be lower in basicity than the alkyllithiums that would generate from the other ligands on the complex. This in turn would also explain the better reactivity of these complexes.

Scheme 1-7: The equilibrium operative in ate complex solutions.

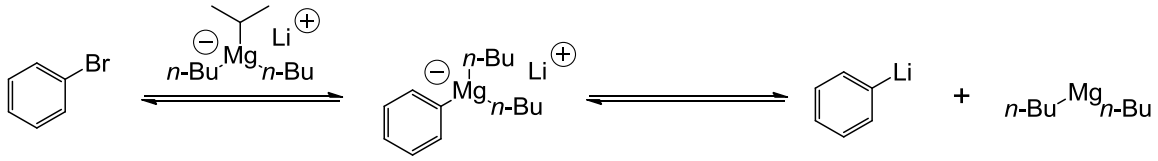

1-25

Looking at the reactivity pattern these species are nucleophilic in nature and thus are active in reactions where anionic reagents are used. Various kinds of reactions have been reported using different magnesate complexes.[29,30,32,36-38] We will limit ourselves to the metal halogen exchange reactions of magnesates in this section since we are attempting to enhance the reactivity of a Grignard reagent.

1.1.3.3 Magnesate complexes in Mg/X exchange reactions

The first use of magnesates as reagents in Mg/X exchange reactions was reported by Oshima and co-workers in the year 2000.[39] Looking at the exchange reactions of aryl halides with RMgX reported by Knochel, et al,[15] Oshima suggested that ate complexes of magnesium should react better than normal organomagnesium compounds owing to greater nucleophilicity of the transfer ligands on the magnesates. A series of aryl halides **1-26** were tested for exchange with magnesates *n*-Bu_3MgLi and *i*-$PrBu_2MgLi$. The exchange reaction was successful for various polyfunctional aryl halides in good yields. The results are summarized in Table 1-2.

Table 1-2: Oshima's magnesates/halogen exchange with aryl halides and quenching with electrophile.[39]

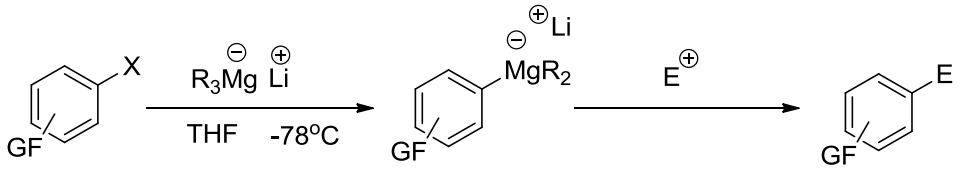

1-27 **1-28**

Entry	ArX	Reagent	Electrophile	Product	Yield%
1	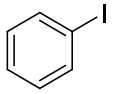	A	*n*-$C_6H_{13}CHO$	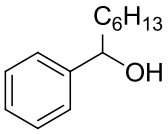	80
2	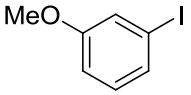	A	PhCHO	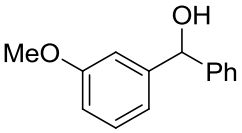	93
3	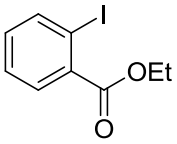	A	*n*-$C_6H_{13}CHO$	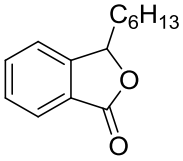	60
4	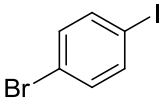	A	CH_2=$CHCH_2Br$	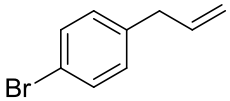	73
5	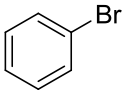	A	C_2H_5CHO	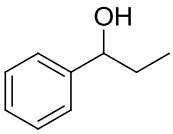	87
6	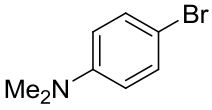	A	C_2H_5CHO	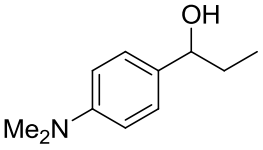	94

7	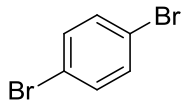	B	C_2H_5CHO	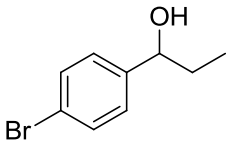	78
8	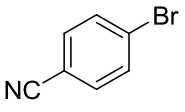	B	$^{n}C_6H_{13}CHO$	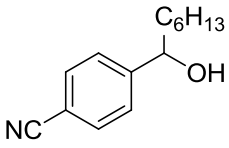	60
9	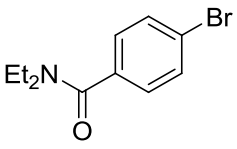	B	$CH_2=CHCH_2Br$	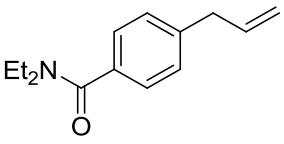	79

Reagent A: *n*-Bu_3MgLi; Reagent B: *i*-$PrBu_2MgLi$.

As seen here, not only do the aryl iodides undergo a facile exchange but the same is observed for aryl bromides. Various functional groups like ester, halogen, amide, nitrile, triamino etc. are tolerated in these reaction conditions. Good yields are obtained for aromatic compounds having activating substituents (Entry 2, 6), and a comparatively lower yield is obtained for compounds with deactivating substituents (Entry 3, 6), which is reasonable considering the nucleophilic transfer of the aryl group on to the metal center. For exchange reactions of aryl bromides, *i*-$PrBu_2MgCl$ was found to be more effective than Bu_3MgCl, which is more effective in case of aryl iodides. This new procedure for exchange was then tried on various alkenyl iodides. Some representative examples from this study are summarized in Table 1-3

Table 1-3: Oshima's magnesate/halogen exchange reactions of alkenyl iodides.[39]

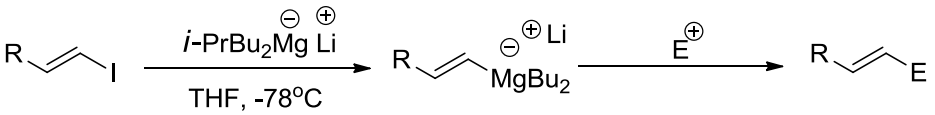

R-X	Electrophile	Product	Yield %
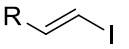 R = $C_{10}H_{21}$	D_2O	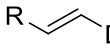	93
	Me_3SiCl	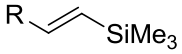	93
	PhCHO	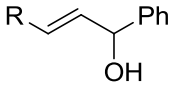	69
 R = $C_{10}H_{21}$	Me_3SiCl	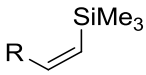	83
	PhCHO	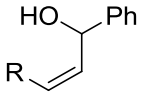	78
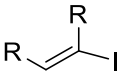 R = $C_{10}H_{21}$	D_2O	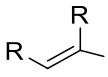	87
	PhCHO	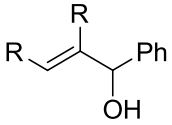	87
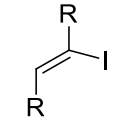 R = $C_{10}H_{21}$	D_2O	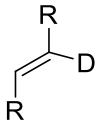	88
	PhCHO	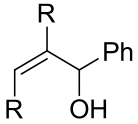	70
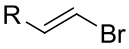 R = $C_{10}H_{21}$	Me_3SiCl	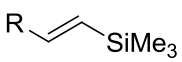	29
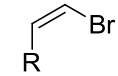 R = $C_{10}H_{21}$	Me_3SiCl	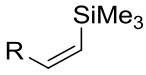	59

As observed from the table, good yields were obtained for the exchange reactions after subsequent trapping with electrophiles with both E and Z alkenyl compounds. Complete retention of configuration was observed in each case. In contrast to the reactions with aryl compounds, the alkenyl bromides react sluggishly in this reaction giving poor yields.

Oshima and co-workers further investigated the uses of aryl magnesates derived from exchange reactions of various polyfunctional aryl halides **1-29** in the titanium mediated self-coupling reactions of magnesates **1-30**. (Scheme 1-8).[40] Good yields were obtained in each case [4-Me (82%), 4-OMe(80%), 3-Br(74%), 4-CF_3(74%)], signifying an important application of magnesates.

Scheme 1-8: Oshima's titanium mediated self-coupling reactions of magnesates.[40]

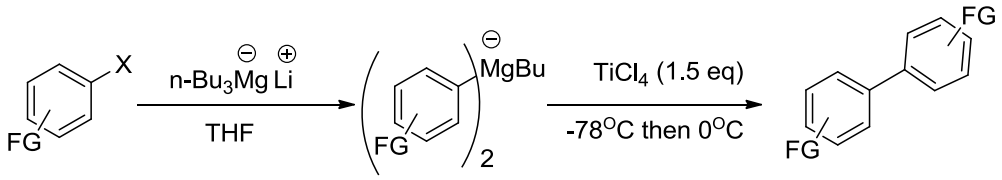

1-29 **1-30** **1-31**

X= Br, I

FG = Me, OMe, Br, CF_3,

The exchange reaction thus was proven to be a useful in the synthesis and reactions of magnesates of aryl halides. The reaction was next extended to various heteroaryl halides, using the same procedure, magnesate reagent in THF solvent (Table 1-4).[41]

Table 1-4: Oshima's magnesate/halogen exchange of heteroaryl halides.[41]

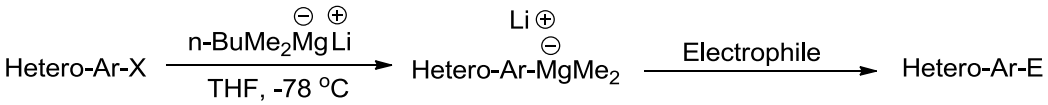

Entry	Substrate	Electrophile	Product	Yield %
1	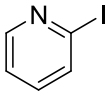	EtCHO	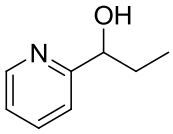	58
2	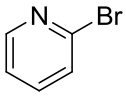	EtCHO	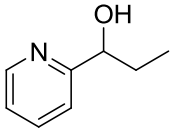	67
3	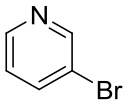	EtCHO	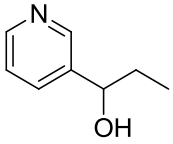	73
4	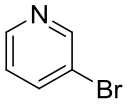	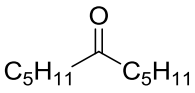	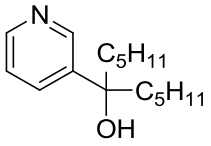	49
5	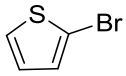	PhCHO	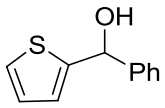	78

Again good yields were observed for most of the trapped products, signifying good tolerance to the heteroatom in this reaction. The only exception observed involved the trapping by a bulky electrophile, where steric hindrance might be the reason for a poor yield (Entry 4).

The reaction was further tried for dibromo compounds by Iida and co-workers. [42] The dibromides were treated with tributyl magnesate and the resulting aryl butyl magnesates were trapped using dimethyl formamide followed by acid work-up (Table 1-5). The overall reaction was the formylation of the aryl and heteroaryl dibromides, where magnesate was the intermediate.

Table 1-5: Iida's formylation reactions of aryl-heteroaryl dibromides via magnesate intermediates.[42]

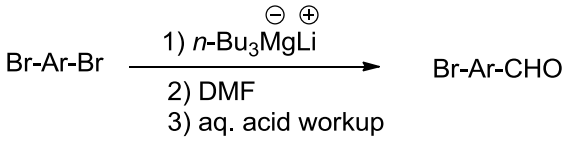

Substrate	Conditions	Product	Yield %
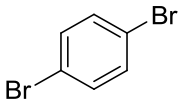	0 °C, 5h	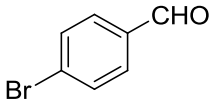	84
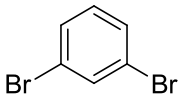	0 °C, 1.5h	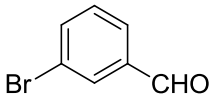	99
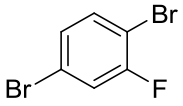	0 °C, 1h	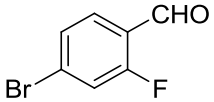	92
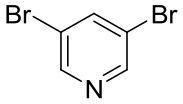	-10 °C, 1.5h	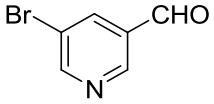	78
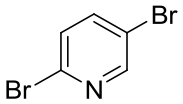	0 °C, 1.25h	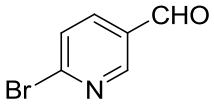	71
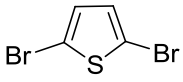	-10 °C, 3h	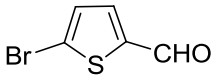	73

All electrophilic quenching steps carried at 0°C and then warmed to R.T

The study revealed various aspects of this reaction, most compelling being reaction conditions. All the reactions were performed at non-cryogenic temperatures, suggesting good thermal stability of the magnesate intermediate. Another important observation was that of the investigation of ratios of mono and di-formylation. Mono formyl product was observed almost exclusively in all the reactions, indicating that only one halogen is exchanged during the magnesate formation step.

J. Xu and co-workers reported the exchange reactions of aryl compounds bearing electron-rich species using different magnesates.[43] Various magnesation resistant substituents like the hydroxyl and amine were tried for exchange. (Scheme 1-9).

Scheme 1-9: Xu's magnesations of hydroxyl group containing aryl halides.[43]

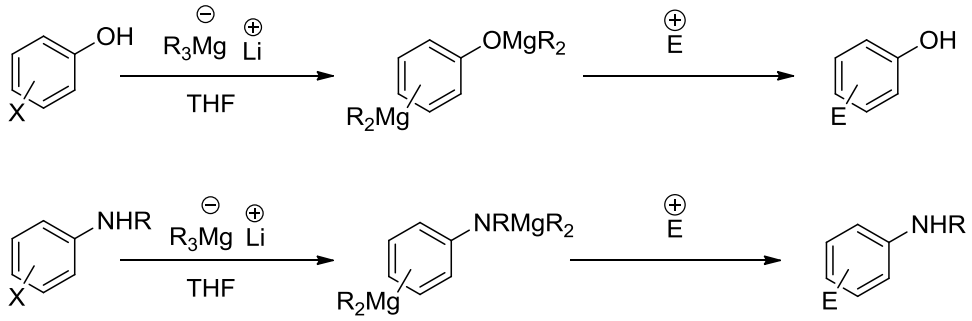

A comparative study was performed between organomagnesium reagents and magnesate reagents. In most of the cases, magnesate reagents prove to be better exchange reagents than the conventional organomagnesium compounds. The exchange reaction was tried on indolyl iodide for the first time and magnesate reagents prove to be excellent reagents for the exchange (Scheme 1-10).

Scheme 1-10: Xu's magnesate/halogen exchange reactions on indolyl iodides.[43]

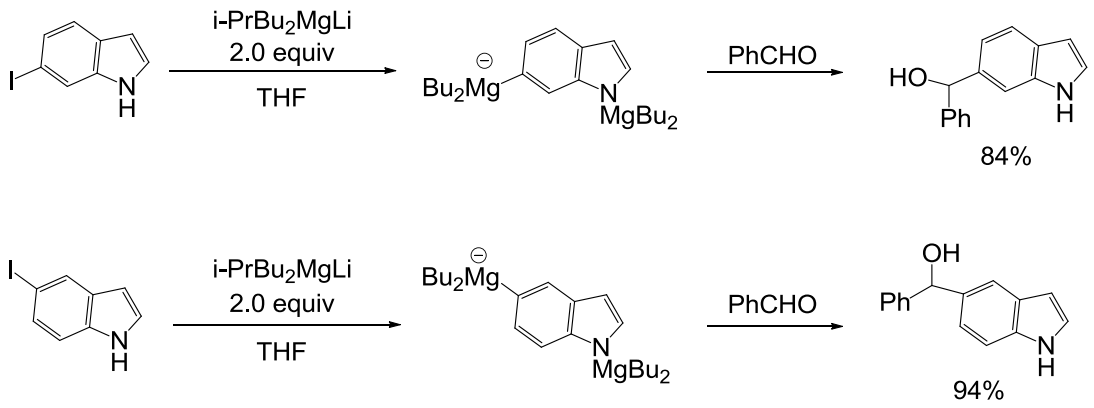

The exchange reactions of alkenyl halides was again taken up for study by Sato and co-workers, where selective Mg/I exchange reactions of 1,4 di-iodo-1,3-butadiene

were studied.[44] The subsequent quenching reactions were carried out by water and the products isolated. Various electrophiles and substituents were tried and the resulting products studied for explanations on the reaction (Table 1-6). Good yields are observed for all the available substrates. Here, regioselectivity is observed due to the presence of silyl group at R_1 position.

Table 1-6: Fukuhara's magnesate exchange reactions of 1,4 di-iodo alkadienes. [44]

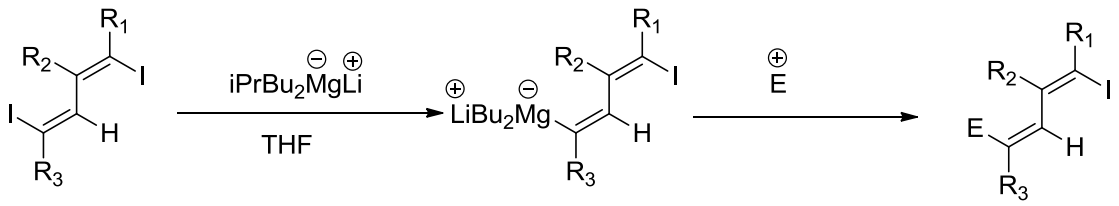

Substrate			Electrophile	Product	Yield
R_1	R_2	R_3		E =	%
$SiMe_3$	C_6H_{13}	C_6H_{13}	H_2O	H	83
$SiMe_3$	C_6H_{13}	$SiMe_3$	H_2O	H	84
$SiMe_3$	C_6H_{13}	*c*-C_6H_{11}	H_2O	H	79
C_3H_7	C_3H_7	C_3H_7	H_2O	H	86

Finally, the examples of magnesate mediated exchanges of alkyl halides are still a rarity and not many reactions have been reported. Oshima and co-workers have reported the only observed magnesation reaction of cyclopropyl bromide **1-32** with tributylmagnesate.(Scheme 1-11).[41] It was postulated that the exchange reactions of alkyl halides are rare because of competition between the transfer aptitude of the alkyl groups previously present on the ate complex with the substrate alkyl group.[41] If there is no compelling difference between the basicity's of the ligands on the ate complex, there is no driving force for the exchange to occur and thus not many examples are observed.

Scheme 1-11: Oshima's magnesate exchange of cyclopropyl bromide. [41]

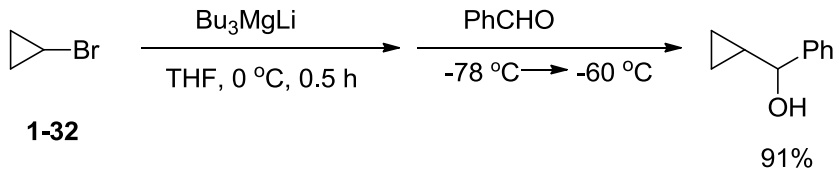

Throughout this section, it was demonstrated that the Mg/X exchange reactions of magnesate complexes are extensively useful in case of aryl, heteroaryl and alkenyl halogen compounds. These reagents have proven to be better than the organomagnesium reagents because of the faster rate of reactions and better yields are obtained. In section 1.2, we will demonstrate our observations on the Mg/X exchange reactions on bromonitrile **1-20** with magnesate complexes and the subsequent reactions of the new magnesate species with electrophiles. The relative paucity of examples of Mg/X exchange reactions at sp^3 carbon centers even with strong reagents such as magnesates, aptly demonstrates the fundamental problem of driving force in such reactions due to the lack of large enough basicity difference. In the next section we will briefly review the available examples of Mg/X exchange reactions of alkyl (sp^3) halides, particularly secondary sp^3 alkyl halides as these reactions could be potential methods for synthesizing C_α-chiral Grignard reagents.

1.1.4 Mg/X exchange routes to secondary sp^3 Grignards – potential method for the synthesis of chiral Grignards

The utility of organometallic reagents in various complicated synthetic procedures has been established evidently by over a century of skilled and painstaking research.[45,46] Although conventional methods like direct oxidative addition of activated metals to organic halides,[47-52] carbometallation,[53] and hydrometallation[54] still remain the most used methods for introduction of metals in organic compounds, the presence of sensitive functional groups often creates a problem of competing reactions and makes their convenient use a problem in many cases.

A solution to this problem appeared after the discovery of Lithium-Halogen (Li/X) exchange reactions by Wittig et al. and Gilman and co-workers.[15] The functional group tolerance was still low in case of organolithium compounds due to their high reactivity but, the organomagnesium reagents are better in this respect owing to their relatively lower reactivity. Metal-halogen exchange reactions provide an access to various polyfunctionalized organometallic reagents, which is an important feature of these reactions and makes them one of the most useful reactions in organic synthesis. Various polyfunctionalized organolithium and organomagnesium compounds have been synthesized using the metal halogen exchange reactions.[55] The various aspects and applications of this reaction have been summarized by Knochel and co-workers.[15,55] In this section we will briefly review at magnesium-halogen (Mg/X) exchange reaction from the viewpoint of hybridization of the α-carbon of the alkyl halide used and then demonstrate our studies towards achieving Mg/X exchange with secondary sp^3 alkyl halides possessing an appropriately placed activator group.

1.1.4.1 Magnesium –Halogen (Mg/X) exchange reactions on aryl and alkenyl (sp^2) halides

In two review articles,[15,38] and a detailed book chapter,[56] Knochel and co-workers have demonstrated the manifold utility of the Mg/X exchange reactions in the synthesis of aryl and alkenyl Grignard reagents. In this section we look at this reaction with respect to the mechanism and driving force. The common accepted ionic mechanism for Mg/X exchange reaction between an aryl halide and RMgCl based on ate complexes of iodo halides observed by Hoffmann is shown in Figure 1-6.[57,58]

Figure 1-6: Ionic Mechanism for Mg/X exchange between Ar-X and RMgCl

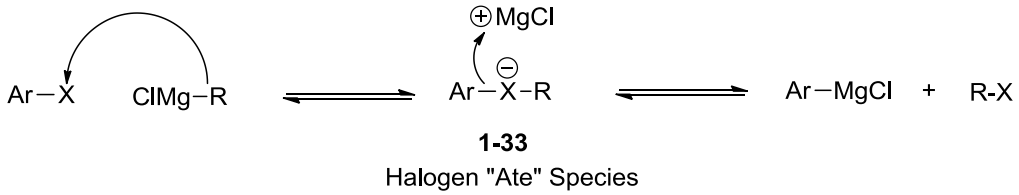

The initial step is thought to involve the formation of halogen ate complex species **1-33**. The subsequent formation of aryl Grignard species is favored by equilibrium owing to its lower basicity in comparison to the alkyl Grignard reagent used as a reagent. The reaction thus works well with most aryl and alkenyl halides due to the lower basicity of the resulting Grignard. A large number of reactions aryl halides bearing various functional groups have been known to undergo facile Mg/X exchange reactions (Scheme 1-12).[15] Similar examples about heteroaryl halides, alkenyl halides can be found in the review articles and chapters mentioned above and will not be discussed here.

Scheme 1-12: Mg/X exchange reactions of various polyfunctional aryl halides studied by Knochel.

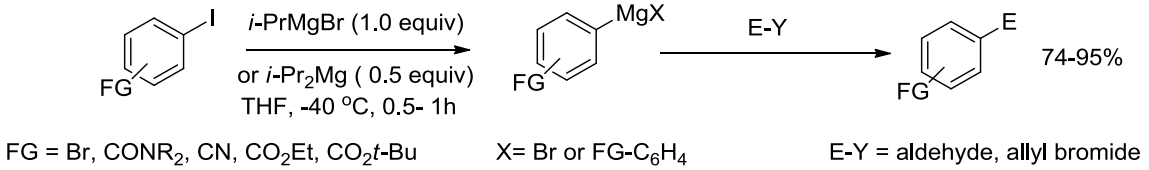

FG = Br, $CONR_2$, CN, CO_2Et, CO_2t-Bu X= Br or FG-C_6H_4 E-Y = aldehyde, allyl bromide

1.1.4.2 Magnesium –Halogen (Mg/X) exchange reactions on alkyl (sp^3) halides

As compared to aryl halides, Mg/X exchange reactions of alkyl halides are difficult to achieve. As shown in Figure 1-6, the second step of the Mg/X exchange mechanism is driven by basicity. As can be expected, this creates a problem in case of alkyl halides as most alkyl ligands on the halogen ate complex in these cases will have comparable basicity. In those cases where there are carbanion stabilizing group on the α-sp^3 carbon, the basicity of the resulting alkyl Grignard reagent is lower and we get an exchange reaction. On the other hand if no such group is present on this carbon atom, the basicity difference even if exists is not significantly high enough to push the reaction forward. Similarly primary halides generate less basic primary ligands in the halogen ate complex as opposed to higher basic secondary and tertiary carbon ligands generated by the corresponding secondary and tertiary halides. Consequently the reaction can be driven forward by exploiting this basicity difference.

Negishi and co-workers for the first time demonstrated that using a strong enough organolithium, the metal-halogen exchange reaction could be driven forward.[59] The Li/I exchange reaction is typically unsuccessful if *n*-butyllithium (*n*-BuLi) is used. However when 2 equiv of a stronger organolithium like *t*-butyllithium (*t*-BuLi) was used, a facile exchange reaction was observed (Scheme 1-13). Several primary alkyl iodides were

shown to undergo the exchange reaction at low to room temperatures. The resulting organolithium was monitored using ^{1}H-NMR or by monitoring the yield of trapping the primary organolithium using Me_3SiCl or back-iodination using I_2.

Scheme 1-13: Negishi's exchange/trapping reactions of alkyl iodides using *t*-BuLi.[59]

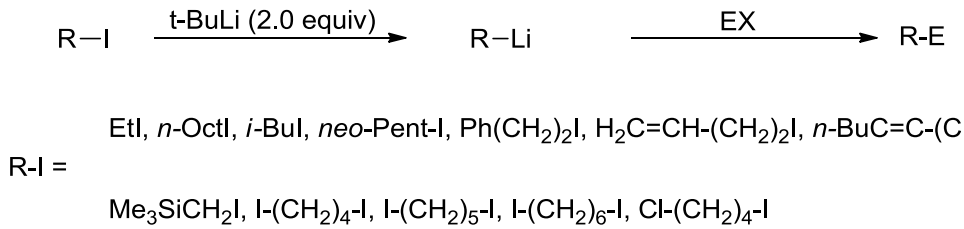

If the mechanism of the exchange reaction between the alkyl iodide and *t*-BuLi follows a pathway similar to the one shown in Figure 1-5, it can be postulated that the reaction is driven by the higher basicity of the *t*-Butyl ligand on the corresponding halogen ate complex in comparison to the primary alkyl ligand. A similar reaction with secondary alkyl halides is however not successful. This could be because of the similar basicity of the alkyl ligands in the corresponding halogen ate complex which prevents a forward reaction from happening. Because of this factor there are not many available examples of Mg/X exchange reaction on secondary alky halides. The only available examples are those with certain activated alkyl halides. In such cases the activating group on the α–Carbon of the alkyl halide is responsible for a successful Mg/X exchange reaction.

Knochel and co-workers achieved Mg/X exchange of the cis-cyclopropyliodoester **1-34** to the corresponding Grignard **1-35**. Here the initial Mg/X exchange works since the new Grignard reagent **1-35** is less basic than the reagent isopropyl magnesium chloride.[25] The formation of **1-35** is deduced to be stereoselective by observing only cis-ketoester

product**,** following transmetallation-benzoylation of **1-35** (Scheme 1-14).[60]

Scheme 1-14: Knochel's Mg/X exchange reaction with cyclcopropyliodoester.[60]

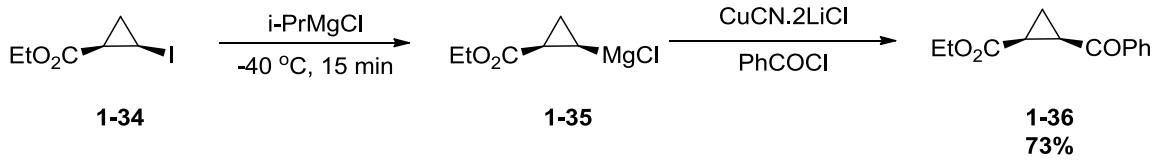

1-34 **1-35** **1-36**
73%

As shown in the earlier section, Hoffmann studied the Mg/X exchange reaction of 1,1-dihaloalkanes with a Grignard reagent bearing a chiral ligand (Scheme 1-15).[61] Again the lower basicity of the new Grignard reagent **1-38** to the reagent *i*-PrMgL* is the reason for the Mg/I exchange reaction. The resulting Grignard **1-38** was quenched with benzaldehyde in presence of Lewis acidic catalyst Me_2AlCl to yield a major syn diastereomer **1-39** in good yield but moderate enantiomeric excess.

Scheme 1-15: Hoffmann's Mg/X exchange reactions of α–halo alkyl halides.[61]

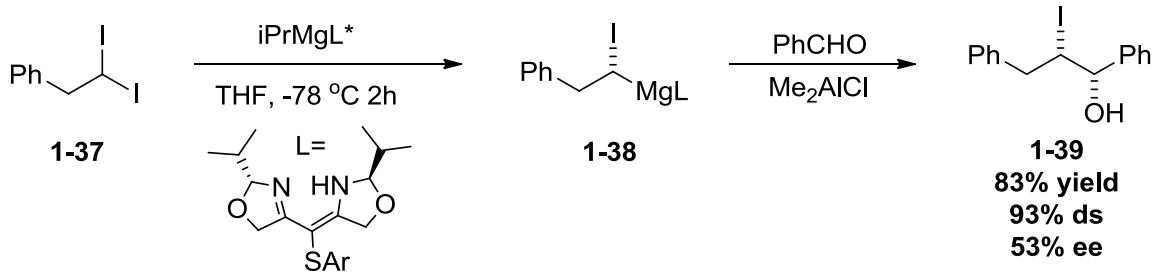

1-37 **1-38** **1-39**
83% yield
93% ds
53% ee

Along with the halogen exchange reactions, Hoffmann studied the sulfoxide exchange reactions to generate secondary chiral Grignard reagents (Scheme 1-16).[62] The activated α–alkoxy sulfoxide **1-40** was conveniently converted to the corresponding Grignard **1-41** at low temperatures. The subsequent electrophilic reaction with benzaldehyde yielded the alcohol **1-42** in good yield and excellent diastereomeric ratio. Similarly, sulfoxide/Mg exchange reaction was used to generate chiral Grignard reagent **1-44** from the chiral

enantioenriched sulfoxide **1-43** (93% *ee*). The reaction of **1-44** with benzaldehyde generated the epoxide **1-45** in 70% yield without loss of enantiomeric excess (93%).

Scheme 1-16: Sulfoxide/Mg exchange reactions toward secondary Grignard reagents

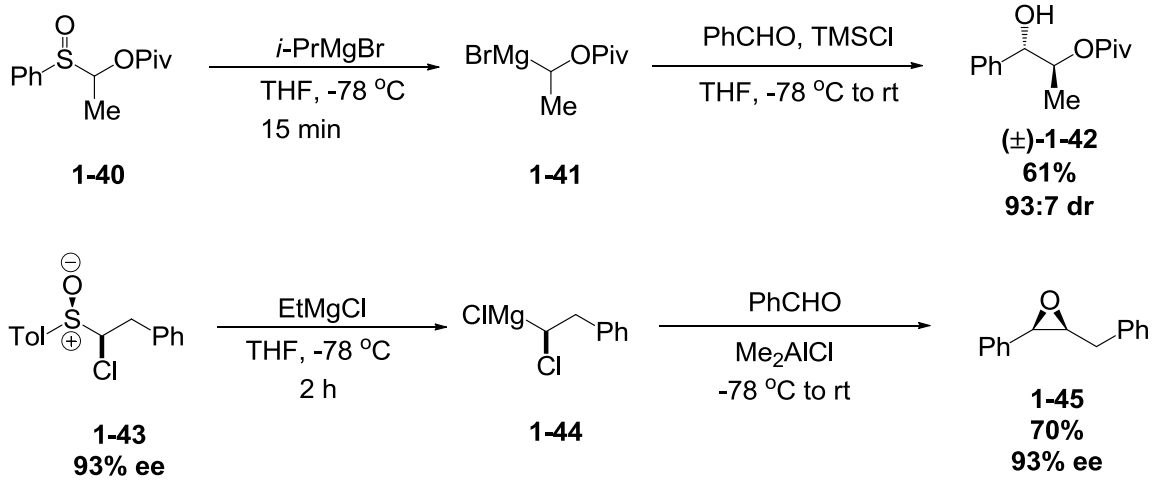

We hypothesized that sulfoxide exchange reactions will follow a mechanism similar to the ionic mechanism halogen exchange reactions (Figure 1-7), where the initial step follows the addition of the Grignard alkyl group to the sulfoxide sulfur, generating a 4-coordinate sulfur intermediate **1-46**. This is then followed by elimination of the least basic ligand generating the Grignard. Again the driving force for this reaction could be the lower basicity of the new Grignard species as compared to the initially used Grignard reagent.

Figure 1-7: Postulated mechanism for sulfoxide/Mg exchange reaction.

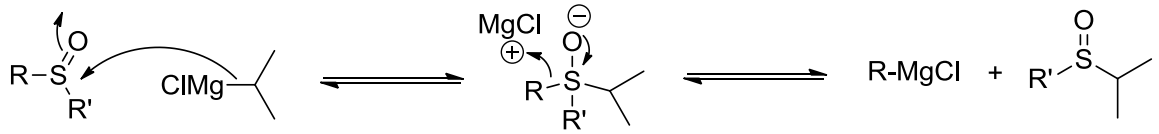

1-46

1.1.5 Appropriately placed activators to assist Mg/X exchange reactions

A conceptually appealing approach to effect metal-halogen exchange reactions is the inclusion of appropriately placed activators that direct and assist the exchange process. Pendant alkoxy groups have been successfully used in assisting intramolecular Li-Halogen, Li-Sulfur, Li-Tellurium exchange reactions.[63] Here the pendent alkoxides help by intramolecularly delivering the lithium reagent close to the reaction site. Based on this strategy, Knochel and co-workers have attempted to carry out Mg/X exchange reactions of certain γ–hydroxyl and δ-hydroxyl group containing primary sp^3 alkyl halides **1-47** (Scheme 1-17).[64] A protocol of first treatment with 1.1 equivalents of Grignard reagent (*i*-PrMgCl) followed by 2.2 equivalents of organolithium reagent (*n*-BuLi) is used to carry out the transformation. The intermediate Grignard species is the internally chelated cyclic species **1-48**, which upon trapping with carbonyl electrophiles yielded the corresponding alcohols **1-49** in moderate to good isolated yields.

Scheme 1-17: Directed I/Mg exchange reactions of γ and δ–hydroxyl group containing primary sp^3 alkyl halides.

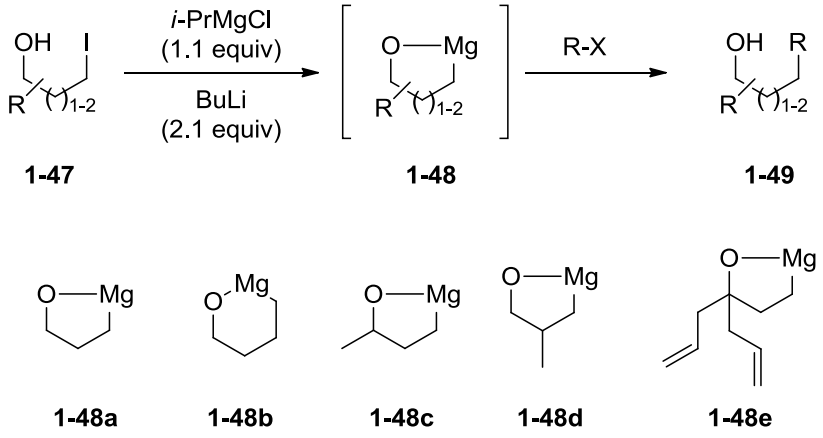

Grignard species such as **1-48a – 1-48e** were shown to react with a variety of electrophiles. The mechanism of this reaction was also postulated, which is shown in Figure 1-8. The initial step was the conversion of the halo-alcohol to the corresponding magnesium alkoxide **1-51** by deprotonation. After the addition of the *n*-BuLi, the mechanism can advance by either of the two pathways - the formation of magnesate species **1-52** or, formation of organolithium species **1-53** both of which lead to the cyclic Grignard or ate species **1-54**. The likely driving force of this mechanism is formation of the cyclic Grignard species, which is less reactive than both intermediate organolithium species **1-53** and magnesate species **1-52** (Figure 1-8).

Figure 1-8: Suggested mechanism of directed Mg/X exchange reaction.

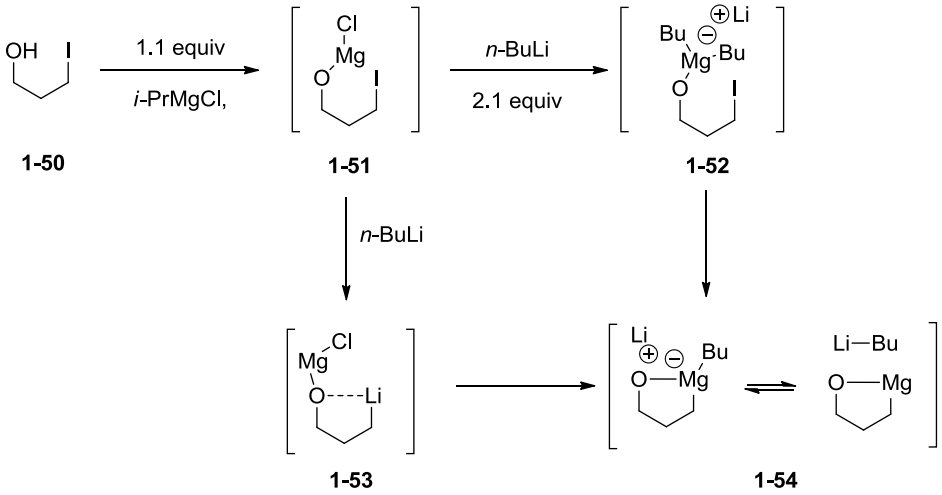

Similar directed Mg/X exchange reactions were again studied by Knochel et.al (Scheme 1-17).[65] Addition of 1.1 equivalents of bidentate magnesate species **1-57** or 0.65 to 1.1 equivalents of lithium diisopropyl magnesate reagents **1-56** were used in place of the combination of two organometallic reagents. Also, the directing group this time was a protected alkoxy group as opposed to the hydroxyl group in the example above. The resulting Grignard reagents were successfully trapped using alkyl halide, ketone, and acid

chloride electrophiles in good yields after transmetalating with CuCN·LiCl. A variety of different Grignard species bearing γ–activator groups **1-60** – **1-65** have been synthesized using the method (Scheme 1-18).

Scheme 1-18: Mg/X exchange reactions of alkyl halides bearing γ–activator groups

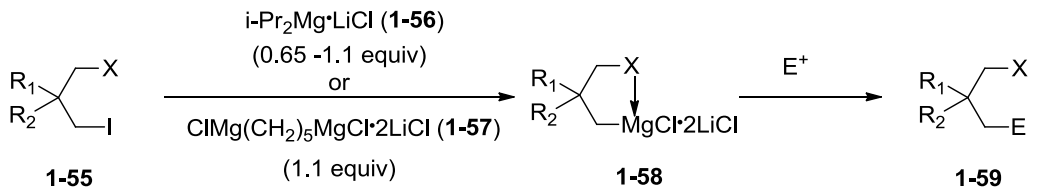

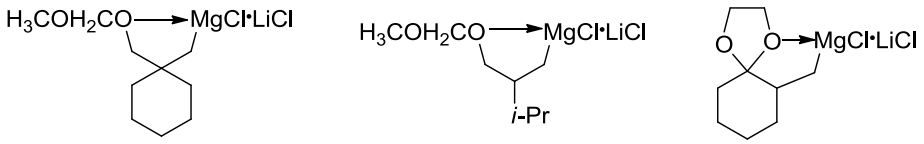

1-60 **1-61** **1-62**

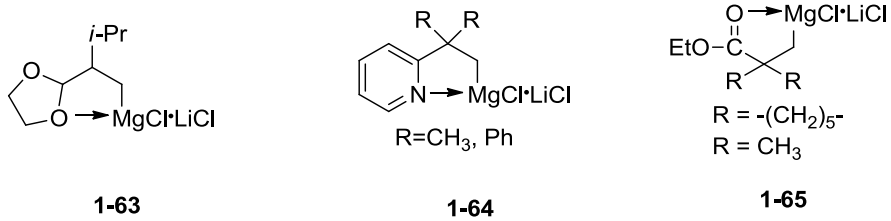

1-63 **1-64** **1-65**

Recently, Fleming and co- workers employed a 1,3 induction protocol for a diastereoselective synthesis of magnesio nitrile **1-69** (Scheme 1-19) through directed deprotonation .[66] The strategy involved formation of magnesium alkoxide **1-67** followed by inclusion of one more equivalent of *i*-PrMgCl for the formation of ate complex **1-68**. This ate species then carries out the intramolecular deprotonation leading to the cyclic magnesio nitrile **1-69**. Diastereoselectivity is induced by the side from which the deprotonating isopropyl group is delivered. The resulting Grignard is then quenched in high yields using various electrophiles in moderate to high yields. Although this is not an

example of Mg/X exchange reaction, the induction of diastereoselectivity is important to mention at this point.

Scheme 1-19: Fleming's diastereoselective metalated nitrile formation by 1-3 induction/deprotonation.

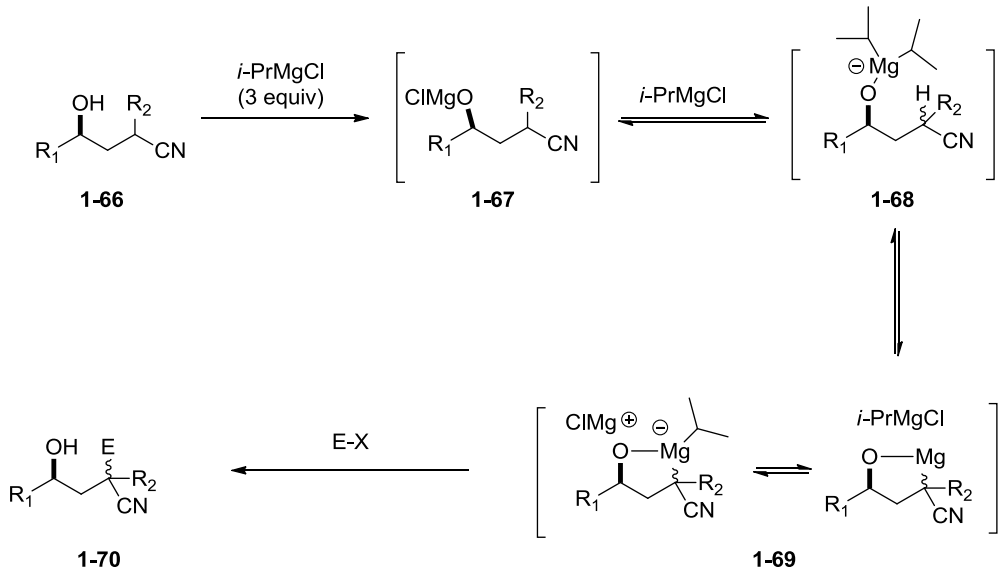

This method although successful with the activation of primary alkyl halides for Mg/X exchange reaction and deprotonative magnesiation reaction, has yet not been proved to be useful for activation of secondary alkyl halides for Mg/X exchange reaction. If this method does work with secondary alkyl halides, then it could potentially be used as a method in the synthesis of C-Chiral Grignard reagents. In section 1.3 we will discuss our experiments towards achieving such reactions using some γ-hydroxyl secondary alkyl halides.

1.2 Results and Discussions: Reactions of 1-magnesio-2,2-diphenyl cyclopropylcarbonitrile 1-21 with electrophiles – Reactivity studies.

As discussed in section 1.1.1, the first example of the enantioenriched 1-magnesio-2,2-diphenyl cyclopropylnitrile **1-21** was reported by Carlier and Zhang.[7] Unfortunately though, **1-21** was not reactive towards carbon electrophiles, and no significant carbon substituted product was obtained (Table 1-1). It was stipulated that the steric hindrance of the two phenyl substituents on **1-21** or its low nucleophilicity at low temperatures was the reason for the reduced reactivity towards electrophiles. To tackle this problem, we devised a three pronged approach. First, the development of magnesio cyclopropylnitrile reagents bearing smaller substituents to the phenyl rings in **1-21** and study of their Mg/X exchange reactions to determine if steric factors were actually responsible for the low reactivity. Second, we attempted the activation of **1-21** at low temperature by using in-situ activation protocols to get reactions at these temperatures with electrophiles. Finally, the synthesis of analogous highly nucleophilic organometallic reagents such as lithium trialkyl magnesates and their reactions with electrophiles were attempted to determine if this was the problem with **1-21**. In this section, we will describe our studies towards achieving electrophilic substitution reactions of **1-21** and then the results of experiments using the protocols mentioned above.

1.2.1 Development of magnesio cyclopropylnitrile reagents bearing smaller substituents and study of their Mg/X exchange reactions.

Assuming that the steric hindrance of the 2,2-diphenyl substituents is responsible for the lower reactivity of **1-21**. We first focused on the synthesis of alternate 1-bromo-2,2-dialkyl-cyclopropylnitrile reagents (Scheme 1-20). The two substituents at the 2

position however are necessary since these make such Grignard reagents enantiomeric. The analogous compounds bearing a single substituent however are diastereomeric. We initially chose racemic (±)-1-bromospiro[2.5]octane-1-carbonitrile (±)-**1-76** as the substrate for this study. Since measuring the reactivity of the Grignard generated by a Mg/X exchange reaction was the initial purpose of this study, we decided to use (±)-**1-76** in place of its synthetically challenging enantiopure analogue. (±)-**1-76** was synthesized using Walborsky's protocol for synthesis of analogous 1-bromo-1-methylspiro[2.5]octane over 6 steps starting from cyclohexanone as described in Scheme 1-20.

Scheme 1-20: Synthesis of (±)-1-bromospiro[2.5]octane-1-carbonitrile - (±)-**1-76**.

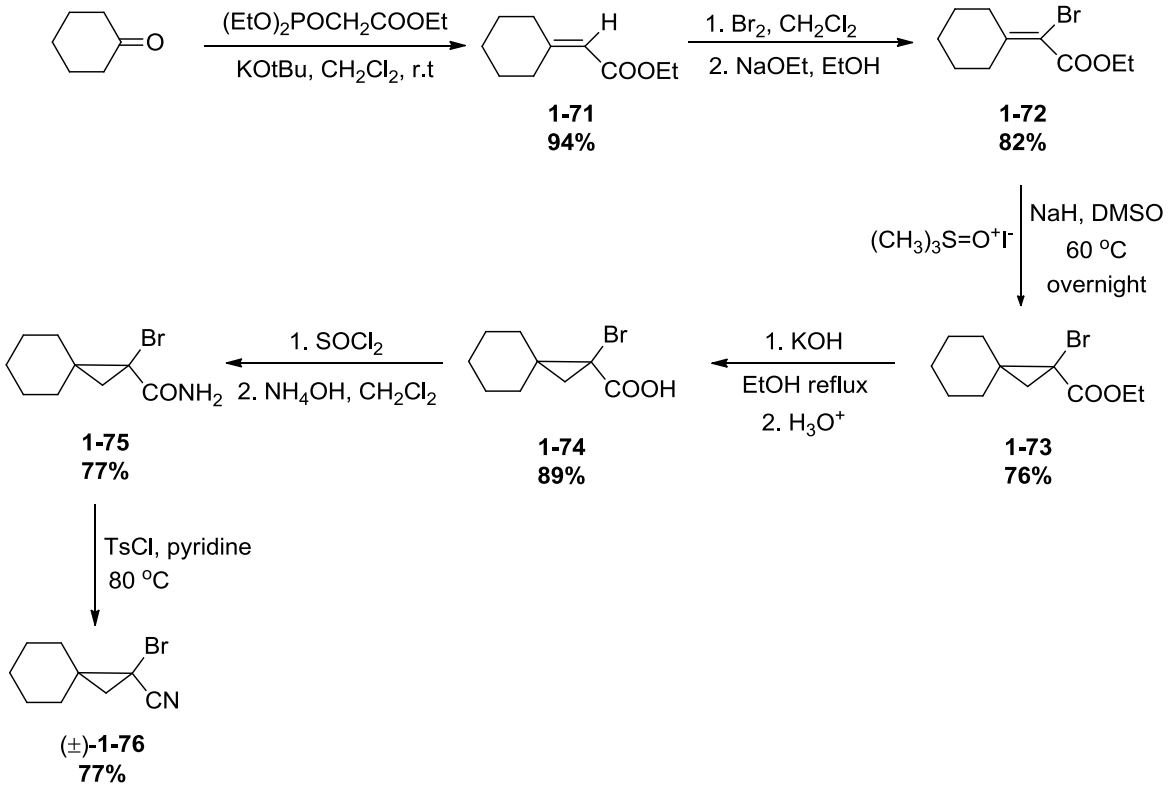

The synthesis began with the Horner – Wadsworth – Evans olefination of cyclohexane using triethylphosphono acetate to yield the α,β -unsaturated ester **1-71** in 94% yield. This was then converted to bromoester **1-72** in 72% yield via a bromine

addition followed by elimination reaction. The bromoester **1-72** was then subject to the Corey-Chaykovsky cyclopropanation reaction using trimethyl sulfoxonium iodide in DMSO under basic conditions to yield the cyclopropyl bromoester **1-73** in 76% yield which was subject to basic ester hydrolysis to yield bromoacid **1-74** in 89% yield. Amide **1-75** was then synthesized in overall 76% yield from **1-74** by an acid chloride formation/amidation reaction. The final (±)-1-bromospiro[2.5]octane-1-carbonitrile (±)-**1-76** was then synthesized in 76% yield from **1-75** by a dehydration reaction using TsCl in pyridine. The Mg/Br exchange/trapping reactions were then attempted on (±)-**1-76** using Carlier and Zhang's standardized protocol for reactions of **1-21** (Table 1-7).

Table 1-7: Mg/X exchange/trapping reactions of (±)-**1-76**.

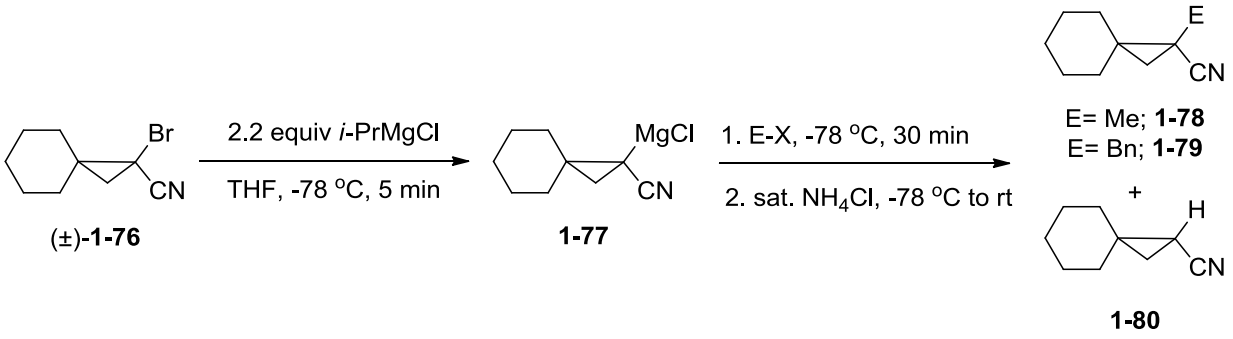

Entry	E-X	Product	Product yield mol%	1-80 mol%
1	MeI	**1-78**	0	>90%
2	BnBr	**1-79**	0	>90%
3	D_2O	[D_1]-**1-80**	>90%	N.A

The corresponding Grignard reagent **1-77** was again found to be completely unreactive towards carbon electrophiles. Methyl iodide (MeI) (Entry 1) and benzyl bromide (BnBr) (Entry 2) both gave no observable substitution products even after

stirring for 30 minutes with the Grignard reagent at this temperature with >90% isolated yields of product of quenching spiro[2.5]octane-1-carbonitrile **1-80**. However as seen before, **1-77** also gave 1-deuterio-spiro[2.5]octane-1-carbonitrile substrate [D_1]-**1-80** in >90% isolated yields (Entry 3).

To check if any significant reaction happens at higher temperatures we next examined the reaction of **1-77** with BnBr at warmer temperatures of -61, -42, -20 and 0 ^{o}C (Table 1-8). If the reaction proceeds to completion at higher temperature, a problem of low nucleophilicity of **1-77** can be envisioned to be the reason for its low reactivity towards carbon electrophiles. As expected, the reaction proceeds towards completion as the temperature is raised above -20 ^{o}C giving approx. 95% isolated yield of **1-79**.

Table 1-8: Reaction of **1-77** with BnBr at elevated temperatures.

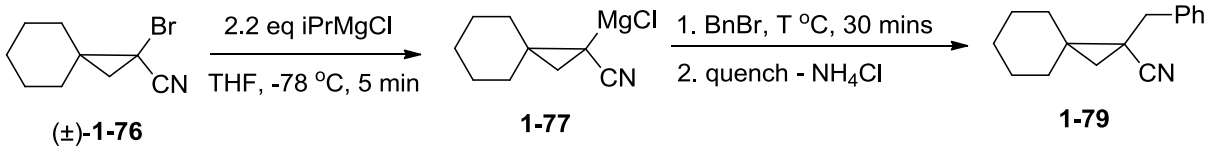

(±)-**1-76** **1-77** **1-79**

Entry	Temp *T* (^{o}C)	1-79 mol% [a]
1	-78	0
2	-61	7
3	-42	24
4	-21	94
5	0	91

[a] Isolated yield of 1-78b

The observation of successful electrophilic quench reactions at -20 ^{o}C, prompted us to attempt the synthesis of enantiopure **1-76**. Walborsky and co-workers have reported the resolution of 1-bromospiro[2.5]octane-1-carboxylic acid compound **1-74**, by the use of enantiomerically pure dehydroabeityl amine (Scheme 1-20 a). However, the reported

yield of the enantiopure **1-74** at the end of the procedure was extremely low (1.5 g (+)-**1-74** starting from 22.0 g of (±)-**1-74**). Our attempts at performing this procedure on 1 g of starting bromoacid (±)-**1-74** yielded only trace amounts of the desired salt. Due to these discouraging low yields, we decided to look for alternate procedures for the resolution of **1-74** (Scheme 1-21 b,c).

Scheme 1-21: Published (a) and attempted (b, c) resolutions of bromo acid **1-74**.

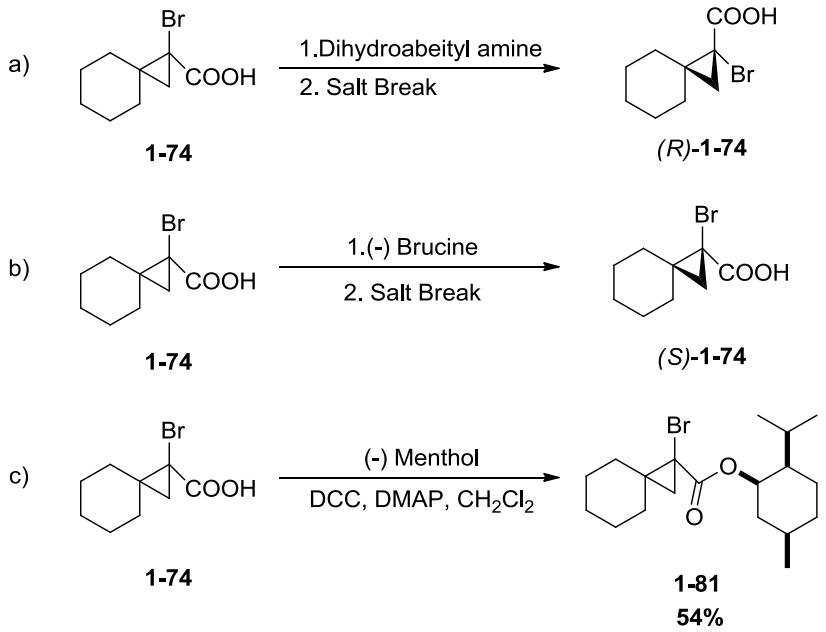

At the point of the writing of this dissertation, we have not been successful in finding a successful method for the resolution of **1-74**. Attempts to resolve **1-74** by using (-) Brucine were not successful (Scheme 1-20b). The respective diastereomeric salts were not separable by recrystallization which is the common technique for such separations. Similarly even though the synthesis of the corresponding menthyl ester **1-81** was successful in moderate yields, the separation of the two diastereomers was also not successful by crystallization or chromatography.

Our failure in determining a convenient method for synthesizing **1-76** as a single enantiomer prompted us to re-investigate the reactivity of **1-21**. The enantiopure 1-bromo-2,2-diphenyl cyclopropylnitrile (*S*)-**1-20** was synthesized using the method provided by Carlier and Zhang.[7] First, we will discuss our studies on the effect of increasing the temperature of the electrophilic quench of **1-21** similar to Table 1-7 above. The Mg/X exchange reaction to yield **1-21** was carried out in two solvents: Et_2O and THF (Table 1-9). The effect solvent on the structure and dynamics of the Grignard reagent derived from **1-20** will be discussed in Chapter 2.

Table 1-9: Effect of temperature on reactivity of **1-21**.

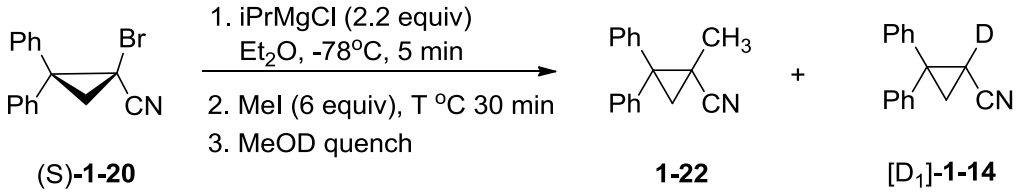

(S)-**1-20** **1-22** [D_1]-**1-14**

Entry	Solvent	T °C	1-22 mol% [a] (er (R:S)) [b]	[D_1]-1-14 mol% [a]
1	Et_2O	-78	0	>99
2		-42	0	>99
3		-20	14 (57:43)	86
4	THF	-78	15 (53:47)	85
5		-42	49 (52:48)	51
6		-20	61 (51:49)	39

[a] Calculated from ^{1}H-NMR spectroscopy of the product mixture.

[b] Calculated by CSP-HPLC analysis of **1-22**

As is seen in entries 1-3, at -78 and -42 °C, no alkylation product **1-22** is observed in Et_2O. However, at -20 °C some alkylation product **1-22** is detected. The same trend is followed in THF, but at all temperatures significantly more alkylation product is

observed in THF than in Et_2O. At any temperature T, alkylation yields are higher in THF than in Et_2O. However, alkylation products observed are substantially racemic. The reason for this was the reduced configurational stability of **1-21** at higher temperatures in Et_2O and all temperatures in THF. We will describe this subject further in Chapter 2. To overcome such a conflict it is important to devise methods to activate these Grignard reagents at colder temperatures. In the next section, we discuss our experiments towards such activations.

1.2.2 In-situ activation of 1-magnesio-2,2-diphenyl cyclopropylnitrile 1-21

Lewis base activation of Lewis acidic reagents has been discussed in a seminal review by Denmark and Buetner.[28] In situ activation of Grignard reagents by using Lewis basic donor compounds such as different ionic and non-ionic bases can be envisioned to proceed through formation of an activated complex of the type **1-82** by co-ordination of the donor base to the Lewis acidic Mg-metal center (Scheme 1-22).[28] This activated complex can possess enhanced electron density on the ligands and as a result increase their nucleophilicity towards electrophiles. Such activations of Grignard reagents with *N*-heterocyclic carbenes and other Lewis basic molecules have been studied by Hoveyda and Lee.[67] Enhanced activity of the resulting Grignard complex towards various electrophiles is demonstrated.

Scheme 1-22: Lewis base activation of Grignard reagents.[67]

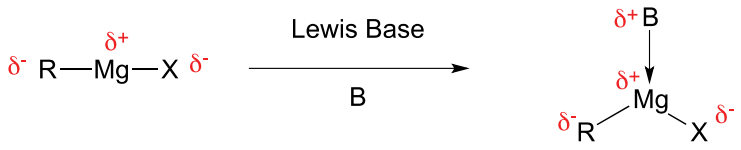

1-82

We began our study by first reinvestigating the reactions of **1-21** with various carbon electrophiles (Table 1-10), to first check if any electrophile generates appreciable amounts of product without the need of such activation. Carbon electrophiles such as methyl iodide (MeI), benzyl bromide (BnBr), and allyl bromide, carbonyl electrophile like benzoyl chloride were studied. Note that the alkylation reactions were racemizing in THF and at higher temperatures in Et_2O (Table 1-9). As we will describe in Chaper 2, the configurational stability of **1-21** is better in Et_2O/toluene mixtures, and thus we attempted these reactions with and without Lewis base in these solvent mixtures. The reaction temperature was maintained at -78 ^oC over the 30 minutes and the reaction was quenched at this temperature. The activation of **1-21** was then attempted using stoichiometric amounts of different Lewis bases such as amines (Entry 5-6), triphenylphosphine (Entry 7), and *N*-heterocyclic carbene catalysts **1-83** and **1-84** (Entry 8-9) (Table 1-10). Methyl iodide was chosen as the electrophile because of the ease of workup of since the excess electrophile is volatile. The order of addition was chosen as shown since we needed the electrophile to be present during the activation step, to avoid racemization from the activated complex before reaction.

Table 1-10: Reactions of **1-21** with different electrophiles and attempted reactions for activation of **1-21** using different Lewis bases.

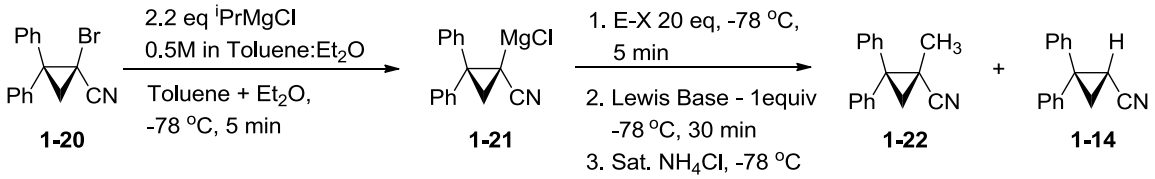

Entry	Lewis Base	Electrophile E-X	1-20 mol%[a]	1-22 mol%[a]	1-14 mol%[a],
1	None	CH_3I	<0.5	0	>99
2	None	BnBr	<0.5	0	>99
3	None	Allyl Bromide	<0.5	0	>99
4	None	Benzoyl Chloride	<0.5	0	>99
5	Pyridine	MeI	<0.5	0	>99
6	Triethylamine	MeI	<0.5	0	>99
7	Triphenyl Phosphine	MeI	<0.5	0	>99
8	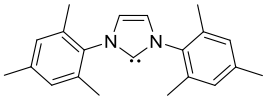 1-83	MeI	<0.5	0	>99
9	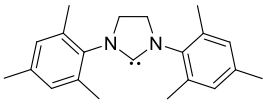 1-84	MeI	<0.5	0	>99

[a] Calculated from ^{1}H-NMR spectra of the product mixture

No appreciable amounts of products were seen with the Lewis bases attempted.. Various other Lewis bases were thought, but owing to their insolubility in these solvent mixtures at low temperatures, their use was not possible. Another form of Lewis base activation popular in the literature is the Ate complex methodology where the reactive complexes are identical to the activated complex **1-82**. The Lewis base in this case is an

anionic alkyl or halide ligand rather than a neutral nitrogen or phosphorus Lewis base. In section 1.1.2 we have discussed the reactivity of magnesate complexes as compared to traditional Grignard reagents. In the next section, we will discuss our experiments at exploiting the higher reactivity of magnesate complexes in our problem.

1.2.3 Exploration of anionic magnesates formed from bromonitrile 1-20

In section 1.1.2 we have discussed the advantages of magnesate complexes over conventional organomagnesium reagents. The exchange reactions of cyclopropyl halides with lithium trialkyl magnesate and its subsequent reactions with electrophiles were demonstrated (Scheme 1-10).[40] We next planned to synthesize the corresponding lithium magnesate reagents **1-85 - 1-88**, which would then be tested in exchange/electrophilic trapping with reactions similar to **1-21** for reactivity towards electrophiles (Scheme 1-23).

Scheme 1-23: Proposed formation of highly nucleophilic lithium magnesate reagents and their trapping reactions.

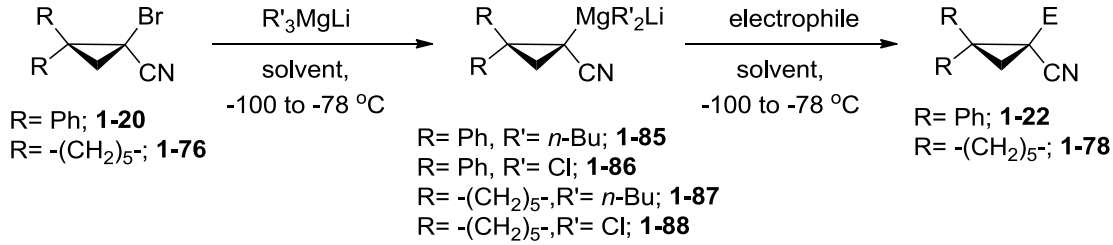

We began by first studying the Mg/Br exchange reactions of (±)-1-bromospiro[2.5]octane-1-carbonitrile (±)-**1-76** with the lithium isopropyldibutyl magnesate (*i*-PrBu$_2$MgLi) reagent **1-25** (synthesized in the same reaction flask by mixing 1 equiv i-PrMgCl and 2 equiv *n*-BuLi) and the commercial (Turbo-Grignard®, Sigma Aldrich) ate reagent complex of isopropyl magnesium chloride and lithium chloride (*i*-PrMgCl·LiCl) (Table 1-11). All reactions were attempted and quenched at -78 °C to

check if the organometallic reagent was reactive at this temperature. MeI and BnBr were chosen as the electrophiles for these studies. The organometallic species **1-77** and magnesates **1-87** and **1-88** are the putative intermediates in these reactions. As seen from Table 1-11, the higher nucleophilicity of **1-87** and **1-88** is clearly demonstrated. As seen before, the reaction of Grignard **1-77** did not proceed at these temperatures (Entry 1), but fortunately, the reactions of both **1-87** and **1-88** with both electrophiles were successful with >90% yields observed in both cases (Entry 2-5).

Table 1-11: Reactions of (±)-1-bromospiro[2.5]octane-1-carbonitrile (±)-**1-76** with magnesate reagents

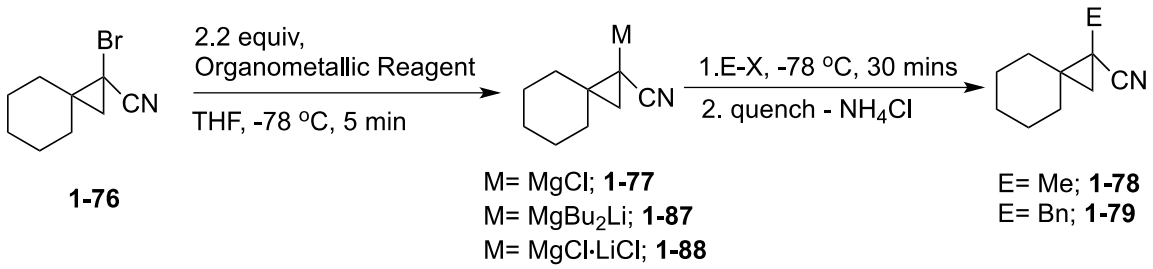

1-76

M= MgCl; **1-77**
M= $MgBu_2Li$; **1-87**
M= MgCl·LiCl; **1-88**

E= Me; **1-78**
E= Bn; **1-79**

Entry	Organometallic Reagent	Putative Intermediate	Electrophile	Product	Product mol%[a]
1	*i*-PrMgCl	**1-77**	BnBr	**1-79**	0
2	*i*-$PrBu_2MgLi$	**1-87**	MeI	**1-78**	89%
3	*i*-$PrBu_2MgLi$	**1-87**	BnBr	**1-79**	91%
4	*i*-PrMgCl·LiCl	**1-88**	MeI	**1-78**	95%
5	*i*-PrMgCl·LiCl	**1-88**	BnBr	**1-79**	94%

[a] isolated yields of

These successful results with (±)-1-bromospiro[2.5]octane-1-carbonitrile (±)-**1-76** were encouraging. However our inability to synthesize **1-76** as a single enantiomer,

prompted us to switch back to bromonitrile (*S*)-**1-20** for the study (Table 1-12). Protocols identical to those shown in Table 1-11 above were followed. Similar to the above results, the complexes **1-85** and **1-86** both provided excellent yields (>90%) of the corresponding substitution products **1-22** (Entry 2-3); however these products were completely racemic. The racemic products meant that either the organometallic reagent is configurationally unstable or that the electrophilic quenching reaction is non-retentive. To determine which scenario was true in this case, we quenched the intermediate **1-85** and **1-86**, 5 minutes after their formation at the same cold temperatures they were formed with D_2O. The resulting product [D_1]-**1-14** were again formed in high yields (>90%) but were completely racemic. This result demonstrated the relatively low configurational stability of the putative intermediates **1-85** and **1-86** as compared to **1-21** where highly enantioenriched [D_1]-**1-14** was isolated. Whether **1-85** and **1-86** are actual reactive intermediates in these reactions will be discussed below.

Table 1-12: Reactions of enantiopure 1-bromo-2,2-diphenyl cyclopropylnitrile (*S*)-**1-20** with magnesate reagents.

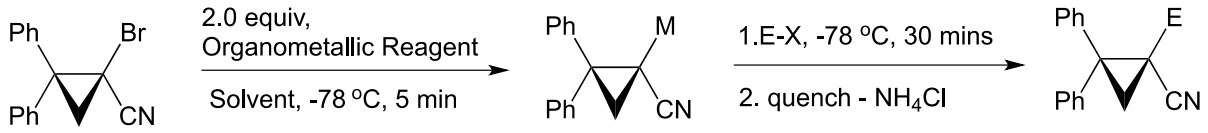

(S)-**1-20**

M= MgCl; **1-21**
M= $MgBu_2Li$; **1-85**
M= MgCl•LiCl; **1-86**

1-22

Entry	Organometallic Reagent	Putative Intermediate	Solvent	E-X	Product	Product mol% [a]	er [b] (R:S)
1	*i*-PrMgCl	**1-77**	THF	MeI	**1-22**	0	ND
2	*i*-$PrBu_2MgLi$	**1-85**		MeI	**1-22**	>90	54:46
3	*i*-PrMgCl·LiCl	**1-86**		MeI	**1-22**	>90	55:45
4	*i*-$PrBu_2MgLi$	**1-85**		D_2O	[D_1]-**1-14**	>90	52:48
5	*i*-PrMgCl·LiCl	**1-86**		D_2O	[D_1]-**1-14**	>90	55:45
6	*i*-$PrBu_2MgLi$	**1-85**	Et_2O	MeI	**1-22**	>90	53:47

[a] Calculated from ^{1}H-NMR spectroscopy of the product mixture
[b] Calculated by CSP-HPLC analysis of **1-22**

Again in this case it is important to note that an equilibrium could exist in this solution, which could generate the organolithium compound **1-18** (Scheme 1-24).

Scheme 1-24: Equilibrium thought to exist in Mg/X exchange reactions of **1-76** with magnesates.

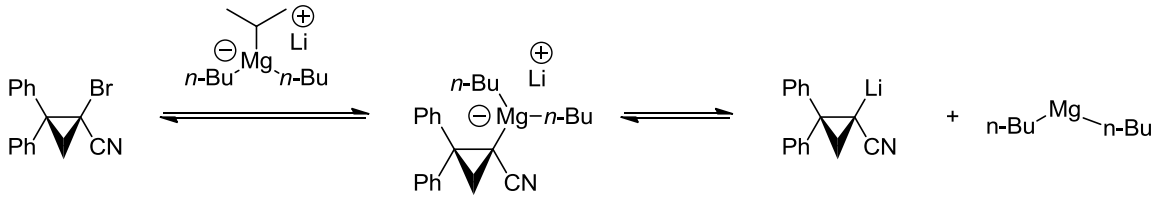

(*S*)-**1-20** **1-85** **1-18**

It is known from the work of our previous group member Dr. Yiqun Zhang, that such species is reactive towards carbon electrophiles. [68] Besides it was also shown that these

organolithium species are configurationally unstable. The observed racemic products with electrophiles shown in Table 1-12 could thus be the results of the electrophilic trapping of **1-18**. The effect of solvent on the configurational stability of **1-85** could lead to racemic products too, however as observed from the reaction in Et_2O (Entry 6), this was unlikely.

1.2.4 Conclusions for attempted Lewis base activation of cyclopropyl Grignard reagents

We began our study with the proposal that the steric hindrance provided by the 2,2 diphenyl substituents was responsible for the low reactivity of **1-21** at low temperatures. While the substrate **1-76** bearing slightly smaller substituents was successfully synthesized, we were not able to synthesize it as a single enantiomer. Nevertheless, we saw that the corresponding Grignard reagent **1-77** was not reactive at low temperatures (Table 1-9). Attempts at activation of Grignard reagent **1-21** using various neutral Lewis bases was not successful. No product was seen in any cases as seen from Table 1-10. However, since an exhaustive search of compatible Lewis bases was not performed, this study remains incomplete. Alternate magnesate reagents **1-85** and **1-88** proved to be substantially better nucleophiles than the traditional Grignard species **1-21** and **1-77** at low temperatures of -78 ^{o}C, giving excellent yields of the electrophilic quench products **1-22** and **1-78** (Tables 1-11 and 1-12). However, application of the magnesate strategy to enantiopure (*S*)-**1-20** gave completely racemic products. Further analysis of these reactions by the direct quench of intermediate **1-85** and **1-86** showed that these reagents were configurationally unstable and racemized within the 5 minutes time interval between their synthesis and quench. However the intermediacy of the

organolithium species **1-18** could also be a possible reason for the observed higher nucleophilicity and low configurational stability.

The results discussed in the three sections above demonstrate the classic conflict in the development of chiral organometallics. When we attempted to get a useful reaction with enantioenriched **1-21**, the reaction conditions (temperature) had to be modified and eventually its enantiomeric purity was compromised while under the conditions where the configurational stability of such reagents is high, no reaction was observed. To understand the enantiomerization process of such reagents was important in attempting to enhance their further utility. The task of measuring the configurational stability of **1-21** at different temperatures and in different solvents was then undertaken. Attempts were made at understanding the mechanism of enantiomerization of **1-21** in solvents for the first time, by measuring the reaction orders. All these experiments will be discussed in detail in chapter 2.

1.3 Results and Discussion: Towards γ-hydroxyl directed Mg/X exchange reactions on secondary alkyl halides – A potential method for synthesizing chiral Grignard reagents.

We discussed in section 1.2, the experiments we performed on the reactions of enantiopure Grignard reagents. However, looking at the relative paucity of chiral Grignard reagents it is clear that there are not many efficient methods of synthesis of such reagents. Traditional metal insertion methods for the synthesis of Grignard reagents are typically not useful in the synthesis of chiral Grignard reagents since they are racemizing.[3,69] As discussed in section 1.1.3, Mg/X exchange reactions on secondary alkyl halides are unknown in the literature. We also discussed the Mg/X exchange

reactions performed by Knochel and co-workers on the γ and δ–hydroxyl group containing primary sp^3 alkyl halides. The proposed mechanism for such reactions was also discussed (Figure 1-7). In this section we discuss our experiments towards extending this γ-activation methodology to secondary alkyl halides bearing γ-hydroxyl group.

1.3.1 Synthesis and Mg/X exchange reactions of certain γ-hydroxyl group containing alkyl halides.

3-Iodo-5-phenylpentan-1-ol substrate **1-93** was initially chosen as the model substrate for γ-hydroxy alkyl halides. Compound **1-93** was synthesized over 5 steps starting from ethyl acetoacetate (Scheme 1-25). Ethyl acetoacetate was selectively alkylated by synthesizing dianion intermediate to yield ethyl 3-oxo-5-phenylpentanoate **1-89** in 72% yield. **1-89** was then subject to lithium aluminum hydride (LAH) reduction to give diol 1-90 in 80% yield. Selective silyl protection was then performed on the primary hydroxyl to give compound **1-91** in 78% yield. This protected diol compound **1-91** was then halogenated using iodine with triphenylphosphine (PPh_3) and imidazole to yield the required protected iodo-alcohol **1-92** in good yields. Finally the protecting group was selectively removed using mild acidic conditions to provide the desired 3-iodo-5-phenylpentan-1-ol substrate **1-93**.

Scheme 1-25: Synthesis of 3-iodo-5-phenylpentan-1-ol substrates **1-93**.

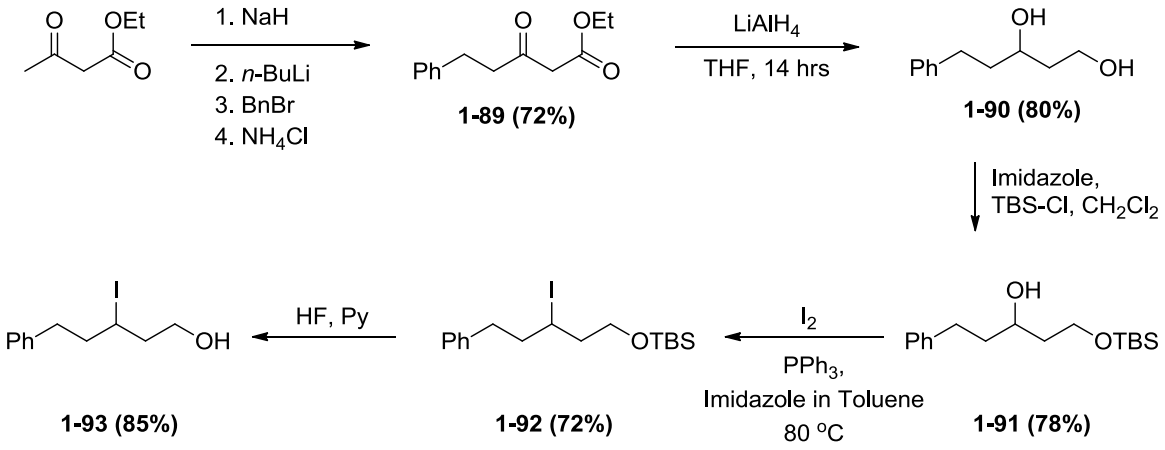

The Mg/X exchange – trapping reactions were then performed on **1-93** to test if the desired directed metalation actually works (Table 1-13). First we checked if addition of 3 equivalents of Grignard reagent *i*-PrMgCl at can carry out the desired transformation at two temperatures (-78 and 0 ^{o}C, Entry 1&2). The subsequent reactions were performed as demonstrated by Knochel and co-workers, first formation of the magnesium alkoxide followed by addition of the desired organolithium reagent. *n*-Butyllithium (*n*-BuLi), sec-butyllithium (*s*-BuLi) and tert-butyllithium (*t*-BuLi) were the organolithium reagents tested.

As can be seen from Table 1-13, the use of *i*-PrMgCl alone at -78 ^{o}C (Entry 1) gave no reaction with >99% leftover starting material isolated. On increasing the reaction temperature to 0 ^{o}C, the β-elimination product **1-96** was the major isolated product (Entry 2). On the other hand, the use of ate complexes gave a reaction even at -78 ^{o}C, but the β–elimination product **1-96** was the only product isolated in these cases (Entries 3-5).

Table 1-13: Mg/X exchange, trapping reactions of 3-iodo-5-phenylpentan-1-ol **1-93**

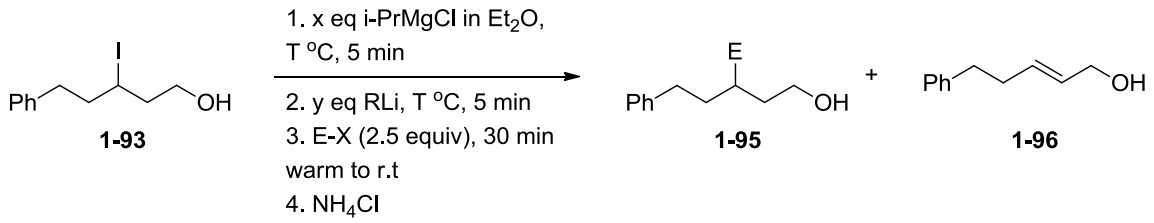

1-93 **1-95** **1-96**

Entry	T °C	x	RLi	y	E-X	1-93[a] mol%	1-95[a] mol%	1-96[a] mol%
1	-78	3	None	-	PhCHO	>99	0	0
2	0	3	None	-	PhCHO	5	0	>90
3	-78	1.1	*n*-BuLi	2.1	PhCHO	8	0	>90
4	-78	1.1	*sec*-BuLi	2.1	PhCHO	13	0	85
5	-78	1.1	*t*-BuLi	2.1	PhCHO	0	0	>95

[a] Calculated from isolated amounts of **1-94**, **1-96** and **1-97** after purification

We postulated that substituting the β–hydrogens with methyl groups was a way around this problem and decided to synthesize substrates **1-101** for this purpose. A pathway similar to Scheme 1-25 above was utilized (Scheme 1-26). The Mg/X exchange reaction on these compounds was next undertaken to check if the strategy actually works (Table 1-14).

Scheme 1-26: Synthesis of 2,2 dimethyl 3-halo-5-phenylpentan-1-ol substrates **1-101**

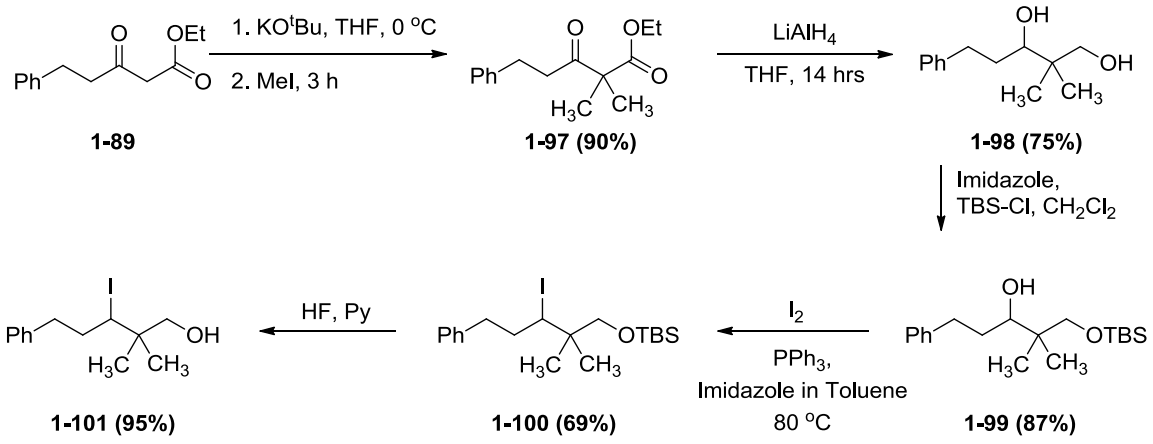

Table 1-14: Mg/X exchange, trapping reactions of 3-iodo-2,2-dimethyl-5-phenylpentan-1-ol **1-101.**

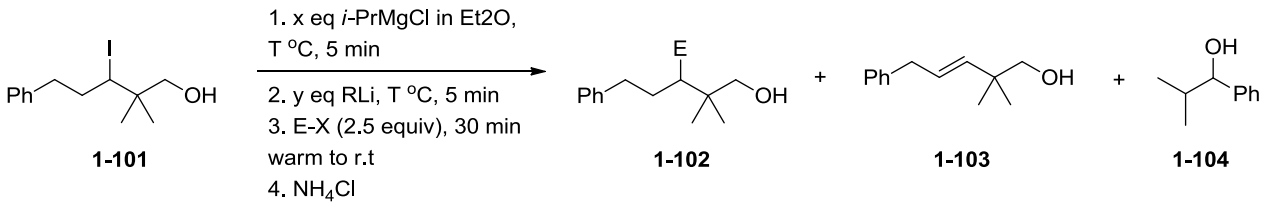

Entry	T °C	x	RLi	y	E-X	1-102 mol%[a]	1-103 mol%[a]	1-104 mol%[a]	1-101 mol%[a]
1	-78	3	None	-	PhCHO	0	0	>95	>95
2	0	3	None	-	PhCHO	0	0	>95	>95
3	-78	1.1	*t*-BuLi	2.1	D_2O	0	0	-	>95
4	0	1.1	*t*-BuLi	2.1	D_2O	0	0	-	>95
5	Rt	1.1	*t*-BuLi	2.1	D_2O	0	0	-	72
6	Reflux	1.1	t-BuLi	2.1	D_2O	0	0	-	>95

[a] Calculated from isolated amounts of **1-101- 1-104** after purification

A similar procedure to the one described in Table 1-13 above was employed. Initially benzaldehyde was used as the electrophile, however a byproduct of the reaction of the isopropyl ate reagent directly with the benzaldehyde **1-104** was found (Entry 1,2). Besides **1-104**, starting **1-101** was isolated in high weight recovery following the reaction. This puzzling result suggested that the intermediate alkoxide magnesate species similar to **1-105** below was in fact getting formed, but instead of performing the intramolecular Mg/X exchange reaction it reacted with the electrophile benzaldehyde. The low basicity difference in the isopropyl ligands on the corresponding alkoxide complex and the alkyl halide fragment could be the reason for this. To overcome this, we followed the strategy of adding 1.1 equivalent of *i*-PrMgCl followed by 2.1 equivalents of *t*-BuLi to generate the magnesium alkoxide species **1-105** (Entry 3-7). This species is expected to be better prepared for Mg/X exchange owing to higher basicity of the *t*-butyl ligands. D_2O was used to quench this reaction in order to minimize the byproducts.

No electrophilic quench product was observed in any case (Entry 1-5) with the recovered **1-101** being the major product. The possible elimination product from the other β– hydrogens is interestingly not observed. Even more frustrating for us was Entry 6, where no electrophilic quench product was obtained even after the use of the highly basic *t*-BuLi reagent at reflux temperatures of Et_2O. These results suggested that even though the initial ate species **1-105** was being formed (suggested by the color change upon addition of each organometallics, see Chapter 4 for detailed experimental description), there was not enough driving force for Mg/X exchange reaction to happen (Figure 1-9) and hence cyclic Grignard **1-106** was not being formed.

Figure 1-9: Possible reason for no-reaction observed in case of Mg/I exchange of **1-101**.

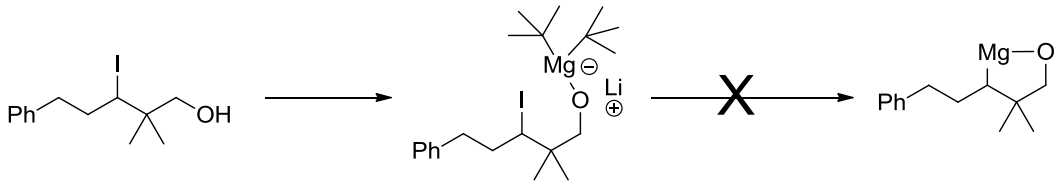

1-101 **1-105** **1-106**

The reason for this could be the lack of difference in basicity of the new organometallic **1-106** and magnesate species **1-105**, which is necessary for the Mg/X exchange reaction. To induce such a difference, we planned the synthesis of one more substrate **1-112**, which should be able to provide a less basic organometallic reagent if an Mg/X exchange reaction happens. The syntheses of **1-112** is described in Scheme 1-25. The only difference from Scheme 1-23 is the initial reaction forming dimethyl species **1-108** and the stronger acids used for deprotection of silyl ether **1-111**.

Scheme 1-27: Synthesis of substrate **1-112**

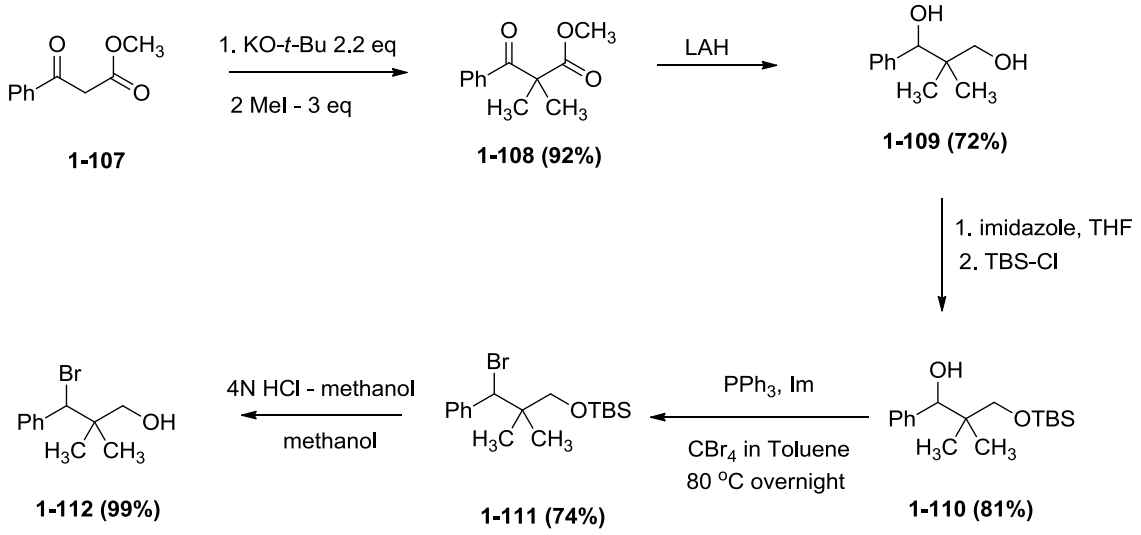

1-107 **1-108 (92%)** **1-109 (72%)** **1-110 (81%)** **1-111 (74%)** **1-112 (99%)**

The Mg/X exchange reactions of **1-112** were then studied similar to those discussed in Tables 1-13 and 1-14. Frustratingly, no substitution product **1-113** was seen

even after the use of higher temperatures and stronger bases (Entry 4-7). The reasons for the non-reactivity of these substrates in these reactions are not clear to us at this point.

Table 1-15: Mg/X exchange-trapping reactions of **1-112**

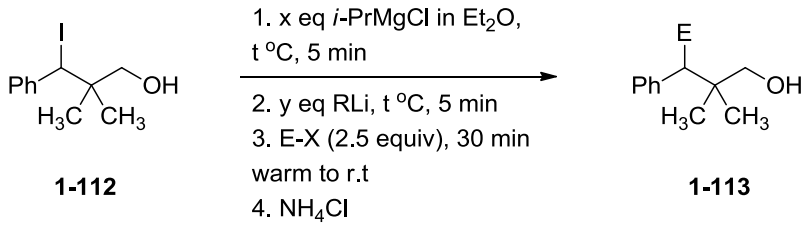

Entry	t °C	x	RLi	y	E-X	1-112 mol%	1-113mol%
1	0	3	None	-	D_2O	>99	0
2	-78	1.1	*t*-BuLi	2.1	D_2O	>99	0
3	0	1.1	*t*-BuLi	2.1	D_2O	>99	0
4	rt	1.1	*t*-BuLi	2.1	D_2O	>99	0

1.3.2 Conclusions for section 1.3

As seen from section 1.3.1 above, the directed Mg/X exchange reactions were unsuccessful, with no formation of the desired trapping products seen. Initially we found that the competing –elimination reactions were prominent in cases where they were possible. While we are sure that the initial magnesium alkoxide formation does take place, the lack of driving force prohibits the Mg/X exchange reaction from taking place. Even where substrates were modified to provide a possible driving force, no product formation was observed. Due to the unfavorable results and lack of insight on potential reasons for the difficulties encountered, we decided to not pursue these studies any further at this point.

1.4 References for Chapter 1

(1) Clayden, J. In *Organolithiums - Selectivity for Synthesis*; Jonathan, C., Ed.; Elsevier: 2002; Vol. Volume 23, p 241.

(2) Gawley, R. E. *Overview of Carbanion Dynamics and Electrophilic Substitutions in Chiral Organolithium Compounds*; Verlag Helvetica Chimica Acta, 2010.

(3) Hoffmann, R. W. *Chem. Soc. Rev.* **2003**, *32*, 225.

(4) Larouche-Gauthier, R.; Elford, T. G.; Aggarwal, V. K. *J. Am. Chem. Soc.* **2011**, *133*, 16794.

(5) Christmann, M.; Bräse, S. *Asymmetric synthesis : the essentials*; Wiley-VCH: Weinheim, 2007.

(6) Fleming, F. F.; Yao, L.; Ravikumar, P. C.; Funk, L.; Shook, B. C. *J. Med. Chem.* **2010**, *53*, 7902.

(7) Carlier, P. R.; Zhang, Y. Q. *Org. Lett.* **2007**, *9*, 1319.

(8) Fleming, F. F.; Shook, B. C. *Tetrahedron* **2002**, *58*, 1.

(9) Arseniyadis, S.; Kyler, K. S.; Watt, D. S. In *Organic Reactions*; John Wiley & Sons, Inc.: 2004.

(10) Vallino, M. *J. Organomet. Chem.* **1969**, *20*, 1.

(11) Boche, G. *Angew. Chem. Int. Ed* **1989**, *28*, 277.

(12) Boche, G.; Harms, K.; Marsch, M. *J. Am. Chem. Soc.* **1988**, *110*, 6925.

(13) Toney, J.; Stucky, G. D. *J. Organomet. Chem.* **1971**, *28*, 5.

(14) Fleming, F. F.; Liu, W. *Eur. J. Org. Chem.* **2009**, *2009*, 699.

(15) Knochel, P.; Dohle, W.; Gommermann, N.; Kneisel, F. F.; Kopp, F.; Korn, T.; Sapountzis, I.; Vu, V. A. *Angew. Chem. Int. Ed* **2003**, *42*, 4302.

(16) Fleming, F. F.; Zhang, Z. Y.; Knochel, P. *Org. Lett.* **2004**, *6*, 501.

(17) Fleming, F. F.; Zhang, Z. Y.; Liu, W.; Knochel, P. *J. Org. Chem.* **2005**, *70*, 2200.

(18) Carlier, P. R. *Chirality* **2003**, *15*, 340.

(19) Walborsky, H. M.; Young, A. E. *J. Am. Chem. Soc.* **1964**, *86*, 3288.

(20) Walborsky, H. M.; Youssef, A. A.; Motes, J. M. *J. Am. Chem. Soc.* **1962**, *84*, 2465.

(21) Padwa, A.; Wannamaker, M. W.; Dyszlewski, A. D. *J. Org. Chem.* **1987**, *52*, 4760.

(22) Masarwa, A.; Marek, I. *Chem.--Eur. J.* **2010**, *16*, 9712.

(23) Simaan, S.; Masarwa, A.; Zohar, E.; Stanger, A.; Bertus, P.; Marek, I. *Chem.--Eur. J.* **2009**, *15*, 8449.

(24) Levin, A.; Marek, I. *Chem. Commun. (Cambridge, U. K.)* **2008**, 4300.

(25) Walborsky, H. M.; Motes, J. M. *J. Am. Chem. Soc.* **1970**, *92*, 2445.

(26) Walborsky, H. M.; Hornyak, F. M. *J. Am. Chem. Soc.* **1955**, *77*, 6026.

(27) Walborsky, H. M.; Hornyak, F. M. *J. Am. Chem. Soc.* **1956**, *78*, 872.

(28) Denmark, S. E.; Beutner, G. L. *Angew. Chem. Int. Ed* **2008**, *47*, 1560.

(29) Mulvey, R. E. *Organometallics* **2006**, *25*, 1060.

(30) Mulvey, R. E.; Mongin, F.; Uchiyama, M.; Kondo, Y. *Angew. Chem. Int. Ed* **2007**, *46*, 3802.

(31) W. Tochtermann *Angew. Chem. Int. Ed* **1966**, *5*, 351.

(32) Ashby, E. C.; Chao, L.-C.; Laemmle, J. *J. Org. Chem.* **1974**, *39*, 3258.

(33) Erwin Weiss *Angew. Chem. Int. Ed* **1993**, *32*, 1501.

(34) Kamienski, C. W.; Eastham, J. F. *J. Org. Chem.* **1969**, *34*, 1116.

(35) Richey, H. G.; Farkas, J. *Tetrahedron Lett.* **1985**, *26*, 275.

(36) Hatano, M.; Matsumura, T.; Ishihara, K. *Org. Lett.* **2005**, *7*, 573.

(37) Krasovskiy, A.; Krasovskaya, V.; Knochel, P. *Angew. Chem. Int. Ed* **2006**, *45*, 2958.

(38) Krasovskiy, A.; Straub, B. F.; Knochel, P. *Angew. Chem. Int. Ed* **2006**, *45*, 159.

(39) Kitagawa, K.; Inoue, A.; Shinokubo, H.; Oshima, K. *Angew. Chem. Int. Ed* **2000**, *39*, 2481.

(40) Inoue, A.; Kitagawa, K.; Shinokubo, H.; Oshima, K. *Tetrahedron* **2000**, *56*, 9601.

(41) Inoue, A.; Kitagawa, K.; Shinokubo, H.; Oshima, K. *J. Org. Chem.* **2001**, *66*, 4333.

(42) Iida, T.; Wada, T.; Tomimoto, K.; Mase, T. *Tetrahedron Lett.* **2001**, *42*, 4841.

(43) Xu, J. Y.; Jain, N. K.; Sui, Z. H. *Tetrahedron Lett.* **2004**, *45*, 6399.

(44) Fukuhara, K.; Takayama, Y.; Sato, F. *J. Am. Chem. Soc.* **2003**, *125*, 6884.

(45) Afarinkia, K. *J. Chem. Soc., Perkin Trans. 1* **1999**, 2025.

(46) de Meijere, A. *Chem. Rev.* **2000**, *100*, 2739.

(47) Burns, T. P.; Rieke, R. D. *J. Org. Chem.* **1987**, *52*, 3674.

(48) Gomez, C.; Huerta, F. F.; Yus, M. *Tetrahedron* **1998**, *54*, 1853.

(49) Gomez, I.; Alonso, E.; Ramon, D. J.; Yus, M. *Tetrahedron* **2000**, *56*, 4043.

(50) Guijarro, A.; Yus, M. *Tetrahedron* **1995**, *51*, 231.

(51) J. Lee, R. V.-O., A. Guijarro, J. R. Wurst, R. D. Reike *J. Org. Chem.* **2000**, *65*.

(52) Ramon, D. J.; Yus, M. *Eur. J. Org. Chem.* **2000**, 225.

(53) Normant, J. F.; Alexakis, A. *Synthesis-Stuttgart* **1981**, 841.

(54) Trost, B. M. *Chem.--Eur. J.* **1998**, *4*, 2405.

(55) Boudier, A.; Bromm, L. O.; Lotz, M.; Knochel, P. *Angew. Chem. Int. Ed* **2000**, *39*, 4414.

(56) Knochel, P.; Kmsovskiy, A.; Sapountzis, L. In *Handbook of Functionalized Organometallics*; Wiley-VCH Verlag GmbH: 2008, p 109.

(57) Hoffmann, R. W.; Bronstrup, M.; Muller, M. *Org. Lett.* **2003**, *5*, 313.

(58) Müller, M.; Brönstrup, M.; Knopff, O.; Schulze, V.; Hoffmann, R. W. *Organometallics* **2003**, *22*, 2931.

(59) Negishi, E.; Swanson, D. R.; Rousset, C. J. *J. Org. Chem.* **1990**, *55*, 5406.

(60) Vu, V. A.; Marek, I.; Polborn, K.; Knochel, P. *Angew. Chem. Int. Ed* **2002**, *41*, 351.

(61) Schulze, V.; Brönstrup, M.; Böhm, V. P. W.; Schwerdtfeger, P.; Schimeczek, M.; Hoffmann, R. W. *Angew. Chem. Int. Ed* **1998**, *37*, 824.

(62) Hoffmann, R. W.; Nell, P. G. *Angew. Chem. Int. Ed* **1999**, *38*, 338.

(63) Yus, M.; Foubelo, F. In *Handbook of Functionalized Organometallics*; Wiley-VCH Verlag GmbH: 2008, p 7.

(64) Fleming, F. F.; Gudipati, S.; Vu, V. A.; Mycka, R. J.; Knochel, P. *Org. Lett.* **2007**, *9*, 4507.

(65) Rauhut, C. B.; Vu, V. A.; Fleming, F. F.; Knochel, P. *Org. Lett.* **2008**, *10*, 1187.

(66) Mycka, R. J.; Steward, O. W.; Fleming, F. F. *Org. Lett.* **2010**, *12*, 3030.

(67) Lee, Y.; Hoveyda, A. H. *J. Am. Chem. Soc.* **2006**, *128*, 15604.

(68) Zhang, Y.; University Libraries, Virginia Polytechnic Institute and State University: Blacksburg, Va., 2007.

(69) Beckmann, J.; Schutrumpf, A. *Org. Biomol. Chem.* **2009**, *7*, 41.

Chapter 2: Solvent assisted enantiomerization of C_α-chiral 1-magnesio-2,2 diphenyl cyclopropylcarbonitrile

Contributions

This chapter is a modified and expanded version of a published communication.[1] Contributions from all co-authors of the communication are described as follows in the order of the names listed. The author of this dissertation (Neeraj N. Patwardhan) synthesized all starting materials (barring the ones purchased commercially), performed all the kinetic experiments and wrote the initial drafts for the communication. Dr. Ming Gao assisted in the design of kinetic experiments, and performed the studies to determine the reaction stoichiometry. Dr. Paul R. Carlier was the principal investigator and mentor for this work and also the corresponding author for the communication.

Incremental Solvation Precedes Ion-Pair Separation in Enantiomerization of a Cyano-Stabilized Grignard Reagent: Patwardhan, N. N.; Gao, M.; Carlier, P. R., *Chemistry – A European Journal* **2011,** *17*, 12250-12253.

2.1 Introduction

In chapter 1, we discussed the importance of efficient synthetic methods in the development of C-chiral Grignard reagents. Apart from efficient retentive synthetic methods and retentive reaction pathways, configurational stability is an important factor that determines the stereochemical outcome of reactions involving chiral organometallics. Evaluating configurational stability and understanding the possible pathways of enantiomerization of chiral organometallics is important in order to increase their utility in asymmetric synthesis. Numerous studies have been performed to measure the configurational stability of chiral organolithium reagents,[2,3] which have not only helped chemists expand their use in asymmetric synthesis,[4] but also have helped in understanding of their structure and mechanism of reactions.[5] The relative scarcity of chiral Grignard reagents is again reflected here, in the fact that very little is known about their configurational stability.[6] In this chapter we will present our attempts to study the configurational stability and enantiomerization mechanism of 1-magnesio-2,2-diphenyl cyclopropylcarbonitrile **2-37** in ethereal solvents.

2.1.1: Common methods used to study configurational stability of chiral organolithium compounds

Before we begin to discuss configurational stability, it is important first to highlight the methods and techniques by which configurational stabilities are measured. We begin this chapter by introducing these techniques and providing a representative example for each technique. Three kinds of experimental strategies have been commonly employed in such studies with chiral organolithium compounds,[3] and we review each in turn.

A. Enantioselective synthesis/trapping method: As the title explains itself, this method involves the synthesis of enantioenriched organolithium reagents followed by trapping them using a suitable electrophile after a delay time *t*. The enantiomeric purity of the products is measured using a suitable analytical method. Using the measured enantio/diasteriomeric purity as a function of time, the configurational stability of the organolithium compound is then assessed. This strategy faces a flaw in the fact that enantioenriched organolithium reagents needed to be synthesized initially. Not only such synthesis is difficult as discussed in Chapter 1, but organolithiums possessing microscopic configurational stability cannot be analyzed using this method as they produce racemic products before efficient trapping experiment can produce the product. Nevertheless, this method has been successfully employed in many applicable cases.[5]

A representative example of this technique is given in Scheme 2-1.[7] Racemization of *N*-ethyl-2-lithiopyrrolidine (**2-1)** which was synthesized from the corresponding enantiopure *N*-ethyl-2-(tributylstannyl)pyrrolidine via a Sn/Li exchange reaction, was followed by trapping the chiral nucleophile with Me_3SiCl. The product mixture (*S*)-**2-2**: (*R*)-**2-2** was then analyzed by CSP-HPLC for enantiomeric excess.

Scheme 2-1: Example for measurement of configurational stability by kinetic methods.

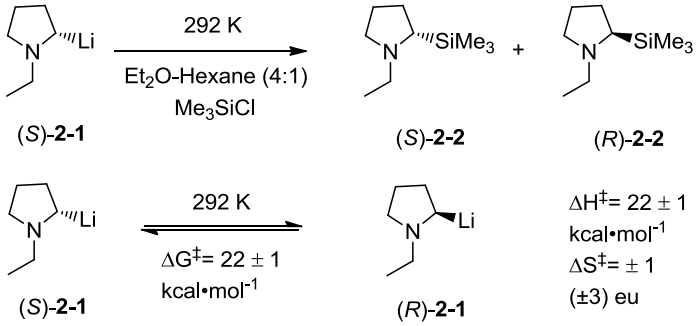

Activation parameters for the enantiomerization process were calculated by measuring the rates of enantiomerization at different temperatures.

B. Hoffmann test for configurational stability: This test involves estimation of configurational stability looking at the kinetic resolution achieved in the reaction of the configurationally stable/labile organolithium reagent with a suitable enantiomerically pure chiral electrophile (typically an amide or an aldehyde). The details of this test, including various modifications and numerous examples have been reviewed by Hoffmann.[8] However, the test only provides a qualitative estimate of the configurational stability and other methods need to be relied upon for quantitative assessment.

C. Variable temperature NMR studies: This method involves the experimental measurement of coalescence temperatures of diastereotopic signals from the organolithium species, followed by estimation of the energy barrier for the enantiomerization/epimerization using Equation (1). This method is generally useful for determining configurational stability of organolithium compounds possessing lower barriers of enantiomerization/ epimerization (half-lives of a few seconds or less).

$$\Delta G^{\ddagger} = RT_c\,(22.96 + \ln(T_c/\sqrt{(\Delta\nu^2 + 6J^2)}) \qquad (1)$$

[T_c = temperature (K), $\Delta\nu$ = peak frequency separation (Hz), J = coupling constant (Hz)].

A representative example of this technique is given in Scheme 2-2, where the enantiomerization of 1-phenylseleno-2-phenyl-ethyllithium (**2-3**) was studied using dynamic NMR. The coalescence temperature was found to be 273 K; using Equation (1) a very low barrier for enantiomerization was calculated as 12.4 kcal/mol at this temperature, which corresponded to a racemization half-life $t_{1/2}$(rac) of 11.3 h, demonstrating the macroscopic configurational stability of this compound at this temperature.

Scheme 2-2: Enantiomerization barrier for 1-phenylseleno-2-phenyl-ethyllithium **2-3**

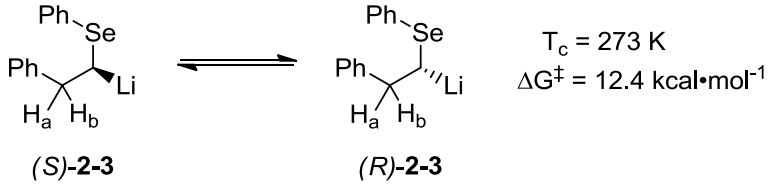

2.1.2 Configurational stability of chiral organolithium compounds

A large number of studies have been reported by various authors that highlight the configurational stability of enantioenriched organolithium compounds.[2,5] Even though the central point of study was the same, each study has to be examined individually as there is as of yet no generalized model for explaining configurational stability of organolithiums. In all cases, unique structural properties of the compound in question have been found to play a key role in determining the configurational stability – thus making any generalized explanation difficult. Three key structural features can be identified to be influential in determining their configurational stability - a) Cyclic/acyclic structure of the metal bearing C_α-carbon, b) Presence of heteroatoms on the C_α-carbon, and c) Presence of internally chelating groups. Clayden has reviewed these and other structural properties of chiral organolithiums in detail.[3] In this section we intend to focus on the effect of extrinsic factors on configurational stability.

Very often the configurational stability is found to be influenced by the conditions employed for the reactions. Amongst these, solvent effects have been suggested to significantly influence configurational stability of organolithiums.[3,4] The effects of identity of solvent;[9-13] influence of co-solvent and additives;[12,14,15] and solvent concentration have all been studied. In this section, we will provide a few representative examples of solvent effects on configurational stability of chiral organolithiums.

2.1.2.1 Solvent effects on configurational stability of chiral organolithium compounds

Although the precise nature of solvent effect varies from compound to compound, in many cases Lewis-basic solvents are known to aid or to prevent racemization of organolithiums. In this section we will discuss both scenarios with some representative examples. In cases where such reagents are known to aid racemization, enhancement of dissociation of the organolithium species is observed. Lewis-basic solvents, co-solvents and additives such as TMEDA (tetramethyl ethylene diamine),[16] DME (dimethoxyethane), THF (Tetrahydrofuran) and in some cases Et_2O (Diethyl ether) are known to act as ligands and coordinate to the Li metal. This coordination substantially weakens the C-Li bond of organolithium **2-4**, leading to its dissociation and formation of separated ion-pair species **2-5** (Scheme 2-3).[2,17] Once the bond dissociates, the carbanion species can undergo inversion leading to *ent*-**2-5**, which in most cases has a low energetic barrier, eventually leading to the racemic organolithium species.

Scheme 2-3: Enantiomerization of organolithium by a dissociative pathway.

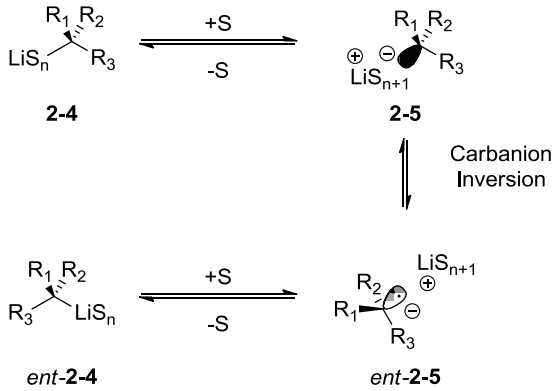

Beak *et al*. reported that the stereochemical outcome of the sparteine/*s*-BuLi deprotonation followed by cyclization reaction of the *N*-Boc protected chloroamine

compound **2-6** was susceptible to strong effects from the reaction solvent (Scheme 2-4).[13] The reaction leading to the cyclized product **2-8** was found to be more stereoselective when performed in non-polar solvents such as toluene (96% ee) and pentane (80% ee) than Lewis-basic-donor solvents such as Et_2O (64% ee) and THF (3% ee). The intermediate organolithium species **2-7** was suggested to be more configurationally stable in non-polar solvents than ethereal solvents.

Scheme 2-4: Configurationally stable organolithium species **2-5**.

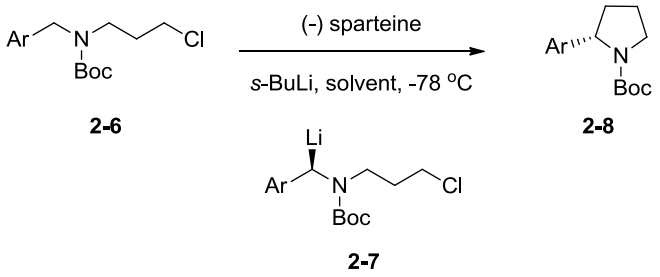

2-6 **2-8** **2-7**

Similar studies on the deprotonation/trapping by allyl chloride on the enantiopure carbamate protected benzyl alcohol **2-9** were performed by Carstens and Hoppe (Scheme 2-5). [18] The reaction was found to be more stereoselective in the nonpolar pentane and weak donor Et_2O than the strong donor THF, again suggesting that the intermediate organolithium was configurationally stable in pentane and Et_2O and unstable in THF.

Scheme 2-5: Deprotonation/alkylation by allyl chloride of **2-9**

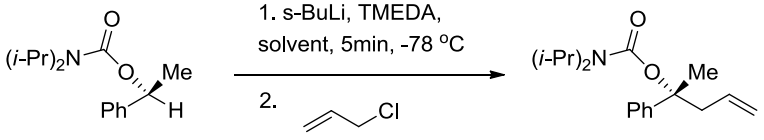

2-9 **2-10**

solvent	%ee (**2-10**)
pentane	83
Et_2O	83
THF	5

Recently, Ikemoto et al. studied the effect of solvents on the stereochemical course of [2,3]Wittig rearrangement reactions of (*S*,*E*)-[3-(Allyloxy)prop-1-ene-1,3-diyl]dibenzene *(S)*-**2-11** and its derivatives. This reaction proceeds through formation of the organolithium species **2-12**, the configurational stability of which determines the stereochemical outcome of the reaction (Scheme 2-6). [9] The product of the reaction *(R)*-**2-13** in different solvents was checked for enantiomeric purity, which showed a prominent solvent effect on this reaction. Best enantiomer ratios are obtained in non-polar solvents, hexane (91:9) and toluene (84:16). The enantiomer ratios for Lewis-basic donor solvents decreased as the donor ability of the solvent increased – 1,4-dioxane (84:16) > TBME (80:20) > Et_2O (67:33) > THP (55:45) > THF (50:50).

Scheme 2-6: Stereochemical outcome of [2, 3] Wittig rearrangement reactions of (*S*,*E*)-[3-(Allyloxy)prop-1-ene-1,3-diyl]dibenzene **2-11**.[9]

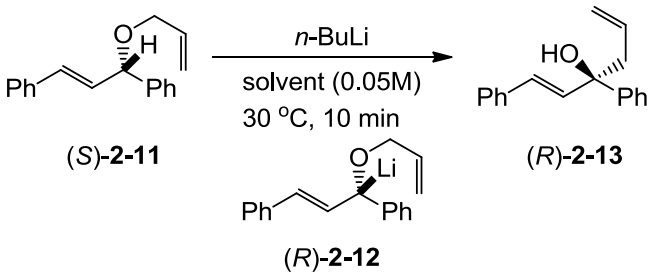

solvent	er (**2-13**)
hexane	91:9
toluene	84:16
1,4 dioxane	84:16
TBME	80:20
Et_2O	67:33
THP	55:45
THF	50:50

As stated before, just like effects of solvents, Lewis-basic additives such as TMEDA, PMDTA HMPA etc. are known to affect configurational stability by aiding the dissociative process.[14,19] Gawley studied the effect of [TMEDA] on the enantiomerization of *N*-Boc-2-lithiopiperidine (*S*)-**2-14** (Scheme 2-7). The starting organolithium **2-14** was synthesized through a Sn/Li exchange reaction in Et_2O solvent at -78 °C and quenched at an appropriate temperature using trimethylchlorosilane which was then analyzed by CSP-

HPLC to check the enantiomer ratios. A first order dependence of the observed enantiomerization rate constant (k_{obs})on [TMEDA] was observed at all temperatures.[15]

Scheme 2-7: Enantiomerization of *N*-Boc-2-lithiopiperidine (*S*)-**2-14**

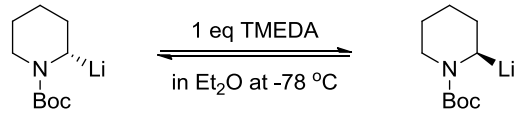

(*S*)-**2-14** (*R*)-**2-14**

Like the dissociative process described above, associative enantiomerization processes have also been shown to be subject to considerable solvent effects (Scheme 2-8). In such cases, a retardation of the enantiomerization by presence of Lewis basic solvents is observed. Here, the association of two or more organolithium molecules to generate aggregate species **2-16** is the key step towards enantiomerization. As expected, solvents that are known to enhance the formation of such aggregates tend to decrease configurational stability. On the other hand, chelating additives such as HMPA, TMEDA, and PMDTA tend to prevent the aggregation. Thus, in such cases, a reverse effect is observed compared to the examples described in Schemes 2-4 – 2-6.[20-24]

Scheme 2-8: Enantiomerization of a chiral organolithium by an associative pathway.

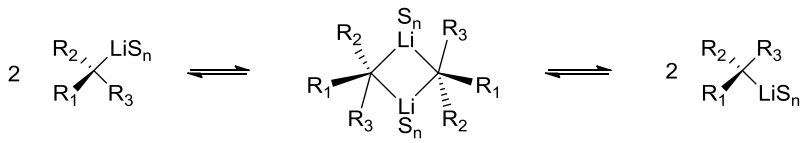

2-15 **2-16** *ent*-**2-15**

Reich et al. investigated the configurational stability of 1-lithio-3, 5-diphenylcyclohexane (axial isomer) **2-17**.[25] The rate of inversion of **2-17** to its equatorial isomer *ent*-**2-17** was found to be strongly dependent on the concentration of the reaction; the higher the concentration, the higher the rate of inversion. Reich suggested the

involvement of an associative process in the inversion. An aggregate such as **2-18**, was thought to be the species from which inversion process was facilitated (Scheme 2-8).[26] The process of inversion was also found to be influenced by the presence of the additive PMDTA (*N,N,N',N'',N''*–pentamethyldiethylenetriamine). This additive prevents the formation of aggregates, thus reducing the rate of inversion 20-fold compared to the rate of inversion in plain THF. The identity and solvating capability of the solvent was shown to have a similar influence on the racemization. Thus, racemization of **2-17** was shown to be slower in THF than in Et_2O, consistent with the better solvating power of THF.

Scheme 2-9: Enantiomerization of 1-lithio-3, 5-diphenylcyclohexane **2-17**

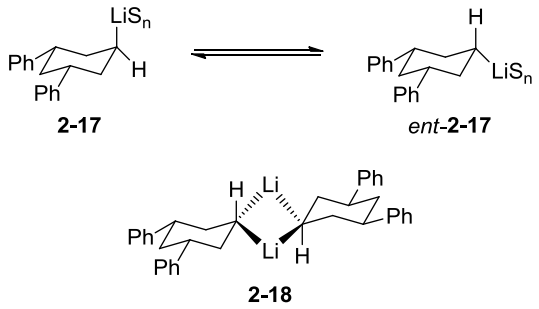

Despite the various examples reported, drawing a generalized explanative picture for the solvent effects on the configurational stability of C-chiral organolithium compounds is not possible, as the final stereochemical outcome of such reactions is always based on a combination of substrate structure and external conditions. In the next section, we will discuss the very few examples available for the studies of configurational stability of organomagnesium compounds.

2.1.3: Configurational Stability of organomagnesium compounds

We discussed in section 1.3, the synthesis of organomagnesium reagents using Mg/X exchange reactions. The utility of this reaction in the synthesis of a few

configurationally stable organometallic reagents was discussed. However, detailed studies of their configurational stability and the factors affecting configurational stability are extremely rare.

The first example of a configurationally stable Grignard reagent was introduced by Walborsky, where the Grignard **2-21** was synthesized by a transmetallation reaction of the corresponding lithio compound **2-20** (Scheme 2-10). [27] The carbonation by CO_2 yielded the corresponding carboxylic acid in 100% optical purity, which suggested that the intermediating Grignard **2-21** and the lithio compound **2-20** are configurationally stable. However, the same Grignard could not be synthesized as a single enantiomer by reaction of (S)-**2-19** with magnesium metal, suggesting the involvement of radical intermediates during the insertion of Mg into the C-Br bond.

Scheme 2-10: Examples of configurationally stable Grignards **2-17** and **2-19**.

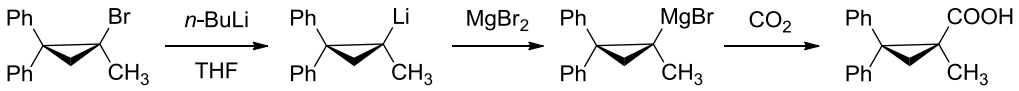

2-19 **2-20** **2-21** **2-22**

Jensen *et al*. studied the configurational stability of exo and endo norbornyl Grignard reagents **2-23** (synthesized as diastereomeric mixtures by metal insertion reaction from the corresponding bromide) using ^{1}H-NMR spectroscopy (Scheme 2-11).[28] When a 59:41 mixture of *endo*-**2-23** to *exo*-**2:23** was subject to reactions with mercuric bromide ($HgBr_2$) and CO_2, the resulting organomercury **2-24** and carboxylic acid **2-25** products were found to be enriched in the *endo*-isomer, consistent with the starting ratio (Scheme 2-11a). *Endo*-**2-23** was then carefully separated from the mixture taking advantage of a selective fast reaction of the exo component with benzophenone (reduction through β–hydride elimination) leading to a precipitate of diphenyl methanol

2-26, byproduct **2-27** and a solution enriched with *endo*-**2-23** (95-100%) (Scheme 2-11b). The subsequent reactions of this enriched solution with $HgBr_2$ and CO_2 yielded **2-24** and **2-25** which were enriched in (>94% in both cases) in the *endo*-isomer. This result indicated that the Grignard *endo*-**2-23** was configurationally stable.

Scheme 2-11: Jensen's NMR analysis of norbornyl Grignard **2-23**

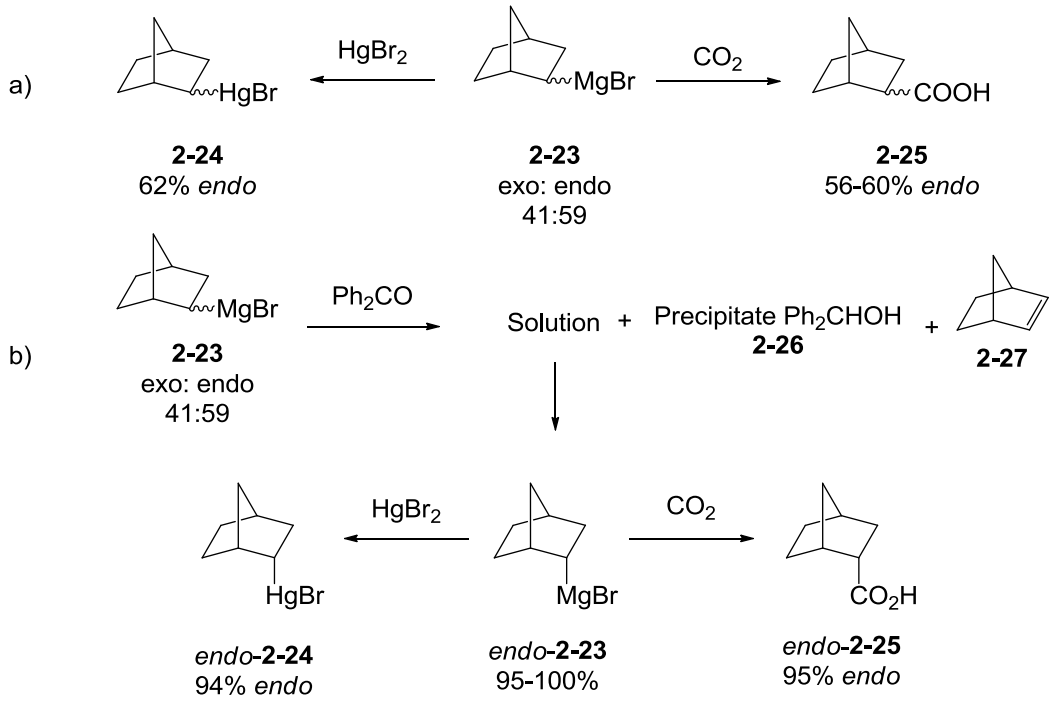

Similarly, Whitesides et al. studied the configurational stability of alkyl magnesium reagents using dynamic NMR. It was found that primary alkyl magnesium compounds underwent rapid inversion of configuration. The inversion barrier for secondary alkyl organomagnesiums on the other hand was higher than that for the primary alkyl halide compounds.[29,30]

Apart from these early examples, investigations performed by Hoffmann on the Mg/Sulfoxide exchange reactions on enantioenriched 1,1-dihaloalkanes provided valuable insights into the configurational stability of Grignard reagents (Scheme 2-12).[31-

[33] α-halo Grignard compound **2-29** was synthesized from the enantiomerically pure sulfoxide **2-28** prepared by through a sulfoxide/Mg exchange reaction.[33]

Scheme 2-12: Hoffmann's investigations into the synthesis and configurational stability of Grignard reagent **2-29**.

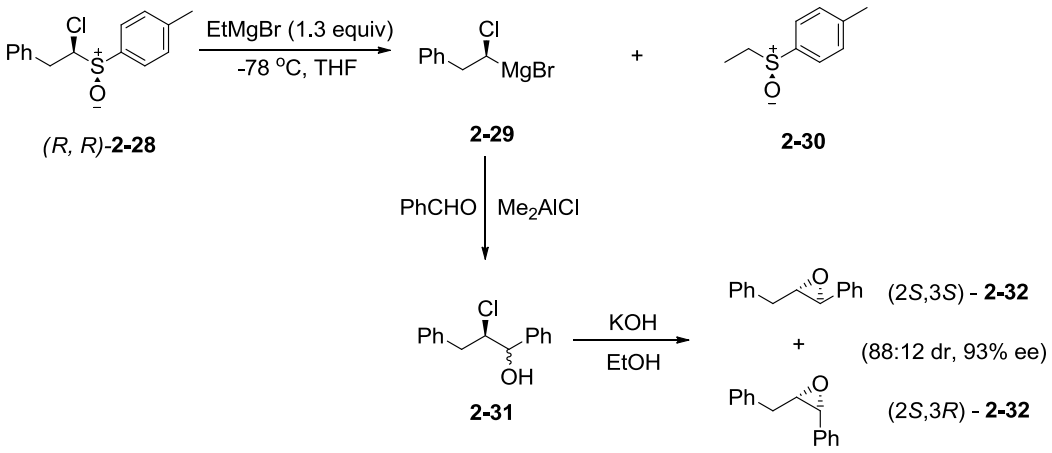

The reaction of **2-29** with PhCHO/Me_2AlCl yielded the corresponding chlorohydrin **2-31** which was then treated with a base to convert to the corresponding *cis* and *trans*-epoxide **2-32**, as a mixture of diastereomers, which were analyzed by ^{1}H-NMR analysis in presence of [Eu(hfc)$_3$] (hfc = 3-(heptafluoropropylhydroxymethylene)-d-camphorate).[33] The resulting epoxide **2-32** was formed in an 88:12 diastereomer ratio; each diastereomer was present in 93% ee, suggesting that the Grignard **2-29** was enantiomerically enriched and configurationally stable on the reaction timescale.

When a similar reaction was performed with related sulfoxide compound **2-33** and an excess of EtMgCl (5-10) equivalents, the resulting chiral Grignard reagent was **2-35** where the chloro functional group was substituted by an ethyl group (Scheme 2-13).[31] The trapping of this Grignard by a PhNCS, yielded compound **2-37**, which was found to be having a 93% *ee* – again suggesting a configurationally stable Grignard **2-35**. **2-35**

was also trapped with a number of oxidizing reagents generating the corresponding hydroxyl compound **2-35**. The hydroxyl product was analyzed by CSP-HPLC for enantiomeric excess, which showed that as long as the reaction was performed in cold temperatures (-78 to -30 ^{o}C) the product was enantiomerically enriched.

Scheme 2-13: Configurationally stable Grignard reagent **2-35**

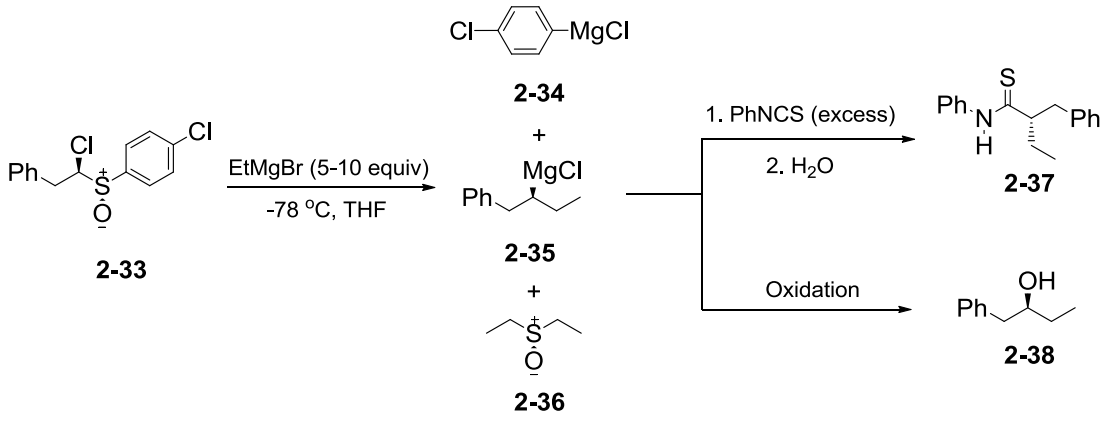

However as the temperature of its trapping reaction with oxidant was warmed to above -10 ^{o}C, racemic products were obtained. It was concluded that the racemization follows a first order process (k_{rac} = 3.46 ± 0.05 ×10^{-5} s^{-1}) with a half-life of 5 hours at -10 ^{o}C.

Although these examples illustrate that certain Grignard reagents can be configurationally stable, no general conclusions can be drawn. Also, providing a conclusive mechanistic picture towards their enantiomerization process is difficult, owing to the complex solution structure of these reagents. As will be discussed in chapter 3, aggregation, solvation, and disproportionation (scrambling) by competitive equilibration processes all contribute to this complexity. We believe it would be valuable to develop an understanding of these processes, in order to expand their use in asymmetric synthesis. As explained in section 1.1.1, metalated nitriles are valuable reagents in the synthesis of a

variety of compounds. In the next several sections, we will describe our efforts towards measuring the configurational stability of an enantioenriched metalated nitrile **2-40**.

2.2 Investigation of configurational stability of 1-magnesio-2,2-diphenyl-cyclopropylcarbonitrile 2-40.

As explained in section 1.1.1, the first example of an enantioenriched metalated nitrile was reported by Carlier et al,[34] where **2-40** was synthesized using a Mg/Br exchange reaction from the corresponding enantiopure bromonitrile **2-39**. It was demonstrated that 2.2 equivalents of the reactant isopropyl magnesium chloride (*i*-PrMgCl) was needed for an efficient exchange reaction at the very low reaction temperature of 173 K. The Grignard was subsequently quenched using D_2O giving very high yields of the deuteriated nitrile [D_1]-**2-41** (Scheme 2-14) which was found to be highly enantioenriched using CSP-HPLC analysis.

Scheme 2-14: Mg/Br exchange/D_2O trapping reactions reported by Carlier *et al*.

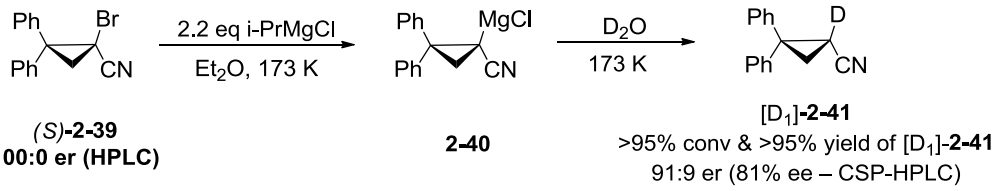

This study demonstrated the utility of Mg/X exchange reaction as a useful method to synthesize the chiral Grignard reagent. A kinetic protocol was then employed to investigate the configurational stability of **2-40**. The depletion of % *ee* of [D_1]-**2-41** was measured after quenching **2-40** at different time intervals. Since the D_2O quench can be considered to be a very fast reaction, it was assumed that the enantiomeric excess (*ee*) of [D_1]-**2-41** is equal to the *ee* of **2-40** before quench. The rate constant k_{rac} for racemization was then calculated from the slope of the plot of ln (%*ee*/100) vs time (Figure 2-1),

treating the racemization process as a first order reaction. Using k_{rac}, the half-life of racemization was calculated, which was found to be 11.4 h, implying that **2-40** was configurationally stable on a macroscopic timescale at this temperature.

Figure 2-1: Plot of ln ((%*ee*([D_1]-**2-41**))/100) vs delay time *t* (s) in Et_2O at 173 K. Data replicated from the published article by Carlier et al.[34]

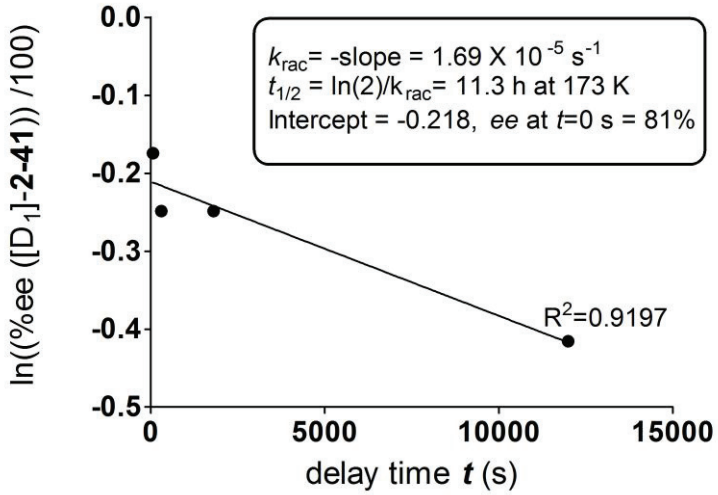

The intercept of the line on the y-axis was used to calculate the extrapolated % *ee* (81%) at t = 0 s. This result showed that at t = 0 s or at the moment it is formed, the Grignard **2-40** has 81% *ee*, suggesting that the Mg/Br exchange reaction is not completely retentive. The complete stereochemical course of this reaction can be summarized by Figure 2-2. The Grignard **2-40** is formed by an Mg/Br exchange from enantiopure bromonitrile **2-39**. [2] Resulting Grignard reagent **2-40** is enantioenriched (but not enantiopure), suggesting a competing invertive component to the Mg/Br exchange process. Once formed, the enantioenriched **2-40** undergoes enantiomerization to *ent*-**2-40** by some pathway, ultimately leading to diminished *ee* of [D_1]-**2-41** over time. Looking at Figure 2-2, two questions arise. Firstly, is Mg/Br exchange reaction not perfectly

retentive as opposed to the observed retentive course of Li/X exchange? [3] Secondly what is the mechanism of enantiomerization of **2-40**?

Figure 2-2: Plausible stereochemical pathway involved in synthesis and quench of **2-40** (Structure **2-40** does not imply any particular solvation or aggregation state)

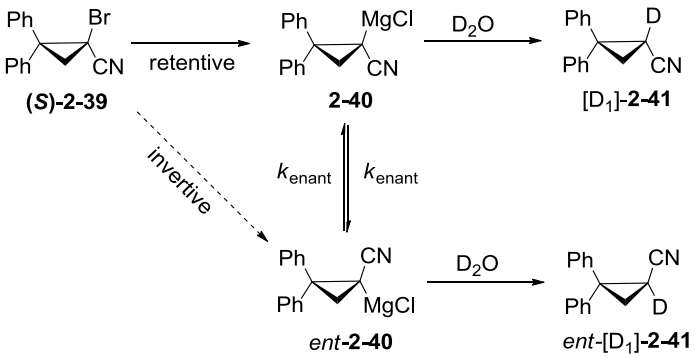

Various different mechanisms of enantiomerization have been proposed to be involved in cases of enantiopure organolithium compounds as discussed in section 2.1. In addition, involvement of a conducted tour pathway has been computationally studied by Carlier on the identical lithio-2,2-diphenyl cyclopropylnitrile **2-42** (Scheme 2-15).[35]

Scheme 2-15: Conducted tour pathway for enantiomerization of lithio-2,2-diphenyl cyclopropylnitrile **2-42**

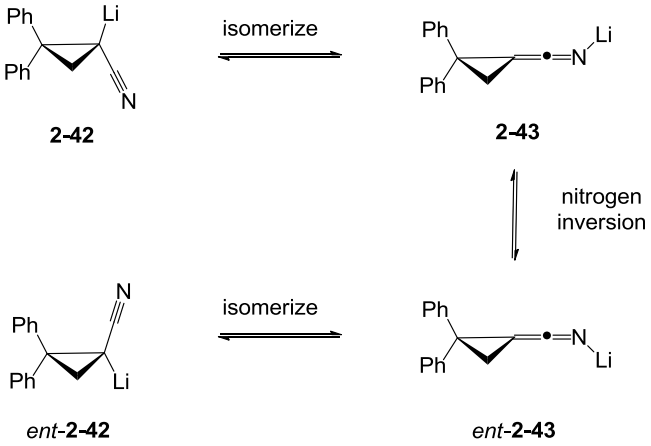

The *C*-lithio nitrile **2-42** undergoes isomerization to an *N*-lithio species **2-43**, which was thought to undergo enantiomerization through nitrogen inversion. A low enthalpic barrier $\Delta H^{\ddagger}$ = 6.7 kcal/mol was found at B3LYP/6-31+G*. [35] Another plausible enantiomerization mechanism is the solvent assisted ion-pair separation mechanism (Scheme 2-16).[36] The capture of one or more molecules of solvent by a contact ion-pair species **2-44** (CIP) leads to formation of solvent separated ion-pair species **2-45** (SIP), which can then enantiomerize through a carbanion inversion leading to the enantiomeric species ent-**2-45** (SIP).

Scheme 2-16: Solvent assisted ion pair separation mechanism for enantiomerization

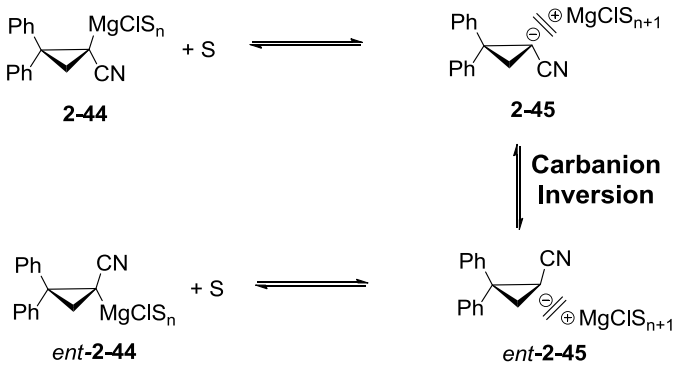

The barrier for inversion of the analogous unsubstituted cyclopropylnitrile carbanion has been shown to be low.[35] If such a mechanism is operative, it can be envisioned that the identity of the solvent should have some influence on the process.

2.3 Reinvestigation of the configurational stability of 2-40 – new improved protocol

We started this study with a goal to find answers to the questions raised by the earlier communication of Carlier *et al.*[35] The primary objective of this study was to identify which of the above-mentioned pathways was operational in the enantiomerization. Also, since Mg/Br exchange reaction method was shown to generate a

highly enantioenriched Grignard reagent for the first time, we studied this process for possible expansion toward synthesis of newer enantioenriched Grignard reagents. Our initial approach was directed towards probing the involvement of solvent in the enantiomerization process, which was prompted by a curious observation showing significantly depleted er values when the same reaction as in Scheme 2-14 was repeated using tetrahydrofuran (THF) as a solvent. To carry out these studies, we developed a new kinetic protocol, improved from the earlier studies. But before we get into the experimental details, the kinetic expressions we used to analyze our experimental data need to be discussed first.

2.3.1 Derivation of expression used to calculate enantiomerization rate constant k_{enant}

As can be seen in various different examples of kinetic studies towards configurational stability, the process of racemization is considered a first-order reversible reaction, the integrated rate law for which is given by equation 7 below or by some of its variant defined by the respective authors of the study. However it is important to demonstrate how this expression is derived.

Consider the inter-conversion of two enantiomers, (*R*)- and (*S*)-**1** (equation 2). We define the first order rate constant for conversion of one enantiomer to the other (enantiomerization) as k_{enant}.

$$(R)\text{-}\mathbf{1} \underset{k_{enant}}{\overset{k_{enant}}{\rightleftharpoons}} (S)\text{-}\mathbf{1} \qquad (2)$$

Following Conners,[37] we apply the integrated rate law in equation 3, where c_R is the concentration of the (*R*)-enantiomer at any time *t*, c^e_R is the concentration of the (*R*)-enantiomer at equilibrium, and c^0_R is the concentration at time 0.

$$\ln \left[\frac{c_{\mathbf{R}} - c^{\mathrm{e}}_{\mathbf{R}}}{c^{0}_{\mathbf{R}} - c^{\mathrm{e}}_{\mathbf{R}}} \right] = -(k_{\mathrm{enant}} + k_{\mathrm{enant}})t = -2k_{\mathrm{enant}}t \qquad (3)$$

Since the term in brackets is dimensionless, we can replace concentration *c* with mole fraction *X*

$$\ln \left[\frac{X_{\mathbf{R}} - X^{\mathrm{e}}_{\mathbf{R}}}{X^{0}_{\mathbf{R}} - X^{\mathrm{e}}_{\mathbf{R}}} \right] = -2k_{\mathrm{enant}}t \qquad (4)$$

By definition, $X^e_R = 0.5$, and since we assume pure (*R*)-enantiomer at $t = 0$, $X^0_R = 1.0$. Thus equation 3 simplifies as follows.

$$\ln \left[\frac{X_{\mathbf{R}} - 0.5}{0.5} \right] = \ln(2X_{\mathbf{R}} - 1) = -2k_{\mathrm{enant}}t \qquad (5)$$

To allow for the more general case where one starts with pure (*S*)-enantiomer, we note that $X_R = 1 - X_S$ and show that $(2X_R - 1)$ and $(2X_S - 1)$ are equal and opposite.

$$2X_R - 1 = 2(1 - X_S) - 1 = 1 - 2X_s = -(2X_s - 1) \qquad (6)$$

A general equation can be obtained from equation 4 by placing an absolute value on the term in parentheses, giving equation 6.

$$\ln(|2X_{\mathbf{R}} - 1|) = -2k_{\mathrm{enant}}t \qquad (7)$$

Note that equation 6 describes the kinetics of racemization: conversion of a collection of single enantiomers to an equilibrium mixture of (*R*)- and (*S*)-enantiomers. This first-order approach to equilibrium occurs with a rate constant $k_{rac} = 2k_{enant}$, and corresponding half-life $t_{1/2}$(rac).[38]

$$k_{rac} = 2k_{enant} \qquad t_{1/2}(\text{rac}) = (\ln 2)/k_{rac} \tag{8}$$

Finally we note the following relationships between X_R, er, and %*ee*:

$$\text{er} = 100*X_R : 100*(1 - X_R) \tag{9}$$

$$\%\text{ee} = 100 *|X_{\mathbf{R}} - X_S| = 100 *|2X_{\mathbf{R}} - 1| \tag{10}$$

2.3.2 Experimental details of the new protocol to study enantiomerization

At the beginning of our study, we followed the standard strategy of synthesizing the enantioenriched Grignard **2-40** by an Mg/Br exchange reaction from the bromonitrile **2-40**, allowing the Grignard to enantiomerize for specific delay times between 60 to 3600 s and then trapping the Grignard using a deuterium quench (Scheme 2-14) The deuterio product [D_1]-**2-41** is then analyzed for conversion, yield and %deuterium incorporation using ^{1}H-NMR spectroscopy and, for enantiomer ratio (er) by CSP-HPLC. As mentioned earlier, we observed that the enantiomer ratios were significantly depleted when the same Mg/Br exchange/ trapping with D_2O reaction was performed in tetrahydrofuran (THF) as the solvent. This prompted us to study the enantiomerization of **2-40** in three different solvents, Diethyl Ether (Et_2O), 2-methyltetrahydrofuran (2-MeTHF) and, tetrahydrofuran (THF). However, our initial experiments were marred with error in the observed values of *er* and consequently the k_{enant}. The error was quite large at the temperature of 173 K,

which had the lowest value for k_{enant}. This inconsistency in our results prompted us to modify our experimental protocol for this study.

The first improvement we made to the reported protocol was the introduction of new method for temperature control. A cooling bath made of diethyl ether and dry ice has been traditionally used to attain the low reaction temperature of 173 K (-100 ^{o}C). However, we were never able to attain this temperature in our laboratories using this mixture in our cooling bath. The temperature was found to be significantly warmer (189 K) and fluctuating unreliably, using all different thermometers available (alcohol thermometers, digital thermometers). To solve this problem we switched to a slush bath made of a mixture of liquid N_2 and methanol. This mixture when formed in the required slush form, stays consistently around 175 ± 2 K over the duration of the experiment, thus minimizing the error in measurement of the *er* introduced by poor temperature control.

The second major improvement was the use of a different quench in place of D_2O. The room temperature D_2O used as a quench can warm the reaction mixture before complete quench, leading to increased racemization. Also since D_2O forms a clump of ice as soon as it is added to the cold reaction mixture, the mixing of the reaction solution is stopped, thus leading to a partial quench of the Grignard, which is quenched as the ice melts. Both these phenomena may explain the low values for extrapolated er at t = 0 s and other short reaction time at t = 1 min. The use of monodeuteriated methanol (CH_3OD) that has been precooled to the respective reaction temperature (liquid) as a quench works better than D_2O, as demonstrated in the next section.

2.4 Measurement of enantiomerization rates and corresponding activation parameters

The first aim of our study was towards measurement of activation parameters pertaining to the enantiomerization process. The improvements in our experimental protocol allowed us to measure the k_{enant} at 4 different temperatures in Et_2O: 175 K, 195 K, 212 K and 231 K. In THF and 2-MeTHF, 3 different temperatures were employed: 175 K, 195 K, and 212 K. The study at temperature of 231 K was not attempted in 2-MeTHF and THF, due to the near racemic products obtained in these conditions. These rate constants were then analyzed using the Eyring equation (Equation 11), to determine activation free energy $\Delta G^{\ddagger}$ at these temperatures.

$$\Delta G^{\ddagger} = -RT*\ln[(k_{enant}*h)/(k_B*T)] \text{ (kcal/mol)} \quad (11)$$

2.4.1 Studies in diethyl ether (Et_2O)

Figure 2-3 shows the linear plot of Equation 7, at four temperatures in diethyl ether (Et_2O) solvent. Table 2.1 shows the calculated values of k_{enant}, $\Delta G^{\ddagger}$ at the respective temperature and the extrapolated er at t = 0 at that temperature. As expected, the values of k_{enant} are small at lower temperatures. Also, the extrapolated values of er at t = 0 are larger at lower temperatures, suggesting higher retentive behavior of the Mg/Br exchange reaction at these temperatures. It is important to note that the values of k_{enant} at 175 K and extrapolated er at t = 0 are significantly better than the previously reported ones at 173 K. The superiority of the use of our new protocol is demonstrated by this result.

Figure 2-3: Plot of ln (|2X_R([D_1]-**2-41**)-1|) vs delay time *t* for reactions in Et_2O

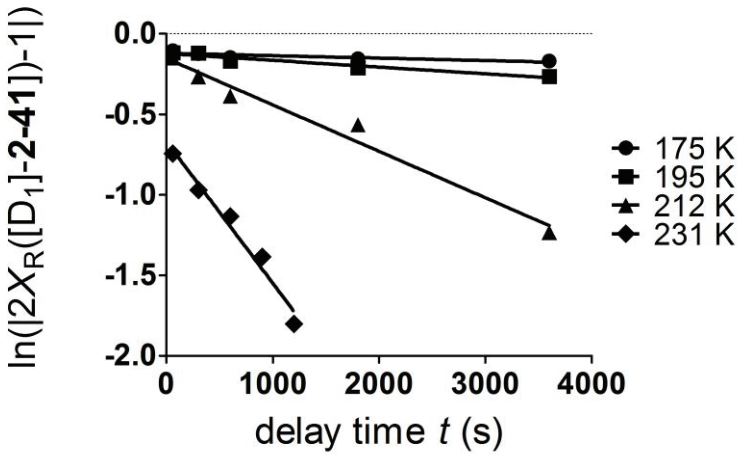

Table 2-1: Enantiomerization rate constants and activation free energies at four temperatures in Et_2O

T **(K)**	k_{enant} **X** (10^6) (s^{-1})[a]	$\Delta G^{\ddagger} = -RT*\ln((h/k_B T)*k_{enant})$ **(kcal/mol)**[b]	**Extrapolated er at** ***t*** **=0** [c]
175	7.6 ± 2.6	14.2 ± 0.1	95 : 5
195	20.8 ± 3.3	15.5 ± 0.05	94 : 6
212	144.2 ± 13.3	16.0 ± 0.04	91 : 9
231	440.1 ± 41.6	16.9 ± 0.04	74 : 26

[a] Calculated from the error in slope of the line using error analysis package in Microsoft-Excel 2007
[b] Calculated from the Eyring equation $\Delta G^{\ddagger} = -RT*\ln[(k_{enant}*h)/(k_B*T)]$. Error in $\Delta G^{\ddagger}$ was calculated as $RT*(\text{error } k_{enant})/k_{enant}$.
[c] Calculated from the intercept of the line on y-axis.

2.4.2 Studies in 2-methyl tetrahydrofuran (2-MeTHF) and tetrahydrofuran (THF)

Like Et_2O, 2-MeTHF and THF are commonly used donor solvents in Grignard reactions. Both 2-MeTHF and THF have the advantage of higher boiling points compared to Et_2O. These advantages are, less evaporation, greater safety, and the possibility to use higher reaction temperatures. However, THF is known to be a better ligand than Et_2O, which means that it possesses better ability to solvate the magnesium metal. As a consequence, we can expect our reaction to perform differently in THF as compared to

Et_2O. The results for similar studies in 2-MeTHF are shown in Figure 2-4 and Table 2-2, and the results in THF are shown in Figure 2-5 and Table 2-3. As explained above, reactions at 231K were not attempted in these two solvents, due to the near racemic products obtained at these temperatures.

Figure 2-4: Plot of ln ($|2X_R([D_1]$-**2-41**$)-1|$) vs delay time *t* for reactions in 2-MeTHF

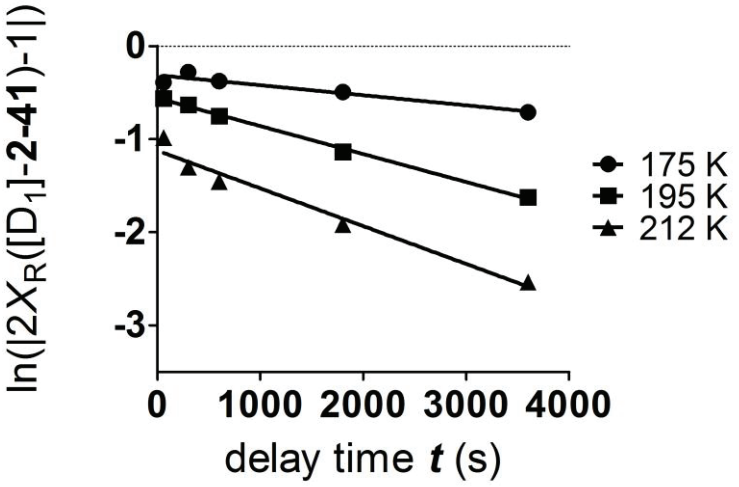

Table 2-2: Enantiomerization rate constants and activation free energies at three temperatures in 2-MeTHF

Temp (^{o} K)	**k_{enant} X (10^6) (s^{-1})[a]**	**$\Delta G^{\ddagger}$=-RT*ln((h/k_BT)*k_{enant}) (kcal/mol)[b]**	**Extrapolated er at t=0 [c]**
175	54.0 ± 9.6	13.5 ± 0.06	87 : 13
195	150.1 ± 4.2	14.7 ± 0.01	79 : 21
212	202.9 ± 20.3	15.9 ± 0.04	66 : 34

[a] Calculated from the error in slope of the line using error analysis package in Microsoft-Excel 2007
[b] Calculated from the Eyring equation $\Delta G^{\ddagger} = -RT*\ln[(k_{enant}*h)/(k_B*T)]$. Error in $\Delta G^{\ddagger}$ was calculated as RT*(error k_{enant})/k_{enant}.
[c] Calculated from the intercept of the line on y-axis.

Figure 2-5: Plot of ln (|2X_R([D_1]-**2-41**)-1|) vs delay time *t* for reactions in THF

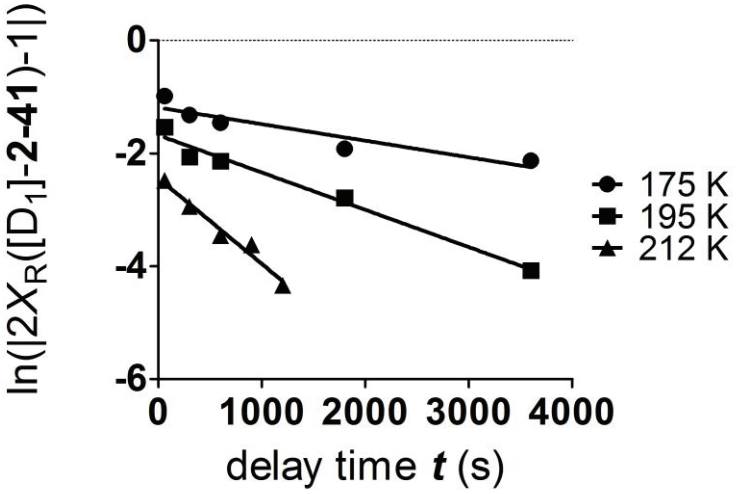

Table 2-3: Enantiomerization rate constants and activation free energies at three temperatures in THF

Temp (^{o} K)	**k_{enant} X (10^6) (s^{-1})[a]**	**$\Delta G^{\ddagger}$=-RT*ln((h/k_BT)*k_{enant}) (kcal/mol)[b]**	**Extrapolated er at t=0 [c]**
175	146.5 ± 32.9	13.3 ± 0.1	67 : 33
195	175.3 ± 32.5	146 ± 0.1	59 : 41
212	760.5 ± 75.1	15.3 ± 0.04	54 : 46

[a] Calculated from the error in slope of the line using error analysis package in Microsoft-Excel 2007
[b] Calculated from the Eyring equation $\Delta G^{\ddagger} = -RT*\ln[(k_{enant}*h)/(k_B*T)]$. Error in $\Delta G^{\ddagger}$ was calculated as RT*(error k_{enant})/k_{enant}.
[c] Calculated from the intercept of the line on y-axis.

As seen from Table 2-2 and Figure 2-3, the enantiomerization rate constant k_{enant} at 175 K was sevenfold faster in 2-MeTHF as compared to Et_2O. On the other hand, from Table 2-3 and Figure 2-4 we can see that k_{enant} at 175 K was nineteen fold faster in THF than that in Et_2O. Also, the extrapolated er at t = 0 in 2-MeTHF were lower at all studied temperatures as compared to Et_2O and following a similar trend, the extrapolated er values at t = 0 in THF were significantly worse than in Et_2O. A less retentive Mg/Br exchange in 2-MeTHF as compared to Et_2O and even less retentive Mg/Br exchange in

THF were possibly the reason behind these observed small extrapolated er values.

2.4.3 Calculation of Activation parameters in three solvents

These divergent results in three of the most commonly used solvents for Grignard reaction are consistent with our suspicion of significant involvement of the solvent in the both the Mg/Br exchange and enantiomerization processes. The plot of $\Delta G^{\ddagger}$ vs T, which is justified by the Equation 12 below, was then used to determine enthalpy of activation $\Delta H^{\ddagger}$ and entropy of activation $\Delta S^{\ddagger}$ (Equation 13 & 14) (Figure 2-6)

$$\Delta G^{\ddagger} = \Delta H^{\ddagger} - T\Delta S^{\ddagger} \quad (12)$$

From plot of $\Delta G^{\ddagger}$ vs T

$$\Delta H^{\ddagger} = \text{Intercept on Y axis (At T = 0, kcal/mol)} \quad (13)$$

$$\Delta S^{\ddagger} = \text{slope}*-1000\ (\text{cal}\cdot\text{mol}^{-1}\cdot\text{K}^{-1})\ (\text{eu}) \quad (14)$$

Figure 2-6: Plot of calculated $\Delta G^{\ddagger}$ values versus temperature T and activation parameters for the enantiomerization of **2-40** calculated using the Eyring equation. Where error bars are not seen, they are smaller than the symbol employed.

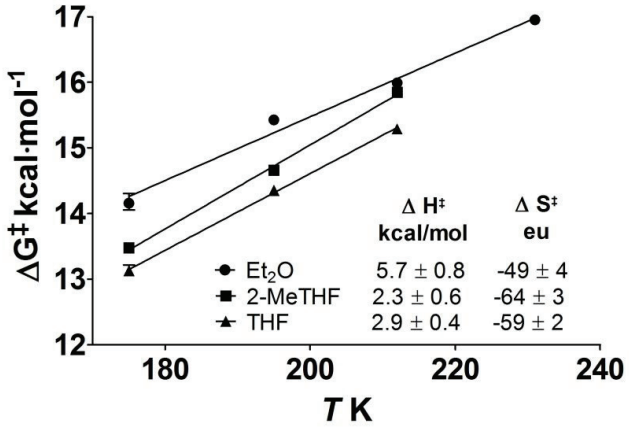

In all three solvents, large negative entropies of activation $\Delta S^{\ddagger}$ were calculated (Et_2O: -49 ± 4 eu; 2-MeTHF: -64 ± 3 eu; THF: -59 ± 2 eu), accompanied by relatively

small enthalpies of activation $\Delta H^{\ddagger}$ (Et_2O: 5.7 ± 0.8 kcalmol^{-1}; 2-MeTHF: 2.3 ± 0.6 kcalmol^{-1}; THF: 2.9 ± 0.4 kcalmol^{-1}). Such large negative numbers for activation entropy have been previously observed by various authors for enantiomerization processes of organolithium reagents **2-46** – **2-49** (Figure 2-7). [5,20,39,40]

In all the cases, the involvement of the solvent-assisted ion-pair separation mechanism has been proposed (Scheme 2-15). Two distinct phenomenon have been proposed as the origin of the negative entropy of activation: either an increase in solvation number concerted with ion pair separation (solvent capture), or rearrangement of the secondary solvent shell during Li-C cleavage of a fully-solvated contact ion-pair, to stabilize developing charge separation (solvent electrostriction) These two concepts are discussed further in section 2.8.

Figure 2-7: Negative activation entropies reported for racemization of chiral organolithiums **2-46** – **2-49**. [5,20,39,40]

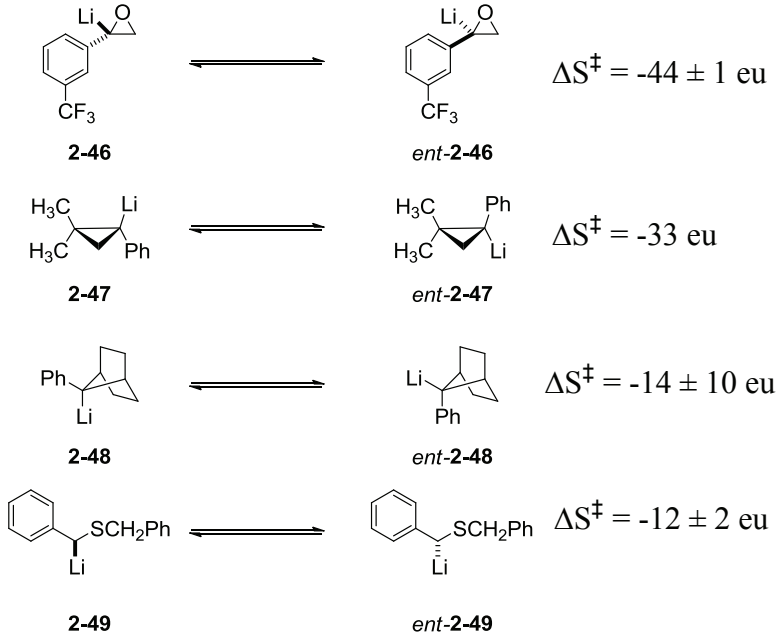

Another possible source of negative entropy of activation is the involvement of aggregation of Grignard **2-40** on the reaction pathway. The suggestion that aggregation is source of enantiomerization has been proposed in case of enantiomerization of organolithium reagents (see schemes 2-8 and 2-9).[25] Scheme 2-17 describes aggregation by the example of dimerization of **2-40**. Two particles combining to give a single particle could be the source of the observed large negative $\Delta S^{\ddagger}$.

Scheme 2-17: Dimerization of Grignard **2-40**.

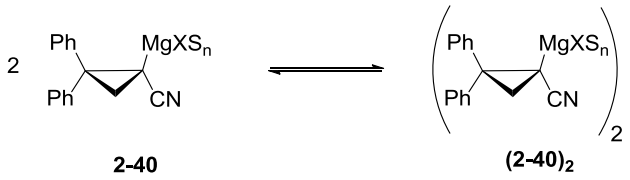

Although the two pathways discussed above have been proposed by various authors to be involved in enantiomerization processes, there is a need to definitively identify which pathway is involved and distinguish them from each other. Additionally, the role of solvent in the ion-pair separation process needs to be precisely identified. Is rate-determining solvent capture the origin of the negative entropy of activation? Is solvent capture followed by ion-pair separation a concerted process? Or is it a stepwise process where solvation precedes ion pair separation similar to an addition- elimination process. These possibilities can be distinguished by the measurement of reaction orders with respect to all components involved.

2.5 Measurement of reaction orders to determine enantiomerization pathway involved.

The strategy of measurement of reaction orders with respect to the components of a reaction is a standard technique to probe the role of individual components in a reaction.[38,41] The kinetic method of "flooding",[38] is used in these cases where the influence of variation of the concentration of the respective component on the observed rate constant is measured. In this case, we decided to measure the reaction orders with respect to:

a) The Grignard reagent **2-40**, to test the hypothesis that aggregation of **2-40** is on the reaction pathway.
b) The donor solvent – to test the hypothesis that the solvation-number of **2-40** increases in the rate-determining transition structure.

2.5.1 Measurement of reaction order with respect to Grignard reagent 2-40

To address the possibility that the large negative $\Delta S^{\ddagger}$ observed was due to aggregation of **2-40** on the enantiomerization path (Scheme 2-16), the reaction order with respect to [**2-40**] needs to be measured. Besides, our first order treatment of the enantiomerization process has not been convincingly justified yet, as the decay of er of **2-41** is not measured for more than 3 half-lives, as the standard protocol requires. The measurement of k_{enant} at different concentrations of [**2-40**] will not only be useful in determining the order of the reaction in [**2-40**], but also to validate our first order treatment of the enantiomerization process. Here, since the concentration of [**2-40]** in solution is not directly measureable (as it is in-situ formed after the first Mg/Br exchange reaction), we decided to vary the easily measurable $[Mg]_{total}$: the total concentration of all

the Grignard reagents at any time in the solution. Note that, the $[Mg]_{total}$ at any time interval on the reaction pathway is equal to the initial concentration of *i*-PrMgCl ($[i\text{-PrMgCl}]^0$), since the sum of concentrations of the Grignard reagents generated from Mg/Br exchange will always be equal to $[i\text{-PrMgCl}]^0$. However, since this term is not included in our integrated rate law, it is important first to justify its use here. As can be derived from equation 5 – section 2.3 above,

$$(2X_R\text{-}1) = \frac{[(R)\text{-}\mathbf{2\text{-}40}] - [(R)\text{-}\mathbf{2\text{-}40}]^e}{[(R)\text{-}\mathbf{2\text{-}40}]^0 - [(R)\text{-}\mathbf{2\text{-}40}]^e} \qquad (15)$$

Where, $[(R)\text{-}\mathbf{2\text{-}40}]$, $[(R)\text{-}\mathbf{2\text{-}40}]^e$, and $[(R)\text{-}\mathbf{2\text{-}40}]^0$ are the time-dependent, equilibrium, and initial concentrations of (*R*)-**2-40**. $[(R)\text{-}\mathbf{2\text{-}40}]^e$ and $[(R)\text{-}\mathbf{2\text{-}40}]^0$ are both proportional to $[Mg]_{total}$, and $[(R)\text{-}\mathbf{2\text{-}40}]$ is related to $[Mg]_{total}$ by exponential decay from $[(R)\text{-}\mathbf{2\text{-}40}]^0$. Thus, although the first-order rate constant k_{enant} does not measure the decay of [Mg], it measures the rate of decay of the excess concentration of (*R*)-**2-40** over its equilibrium value, which is related to $[Mg]_{total}$. It is therefore appropriate to study the effect of varying $[Mg]_{total}$ on k_{enant}. Thus in our study, the enantiomerization rate constant k_{enant} was measured at 195 K over a 25-fold range in $[Mg]_{total}$, from 0.063 to 0.0025 M (Figure 2-8 and Table 2-4).

Figure 2-8: Plot of ln($2X_R$([D_1]-**2-41**)-1) vs delay time *t* at different $[Mg]_{total}$

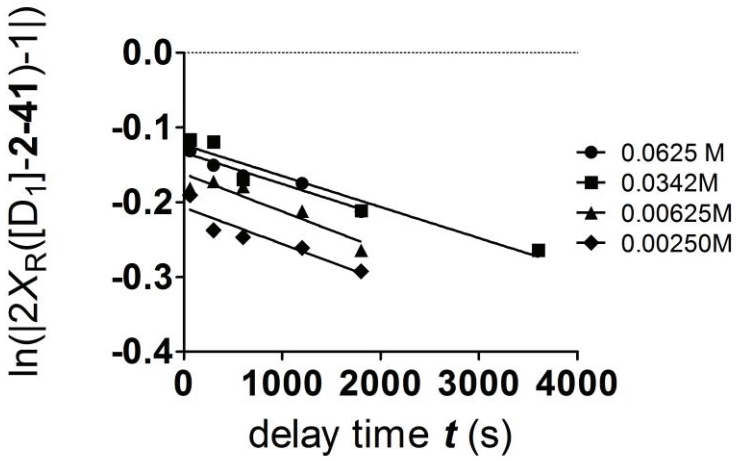

Table 2-4: Measurement of first order enantiomerization rate constants k_{enant} at different $[Mg]_{total}$ at 195 K.

Entry	$[Mg]_{total}$ M	$k_{enant} \times 10^6$ (s^{-1}) [a]	er ($t = 0$) [b]
1	0.0625	21.0 ± 3.3	94 : 6
2	0.0342	20.8 ± 3.3	94 : 6
3	0.00625	25.2 ± 5.4	92 : 8
4	0.00256	24.3 ± 5.7	91 : 9

[a] Calculated from the error in slope of the line using error analysis package in Microsoft-Excel 2007
[b] Calculated from the intercept of the line on y-axis.

If Grignard reagent aggregation were on the enantiomerization pathway, the measured first order rate constants k_{enant} would increase with increasing $[Mg]_{total}$, since the extent of aggregation would increase with increasing $[Mg]_{total}$. However, as can be seen from the data, there is no change in k_{enant} within experimental error, over the studied concentration range. This result justifies the first order kinetic treatment of our data. Also, it could be confirmed that the reaction is first order with respect to $[Mg]_{total}$ and ruled out required aggregation (or de-aggregation) of **2-40** at this temperature on the enantiomerization path.

2.5.2 Measurement of reaction order with respect to [Et_2O]

To determine if rate-determining solvent capture exists on the reaction pathway, the reaction order with respect to the donor solvent needs to be measured. For these studies we limited ourselves to the use of Et_2O as solvent since the most retentive Mg/Br exchange and smallest enantiomerization rate constants are observed in Et_2O. Also, the structure of the Grignard reagent in solution is considerably simpler in Et_2O than in THF.[42] A wide array of solution structures for Grignard reagents have been proposed in THF, ranging from monomer,[43] to mixed aggregates of extremely complex nature.[44] In Et_2O however, alkyl magnesium chlorides are known by ebullioscopy to be dimeric.[45] X-ray crystallography of Et_2O solvates of RMgCl shows a preference for bis-μ_2-chloro (μ_2-Cl) dimers structural motif in solution.[46,47] A discussion on the structure of Grignard reagents is presented in Chapter 3.

To test the hypothesis that the solvation number of **2-37** increases in the rate-determining transition state, a protocol was developed where the Mg/Br exchange – MeOD trapping reactions were performed in varying concentrations of Et_2O, using toluene as a co-solvent, maintaining a fixed Grignard concentration of 0.00625 M. The amount of solvent and co-solvent used and the resulting [Et_2O] is given in table 2-5.

Table 2-5: Et_2O/Toluene mixture compositions and resulting [Et_2O] used

Entry	Total reaction volume mL [a]	Total volume of Et_2O mL [b]	Total volume of Toluene mL [b]	[Et_2O] M [c]	Equiv of Et_2O [d]
1	10	10	0	9.53	1584
2	10	1	9	0.953	158
3	10	0.246	9.754	0.23	38
4	10	0.153	9.847	0.15	25
5	10	0.059	9.941	0.056	9

[a] $[Mg]_{total}$=0.00625, [b] More detailed discussion of experimental procedures in chapter 4, [c] assuming [Et_2O] in Et_2O = 9.53 at 195 and 212K, [d] with respect to $[Mg]_{total}$

The concentration of Et_2O was varied over a 158-fold range, by gradually flooding the concentration of Et_2O from 0.056 M (9 equiv Et_2O - Entry 5) to 9.5 M (neat Et_2O, 1520 equiv - Entry 1) at two temperatures, 212 K and 195 K. Plots of observed rate constants vs [solvent] have been used for determining reaction order with respect to the solvent. The type of solvent involvement in each case can be explained, looking at these plots. If solvation number of **2-40** changes in the rate determining step, we should see a first order dependence of k_{enant} on [Et_2O]. Such dependences have been observed in kinetic investigations of reactions of lithium di-isopropyl amide,[41] where the observed rate constants were dependent on the concentrations of solvents and additives. Interestingly, counter to our expectations the results of our studies at 195 K and 212 K did not show simple first order dependence of k_{enant} on [Et_2O] (Table 2-6, Table 2-7).

As seen in Figure 2-9, at 195 K, the plots of ln(2X_R([D_1]-**2-41**)-1) vs delay time *t*, show lines having nearly identical slopes. From the slopes of these lines, the rate enantiomerization rate constants were calculated at these [Et_2O] (Table 2-6).

Figure 2-9: Plot of ln(2X_R([D_1]-**2-41**)-1) vs delay time *t* in varying [Et_2O] at 195K

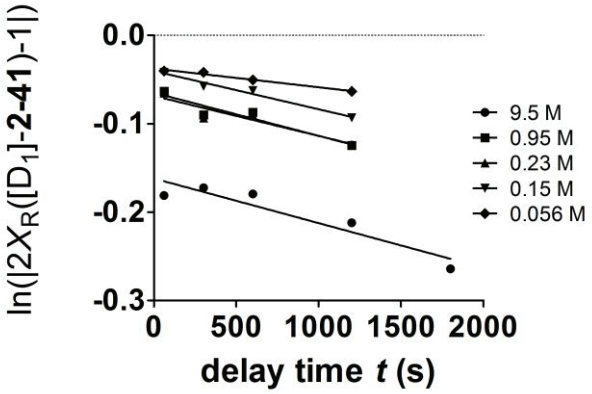

As seen in Table 2-6, k_{enant} remained unchanged until [Et_2O] fell to 0.15 M, after which there was a twofold decrease in k_{enant}. This drop in the observed rate constant was

noticeable but not significant enough to draw a firm conclusion. Note that a small but steady increase in extrapolated er at t = 0 to 98:2 was seen as [Et_2O] decreased. This observation suggested that the Mg/Br exchange reaction is more retentive at these low values of [Et_2O].

Table 2-6: Dependence of k_{enant} and extrapolated t = 0 er of **2-40** on [Et_2O][a] at 195 K

Entry	[Et_2O] M [b]	$k_{enant} \times 10^6$ (s^{-1})	*er* (t = 0)[c]
1	9.5	25.2 ± 5.4	94 : 6
2	0.95	24.4 ± 5.5	97 : 3
3	0.23	22.6 ± 5.8	97 : 3
4	0.15	21.6 ± 2.5	98 : 2
5	0.056	12.9 ± 3.1	98 : 2

[a] Reactions performed at [Mg]total=0.00625 M. [b] Concentration of Et_2O in toluene, assuming neat Et_2O is 9.5 M at 195 K. [c] Extrapolated.

These experiments were then repeated at a higher temperature of 212 K. Compared to Fig 2-9, the slopes of lines of ln($2X_R$([D_1]-**2-41**)-1) vs t in Figure 2-10 have different slopes at each [Et_2O]. Consequently, the k_{enant} can be seen to be significantly increased (14.5-fold) from the lowest [Et_2O] (0.056 M) to pure Et_2O (9.5 M) (Table 2-7).

Figure 2-10: Plot of ln($2X_R$([D_1]-**2-41**)-1) vs delay time t in varying [Et_2O] at 212K

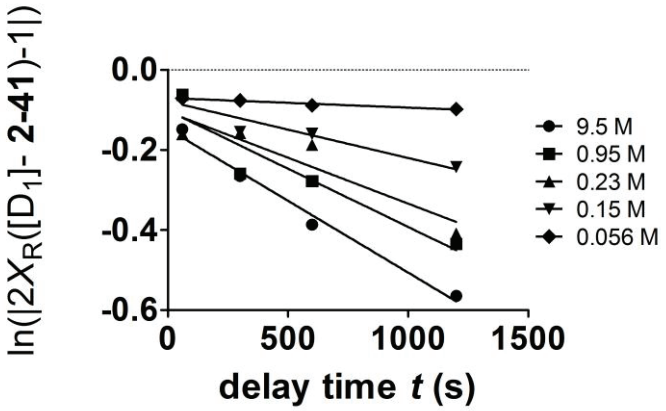

Table 2-7: Dependence of k_{enant} and extrapolated t = 0 er of **2-40** on $[Et_2O]$[a] at 212K

Entry	$[Et_2O]$ M [b]	$k_{enant} \times 10^6$ (s^{-1})	*er* (t = 0)[c]
1	9.5	179.4 ± 14.7	91 : 9
2	0.95	145.3 ± 37.9	95 : 5
3	0.23	114.5 ± 31.8	95 : 5
4	0.15	70.8 ± 17.8	96 : 4
5	0.056	12.4 ± 1.6	96 : 4

[a] Reactions performed at [Mg]total=0.00625 M. [b] Concentration of Et_2O in toluene, assuming neat Et_2O is 9.5 M at 212 K. [c] Extrapolated.

Figure 2-11 and 2-12 show the plots of observed k_{eanant} vs $[Et_2O]$ at 195 and 212 K respectively. As seen in both figures, the observed enantiomerization rate constant k_{enant} "leveled out" or reached a saturation value after a certain $[Et_2O]$ was reached. In other words, after the saturation point, k_{enant} is independent of $[Et_2O]$. This type of observation has been commonly referred as saturation kinetics.[48-51]

Fig 2-11: Plot of k_{enant} versus $[Et_2O]$ in toluene co-solvent at 195 K at $[Mg]_{total}$ = 0.006 M

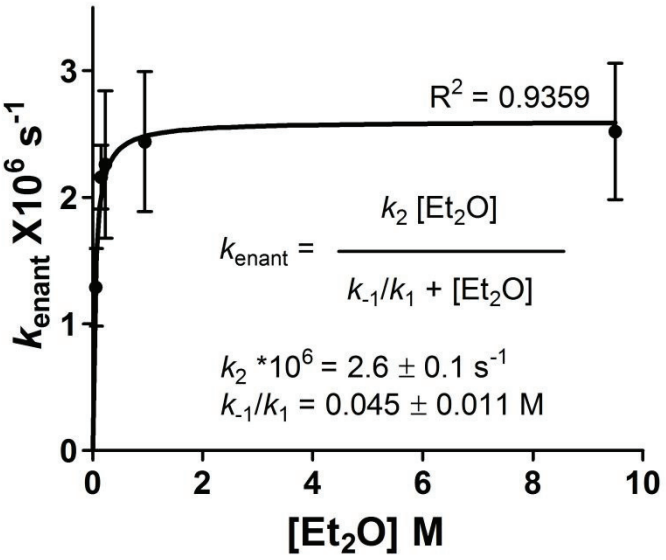

Fig 2-12: Plot of k_{enant} versus $[Et_2O]$ in toluene co-solvent at 212 K at $[Mg]_{total}$ = 0.006 M

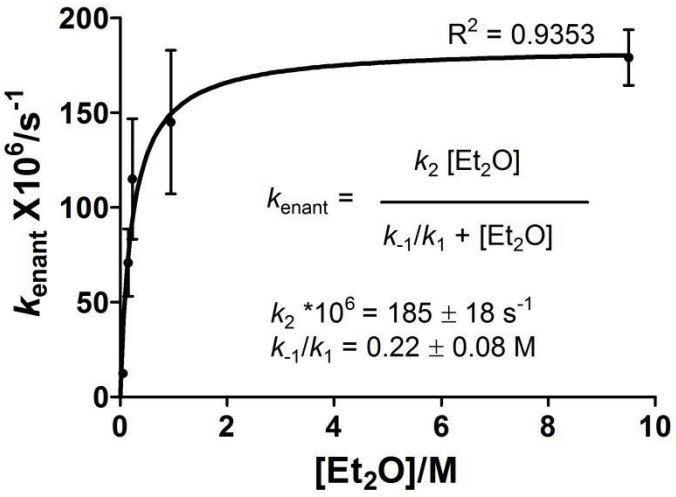

Saturation behavior with respect to [donor solvent] has been reported for the deprotonation of hydrazones by LDA in TMEDA/ hexanes,[52] and deprotonation of ketones by LiHMDS in R_3N/toluene. [51] These types of saturation behaviors with respect to [Solvent] are generally attributed to the change in the observable form of the reactant – which in this case can be the change in the solvation number of the Grignard species in solution.[41]

Looking at our results, we concluded that, at 212 K, the solvation number of the resting solution species changes as we go from low $[Et_2O]$ (0.056 M to 0.22 M), to higher $[Et_2O]$ (> 0.22 M). Thus at high $[Et_2O]$ there is no change in the solvation number of the reactive species in the rate determining step.[53,54] Therefore it can be concluded that the large negative entropy of activation for enantiomerization ($\Delta S^{\ddagger}$ = 49 ± 4 eu) measured in pure Et_2O cannot be attributed to solvent capture in the rate-determining transition structure, and must therefore be due to solvent electrostriction, which is discussed in the next sections.

2.6 Determination of stoichiometry of Mg/X exchange-trapping reaction of 2-39

Before we proceed to propose mechanism of enantiomerization, it is first important to discuss the studies towards understanding the stoichiometry of the Mg/Br exchange-trapping reaction of **2-39** performed by Dr. Ming Gao as a part of this project.[1] The studies on the reaction stoichiometry were performed by running the Mg/X exchange-MeOD trapping at 212 K in Et_2O for 5 min, using varying amounts of the Grignard reagent *i*-PrMgCl (Table 2-8). The amounts of deuteriation product [D_1]-**2-41** was monitored using ^{1}H-NMR and byproduct isopropyl bromide (*i*-PrBr) **2-50** from the Mg/Br exchange reaction,[55] was monitored by GC/MS, using mesitylene as an internal standard to find the composition of the worked up solution and the extent of Mg/Br exchange.

Table 2-8: Studies towards determining reaction stoichiometry.

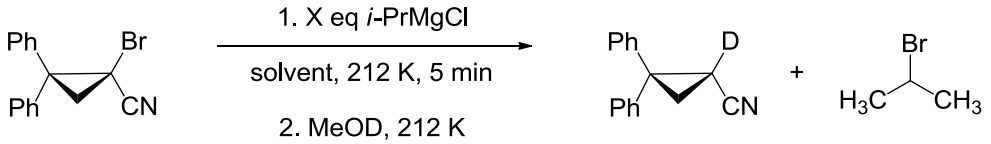

2-39 **[D_1]-2-41** **2-50**

Entry	Solvent	Equivalents of *i*-PrMgCl (X)	Mol % [D_1]-**2-41** [a]	Mol % **2-50** [b]
1	Et_2O	1.1	59 ± 5	65 ± 4
2		2.2	>98	92 ± 4
3	THF	1.1	>95	90 ± 4

[a] Calculated from the ratios of the diastereotopic methylene signals of [D_1]-**2-41** in the ^{1}H NMR spectrum. [b] Calculated from the expected amount of iPrBr measured by GC/MS, with mesitylene as internal standard

Reaction of **2-39** with 1.1 equiv *i*-PrMgCl in Et_2O (measured by titration, at 10 min, 212 K, CH_3OD quench), gave only (59 ± 5) % conversion of [D_1]-**2-41** (^{1}H NMR), and (65 ± 4) % of the expected amount of *i*-PrBr (measured by GC/MS, with mesitylene as internal standard). Increasing the amount of *i*-PrMgCl to 2.2 equiv gave >98% conversion of [D_1]-**2-41**, and (92 ± 4) % of the expected amount of **2-50**. We account for

these observations by proposing that *i*-PrMgCl, which is known to be a dimer in Et_2O (see chapter 3 section 3.1.1), reacts quickly with one equivalent of **2-36**, to form 1 equiv of heterodimer **2-51** (mixed dimer of **2-40** and *i*-PrMgCl) and 1 equiv *i*-PrBr (Scheme 2-18-a). On the other hand, identical studied of the reaction in THF with 1.1 equivalents of reagent *i*-PrMgCl shows >95% consumption of **2-39** and 90 ± 4% of the expected amount of **2-50**, consistent with the expected monomeric state of iPrMgCl in THF.

Scheme 2-18: Proposed scenario for Mg/Br exchange reaction of **2-39**

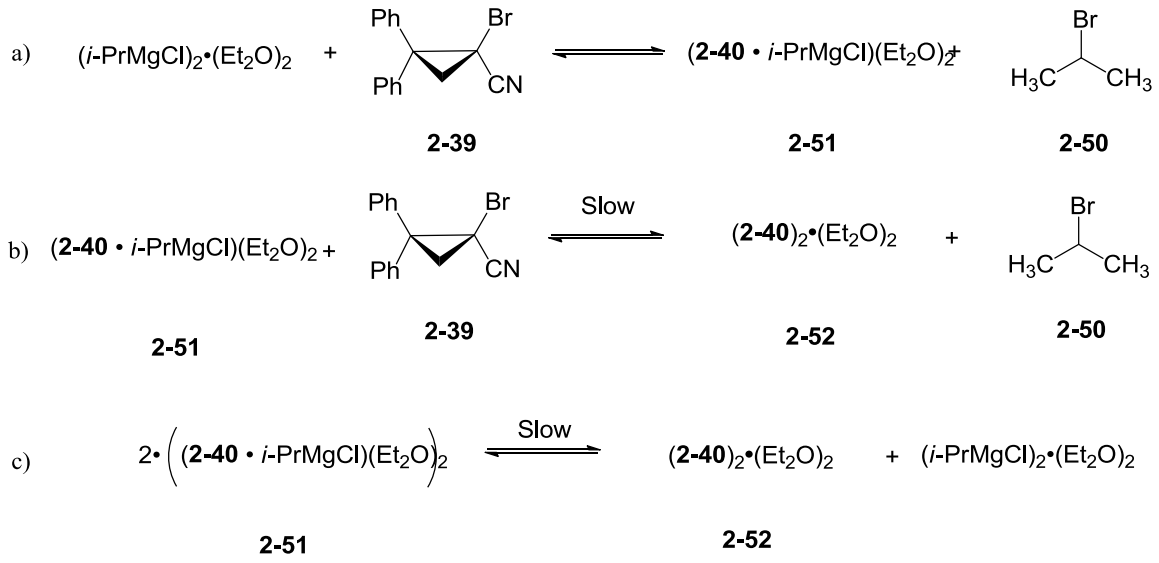

The reaction of this heterodimer **2-51** with another equivalent of **2-39** to form an equivalent of homodimer **2-52** and one equivalent of *i*-PrBr is apparently slow under the reaction conditions employed (Scheme 2-18-b). Similarly, the disproportionation reaction of **2-51** to regenerate the reactive iPrMgCl homodimer and a homodimer **2-52** must also be slow (Scheme 2-18-c). For the purpose of this study, we assumed that the mixed dimer (heterodimer) **2-51** was the predominant solvent structure of our magnesio-cyclopropylnitrile **2-40**.

2.7 Derivation of expression to relate k_{enant} to [Et_2O]

To derive the expression relating k_{enant} to [Et_2O] (shown in Figures 2-6, 2-7 (equation 22 below)), we considered that the enantiomerization process consisted of two reversible steps, formation of a higher solvated species followed by enantiomerization of this higher solvated species (Equation 16). For the sake of simplicity in the derived equation, we restricted ourselves to addition of only one ligand (solvent) even though our kinetic studies does not allow us to definitively distinguish between the additions of one or more ligand molecules.

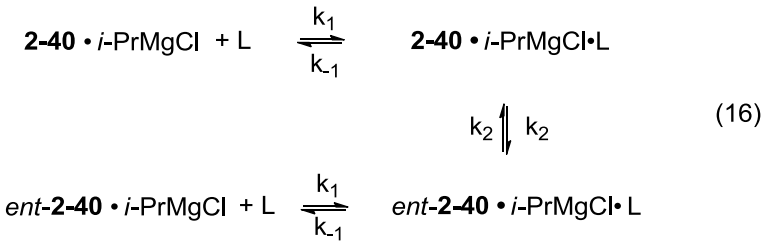

(16)

(Note that as drawn, the starting structure **2-40**·*i*-PrMgCl does not imply any particular structure or solvation state)

Following our standard strategy we define [**2-40**·*i*-PrMgCl]$_{total}$

$$[\mathbf{2\text{-}40} \cdot i\text{-PrMgCl}]_{total} = [\mathbf{2\text{-}40} \cdot i\text{-PrMgCl}] + [\mathbf{2\text{-}40} \cdot i\text{-PrMgCl} \cdot L] \qquad (17)$$

Rearranging equation 17

$$[\mathbf{2\text{-}40} \cdot i\text{-PrMgCl}] = [\mathbf{2\text{-}40} \cdot i\text{-PrMgCl}]_{total} - [\mathbf{2\text{-}40} \cdot i\text{-PrMgCl} \cdot L] \qquad (18)$$

Assuming that $k_{-1} >> k_2$, we can consider **2-40**·*i*-PrMgCl and **2-40**·*i*-PrMgCl·L to be in equilibrium, and substitute equation 89 into the equilibrium expression arising from equation 16

$$k_{-1}/k_1 = \frac{[\mathbf{2\text{-}40} \cdot i\text{-PrMgCl}][L]}{[\mathbf{2\text{-}40} \cdot i\text{-PrMgCl} \cdot L]} = \frac{\{[\mathbf{2\text{-}40} \cdot i\text{-PrMgCl}]_{total} - [\mathbf{2\text{-}40} \cdot i\text{-PrMgCl} \cdot L]\}\,[L]}{[\mathbf{2\text{-}40} \cdot i\text{-PrMgCl} \cdot L]} \quad (19)$$

Simplifying equation 19

$$k_{-1}/k_1 = \frac{[\mathbf{2\text{-}40} \cdot i\text{-PrMgCl}]_{total}\,[L]}{[\mathbf{2\text{-}40} \cdot i\text{-PrMgCl} \cdot L]} - [L] \quad (20)$$

Rearranging equation 20

$$[\mathbf{2\text{-}40} \cdot i\text{-PrMgCl} \cdot L] = \frac{[\mathbf{2\text{-}40} \cdot i\text{-PrMgCl}]_{total}\,[L]}{k_{-1}/k_1 + [L]} \quad (21)$$

To relate the observed enantiomerization rate constant k_{enant} to [L] and microscopic rate constants k_2, k_{-1}, and k_1, we note that the forward rate of conversion (chemical flux) of **2-40**•*i*-PrMgCl to *ent*-**2-40**•*i*-PrMgCl can be written both in terms of $[\mathbf{2\text{-}40} \bullet i\text{-PrMgCl}]_{total}$, and in terms of the discrete solvate [**2-40**•*i*-PrMgCl•L]

$$k_{enant}[\mathbf{2\text{-}40} \cdot i\text{-PrMgCl}]_{total} = k_2\,[\mathbf{2\text{-}40} \cdot i\text{-PrMgCl} \cdot L] \quad (22)$$

Substituting equation 22

$$k_{enant}[\mathbf{2\text{-}40} \cdot i\text{-PrMgCl}]_{total} = \frac{k_2\,[\mathbf{2\text{-}40} \cdot i\text{-PrMgCl}]_{total}\,[L]}{k_{-1}/k_1 + [L]} \quad (23)$$

Simplifying equation 23

$$k_{enant} = \frac{k_2\,[L]}{k_{-1}/k_1 + [L]} \quad (24)$$

2.8 Solvent electrostriction as the probable cause of large negative entropy of activation

Solvent electrostriction can be defined as the charge counterbalancing effect provided by reordering of solvent molecules around a dipole. Figure 2-13 shows a cartoon representing this effect by THF molecules around a dipole.[56] As this reordering happens, a "more ordered" bulk solvent structure is formed, which gives rise to negative $\Delta S^{\ddagger}$ values.[57,58]

Figure 2-13: Solvent electrostriction – cartoon representation.[56]

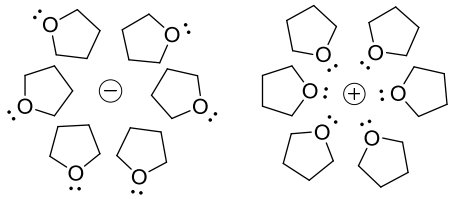

Highly negative entropies of activation have been seen in several cases for dissociative reactions involving carbocationic intermediates. Most notable examples in this series are the "ionogenic" reactions, where generation of an ion-pair is involved on the reaction pathway. In most of these examples, rate-limiting coordination of solvent is not likely, and solvent electrostriction provides a reasonable explanation for the observed large negative $\Delta S^{\ddagger}$ values (Scheme 2-19).[57-60]

Scheme 2-19: Ionogenic reactions showing large negative values for $\Delta S^{\ddagger}$. [61,62]

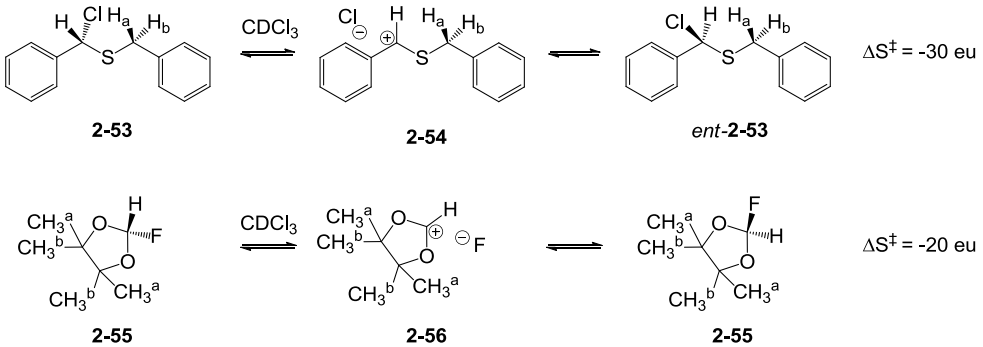

Oki observed the enantiomerization of (S)- α-chlorodibenzyl sulfide **2-53** by following the chemical exchange of H_a and H_b and the inversion of 2-fluoro-4,4,5,5-tetramethyl-1,3-dioxolane **2-55** by following the chemical exchange of CH_3^a and CH_3^b using Dynamic NMR spectroscopy.[61,62] The process in both cases can be imagined to happen through formation of the dissociated intermediates **2-54** and **2-56** respectively. Surprisingly, large negative entropies of activation are found for these processes in a non-polar solvent like $CDCl_3$. In these cases, there can be no co-ordination of the solvent to the ions, thus solvent electrostriction – reordering of the solvent shell around the dipole in **2-54** and **2-56** - provides a better explanation to the large negative $\Delta S^{\ddagger}$ values observed.

Similarly, in case of Grignard **2-40** it can be envisioned that ion pair separation, which is by definition an ionogenic (dissociative) process, gives rise to a large dipole. The ethereal solvent then reorders around this newly formed dipole; giving rise to the large negative $\Delta S^{\ddagger}$ values.

2.9 Plausible mechanism for enantiomerization of 2-40.

Looking at these results we could then provide a plausible sequence for the process of enantiomerization of **2-40**. As discussed earlier and as will be discussed in in Chapter 3, based on the available X-ray crystal structures of Et_2O–solvates of RMgCl and other bis(μ-Cl) dimers at low [Et_2O], **2-40**·*i*-PrMgCl most likely exists as a di-solvate. Based on our DFT calculations (Chapter 3), we can propose that the disolvated dimeric species is the dominant dimeric species in the solution. Nevertheless, our results of the kinetic studies demonstrated that -

a) Solvent plays a key role in the enantiomerization process as seen from the divergent results in three ethereal solvents

b) Solvent capture precedes the ion-pair separation step as seen from the fact that enantiomerization rate constant k_{enant} has a saturating dependence on [Et_2O] above [Et_2O] = 1 M

c) The large negative entropy of activation observed in pure Et_2O probably comes from the electrostriction of the solvent, suggesting an ionogenic TS involved in the rate-limiting step.

Based on these observations, we can propose the precise timing of the solvation event and a plausible mechanistic sequence (Scheme 2-20).

Scheme 2-20: Proposed mechanism of enantiomerization of heterodimer **2-51** in Et_2O solvent.

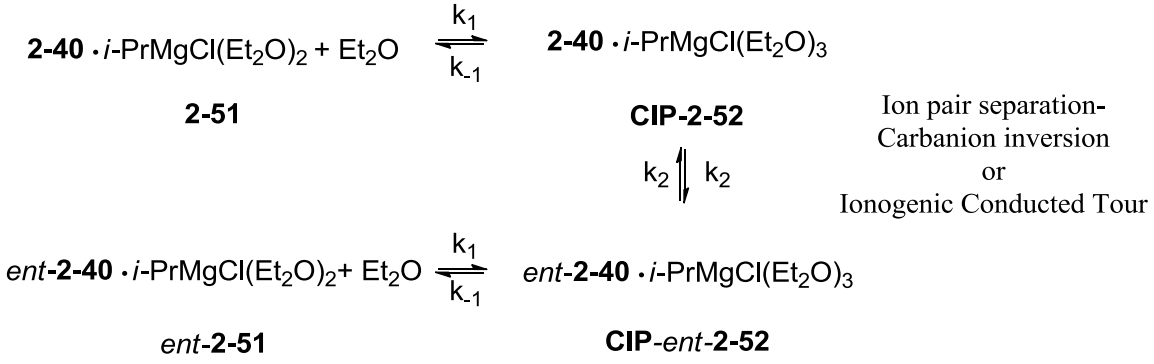

At low [Et_2O], the disolvated heterodimer **2-51**, which is likely to be the major species in solution, undergoes a solvent capture leading to higher solvated species **2-52**, which then undergoes enantiomerization possibly by ion pair separation - carbanion inversion process leading to the enantiomeric species *ent*-**2-52**. At high [Et_2O], the higher solvated species **2-52** is the dominant solution species. Thus, in this domain the mechanism begins with the higher solvated species **2-52** undergoing ion-pair separation, followed by the enantiomerization. It is important to note at this point that the ion pair separation and enantiomerization steps are indistinguishable by kinetic studies as both do

not involve change in any measurable concentration term. However, looking at reported rates for solvent addition, ion pair separation and carbanion inversion, in case of some organolithium compounds, it can be predicted that the ion-pair separation step may be the rate-limiting step out of the three.[63,64]

Our computational studies towards determination of the structure of the heterodimer and possible solvation state will be discussed in detail in chapter 3. However, based on the literature we have identified some probable structures for the disolvate **2-51** and trisolvate **2-52**. (Scheme 2-21).

Scheme 2-21: Possible structures for resting solution species and higher solvated species.

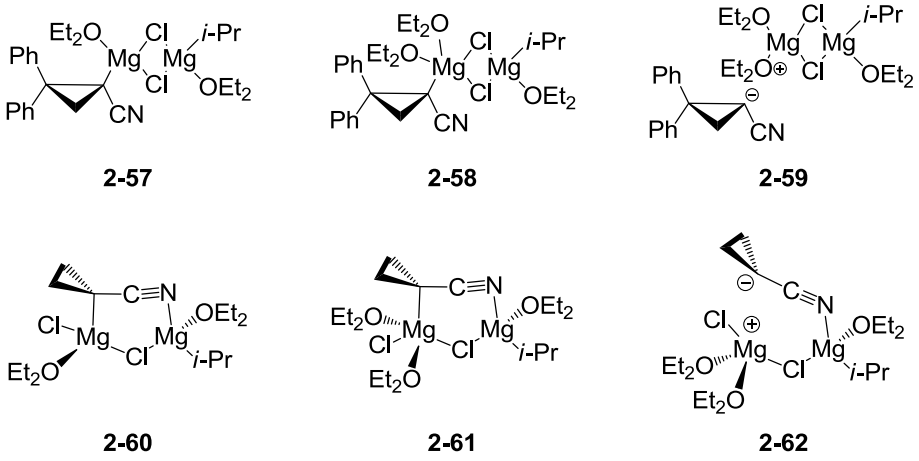

As stated before, X-ray crystal structures of Et_2O–solvates of RMgCl are found to be disolvated bis(μ-Cl) dimers suggesting that the heterodimer structure could be as shown by **2-57**. However, based on the available crystal structure for 2,2 dimethyl-1-lithio cyclopropylnitrile obtained by Boche (see chapter 1 section 1.1), a different disolvated structure like **2-60** is proposed, where the nitrile nitrogen co-ordinates to the other lithium atom forming a –CN bridge in place of one chloro bridge of the bis-μ-chloro (μ-Cl) dimer.[65] For the higher solvated species, the corresponding trisolvated

structures **2-58** and **2-61** are suggested where one of the magnesium atoms goes to 5-coordinate trigonal bipyramidal geometry to accommodate the new solvent molecule.[66] These higher solvated species can then undergo ion pair separation giving SIP species **2-59** or **2-62**, through which enantiomerization by carbanion inversion could happen.[36]

Lastly, we would like to point out that a "conducted tour" pathway,[35] to directly generate an ion-pair **2-63** from the trisolvated bis(μ-Cl) dimer might also be consistent with observed $\Delta S^{\ddagger}$ value since a larger dipole can be expected for such a species. It is important to note that the process of ion-pair separation shown with **2-61**→**2-62**, can also be considered as an ionogenic conucted tour. The inversion of these carbanions **2-62** and **2-63**, and N→C migration would ultimately lead to enantiomerization. Such an "ionogenic conducted tour" is thus a possible alternative to the ion-pair separation mechanism (Scheme 2-22).

Scheme 2-22: Ionogenic conducted tour mechanism towards enantiomerization of **2-58**

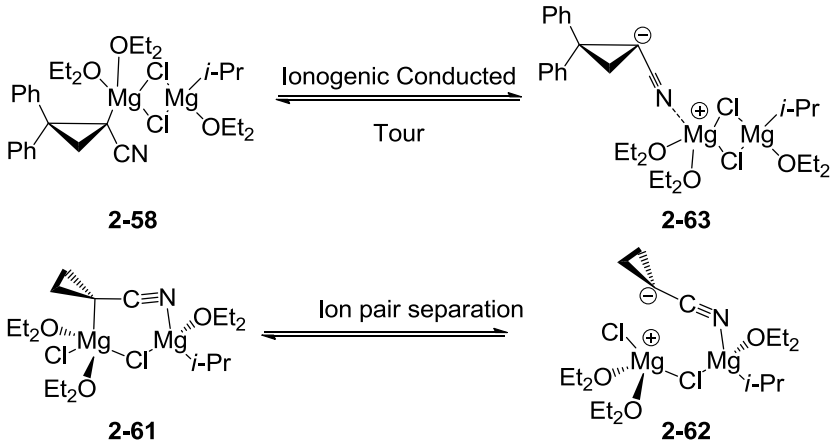

2.10 Conclusions

In conclusion, dramatically different rates of enantiomerization for **2-40** were observed in three ethereal solvents Et_2O, 2-MeTHF and, THF. Both, the Mg/Br exchange

reaction and enantiomerization processes were found to be more retentive in the order Et_2O >> 2-MeTHF~THF. By determining enantiomerization rate constant k_{enant} at different temperatures in different solvents, we were able to determine the activation parameters $\Delta S^{\ddagger}$ and $\Delta H^{\ddagger}$ using the Eyring equation. The activation parameters revealed a large negative entropy of activation ($\Delta S^{\ddagger}$), which was indicative of the solvent-assisted ion-pair separation mechanism on the pathway to enantiomerization. Reaction orders with respect to $[Mg]_{total}$ and the $[Et_2O]$ were measured in order to determine the role of these constituents in the enantiomerization process. The rate of enantiomerization was found to be independent of $[Mg]_{total}$ thus eliminating the idea that aggregation of **2-40** occurred on the enantiomerization path. For the first time, the reaction order in ethereal solvent for enantiomerization of a Grignard reagent was studied. We would note that to the best of our knowledge, such a study has also never been performed on an enantiomerically enriched organolithium. The observation of saturation kinetics in $[Et_2O]$ suggested that ion-pair separation does indeed lie on the enantiomerization reaction path. However since the enantiomerization rate is saturated above $[Et_2O]$ = 1 M, in pure Et_2O there can be no change in solvation number between the resting state of the Grignard reagent and its enantiomerization transition structure. However, we could not rule out the conducted tour pathway for enantiomerization, since it could also generate a large dipole and cause solvent-shell re-ordering. One could surmise that ionization of C-Mg bond leads directly to the *N*-magnesio isomer by some mechanism and eventually enantiomerization. Since ion pair separation is by definition an ionogenic process, we believe the large negative entropy of activation stems principally from solvent electrostriction or reorganization of the secondary solvent shell.

2.11 References for Chapter 2

(1) Patwardhan, N. N.; Gao, M.; Carlier, P. R. *Chem.--Eur. J.* **2011**, *17*, 12250.

(2) Basu, A.; Thayumanavan, S. *Angew. Chem. Int. Ed* **2002**, *41*, 717.

(3) Clayden, J. In *Organolithiums - Selectivity for Synthesis*; Jonathan, C., Ed.; Elsevier: 2002; Vol. Volume 23, p 169.

(4) Clayden, J. In *Organolithiums - Selectivity for Synthesis*; Jonathan, C., Ed.; Elsevier: 2002; Vol. Volume 23, p 241.

(5) Gawley, R. E. *Overview of Carbanion Dynamics and Electrophilic Substitutions in Chiral Organolithium Compounds*; Verlag Helvetica Chimica Acta, 2010.

(6) Hoffmann, R. W. *Chem. Soc. Rev.* **2003**, *32*, 225.

(7) Ashweek, N. J.; Brandt, P.; Coldham, I.; Dufour, S.; Gawley, R. E.; Haeffner, F.; Klein, R.; Sanchez-Jimenez, G. *J. Am. Chem. Soc.* **2005**, *127*, 449.

(8) Hoffmann, R. W. *Test on the Configurational Stability/Lability of Organolithium Compounds*; Verlag Helvetica Chimica Acta, 2010.

(9) Ikemoto, H.; Sasaki, M.; Takeda, K. *Eur. J. Org. Chem.* **2010**, 6643.

(10) Kapeller, D. C.; Hammerschmidt, F. *J. Org. Chem.* **2009**, *74*, 2380.

(11) Marr, F.; Fröhlich, R.; Hoppe, D. *Org. Lett.* **1999**, *1*, 2081.

(12) Perna, F. M.; Salomone, A.; Dammacco, M.; Florio, S.; Capriati, V. *Chem.-Eur. J.* **2011**, *17*, 8216.

(13) Wu, S.; Lee, S.; Beak, P. *J. Am. Chem. Soc.* **1996**, *118*, 715.

(14) Beng, T. K.; Yousaf, T. I.; Coldham, I.; Gawley, R. E. *J. Am. Chem. Soc.* **2009**, *131*, 6908.

(15) Coldham, I.; Leonori, D.; Beng, T. K.; Gawley, R. E. *Chem. Commun. (Cambridge, U. K.)* **2009**, 5239.

(16) Reich, H. J.; Kulicke, K. J. *J. Am. Chem. Soc.* **1995**, *117*, 6621.

(17) Reich, H. J.; Dykstra, R. R. *Angew. Chem. Int. Ed* **1993**, *32*, 1469.

(18) Carstens, A.; Hoppe, D. *Tetrahedron* **1994**, *50*, 6097.

(19) Pearson, W. H.; Lindbeck, A. C.; Kampf, J. W. *J. Am. Chem. Soc.* **1993**, *115*, 2622.

(20) Ahlbrecht, H.; Harbach, J.; Hoffmann, R. W.; Ruhland, T. *Liebigs Annalen* **1995**, 211.

(21) Gawley, R. E.; Zhang, Q. *Tetrahedron* **1994**, *50*, 6077.

(22) Gawley, R. E.; Zhang, Q. *J. Am. Chem. Soc.* **1993**, *115*, 7515.

(23) Kizirian, J.-C. In *Stereochemical Aspects of Organolithium Compounds*; Verlag Helvetica Chimica Acta: 2010, p 189.

(24) Perna, F. M.; Salomone, A.; Dammacco, M.; Florio, S.; Capriati, V. *Chem. Eur. J.* **2011**, *17*, 8216.

(25) Reich, H. J.; Medina, M. A.; Bowe, M. D. *J. Am. Chem. Soc.* **1992**, *114*, 11003.

(26) Clark, T.; Schleyer, P. v. R.; Pople, J. A. *J. Chem. Soc., Chem. Commun.* **1978**, 137.

(27) Walborsky, H. M.; Young, A. E. *J. Am. Chem. Soc.* **1964**, *86*, 3288.

(28) Jensen, F. R.; Nakamaye, K. L. *J. Am. Chem. Soc.* **1966**, *88*, 3437.

(29) Whitesides, G. M.; Roberts, J. D. *J. Am. Chem. Soc.* **1965**, *87*, 4878.

(30) Whitesides, G. M.; Witanowski, M.; Roberts, J. D. *J. Am. Chem. Soc.* **1965**, *87*, 2854.

(31) Hoffmann, R. W.; Hölzer, B.; Knopff, O.; Harms, K. *Angew. Chem. Int. Ed* **2000**, *39*, 3072.

(32) Hoffmann, R. W.; Nell, P. G. *Angew. Chem. Int. Ed* **1999**, *38*, 338.

(33) Hoffmann, R. W.; Nell, P. G.; Leo, R.; Harms, K. *Chem.-Eur. J.* **2000**, *6*, 3359.

(34) Carlier, P. R.; Zhang, Y. Q. *Org. Lett.* **2007**, *9*, 1319.

(35) Carlier, P. R. *Chirality* **2003**, *15*, 340.

(36) Deora, N.; Carlier, P. R. *J. Org. Chem.* **2010**, *75*, 1061.

(37) Connors, K. A. *Chemical Kinetics: The Study of Reactions in Solution*; VCH: New York, 1990.

(38) Espenson, J. H. *Chemical kinetics and reaction mechanisms*; McGraw-Hill ; Primis Custom: New York, 2002.

(39) Capriati, V.; Florio, S.; Perna, F. M.; Salomone, A. *Chem.-Eur. J.* **2010**, *16*, 9778.

(40) Hoell, D.; Schnieders, C.; Müllen, K. *Angew. Chem. Int. Ed* **1983**, *22*, 299.

(41) Collum, D. B.; McNeil, A. J.; Ramirez, A. *Angew. Chem. Int. Ed* **2007**, *46*, 3002.

(42) Silverman, G. S.; Rakita, P. E.; Editors *Handbook of Grignard Reagents* CRC-Press: New York, 1996.

(43) Vallino, M. *J. Organomet. Chem.* **1969**, *20*, 1.

(44) Sakamoto, S.; Imamoto, T.; Yamaguchi, K. *Org. Lett.* **2001**, *3*, 1793.

(45) Walker, F. W.; Ashby, E. C. *J. Am. Chem. Soc.* **1969**, *91*, 3845.

(46) Dohmeier, C.; Loos, D.; Robl, C.; Schnöckel, H.; Fenske, D. *J. Organomet. Chem.* **1993**, *448*, 5.

(47) E. Hibbs, D.; Jones, C.; F. Richards, A. *J. Chem. Soc., Dalton Trans.* **1999**, 3531.

(48) DePue, J. S.; Collum, D. B. *J. Am. Chem. Soc.* **1988**, *110*, 5524.

(49) Gupta, L.; Hoepker, A. C.; Singh, K. J.; Collum, D. B. *J. Org. Chem.* **2009**, *74*, 2231.

(50) Gupta, L.; Ramírez, A.; Collum, D. B. *J. Org. Chem.* **2010**, *75*, 8392.

(51) Zhao, P.; Collum, D. B. *J. Am. Chem. Soc.* **2003**, *125*, 4008.

(52) Bernstein, M. P.; Romesberg, F. E.; Fuller, D. J.; Harrison, A. T.; Collum, D. B.; Liu, Q. Y.; Williard, P. G. *J. Am. Chem. Soc.* **1992**, *114*, 5100.

(53) Sun, X.; Collum, D. B. *J. Am. Chem. Soc.* **2000**, *122*, 2459.

(54) Sun, X.; Collum, D. B. *J. Am. Chem. Soc.* **2000**, *122*, 2452.

(55) Hoffmann, R. W.; Bronstrup, M.; Muller, M. *Org. Lett.* **2003**, *5*, 313.

(56) Szwarc, M. *Acc. Chem. Res.* **1969**, *2*, 87.

(57) Kwart, H.; Lilley, T. H. *J. Org. Chem.* **1978**, *43*, 2374.

(58) Kwart, H.; Silver, P. A. *J. Org. Chem.* **1975**, *40*, 3019.

(59) Dvorko, G. F.; Koshchii, I. V.; Ponomareva, É. A. *Theoretical and Experimental Chemistry* **2003**, *39*, 99.

(60) McManus, S. P.; Somani, S.; Harris, J. M.; McGill, R. A. *J. Org. Chem.* **2004**, *69*, 8865.

(61) Oki, M. *Pure Appl. Chem.* **1989**, *61*, 699.

(62) Oki, M.; Ikeda, H.; Toyota, S. *Tetrahedron Lett.* **1998**, *39*, 7729.

(63) Lucht, B. L.; Collum, D. B. *J. Am. Chem. Soc.* **1994**, *116*, 6009.

(64) Lucht, B. L.; Collum, D. B. *J. Am. Chem. Soc.* **1995**, *117*, 9863.

(65) Boche, G. *Angew. Chem. Int. Ed* **1989**, *28*, 277.

(66) Erwin Weiss *Angew. Chem. Int. Ed* **1993**, *32*, 1501.

Chapter 3: DFT studies on solvation and ion-pair separation of Grignard reagents

3.1 Introduction and motivation

In the first two chapters of this dissertation, we summarized two aspects of our studies towards C_α-chiral Grignard reagents, attempts at their synthesis, reactions and then studies towards understanding the configurational stability of a chiral magnesio cyclopropylcarbonitrile. In this chapter we describe our computational studies to understand solvation and its implications on the structure of Grignard reagents, and finally the ion-pair separation of such compounds under the influence of the solvent. The structure of Grignard reagents has been a topic of significant amount of research ever since they were introduced over a century ago.[1-5] However, the structure of Grignard reagents in solution is still a topic of discussion and debate.[6,7] Figure 3-1 shows the three equilibria operating in Grignard solutions that complicate the analysis of Grignard reagent structure. Equilibrium I is the dimerization equilibrium, II is the Schlenk equilibrium,[8,9] and III is the heterodimerization equilibrium. The position of these equilibria is dictated by several factors such as concentration, the identity of the halide, and the identity of the solvent.

Figure 3-1: The Schlenk and dimerization equilibriums prevalent in Grignard solutions

$$(RMgX)_2 \overset{I}{\rightleftharpoons} 2\ R\text{-}Mg\text{-}X \overset{II}{\rightleftharpoons} R_2Mg + MgX_2 \overset{III}{\rightleftharpoons} R_2Mg{\bullet}MgX_2$$

In this chapter, we will first briefly review some of the experimental and computational studies on Grignard reagent structure in the solid and solution states and then present our computational studies towards understanding solvation and ion pair separation. Two types of Grignard reagents are studied. First, methylmagnesium chloride (MeMgCl) was studied for its relative simplicity. Second, we modeled the magnesio

cyclopropylcarbonitrile **3-26** because of its similarity to the magnesio cyclopropylcarbonitrile **2-40** studied in Chapter 2.[10]

3.1.1 Experimental studies of Grignard reagent structure

In this section, we will first discuss some representative studies on Grignard reagent structure using X-ray crystallography, which will be followed by a brief discussion on the studies of Grignard reagent structure in solution. This section however does not comprehensively cover the entire topic of Grignard reagent structure. Excellent books and review articles have been published on this subject that are a valuable references source for this section. [6,7,11,12] Any references to these sources are duly acknowledged by citation.

X-ray crystal structure analysis is a valuable tool in understanding the structure and composition of organometallic compounds.[7,13] However, the crystallization of Grignard reagents (organomagnesium halides) is found to be experimentally challenging with only a few crystal structures of these compounds reported in the literature.[7] Crystal structures of organomagnesium halides bearing ligands such as TMEDA,[14,15] N^1,N^1,N^2,N^2-tetraethylethane-1,2-diamine,[16] Sparteine,[7] triethyl amine,[17] 15-crown-4 and 18-crown-5,[18] are known. These structures although interesting will not be discussed here since we eventually intend to focus on the structure of Grignard reagents in ethereal solutions.

X-ray crystal structures of ethereal solvates of Grignard reagents (organomagnesium halides) are relatively rare. The structure of the alkyl fragment, and the ethereal solvent that these crystals are obtained from has been shown to influence the types of structure observed. The crystal structures of Et_2O solvates are discussed first.

The X-ray crystal structure studies of ether solvates of organomagnesium chlorides and bromides are discussed separately to distinguish between the types of the structures observed for these compounds. The early X-ray crystal structure studies on structure of phenyl magnesium bromide dietherate **3-1** by Stucky et al. showed the monomeric disolvated structure of these compounds.[19,20] Similarly, Guggenburger et al observed the monomeric dietherate structure for ethylmagnesium bromide **3-2**.[21] Finally Engelhardt et al found a similar structure for the dietherate of the bulky triphenylmethyl magnesium bromide **3-3**. Figure 3-2 shows representations of these crystal structures. It is important to note that similar structures are observed regardless of the structure of the alkyl/aryl group.

Figure 3-2: Representations of observed X-ray crystal structures of EtMgBr•□$OEt_2)_2$, PhMgBr•$OEt_2)_2$, and $(Ph)_3$CMgBr•$OEt_2)_2$.

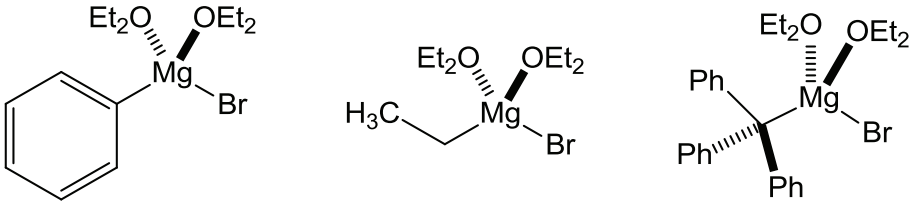

3-1 **3-2** **3-3**

To the best of our knowledge, there are only two X-ray structures reported for diethyl ether solvates of organomagnesium chlorides to date. These compounds crystallize from diethyl ether solutions as disolvated dimers featuring a bis(μ-Cl) bridge.[7] Dohmier and co-workers obtained the crystals of cyclopentadienyl magnesium chloride **3-4** from diethyl ether solutions as bis(μ-Cl) dimers where the two chlorine atoms formed bridges between the two magnesium atoms.[22] The structure was found to be disolvated with the two solvent ligands on opposite faces of the central bis(μ-Cl) dimer structure

(*trans*). The η^5 hapticity of the cyclopentadienyl group is also clearly visible in the structure. Hibbs and co-workers also reported a similar structure for the phosphavinyl Grignard reagent **3-5**. [23] Representations of these structures are shown in Figure 3-3.

Figure 3-3: Representations of observed structures of organomagnesium chlorides by X-ray crystallography.

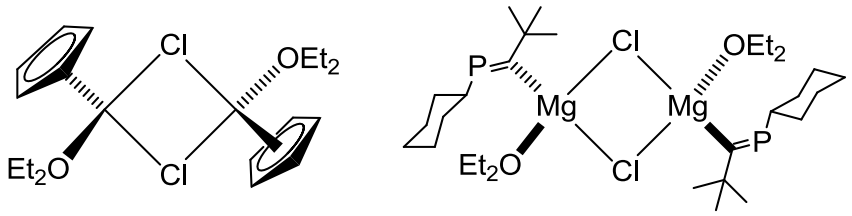

3-4 **3-5**

The X-ray crystal structure analyses of THF-solvates of Grignard reagents however suggest a complex scenario. Different kinds of structures ranging from monomers to higher aggregates have been seen in case of crystals isolated from THF solutions. Early crystal structure studies by Valino showed a trisolvated monomeric structure **3-6** for methylmagnesium bromide ($MeMgBr \bullet THF)_3$) in THF.[24] Toney et al. subsequently showed a complex tetrameric structure **3-7** for THF solvate of $EtMgCl \bullet MgCl_2$. [25] More recently, several Grignard reagents were studied by Sakamoto and co-workers using X-ray crystal structure analysis.[26] Tetrameric complexes of the stoichiometry $(RMgCl \bullet MgCl_2)_2$ similar to the one observed 30 years earlier by Toney et al. were again seen for THF solvates of methyl, phenyl, *t*-Butyl and benzyl magnesium chloride reagents **3-8** to **3-10**. Again it is important to note that similar structures were observed for different alkyl groups. Structures of the stoichiometry $RMgCl \bullet 2MgCl_2$ shown by **3-11** and **3-12** were found for the crystals of *t*-butyl magnesium chloride and phenyl magnesium chloride**.** Finally, a structure of stoichiometry $(2RMgCl \bullet MgCl_2)_2$

shown by **3-13** was also observed in crystals of phenyl magnesium chloride. The representations of all these structures are shown in Figure 3-4.

Figure 3-4: X-ray crystal structures observed for various THF solvates of Grignard compounds.

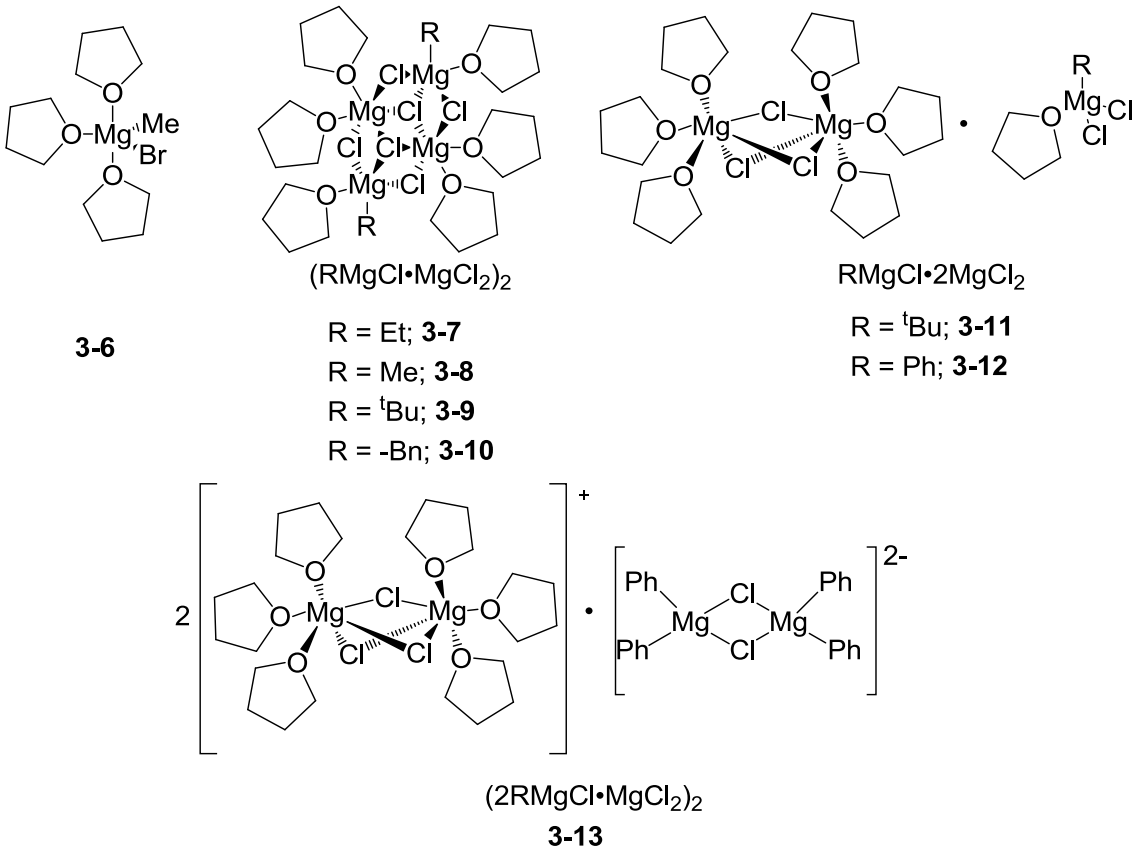

Although the origin of these tetrameric structures have not been discussed by the authors, a disproportionating equilibrium shown in Scheme 3-1 below could be postulated in the THF solutions of these Grignard reagents. The complex **3-15** could be formed via this disproportionation before it crystallizes out of solution as a THF solvate.

Scheme 3-1: Disproportionating equilibrium proposed in THF solutions

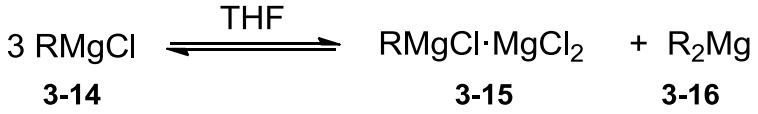

Based on the crystal structures discussed, we can reach a preliminary conclusion. With these large varieties of structures observed for THF solvates of Grignard reagents, making an accurate estimation of the solution structure becomes difficult. Comparatively in case of Et_2O solvates, a fairly predictable scenario is observed. The organomagnesium bromides crystallized as monomers whereas, all known organomagnesium chlorides form bis(μ-Cl) dimeric structures. However, a limitation with making an estimate on solution structure from crystal structures is that the species in a solution may not be the same that crystallizes out of it.[6] For this purpose methods that address structure in solution need to be employed.

Various techniques have been attempted to attain information about solution structure. Amongst these, calorimetric methods,[27-29] isotopic labeling methods,[30,31] and NMR methods (including ^{25}Mg NMR)[5,32-35] have been employed to deduce valuable information on the position of the Schlenk equilibrium. However, no information on the aggregation state of the studied compounds was obtained by these methods. The ebullioscopic molecular weight determination experiments performed by Ashby and co-workers provide the most valuable information about the average aggregation state of Grignard reagents in Et_2O and THF solutions.[6,36] In this study, the elevation in boiling points of the solvent was measured, which is related to the molality of the dissolved solute.[37] Based on the molecular weight of the monomeric species, the weight concentration of the solution, and the boiling point elevation, the average molecularity of the compound in solution can be calculated. In Et_2O, organomagnesium bromides and iodides were found to be monomeric at low concentrations (<0.1 M), but the average aggregation states approached 3.5-4.0 above 2.5 M. On the other hand, organomagnesium

chlorides were found to be dimeric in Et_2O at low concentrations (< 0.1 M) and higher aggregates above 2.5 M. However, all organomagnesium halides and diorganomagnesium compounds studied were found to be monomeric over the entire range of concentrations studied in THF.

This study provided a fundamental picture for the aggregation state not available through any other studies so far. Combining these studies with the solid state information provided by X-ray crystallography, it could be concluded that organomagnesium chlorides exist as bis(μ-Cl) dimers in Et_2O solution. On the other hand organomagnesium bromides and iodides existed as complex oligomers in high concentration solutions and monomers in low concentration solutions. A few computational studies have been attempted to rationalize this scenario. In the next section we will review two important computational studies in this respect.

3.1.2 Computational studies on Grignard reagent structure in solution

Computational investigation of organometallic compounds has been a topic of considerable interest in the recent past as more efficient methods and newer tools in this field continue to advance.[38] Computational modeling of Grignard reagents reported thus far in the literature are typically focused towards understanding their formation,[39] reaction with electrophiles,[40-42] and estimation of the position of the Schlenk equilibrium.[43-45] In our studies, we were interested in modeling the structure of Grignard reagents in solution. The resting solution structure, the energy of the solvation process and the process of solvent assisted ion-pair separation were of greatest interest to us. Such studies for organolithium compounds are known in the literature,[46] but such studies on Grignard reagents are rare.

Ehlers and co-workers performed early DFT studies on Grignard reagents in order to model the Schlenk equilibrium, predict the structure of their solvates in Et_2O solutions, and estimate the energies for the solvation by Et_2O.[47] Solvation of various Grignard species up to the disolvate level was attempted at the modified B-VWN-P DFT method. Furthermore, the energies of dimerization of these Grignard reagents in Et_2O were calculated since X-ray crystals structures for such compounds have been shown to be dimeric in Et_2O. Table 3-1 shows the energies of solvation and energies for dimerization for organomagnesium chlorides studied by the authors.

Table 3-1: Ehlers et al's B-VWN-P DFT studies towards solvation and dimerization of organomagnesium chlorides. [47]

Entry	Process	ΔE kcal.mol^{-1}
	$RMgCl + Et_2O \longrightarrow RMgCl{\cdot}Et_2O$	
1	$MeMgCl{\bullet}Et_2O$	-17.1
2	$EtMgCl{\bullet}Et_2O$	-16.7
3	$PhMgCl{\bullet}Et_2O$	-17.7
	$RMgCl{\cdot}Et_2O + Et_2O \longrightarrow RMgCl{\cdot}(Et_2O)_2$	
4	$MeMgCl{\bullet}(Et_2O)_2$	-11.6
5	$EtMgCl{\bullet}(Et_2O)_2$	-11.1
6	$PhMgCl{\bullet}(Et_2O)_2$	-13.3
	$2\ RMgCl \longrightarrow (RMgCl)_2$	
7	$(MeMgCl)_2$	-33.3
8	$(EtMgCl)_2$	-33.0
9	$(PhMgCl)_2$	-35.3
	$2\ RMgCl{\cdot}Et_2O \longrightarrow (RMgCl{\cdot}Et_2O)_2$	
10	$(MeMgCl{\bullet}Et_2O)_2$	-26.5
11	$(EtMgCl{\bullet}Et_2O)_2$	-27.2
12	$(PhMgCl{\bullet}Et_2O)_2$	-30.1

As can be seen (Table 3-1), addition of solvent on all Grignard species studied was exothermic. In addition, the first solvation step was always more exothermic than the

subsequent solvation steps (compare entries 1-3 with 4-6).[47] Energies for dimerization of the unsolvated and monosolvated monomer species were also calculated (entries 7-12). However, formation of these bis(μ-Cl) dimers from the solvated species was less preferred than from the unsolvated species. For all the organomagnesium chloride compounds studied, the disolvated *trans*- bis(μ-Cl) dimer species similar to **3-5** above were the most stable isomers at the disolvated level.

Recently the solution structures of methyl magnesium chloride (MeMgCl) in Et_2O were studied using RISM-MP2 calculation by Mori and co-workers.[48] The energies of various solvated species in Et_2O were compared at RISM-MP2 level. Figure 3-5 shows the three types of solvated species studied. The disolvated monomer species **3-17** was found to be the lowest energy structure between the compared species. Disolvated bis(μ-Cl) dimer **3-19** was calculated to be 4.7 kcal.mole^{-1} higher in energy than two monomers. An interesting trisolvated "linear" or "open" dimer featuring a single μ-Cl ligand was calculated to be similar in energy (0.9 kcal.mole^{-1}) to two monomers **3-17**. The authors thus suggested that the open dimer **3-18** was thus more likely to be dominant in Et_2O solutions than **3-19**.

Figure 3-5: μ_2–Chlorodimer species **3-17** and open linear dimer species **3-19** studied by Mori and co-workers. [48]

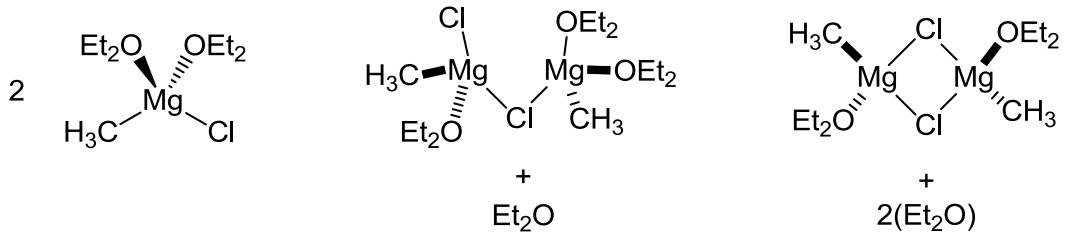

3-17 **0 kcal·mol-1**

3-18 **0.9 kcal·mol-1**

3-19 **4.7 kcal·mol-1**

We began our computations by re-investigating the structure of MeMgCl in Et_2O and Me_2O solvents to determine what the B3LYP method and 6-31G* basis set indicated for the resting solvation state. We begin by discussing the computational methods used for these calculations in the next section and then describe the results of our studies.

3.2 Computational Methods

All calculations were performed using the Gaussian 09 computational chemistry package.[49] The B3LYP method and 6-31G* basis set were chosen for all geometry and transition state optimizations. This basis set was chosen as a compromise between accuracy and computational economy for the large explicit solvates studied in this chapter. The B3LYP/6-31G* calculated geometries were characterized as a minima or transition structure by looking at the vibrational frequency analysis. While the ground state geometries should have zero imaginary frequencies, the transition structure geometries should have one imaginary frequency. The solvated Grignard reagents were studied by constructing multiple starting geometries of the explicit solvates. MP2/6-31G* single point energies at the B3LYP/6-31G* geometry were also determined. Free energy corrections at 195 K to the electronic energies were calculated from frequencies scaled by 0.9804, using the *freqchk* utility of Gaussian 09. Energies and free energies of solvation were calculated to predict equilibrium solvent numbers, as has been demonstrated in other studies.[7,13,22,23,46] Dimethyl ether (Me_2O) and diethyl ether (Et_2O) were the solvents of choice.

Although an exhaustive conformational analysis of all Et_2O solvates is beyond the scope of this study, an attempt at understanding the impact of the conformation of the Et_2O ligand on the electronic energy observed at B3LYP/6-31G* was made. Figure 3-6

shows the four structures of mono-solvated methylmagnesium chloride (MeMgCl) molecules each bearing a different conformation of the Et_2O ligand. No significant difference in the calculated electronic energies was observed at B3LYP/6-31G*. The electronic energies of all four structures were within <0.6 kcal.mol^{-1} from each other. Thus for this chapter, we assumed that the conformation of Et_2O would not significantly influence the electronic energies of the studied explicitly solvated molecules. As expected, the lowest energy conformer **3-20** featured an anti, anti (a, a) conformation of the Et_2O ligand. The highest energy conformer **3-21** was the one where the methyl groups had two gauche interactions (g^+, g^-), thus adopting a *syn*-pentane like conformation.

Figure 3-6: B3LYP/6-31G* optimized geometries and relative energies of mono-solvated monomers of MeMgCl possessing different conformations of solvent Et_2O. Selected bond lengths in Å.

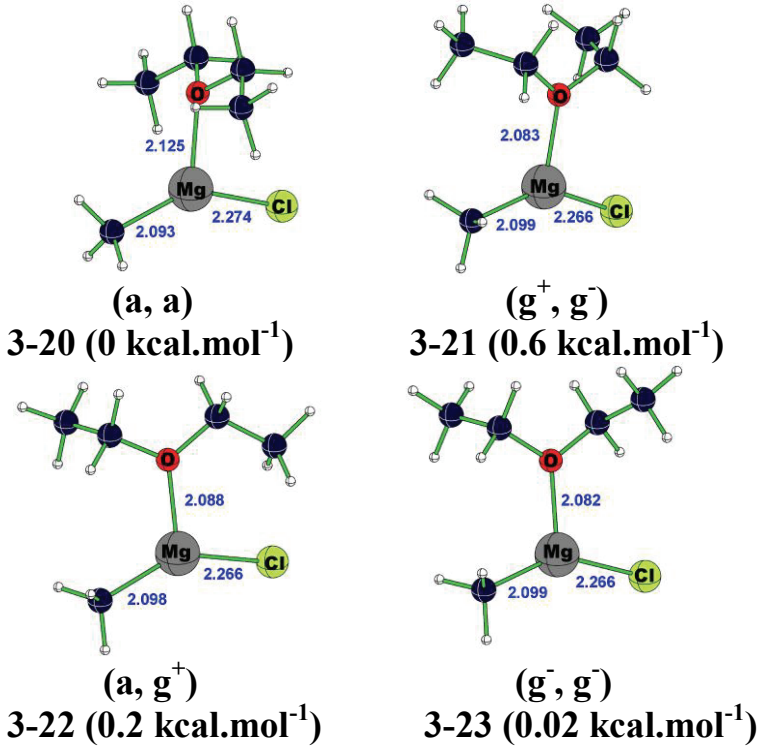

Using this knowledge, the explicit solvates with Et_2O were constructed so as to accommodate the lowest energy (a, a) conformer wherever it was possible. If accommodating this Et_2O conformer led to obvious steric interactions in the structure, the (a, g) or (g^-, g^-)/ (g^+, g^+) were chosen. The use of the (g+, g^-) conformer was avoided.

3.3 DFT studies on the solvation of methylmagnesium chloride (MeMgCl)

We first re-investigated the effect of sequential solvation on monomers and dimers of methyl magnesium chloride (MeMgCl). As discussed above in 3.1.3, computational investigations on the solvated Grignard reagents are rare. [48] The X-ray crystal structure and ebullioscopy experiments reviewed in section 3.1.1 above strongly suggest that organomagnesium chlorides exist as bis(μ-Cl) dimers in diethyl ether (Et_2O) solution at all concentrations. The effect of sequential solvation on the stability of the monomeric and dimeric structures of MeMgCl was studied to determine likely equilibrium solvation numbers. We decided to investigate the explicit solvation using dimethyl ether (Me_2O) and diethyl ether (Et_2O) as the solvent ligands. Owing to the wide array of structures observed for THF solvated Grignard reagents in the X-ray crystal structure analysis,[26] and dominance of the Schlenk equilibrium,[32] we did not study the solvation by THF.

3.3.1 Solvation of MeMgCl monomers

Effect of solvation on MeMgCl monomers with Me_2O and Et_2O was first studied by constructing the explicit solvates of these molecules up to the trisolvated level. B3LYP/6-31G* optimized geometries of the unsolvated and mono-solvates studied are shown in Figure 3-7. The magnesium atom goes from 2-coordinate and linear in the unsolvated structure **3-24** to 3-co-ordinate and planar in the mono-solvated structures **3-**

24•Me_2O and **3-24•Et_2O**. The addition of a solvent leads to slight elongation of the C-Mg and Mg-Cl bonds, as typically seen in solvated organolithium calculations. [46] Furthermore, the shorter bond C-O bond distances observed in Me_2O solvates as compared to Et_2O solvates suggests stronger solvation in the former solvent. In case of structure **3-24•Me_2O**, the solvent was nearly coplanar with the MeMgCl linear structure, while in **3-24•Et_2O** the solvent was orthogonal to the plane of the molecule. This orthogonal structure of **3-24•Et_2O** was found to be 0.4 kcal.mol^{-1} lower in energy than the coplanar structure.

Figure 3-7: B3LYP/6-31G* optimized geometries for unsolvated and mono-solvated structures of MeMgCl monomers. Selected bond lengths in Å.

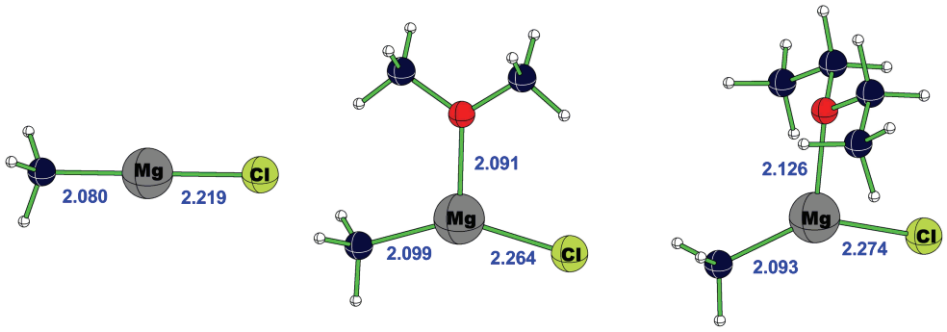

3-24 **3-24•Me_2O** **3-24•Et_2O**

On addition of one more solvent atom, the disolvate structures **3-24•$(Me_2O)_2$** and **3-24•$(Et_2O)_2$** are formed where the magnesium center now adopts a tetrahedral geometry. The addition of this extra solvent atom leads to further elongation of the C-Mg and Mg-Cl bonds compared to the monosolvates. Figure 3-8 shows the B3LYP/6-31G* optimized structures for these disolvates.

Figure 3-8: B3LYP/6-31G* optimized geometries for disolvated structures of MeMgCl monomers. Selected bond lengths in Å.

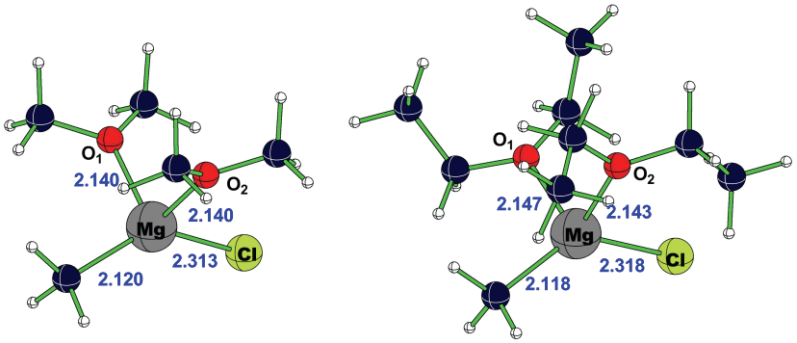

3-24•$(Me_2O)_2$ **3-24•$(Et_2O)_2$**

Further addition of solvent leads to the formation of trisolvates of MeMgCl, where the central magnesium atom now adopts a distorted trigonal bipyramidal structure. Although various starting geometries were explored, in the end only two minima were found: Figure 3-9 shows the B3LYP/6-31G* optimized structures. Calculations at B3LYP/6-31G* revealed that with Me_2O, structure **3-24•$(Me_2O)_3$ -A** which features the methyl and chloride ligands in the equatorial position, is the low energy structure. The other geometry located, **3-24•$(Me_2O)_3$-B** is 3.1 kcal.mole^{-1} higher in energy and features the methyl and chloride ligands in the axial positions. In case of Et_2O, the structure corresponding to **3-24•$(Me_2O)_3$–B** was not found at B3LYP/6-31G*. Instead two structures featuring equatorial methyl and chloride ligands were found, that differed in the conformation of the bound Et_2O ligands. Table 3-2 below summarizes the significant bond lengths in all the optimized structures above.

Figure 3-9: B3LYP/6-31G* optimized geometries for disolvated structures of MeMgCl monomers. Selected bond lengths in Å.

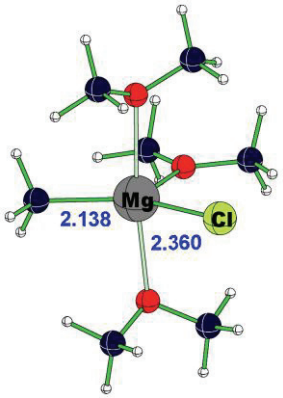

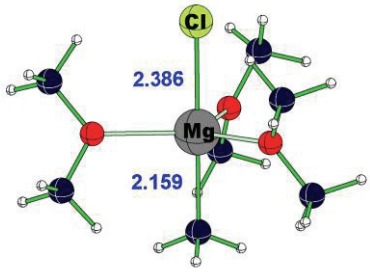

3-24•$(Me_2O)_3$ – A **3-24•$(Me_2O)_3$ - B**

Rel E: **(0 kcal.mol^{-1})** **(3.1 kcal.mol^{-1})**

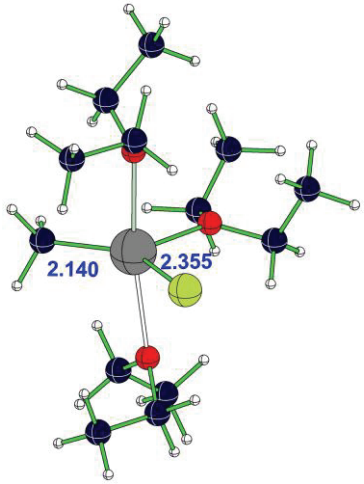

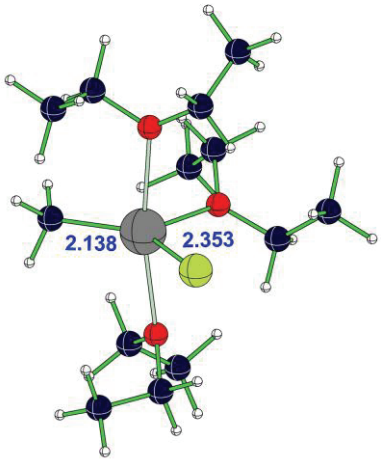

3-24•$(Et_2O)_3$ – A_1 **3-24•$(Et_2O)_3$ – A_2**

Rel E: **(0 kcal.mol^{-1})** **(1.4 kcal.mol^{-1})**

Table 3-2: Tabulation of the bond lengths of the significant bonds in B3LYP/6-31G* optimized structures of monomers **3-24** - **3-24•$(Et_2O)_3$ – B**.

Structure	Cl-Mg Å	Mg-CH_3 Å	O_1-Mg Å	O_2-Mg Å	O_3-Mg Å
3-24	2.219	2.080	-	-	-
3-24•Me_2O	2.264	2.099	2.091	-	-
3-24•Et_2O	2.274	2.093	2.126	-	-
3-24•$(Me_2O)_2$	2.313	2.120	2.140	2.140	-
3-24•$(Et_2O)_2$	2.318	2.118	2.147	2.143	-
3-24•$(Me_2O)_3$-A	2.360	2.138	2.321	2.319	2.136
3-24•$(Me_2O)_3$-B	2.386	2.159	2.288	2.288	2.288
3-24•$(Et_2O)_3$-A_1	2.355	2.140	2.462	2.334	2.155
3-24•$(Et_2O)_3$-A_2	2.353	2.138	2.369	2.414	2.147

The thermodynamics of the solvation in both Me_2O and Et_2O were then calculated from the electronic energies of the lowest energy optimized structures at B3LYP/6-31G*. However, since it is known that B3LYP/6-31G* solvation energies are artificially low for the third solvation of organolithium species,[46,50,51] MP2/6-31G* single point energies on B3LYP/6-31G* optimized geometries were calculated to provide a better estimate of the third solvation energies. In case of trisolvates, structures **3-24•$(Me_2O)_3$-A** and **3-24•$(Et_2O)_3$-A_1** were used for this calculation since they were the lowest energy conformers.

Table 3-3: Thermodynamics of solvation of MeMgCl monomers with Me_2O and Et_2O

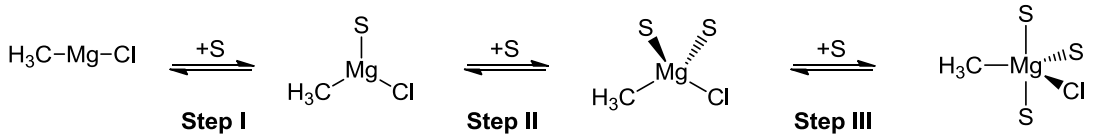

3-24

S= Me_2O; **3-24**•(Me_2O) S= Me_2O; **3-24**•(Me_2O)$_2$ S= Me_2O; **3-24**•(Me_2O)$_3$-**A**

S=Et_2O; **3-24**•(Et_2O) S=Et_2O; **3-24**•(Et_2O)$_2$ S=Et_2O; **3-24**•(Et_2O)$_3$-**A$_1$**

Entry	Method/Basis Set	Solvent	Solvation Step	ΔE_{solv} [a] kcal.mol^{-1}	ΔG_{solv} (195 K)[b, c] kcal.mol^{-1}
1	B3LYP/6-31G*	Me_2O	**I**	-21.9	-14.1
2			**II**	-16.7	-8.9
3			**III**	-5.3	4.2
4	MP2/6-31G* //B3LYP/6-31G*	Me_2O	**I**	-25.7	-17.9
5			**II**	-21.1	-13.2
6			**III**	-11.3	-1.8
7	B3LYP/6-31G*	Et_2O	**I**	-19.0	-11.5
8			**II**	-14.0	-4.2
9			**III**	-3.5	6.3
10	MP2/6-31G* //B3LYP/6-31G*	Et_2O	**I**	-24.0	-16.6
11			**II**	-19.5	-9.7
12			**III**	-11.8	-2.0

[a] Solvation energy ΔE_{solv} in kcal.mol^{-1} at B3LYP/6-31G*, [b] Solvation free energies were calculated from the free energy corrections (at 195 K) to the absolute energies, determined from B3LYP/6-31G* frequencies, scaled by 0.9804. [c] Free energy corrections from B3LYP/6-31G* used to calculate ΔG_{solv} at the MP2/6-31G*// B3LYP/6-31G* level.

The following observations can be made looking at the data in Table 3-3. Regardless of solvent (Me_2O or Et_2O) or solvation step, MP2/6-31G*// B3LYP/6-31G* solvation energies ΔE_{solv} are more exothermic than those from B3LYP/6-31G*. This difference is greatest for the third solvation; for Me_2O the difference is 6.0 kcal.mole^{-1}, and for Et_2O the difference is 8.3 kcal.mole^{-1}. Comparing to Ehler's studies of Et_2O solvation of MeMgCl,[47] the calculated (B3LYP/6-31G*) first and second solvation

energies are slightly (2-3 kcal.mol^{-1}) larger. Solvation free energies ΔG_{solv} are typically 7-8 kcal.mol^{-1} smaller than solvation energies ΔE_{solv}, reflecting the entropic cost of capturing a solvent ligand. Consequently at B3LYP/6-31G*, the third solvation is endergonic whereas at MP2/6-31G*//B3LYP/6-31G* is slightly exergonic.

However, a potential source of error in these calculations is the basis-set superposition error (BSSE), which is commonly found in calculations on reactions where two components combine to give adducts. There would be more basis functions employed in the calculation of the trisolvate species than the basis functions in the corresponding disolvate and solvent, leading to an artificial lowering in the reaction energy. Thus, the third solvation free energies at MP2/6-31G*//B3LYP/6-31G* may be artificially exergonic due to BSSE. Based on previous studies with THF solvates of organolithiums,[46] we expect a counterpoise correction of about +5 to +10 kcal.mol^{-1} for each Et_2O coordination. Thus the disolvate species are likely to be the resting solution structures, although the third solvation could be driven by mass action in pure ethereal solvent.

3.3.2 Solvation of MeMgCl dimers

As discussed in section 3.1 above, organomagnesium chlorides exist as dimers in diethyl ether solution.[19-21] The most common structure for these dimeric compounds observed by X-ray crystal structure is the bis(μ-Cl) dimer where the chlorine atoms form two bridges between the magnesium atoms. Also, as discussed in section 3.1, Mori et al. using the RISM-MP2 methods have studied the solvation of such dimeric structures in Et_2O.[48] In this section, we demonstrate our studies towards the modeling of solvation of bis(μ-Cl) dimers of MeMgCl at the B3LYP/6-31G* level.

As with the monomers in section 3.3.1, the solvation of dimer **3-25** up to the trisolvated species **3-25•(Me_2O)$_3$** and **3-25•(Et_2O)$_3$** was studied at B3LYP/6-31G*. Figure 3-10 shows the B3LYP/6-31G* optimized geometries for unsolvated and mono-solvated structures of MeMgCl bis (μ_2–Cl) dimer **3-25**.

Figure 3-10: B3LYP/6-31G* optimized geometries for unsolvated and mono-solvated structures of MeMgCl bis (μ_2–Cl) dimer **3-25**. Selected bond lengths in Å, signed quantities are the Mulliken charges.

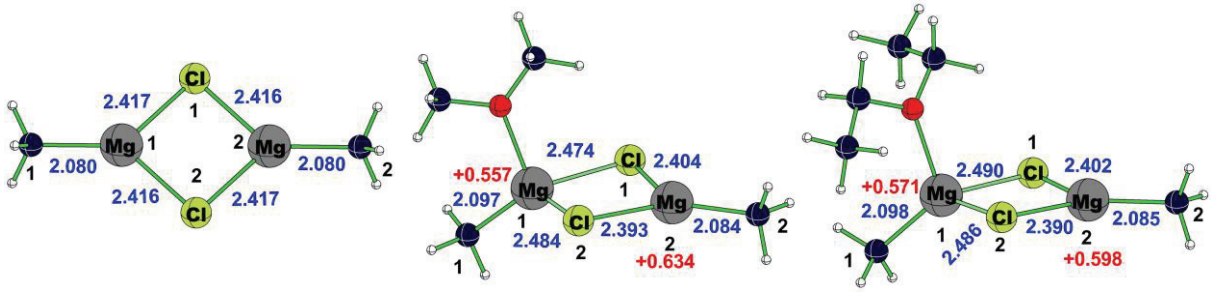

3-25 **3-25•Me_2O** **3-25•Et_2O**

The geometry of unsolvated dimer **3-25** was found to be planar with the central bridging chlorine atoms and the methyl carbons in the same plane. In the mono-solvated structures **3-25•(Me_2O)** and **3-25•(Et_2O)**, addition of a solvent molecule leads to a change in the geometry of the solvated magnesium atom to tetrahedral while the unsolvated atom stays in the planar 3-coordinate structure. Characteristic bond elongation along with distortion of the central 4-membered system is seen.

Addition of one more solvent atom to the monosolvated structures leads to the disolvates; the second molecule is logically added on the unsolvated magnesium atom since it has a higher Mulliken charge. There are two possible structures for the disolvates, first where the solvent ligands on the same face of the central 4-member bridged structure (*cis*-disolvates) and second where the solvent ligands are on opposite faces (*trans*-

disolvates). Figure 3-11 shows the B3LYP/6-31G* optimized geometries and relative energies of the four disolvate structures. As seen from the figure, the *trans*-disolvates in both these solvents were found to be highly symmetric as compared to the *cis*-disolvates. Also, comparison of the electronic energies showed that in both Me_2O and Et_2O the *trans*-disolvates were lower energy structures compared to the *cis*-disolvates.

Figure 3-11: B3LYP/6-31G* optimized geometries and relative energies for four disolvated structures of MeMgCl bis (μ_2–Cl) dimer **3-25**. Selected bond lengths in Å, signed quantities are the Mulliken charges.

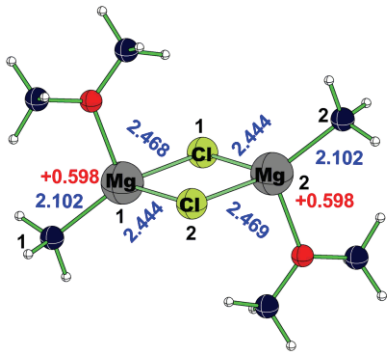

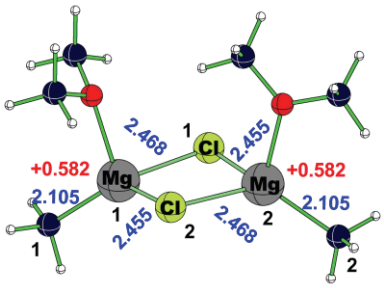

trans-**3-25•$(Me_2O)_2$** *cis*-**3-25•$(Me_2O)_2$**

Rel E: (0 kcal.mol^{-1}) (2.1 kcal.mol^{-1})

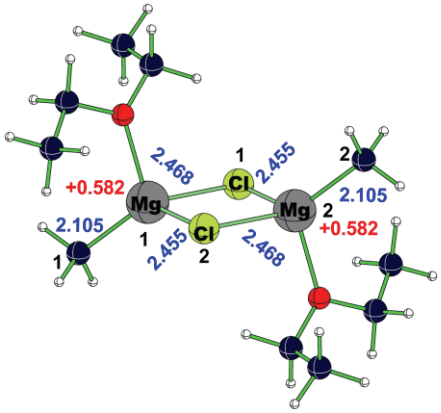

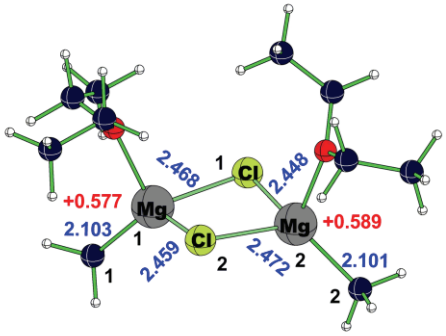

trans-**3-25•$(Et_2O)_2$** *cis*-**3-25•$(Et_2O)_2$**

Rel E: (0 kcal.mol^{-1}) (1.4 kcal.mol^{-1})

Finally, three different structure types were calculated for the trisolvates of these dimers at B3LYP-6-31G*. Here the third solvent can be added to either of the

magnesium atoms in the disolvate structure since they have equal Mulliken charges. The disolvated magnesium in these structures adopts trigonal bipyramidal geometry while the mono-solvated magnesium stays tetrahedral. Figure 3-12 shows the B3LYP/6-31G* optimized geometries and relative energies for the calculated trisolvate species.

Figure 3-12: B3LYP/6-31G* optimized geometries and relative energies for four disolvated structures of MeMgCl bis (μ_2–Cl) dimer **3-25**. Selected bond lengths in Å, signed quantities are the Mulliken charges.

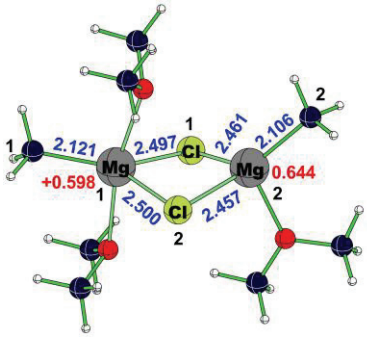

3-25•$(Me_2O)_3$-A
Rel E: (0 kcal.mol^{-1})

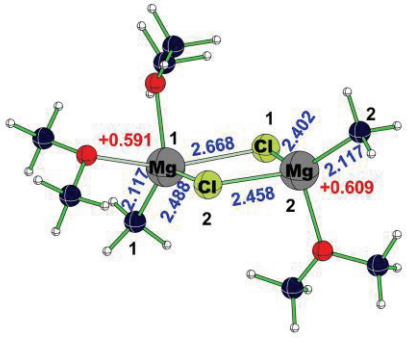

3-25•$(Me_2O)_3$-B
(0.6 kcal.mol^{-1})

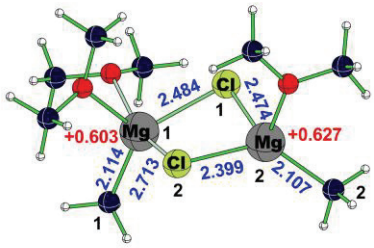

3-25•$(Me_2O)_3$-C
(3.0 kcal.mol^{-1})

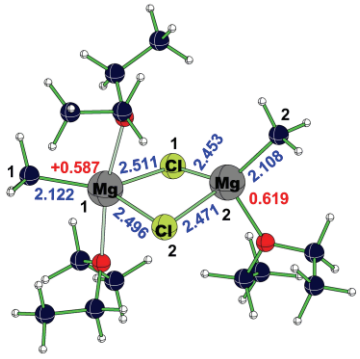

3-25•$(Et_2O)_3$-A
Rel E: (0 kcal.mol^{-1})

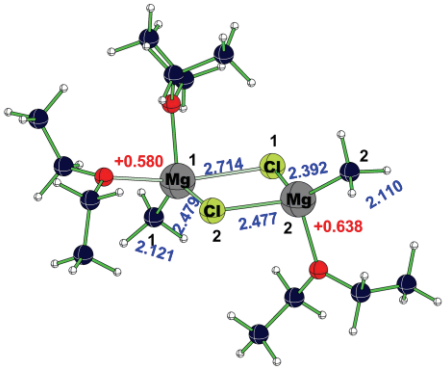

3-25•$(Et_2O)_3$-B
(0.5 kcal.mol^{-1})

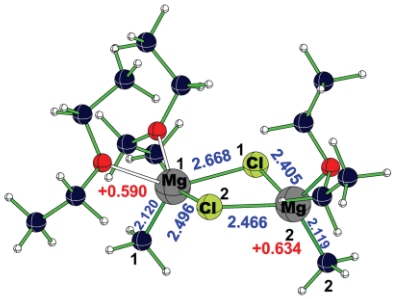

3-25•$(Et_2O)_3$-C
(4.0 kcal.mol^{-1})

In case of **3-25•$(Me_2O)_3$ –A** and **3-25•$(Et_2O)_3$-A**, the 5-coordinate Mg features an equatorial methyl and two axial solvent ligands. In **3-25•$(Me_2O)_3$ –B** and **3-25•$(Et_2O)_3$-**

B, the 5-coordinate magnesium features a methyl group in a pseudo axial position, that is either *trans* (B) or *cis* (C) to the methyl on the four coordinate magnesium. As seen above from the relative energies, structures, **3-25•$(Me_2O)_3$-A** and **3-25•$(Et_2O)_3$-A** were found to be the lowest energy trisolvates, and cis conformers **3-25•$(Me_2O)_3$-C** and **3-25•$(Et_2O)_3$-C** are the highest energy. Table 3-3 shows selected bond-lengths of the various solvated structures of MeMgCl bis(μ-Cl) dimers calculated at B3LYP/6-31G*. As seen with monomers, the Me_2O solvent ligands formed shorter bonds with the magnesium atoms than Et_2O ligands. However the O-Mg bond-lengths are not included in this table to maintain clarity and focus attention on the effect of solvation on the central dimeric structure.

Table 3-4: Tabulation of the bond lengths of the significant bonds in B3LYP/6-31G* optimized structures of monomers **3-25** - **3-25•$(Et_2O)_3$ – C**.

Structure [a]	C_1-Mg_1 Å	Mg_1-Cl_1 Å	Mg_1-Cl_2 Å	C_2-Mg_2 Å	Mg_2-Cl_2 Å	Mg_2-Cl_1 Å
3-25	2.080	2.417	2.416	2.080	2.417	2.416
3-25•Me_2O	2.097	2.474	2.484	2.084	2.393	2.404
3-25•Et_2O	2.098	2.490	2.486	2.085	2.390	2.402
cis-**3-25•$(Me_2O)_2$**	2.105	2.468	2.455	2.105	2.455	2.468
trans- **3-25•$(Me_2O)_2$**	2.102	2.468	2.444	2.102	2.469	2.444
cis-**3-25•$(Et_2O)_2$**	2.103	2.468	2.459	2.101	2.448	2.472
trans- **3-25•$(Et_2O)_2$**	2.105	2.468	2.455	2.105	2.455	2.468
3-25•$(Me_2O)_3$-A	2.121	2.497	2.500	2.106	2.457	2.461
3-25•$(Me_2O)_3$-B	2.117	2.668	2.488	2.117	2.458	2.402
3-25•$(Me_2O)_3$-C	2.114	2.484	2.713	2.107	2.399	2.474
3-25•$(Et_2O)_3$-A	2.122	2.511	2.496	2.108	2.471	2.453
3-25•$(Et_2O)_3$-B	2.121	2.714	2.479	2.110	2.477	2.392
3-25•$(Et_2O)_3$-C	2.120	2.668	2.496	2.119	2.466	2.405

[a] In all the structures above, Mg_1 is solvated in the solvent addition step.

Similar to the monomers, the thermodynamics of solvation of these dimeric structures by Me_2O and Et_2O were then studied at B3LYP/6-31G* and single point

MP2/6-31G*// B3LYP/6-31G* calculations. In case of the disolvates, the *trans* disolvate structures *trans*-**3-25•$(Me_2O)_2$** and *trans*-**3-25•$(Et_2O)_2$** were used for calculations while in case of trisolvates, structure **3-25•$(Me_2O)_3$-A and 3-25•$(Et_2O)_3$-A** were used for calculations as they were the lowest energy conformers of the studied structures.

Table 3-5: Thermodynamics of solvation of MeMgCl dimers with Me_2O and Et_2O

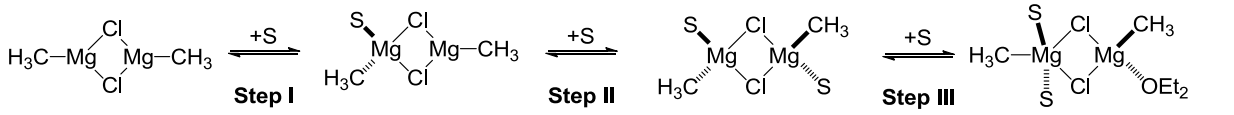

3-25

S= Me_2O; **3-25•**(Me_2O)
S=Et_2O; **3-25•**(Et_2O)

S= Me_2O; *trans*-**3-25•**(Me_2O)$_2$
S=Et_2O; *trans*-**3-25•**(Et_2O)$_2$

S= Me_2O; **3-25•**(Me_2O)$_3$-**A**
S=Et_2O; **3-25•**(Et_2O)$_3$-**A**

Entry	Method/Basis Set	Solvent	Solvation Step	ΔE_{solv} [a] kcal.mol^{-1}	ΔG_{solv} (195 K)[b, c] kcal.mol^{-1}
1			**I**	-19.9	-10.6
2	B3LYP/6-31G*	Me_2O	**II**	-19.4	-12.1
3			**III**	-6.4	3.3
4	MP2/6-31G*		**I**	-24.7	-15.3
5	//B3LYP/6-31G*	Me_2O	**II**	-24.7	-17.4
6			**III**	-12.1	-2.5
7			**I**	-17.7	-8.4
8	B3LYP/6-31G*	Et_2O	**II**	-16.5	-8.0
9			**III**	-4.4	5.3
10	MP2/6-31G*		**I**	-23.7	-14.4
11	//B3LYP/6-31G*	Et_2O	**II**	-23.0	-14.5
12			**III**	-12.0	-2.3

[a] Solvation energy ΔE_{solv} in kcal.mol^{-1} at B3LYP/6-31G*, [b] Solvation free energies were calculated from the free energy corrections (at 195 K) to the absolute energies, determined from B3LYP/6-31G* frequencies, scaled by 0.9804. [c] Free energy corrections from B3LYP/6-31G* used to calculate ΔG_{solv} at the MP2/6-31G*// B3LYP/6-31G* level.

Observations similar to monomers in Table 3-3 can be made. Regardless of solvent (Me_2O or Et_2O) or solvation step, MP2/6-31G*// B3LYP/6-31G* solvation energies ΔE_{solv} are more exothermic than those from B3LYP/6-31G*. This difference is greatest for the third solvation; for Me_2O the difference is 5.7 kcal.mole^{-1}, and for Et_2O the difference is 7.6 kcal.mole^{-1}. Solvation free energies ΔG_{solv} are typically 7-9 kcal.mol^{-1}

smaller than solvation energies ΔE_{solv}, reflecting the entropic cost of capturing a solvent ligand. Again at B3LYP/6-31G*, the third solvation is endergonic whereas at MP2/6-31G*//B3LYP/6-31G* is slightly exergonic. The artificial lowering of these energies by basis set superposition error (BSSE) is again a likely source of error. Thus, the third solvation free energies may be artificially exergonic at MP2/6-31G*//B3LYP/6-31G* due to BSSE. The disolvate species are thus likely to be the resting solution structures for these dimers. The third solvation however could be driven by mass action in pure ethereal solvent.

As discussed in section 3.1.2, Mori et al. have computationally shown a trisolvated open dimer species of MeMgCl bridging through only one chlorine atom.[48] The breaking of one of the chloride bridges leads to adoption of tetrahedral geometry by both the magnesium atoms. To see if such trisolvated open dimer species were lower in energy, we next studied these species at B3LYP/6-31G*. Figure 3-13 shows the B3LYP/6-31G* optimized geometries of these open dimers.

Figure 3-13: B3LYP/6-31G* optimized geometries of trisolvated open dimers. Selected bond lengths in Å, signed quantities are the Mulliken charges.

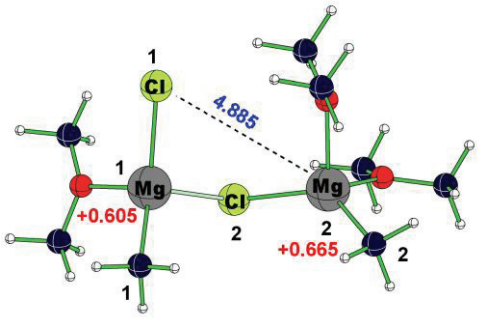

3-25•$(Me_2O)_3$-open

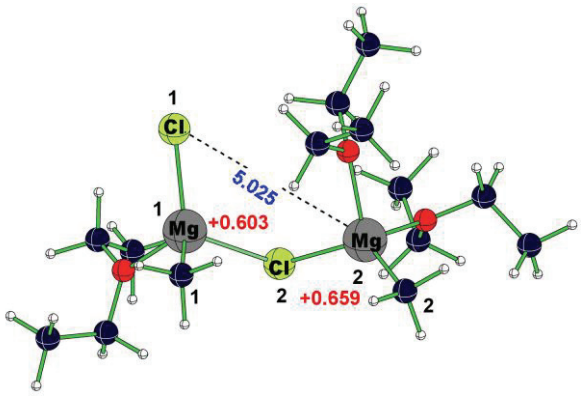

3-25•$(Et_2O)_3$-open

Table 3-6 shows the energy comparison between the lowest energy closed trisolvates and the open solvates. In both cases, the closed species **3-25•$(Me_2O)_3$-A** and **3-25•$(Et_2O)_3$-A** were found to be the lowest energy structures at B3LYP/6-31G*. The energy difference between the closed and open species was found to be 3.8 kcal.mol^{-1} in Me_2O and 3.5 kcal.mol^{-1} in Et_2O at B3LYP/6-31G*. We also tried the optimization of these open dimer structures starting with different starting geometries having different conformational arrangements of the ligands on the magnesium atoms, but in all cases geometry optimization led to the low energy closed trisolvated species. The relative free energies of the two species were calculated which again showed the relative preference for the closed dimer over the open dimer species.

Table 3-6: Relative energies of open and closed trisolvated dimers

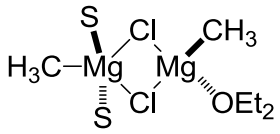

S= Me_2O; **3-25•$(Me_2O)_3$-A**
S=Et_2O; **3-25•$(Et_2O)_3$-A**

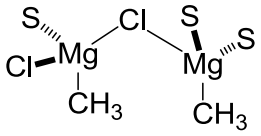

S= Me_2O; **3-25•$(Me_2O)_3$-open**
S=Et_2O; **3-25•$(Et_2O)_3$-open**

Entry	Method/Basis Set	Structure	Rel E [a] kcal.mol-1	Rel G (195K) [b] kcal.mol-1
1		**3-25•$(Me_2O)_3$-A**	0	0
2	B3LYP/6-31G*	**3-25•$(Me_2O)_3$-open**	3.8	2.5
3		**3-25•$(Et_2O)_3$-A**	0	0
4	B3LYP/6-31G*	**3-25•$(Et_2O)_3$-open**	3.5	3.1

[a] Calculated from the electronic energy relative to **3-25•$(Me_2O)_3$-A** and **3-25•$(Et_2O)_3$-A** at B3LYP/6-31G*, [b] Calculated from the free energy corrections (at 195 K) to the absolute energies, determined from B3LYP/6-31G* frequencies, scaled by 0.9804. Calculated relative to **3-25•$(Me_2O)_3$-A** and **3-25•$(Et_2O)_3$-A**.

In their investigations, Mori et.al had shown that the open trisolvate dimer structure **3-18** was more stable than the *trans*-disolvate **3-19** + Et_2O by 3.6 kcal.mol^{-1},

and concluded that this open species was the likely species in solution. However it is not clear if the authors made extensive efforts to locate the closed trisolvate structure in their studies. It seems that this species was neglected in attempts to protect the tetrahedral geometry of the magnesium atoms although, 5-coordinate bipyramidal geometries at magnesium center are known in the literature.[52] Figure 3-14 shows a comparison of the author's calculated energies at B3LYP/6-31G* and MP2/6-31G*// B3LYP/6-31G* levels and those obtained by Mori et al.[48] at RISM-MP2 level.

Figure 3-14: Comparison of energies of trisolvated open dimer with respect to the closed trisolvated dimer and disolvated dimer similar to those reported by Mori et. al.[48]

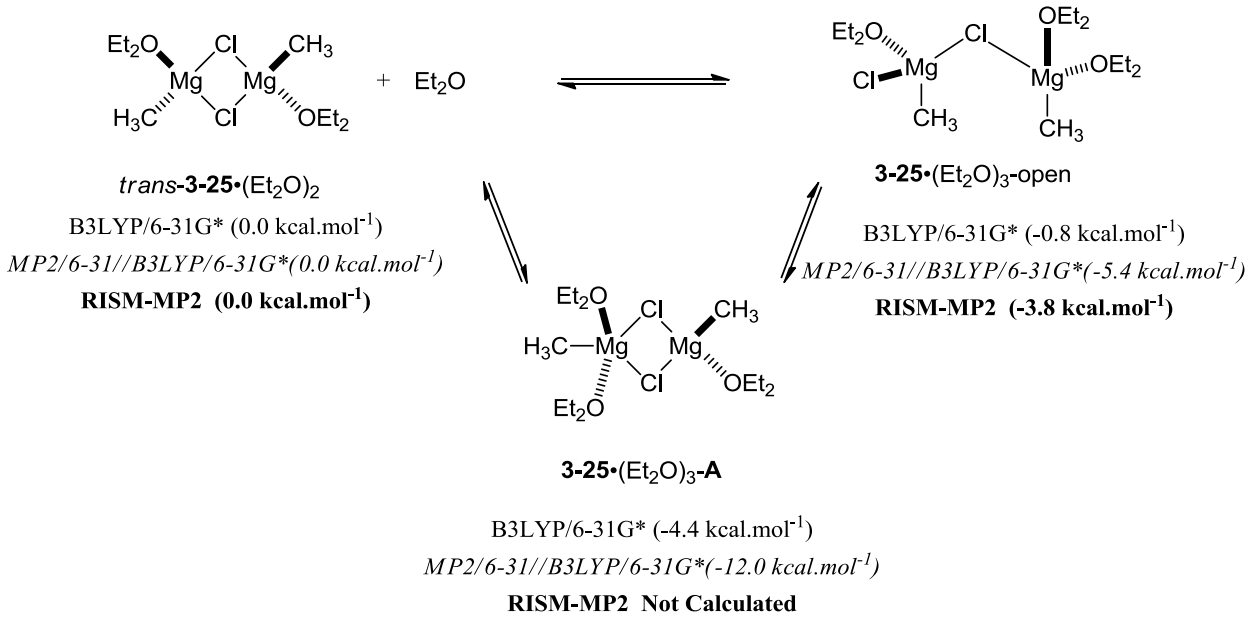

Similar to observations from Mori et al.,[48] the trisolvated open dimer species **3-25•**$(Et_2O)_3$-open was found to be lower in energy than the disolvate bis(μ-Cl) trans-**3-25•(Et_2O)** + Et_2O. The process was found to be more exoenergetic at MP2/6-31G*/B3LYP/6-31G* level (-5.4 kcal.mole^{-1}) than at the B3LYP/6-31G* level as observed in the solvation studies shown in Tables 3-4 and 3-5. However, our calculations

at both B3LYP/6-31G* and MP2/6-31G*// B3LYP/6-31G* levels suggested that the bis(μ-Cl) dimer species **3-25•$(Et_2O)_3$-A** was the lowest energy structure between the three studied species. At B3LYP/6-31G*, the open species **3-25•$(Et_2O)_3$-open** was 3.6 kcal.mol^{-1} higher in energy than the bis(μ-Cl) structure **3-25•$(Et_2O)_3$-A**. This number was significantly larger at the MP2/6-31G*// B3LYP/6-31G* level (6.6 kcal.mol^{-1}) Thus the conclusion drawn by Mori et. al that the tris-solvate open species was the resting solution structure of MeMgCl needs further inspection, with inclusion of the bis(μ-Cl) structure **3-25•$(Et_2O)_3$-A** in the study.

Significant information regarding solvation of these Grignard reagents was gained from this exercise of solvation of MeMgCl monomers and dimers. In addition, we were able to show that the solvation of these Grignard reagents in solution was exergonic up to the disolvated level in case of both monomers and dimers. The third solvation step however was ambiguous as seen from the solvation energies ΔE_{solv} and solvation free energies ΔG_{solv} (195 K) for both monomers and dimers. We would again note that the issue of BSSE makes a precise comparison difficult. We next studied the solvation of the magnesio cyclopropylcarbonitrile reagent **3-26**.

3.4 DFT studies on the solvation/ion-pair separation of 1-magnesio cyclopropylcarbonitrile.

3.4.1 Introduction and motivation

As concluded from our kinetic studies towards enantiomerization pathways of 1-magnesio-2, 2-diphenyl cyclopropylcarbonitrile **2-40**, the process of enantiomerization of **2-40** involves the transformation of a solvated heterodimeric species **2-54** to a higher solvated species **2-55** which then generates a solvent separated ion-pair species **2-56** that possibly enantiomerizes through carbanion inversion (Scheme 2.19, Chapter 2, section 2.8). To characterize similar solvated species and to model the ion-pair separation process, we next performed DFT investigations on the simplified analog 1-magnesio cyclopropylcarbonitrile **3-26.** Again, for reasons of computational economy, the B3LYP method and 6-31G* basis set were chosen. The computational studies of the corresponding NH_3-solvated organolithium species have been published,[53] and previous group member Dr. Yiqun Zhang reported studies of Me_2O solvates of the lithio species in her PhD thesis.[54]

Figure 3-15: 1-Magnesio cyclopropylcarbonitrile species analogous to **2-40**

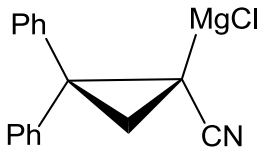

2-40

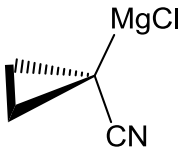

3-26

In this section, we first present our DFT studies of the various heterodimer structures possibly involved in the hypothetical Mg/Br exchange and trapping reactions of bromonitrile compound **3-31**. As concluded by our studies on the stoichiometry of

exchange/trapping reactions in Chapter 2 and looking at the pertinent literature on structure of organomagnesium chlorides in Et_2O solutions, a mixed dimeric species containing two Grignard reagents – the 1-magnesio-2,2-diphenyl cyclopropylcarbonitrile **2-40** and reagent *i*-PrMgCl was involved. Thus the primary emphasis of this study was to model the heterodimers of the cyclopropyl nitrile Grignard **3-26** with isopropyl magnesium chloride (*i*-PrMgCl). To find the resting solution structure of this species and the higher solvated species which was postulated to be involved in ion-pair separation, we then studied the stepwise solvation of these heterodimeric species adding one molecule of Me_2O or Et_2O at a time on the magnesium atoms. Ion-pair separated species generated from these higher solvated species were also examined.

3.4.2 Different unsolvated heterodimeric structures studied

As shown by our studies towards determining the reaction stoichiometry presented in Section 2.6, the initial Mg/Br exchange reaction between 1-bromo-2,2-diphenyl cyclopropylcarbonitrile **2-39** generates a mixed aggregate species of two Grignard reagents, **2-40** and *i*-PrMgCl. The study of possible structures for such mixed dimers (heterodimers) of the analogous 1-magnesio cyclopropylcarbonitrile **3-26** with the starting *i*-PrMgCl were first undertaken. Figure 3-16 shows the three limiting unsolvated heterodimeric structures calculated at B3LYP/6-31G*.

Figure 3-16: Different unsolvated heterodimeric structures modeled at B3LYP/6-31G*

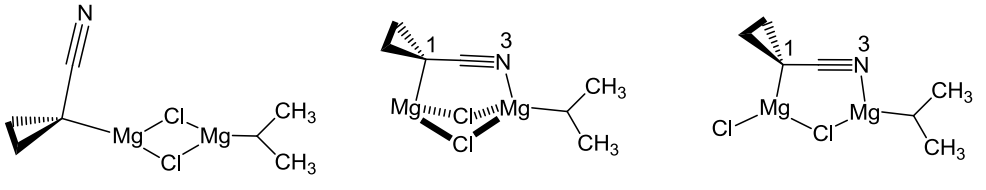

3-27 bis(μ-Cl)-η^1-(C)-cyclopropylnitrile

3-28 bis(μ-Cl)-μ(1,3)-cyclopropylnitrile

3-29 μ-Cl-μ(1,3)-cyclopropylnitrile

Structure **3-27** is the bis(μ-Cl)-η^1-(C)-cyclopropylnitrile formed by the two involved Grignard reagents similar to the bis(μ-Cl) homodimer X-ray crystal structures for RMgCl discussed in Section 3.1. Structure **3-28** involved a similar bis(μ-Cl) dimer moiety along with internal chelation through the nitrile nitrogen. Finally structure **3-29** was the μ-Cl-μ(1,3)-cyclopropylnitrile, reminiscent of the bridging nitrile on the dimer observed by Boche et al. for the analogous 1-lithio-2,2-dimethyl cyclopropylcarbonitrile discussed in Chapter 1.[55] Figure 3-17 shows the B3LYP/6-31G* optimized geometries for **3-27** – **3-29** and Table 3-8 shows selected bond-lengths in these structures.

Figure 3-17: B3LYP/6-31G* optimized geometries of unsolvated heterodimers. Selected bond lengths in Å, signed quantities are the Mulliken charges.

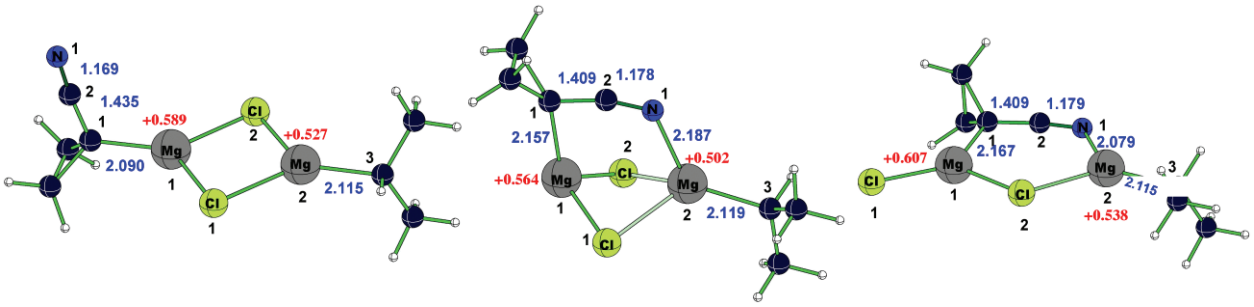

3-27
bis(μ-Cl)-η^1-(C)-cyclopropylnitrile

3-28
bis(μ-Cl)-μ(1,3)-cyclopropylnitrile

3-29
μ-Cl-μ(1,3)-cyclopropylnitrile

Table 3-8: Tabulation of the bond lengths of the significant bonds in B3LYP/6-31G* optimized structures of heterodimers **3-27** - **3-29**

Structure	C_1-Mg_1 Å	C_1-C_2 Å	C_2-N_1 Å	C_3-Mg_2 Å	N_1-Mg_2 Å
3-27	2.090	1.435	1.169	2.115	-
3-28	2.157	1.409	1.178	2.119	2.187
3-29	2.167	1.409	1.179	2.115	2.079

As seen from table 3-6, chelation through the nitrile nitrogen atom leads to a structural change in the nitrile functional group, which is clearly seen in the C_1-C_2 and

C_2-N_1 bond-lengths. Formation of the chelate leads to shortening of the C_1-C_2 bond and elongation of the C_1-N_1 bond as seen in keteniminate species discussed in Chapter 1. The second key feature observed is the elongation of the C_1-Mg_1 bond in the chelated structures. This elongation could potentially lead to bond rupture in the IPS step.

The electronic energies of these three structures calculated at B3LYP/6-31G* were then compared (Table 3-9). μ-Cl-μ(1,3)-cyclopropylnitrile dimer **3-29** was found to be the lowest energy heterodimer. The structure bis(μ-Cl)-μ(1,3)-cyclopropylnitrile **3-28** bearing two chloride bridges along with the nitrile bridge was 8.0 kcal.mole^{-1} higher in energy than **3-29**, indicating an energetic cost for formation of the second chloro bridge. Finally, the bis(μ-Cl)-η^1-(C)-cyclopropylnitrile **3-27** was 5 kcal.mol^{-1} higher in energy than **3-28**, indicating the energetic advantage of the bridging nitrile moiety in **3-28**.

Table 3-9: Relative electronic energies of unsolvated heterodimers **3-27**-**3-29** calculated at B3LYP/6-31G*.

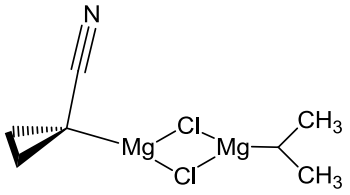

3-27

bis(μ-Cl)-η^1-(C)-cyclopropylnitrile

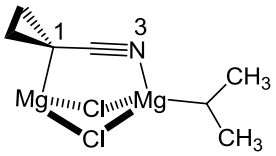

3-28

bis(μ-Cl)-μ(1,3)-cyclopropylnitrile

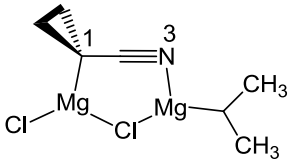

3-29

μ-Cl-μ(1,3)-cyclopropylnitrile

Entry	Method/Basis Set	Structure	Rel E [a] kcal.mol^{-1}
1	B3LYP/6-31G*	**3-27**	13.4
2		**3-28**	8.0
3		**3-29**	0

[a] Electronic Energy ΔE in kcal.mol^{-1} at B3LYP/6-31G*

We next examine how the relative energy of these structural types is affected by ethereal solvation.

3.4.3 Solvation of heterodimers by Me_2O and Et_2O

Heterodimers **3-27** – **3-29** were then solvated sequentially, using dimethyl ether (Me_2O) and diethyl ether (Et_2O). The first solvent molecule was added to the magnesium atom bearing the cyclopropyl ring since it had a higher positive Mulliken charge. The, first solvation step was found to be exoenergetic for all these heterodimers. As shown below, the di and trisolvates were also examined. The subsequent ion pair separation from the trisolvate species in Et_2O is then studied.

3.4.3.1 Mono-solvates of heterodimers 3-27 – 3-29

To begin with, addition of one solvent molecule on all three heterodimers was studied (Figure 3-18). The solvent (Me_2O and Et_2O) molecules were added on to the magnesium atom with the most positive Mulliken charge in the unsolvated structure (Figure 3-17).

Figure 3-18: Mono-solvated heterodimers **3-27 – 3-29**

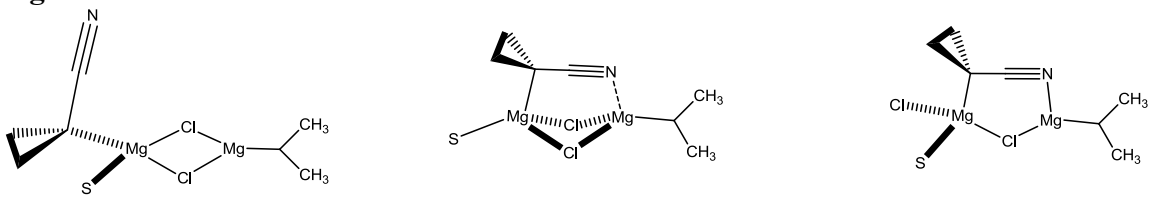

S= Me_2O; **3-27•Me_2O**
S=Et_2O; **3-27•Et_2O**

S= Me_2O; **3-28•Me_2O**
S=Et_2O; **3-28•Et_2O**

S= Me_2O; **3-29•Me_2O**
S=Et_2O; **3-29•Et_2O**

Figure 3-19 shows the optimized geometries for the three Me_2O-mono-solvated species **3-27•Me_2O** - **3-29•Me_2O** and the three Et_2O-mono-solvated species **3-27•Et_2O** - **3-29•Et_2O**. As can be seen in these structures the solvated magnesium atom is 4- co-ordinate and adopts a tetrahedral geometry whereas the unsolvated magnesium atom is 3-co-ordinate and adopts a planar geometry. In the bis(μ-Cl)-μ(1,3)-cyclopropylnitrile structures **3-28•Me_2O** and **3-28•Et_2O** on the other hand, both magnesium atoms are 4-

co-ordinate and adopt a tetrahedral geometry. This is a consequence of the bridging through the nitrile, which also leads to slight neutralization of the positive charge on the unsolvated magnesium as seen from the magnitude of the Mulliken charges on these atoms. Table 3-10 describes selected bond-lengths in these structures.

Figure 3-19: B3LYP/6-31G* optimized geometries and relative energies of mono-solvated heterodimers. Selected bond lengths in Å, signed quantities are the Mulliken charges.

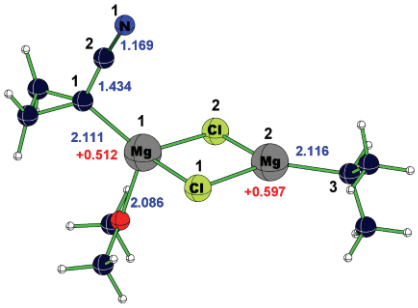

3-27•Me_2O

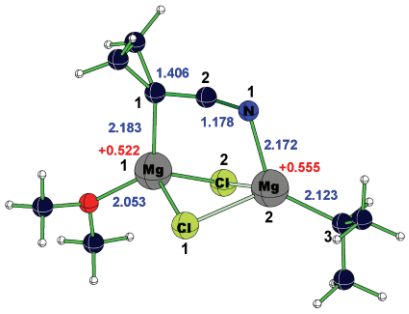

3-28•Me_2O

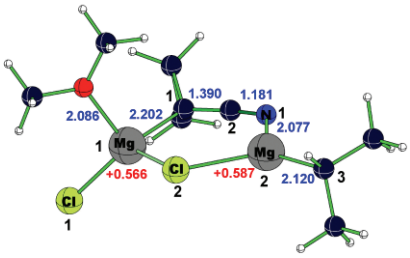

3-29•Me_2O

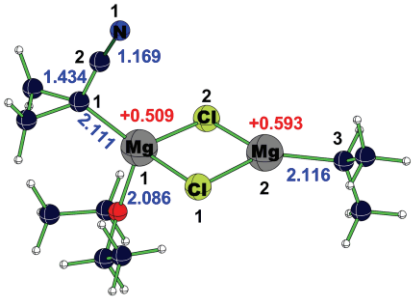

3-27•Et_2O

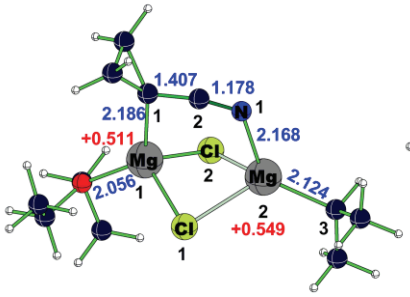

3-28•Et_2O

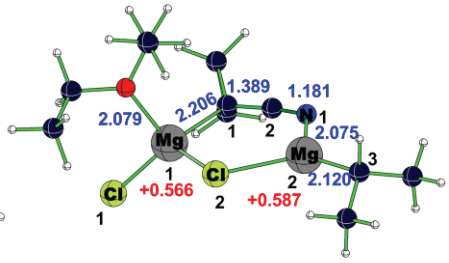

3-29•Et_2O

Table 3-10: Tabulation of the lengths of the significant bonds in B3LYP/6-31G* optimized structures of mono-solvated heterodimers

Structure	C_1-Mg_1 Å	C_1-C_2 Å	C_2-N_1 Å	C_3-Mg_2 Å	N_1-Mg_2 Å
3-27•Me_2O	2.111	1.434	1.169	2.116	-
3-28•Me_2O	2.183	1.406	1.178	2.123	2.172
3-29•Me_2O	2.202	1.390	1.181	2.120	2.077
3-27•Et_2O	2.111	1.434	1.169	2.116	
3-28•Et_2O	2.186	1.407	1.178	2.124	2.168
3-29•Et_2O	2.206	1.389	1.182	2.120	2.075

Finally, the calculated electronic energies of the mono-solvated species both in Me_2O and Et_2O were compared. Recall that for the unsolvated species, μ-Cl-μ(1,3)-cyclopropylnitrile **3-29** was found to be more stable than the bis(μ-Cl)-μ(1,3)-cyclopropylnitrile **3-28** by 8 kcal.mole^{-1} and more stable than bis(μ-Cl)-η^1-(C)-cyclopropylnitrile **3-27** by 13 kcal.mole^{-1}. The monosolvates of these species however are very similar in energy (Table 3-11).

Table 3-11: Relative energies of mono-solvated heterodimers **3-27•Me_2O -3-29•Et_2O**.

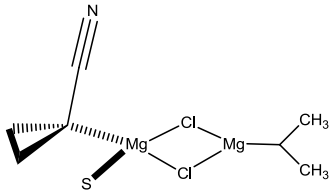

S= Me_2O; **3-27•Me_2O**
S=Et_2O; **3-27•Et_2O**

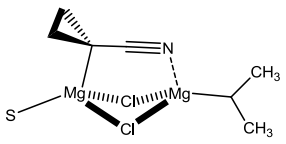

S= Me_2O; **3-28•Me_2O**
S=Et_2O; **3-28•Et_2O**

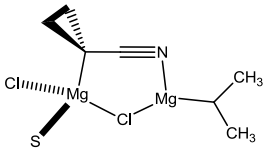

S= Me_2O; **3-29•Me_2O**
S=Et_2O; **3-29•Et_2O**

Entry	Method/Basis Set	Solvent	Structure	Rel E [a] kcal.mol^{-1}
1			**3-27•Me_2O**	0.1
2	B3LYP/6-31G*	Me_2O	**3-28•Me_2O**	0
3			**3-29•Me_2O**	0.2
4			**3-27•Et_2O**	0.6
5	B3LYP/6-31G*	Et_2O	**3-28•Et_2O**	0
6			**3-29•Et_2O**	2.0

[a] Electronic Energy ΔE in kcal.mol^{-1} at B3LYP/6-31G*

3.4.3.2 Disolvates of heterodimers

The monosolvates discussed above were then subject to solvation by one more solvent molecule. Comparison of the Mulliken charges in the mono-solvated structures **3-27•Me_2O - 3-29•Et_2O** showed that the magnesium atom bearing no solvent ligand had a higher positive Mulliken charge. The second solvent molecule was hence added on this magnesium atom. The disolvate μ-Cl-μ(1,3)-cyclopropylnitrile dimers **3-29•$(Me_2O)_2$** and **3-29•$(Et_2O)_2$** and bis(μ-Cl)-η^1-(C)-cyclopropylnitrile dimers **3-27•$(Me_2O)_2$** and **3-27•$(Et_2O)_2$** were both found at B3LYP/6-31G* (Figure 3-20). Interestingly, addition of the second solvent molecule on the mono-solvated *N*-chelated-bis(μ-Cl) dimers **3-28•Me_2O** and **3-28•Et_2O** results in breaking of the nitrile nitrogen chelation, giving the disolvated bis(μ-Cl) dimers **3-27•$(Me_2O)_2$** and **3-27•$(Et_2O)_2$**. Similar to the disolvates of MeMgCl discussed above, two types of disolvates are also possible in these cases, first where the two solvent ligands on the magnesium are on the same side (*cis*-disolvates), and second where they are on opposite faces (*trans*-disolvates).

Figure 3-20: Disolvates of heterodimers **3-27** and **3-29**.

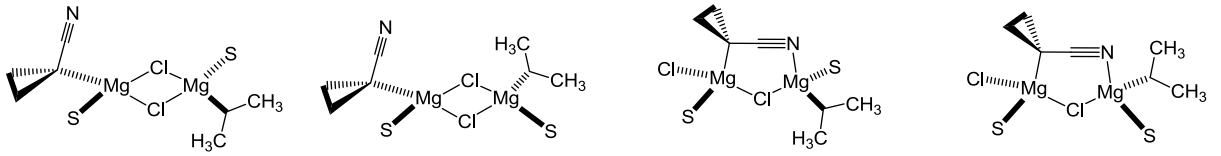

S= Me_2O; *cis*-**3-27•$(Me_2O)_2$**
S=Et_2O; *cis*-**3-27•$(Et_2O)_2$**

S= Me_2O; *trans*-**3-27•$(Me_2O)_2$**
S=Et_2O; *trans*-**3-27•$(Et_2O)_2$**

S= Me_2O; *cis*-**3-29•$(Me_2O)_2$**
S=Et_2O; *cis*-**3-29•$(Et_2O)_2$**

S= Me_2O; *trans*-**3-29•$(Me_2O)_2$**
S=Et_2O; *trans*-**3-29•$(Et_2O)_2$**

Figure 3-21 shows the optimized geometries for the disolvate species in Me_2O and Figure 3-22 shows the optimized geometries for the disolvates in Et_2O. As seen with mono-solvates above, addition of the solvent ligand on the magnesium atom leads to a change in its geometry from planar to tetrahedral. Both magnesium atoms in all the

disolvated dimers were found to be 4-coordinate and tetrahedral. The central bis(μ–Cl) bridge structure in **3-27•(Me$_2$O)$_2$** - **3-27•(Et$_2$O)$_2$** was found to be nearly planar with the solvent and alkyl ligands adopting the *cis*- and *trans*- geometries. Similarly the central μ-chloro and μ(1,3) nitrile bridges in **3-29•(Me$_2$O)$_2$** - **3-29•(Et$_2$O)$_2$** were nearly planar with the other chloride ligand and the isopropyl ligands along with the solvent molecules adopting the *cis*- and *trans*- geometries. Table 3-12 describes selected bond-lengths observed for all disolvate structures in Me_2O and Et_2O.

Figure 3-21: B3LYP/6-31G* optimized geometries of Me_2O-disolvates of heterodimers of **3-27** and **3-29**. Selected bond lengths in Å, signed quantities are the Mulliken charges.

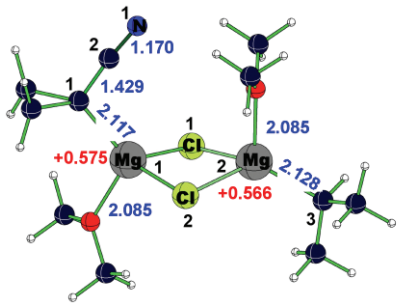

trans- **3-27•(Me$_2$O)$_2$**

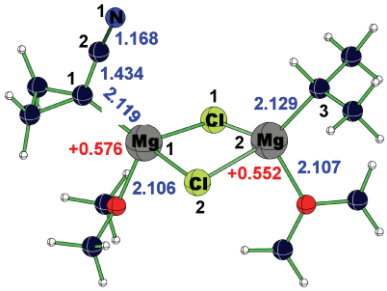

cis- **3-27•(Me$_2$O)$_2$**

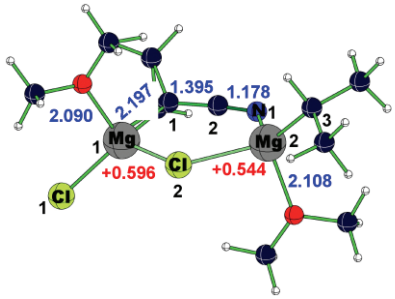

trans- **3-29•(Me$_2$O)$_2$**

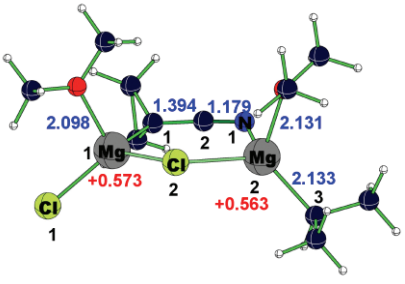

cis- **3-29•(Me$_2$O)$_2$**

Figure 3-22: B3LYP/6-31G* optimized geometries of Et_2O-disolvates of heterodimers of **3-27** and **3-29**. Selected bond lengths in Å, signed quantities are the Mulliken charges.

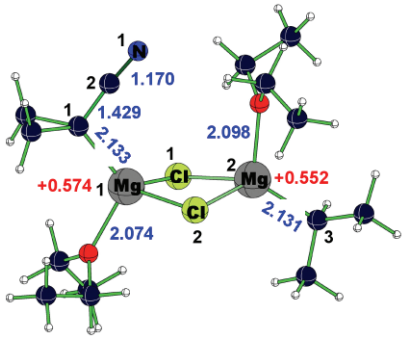

trans- **3-27•$(Et_2O)_2$**

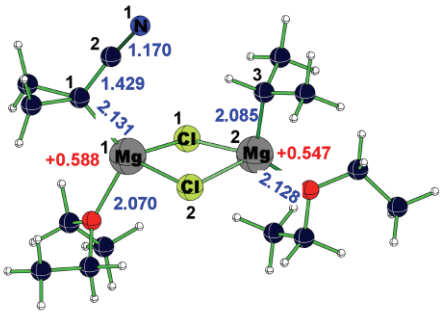

cis- **3-27•$(Et_2O)_2$**

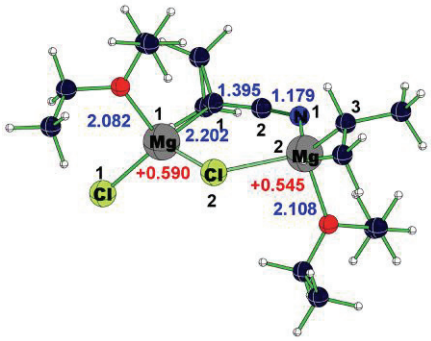

trans- **3-29•$(Et_2O)_2$**

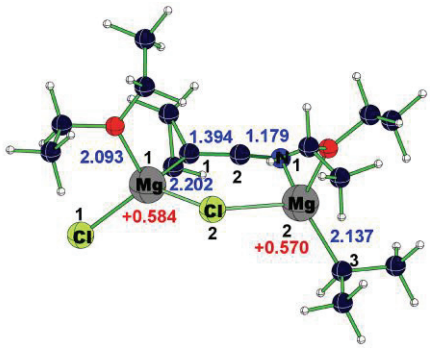

cis- **3-29•$(Et_2O)_2$**

Table 3-12: Tabulation of the bond lengths of the significant bonds in B3LYP/6-31G* optimized structures of disolvated heterodimers

Structure	**C_1-Mg_1** Å	**C_1-C_2** Å	**C_2-N_1** Å	**C_3-Mg_2** Å	**N_1-Mg_2** Å
trans-**3-27•$(Me_2O)_2$**	2.117	1.429	1.170	2.128	-
cis-**3-27•$(Me_2O)_2$**	2.119	1.434	1.168	2.129	-
trans-**3-29•$(Me_2O)_2$**	2.197	1.395	1.178	2.137	2.116
cis-**3-29•$(Me_2O)_2$**	2.200	1.394	1.179	2.131	2.116
trans-**3-27•$(Et_2O)_2$**	2.133	1.429	1.170	2.131	-
cis-**3-27•$(Et_2O)_2$**	2.131	1.429	1.170	2.085	-
trans-**3-29•$(Et_2O)_2$**	2.202	1.395	1.179	2.135	2.120
cis-**3-29•$(Et_2O)_2$**	2.202	1.394	1.179	2.137	2.118

The calculated electronic energies of these disolvates were then compared which showed that irrespective of the structure of the dimer and the attached solvent ligand, the *trans*-disolvate μ-Cl-μ(1,3)-cyclopropylnitrile species was the lowest energy isomer (Table 3-13). At this point, it was clear that the μ-Cl-μ(1,3)-cyclopropylnitrile heterodimers were more stable than the bis(μ-Cl) dimers under both solvated and unsolvated conditions. We thus considered that these structures were likely to be the actual structures of the heterodimers in solution. Thus all further studies were carried out using the μ-Cl-μ(1,3)-cyclopropylnitrile heterodimer structure.

Table 3-13: Relative energies of disolvated heterodimers **3-27-3-29**.

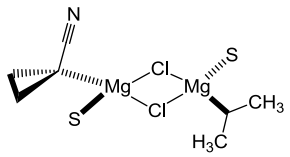

S= Me_2O; *cis*-**3-27•$(Me_2O)_2$**
S=Et_2O; *cis*-**3-27•$(Et_2O)_2$**

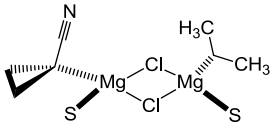

S= Me_2O; *trans*-**3-27•$(Me_2O)_2$**
S=Et_2O; *trans*-**3-27•$(Et_2O)_2$**

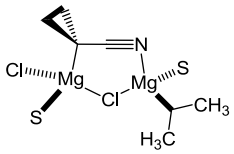

S= Me_2O; *cis*-**3-29•$(Me_2O)_2$**
S=Et_2O; *cis*-**3-29•$(Et_2O)_2$**

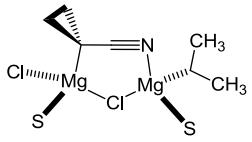

S= Me_2O; *trans*-**3-29•$(Me_2O)_2$**
S=Et_2O; *trans*-**3-29•$(Et_2O)_2$**

Entry	Method/Basis Set	Solvent	Structure	Rel E [a] kcal.mol^{-1}
1			***cis*- 3-27•$(Me_2O)_2$**	15.1
2			*trans*- **3-27•$(Me_2O)_2$**	7.7
3	B3LYP/6-31G*	Me_2O	*cis*- **3-29•$(Me_2O)_2$**	1.8
4			*trans*- **3-29•$(Me_2O)_2$**	0
5			*cis*- **3-27•$(Et_2O)_2$**	19.0
6			*trans*- **3-27•$(Et_2O)_2$**	7.9
7	B3LYP/6-31G*	Et_2O	*cis*- **3-29•$(Et_2O)_2$**	2.0
8			*trans*- **3-29•$(Et_2O)_2$**	0

[a] Electronic Energy ΔE in kcal.mol^{-1} at B3LYP/6-31G*

3.4.3.3 Trisolvates of μ-Cl-μ(1,3)-cyclopropylnitrile heterodimers

The further solvation of the lowest energy disolvated μ-Cl-μ(1,3)-cyclopropylnitrile dimers **3-29•$(Me_2O)_2$** - **3-29•$(Et_2O)_2$** discussed in the above section was then studied. The addition of the solvent molecule can now happen on any of the two magnesium atoms. The two structures arising from third solvation were first studied.

Figure 3-23: Trisolvates of μ-Cl-μ(1,3)-cyclopropylnitrile heterodimer **3-29**.

S= Me_2O; 3-29•$(Me_2O)_3$ - A
S=Et_2O; 3-29•$(Et_2O)_3$ - A

S= Me_2O; 3-29•$(Me_2O)_3$ - B
S=Et_2O; 3-29•$(Et_2O)_3$ - B

Figure 3-24 shows the optimized geometries for the two types of Me_2O and Et_2O trisolvates. As can be seen, the trisolvated magnesium Mg_1 is 5-coordinate and adopts a distorted trigonal bipyramidal geometry, while the other magnesium retains its tetrahedral geometry. As compared to the disolvated structures, the bonds between the solvent ligands and the magnesium atoms were slightly elongated in these trisolvate structures. Table 3-14 describes the significant bond-lengths for these four structures.

Figure 3-24: B3LYP/6-31G* optimized geometries of trisolvated heterodimers **3-29**.

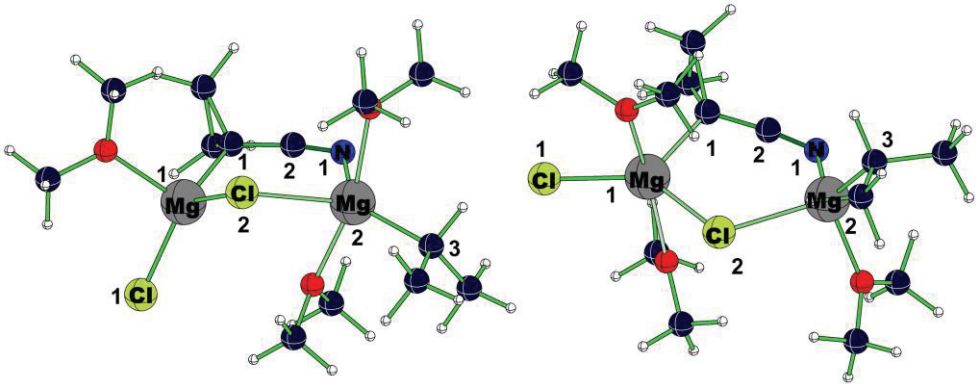

3-29•$(Me_2O)_3$ - A **3-29•$(Me_2O)_3$- B**

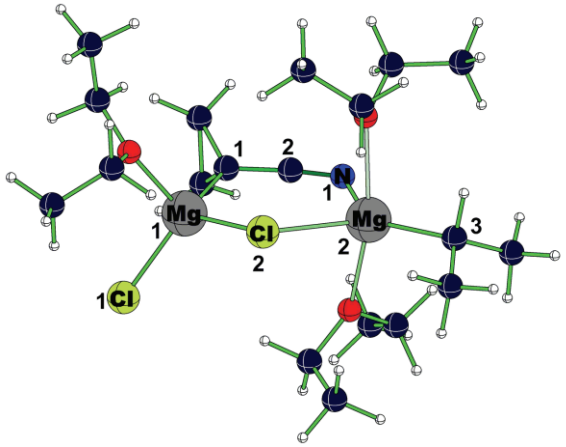

3-29•$(Et_2O)_3$ - A

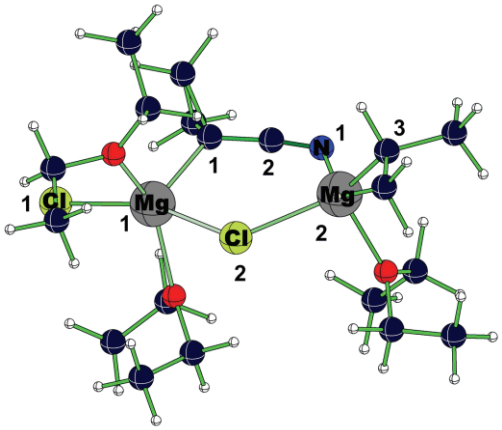

3-29•$(Et_2O)_3$ - B

Table 3-14: Tabulation of the bond lengths of the significant bonds in B3LYP/6-31G* optimized structures of disolvated heterodimers [a]

Structure	**C_1-Mg_1** Å	**C_1-C_2** Å	**C_2-N_1** Å	**C_3-Mg_2** Å	**N_1-Mg_2** Å
3-29•$(Me_2O)_3$ - A	2.203	1.397	1.178	2.159	2.164
3-29•$(Me_2O)_3$ - B	2.235	1.390	1.181	2.137	2.107
3-29•$(Et_2O)_3$ - A	2.206	1.400	1.177	2.169	2.164
3-29•$(EtO)_3$ - B	2.224	1.392	1.180	2.139	2.108

[a] In structures type A above Mg_2 is the one that the new solvent molecule has been added while in structure type B, Mg_1 is the one that the new solvent molecule has been added

The electronic energies of the possible trisolvates in both solvents **3-29•$(Me_2O)_3$ - 3-29•$(Et_2O)_3$** at B3LYP/6-31G* were compared which showed that irrespective of the solvent ligand, a very small preference exists for the trisolvated structures **3-29•$(Me_2O)_3$ –B** and **3-29•$(Et_2O)_3$ –B** (Table 3-15), where the third solvent molecule is added on the magnesium atom attached to the cyclopropyl ring.

Table 3-15: Relative electronic energies of trisolvated heterodimers.

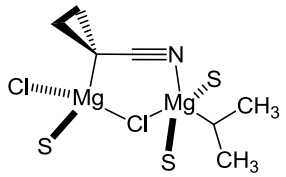

S= Me_2O; 3-29•$(Me_2O)_3$ - A
S=Et_2O; 3-29•$(Et_2O)_3$ - A

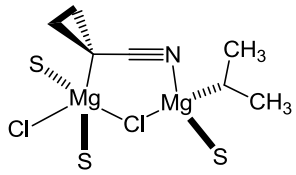

S= Me_2O; 3-29•$(Me_2O)_3$ - B
S=Et_2O; 3-29•$(Et_2O)_3$ - B

Entry	Method/Basis Set	Solvent	Structure	Rel E [a] kcal.mol^{-1}
1			**3-29•$(Me_2O)_3$-A**	0.9
2	B3LYP/6-31G*	Me_2O	**3-29•$(Me_2O)_3$-B**	0
3			**3-29•$(Et_2O)_3$-A**	0.5
4	B3LYP/6-31G*	Et_2O	**3-29•$(Et_2O)_3$-B**	0

[a] Electronic Energy ΔE in kcal.mol^{-1} at B3LYP/6-31G*

The further studies of the solvent assisted ion-pair separation were performed from the solvates of these μ-Cl-μ(1,3)-cyclopropylnitrile heterodimer. But before we discuss the ion-pair separation, first it is important to estimate the resting solution structure of these dimers, and the involved higher solvated species postulated by our kinetic studies. To make this estimation, the thermodynamics of each solvation step is first studied.

3.4.4 Thermodynamics of solvation of μ-Cl-μ(1,3)-cyclopropylnitrile heterodimers

The energy compensation (ΔE_{solv}) involved during each solvation step of the most stable μ-Cl-μ(1,3)-cyclopropylnitrile heterodimers was calculated from the electronic energies of the mono, di and trisolvates at B3LYP/6-31G* and MP2/6-31G*//B3LYP/6-31G* single point levels (Table 3-16).

Table 3-16: Thermodynamics of sequential solvation of μ-Cl-μ(1,3)-cyclopropylnitrile heterodimer **3-29**

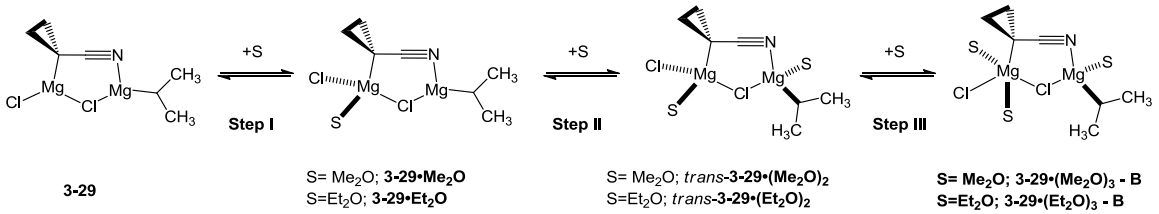

Entry	Method/Basis Set	Solvent	Solvation Step	ΔE_{solv} [a] kcal.mol^{-1}	ΔG_{solv} (195 K)[b] kcal.mol^{-1}
1			**I**	-21.9	-14.5
2	B3LYP/6-31G*	Me_2O	**II**	-19.4	-11.9
3			**III**	-8.4	4.4
4	MP2/6-31G*		**I**	-27.4	-20.0
5	//B3LYP/6-31G*	Me_2O	**II**	-25.5	-18.0
6			**III**	-14.5	-1.6
7			**I**	-20.0	-11.3
8	B3LYP/6-31G*	Et_2O	**II**	-17.8	-9.0
9			**III**	-1.7	8.4
10	MP2/6-31G*		**I**	-26.5	-18.1
11	//B3LYP/6-31G*	Et_2O	**II**	-25.1	-16.3
12			**III**	-10.9	-0.8

[a] Solvation energy ΔE_{solv} in kcal.mol^{-1} at B3LYP/6-31G*, [b] Solvation free energies were calculated from the free energy corrections (at 195 K) to the absolute energies, determined from B3LYP/6-31G* frequencies, scaled by 0.9804. [c] Free energy corrections from B3LYP/6-31G* used to calculate ΔG_{solv} at the MP2/6-31G*// B3LYP/6-31G* level.

Observations similar to the solvation studies on MeMgCl monomers and dimers discussed in Table 3-3 and Table 3-5 can again be made in this case. Regardless of solvent (Me_2O or Et_2O) or solvation step, MP2/6-31G*// B3LYP/6-31G* solvation energies ΔE_{solv} are more exothermic than those from B3LYP/6-31G*. This difference is greatest for the third solvation; in Me_2O the difference is 6.1 kcal.mole^{-1}, and in Et_2O the

difference is 9.2 kcal.mole^{-1}. Solvation free energies ΔG_{solv} are typically 7-9 kcal.mol^{-1} smaller than solvation energies ΔE_{solv}, reflecting the entropic cost of capturing a solvent ligand. Again at B3LYP/6-31G*, the third solvation is endergonic whereas at MP2/6-31G*//B3LYP/6-31G* it is slightly exergonic. However, again the influence of BSSE should be considered due to which these numbers might be artificially lowered. Also similar to MeMgCl dimers it can be deduced that the disolvates are the resting solution species whereas the third solvation step may be driven by mass action although it has very small energy preference.

Based on these studies, we postulated that the disolvate structure *trans*-**3-29•$(Et_2O)_2$** was likely to be the resting solution structure of the heterodimer at low concentration of Et_2O (i.e $[Et_2O]$ = 1 M). The further solvation of this species to **3-29•$(Et_2O)_3$ – B** could be the first step towards formation of the SIP species (Scheme 3-2) and might be favorable in bulk Et_2O. In Et_2O, this trisolvated structure **3-29•$(Et_2O)_3$-B** undergoes an ion-pair separation to yield the separated ion-pair (SIP) species **3-33•$(Et_2O)_3$** through $C_{cyclopropyl}$-Mg bond cleavage which then enantiomerizes through carbanion inversion. Note that the high co-ordination number of the cyclopropyl bearing magnesium atom in **3-29•$(Et_2O)_3$-B** may facilitate IPS both sterically and electronically.

Scheme 3-2: Resting solvation structure *trans*-**3-29•(Et$_2$O)$_2$** and postulated higher solvated species **3-29•(Et$_2$O)$_3$-B**

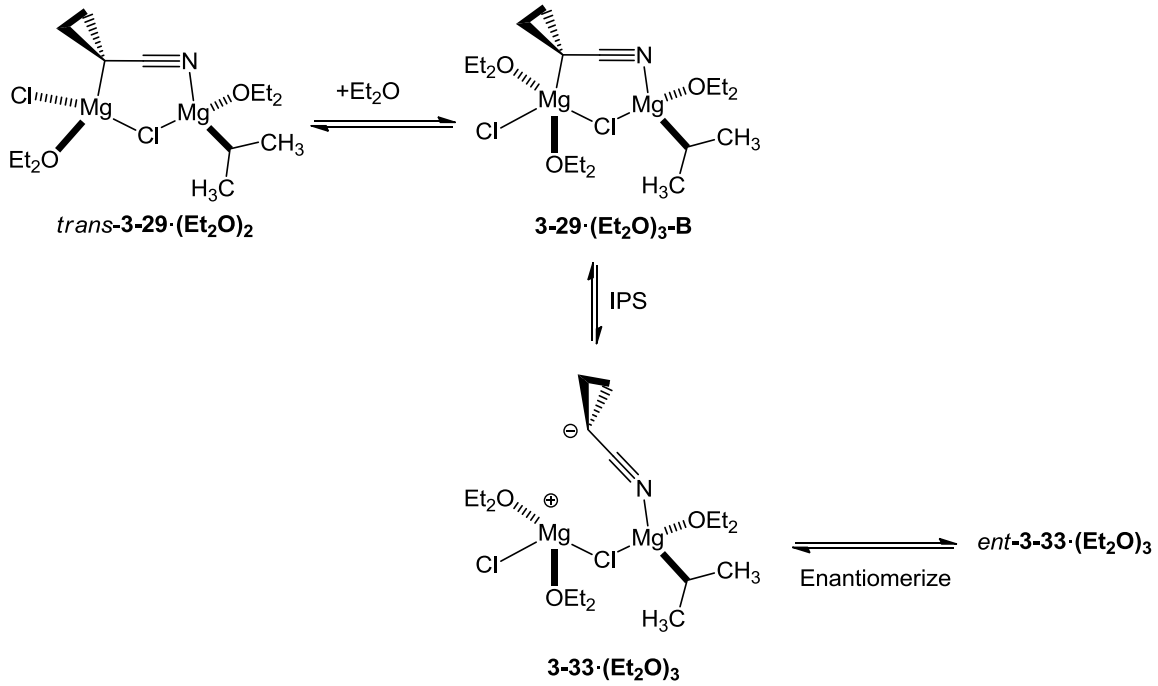

3.4.5 Ion-pair separation from trisolvate species 3-29•(Et$_2$O)$_3$-B in Et$_2$O

As explained above, the trisolvate species **3-29•(Et$_2$O)$_3$-B** was the proposed higher solvate species that undergoes ion-pair separation to yield the separated ion-pair species (SIP) **3-33•(Et$_2$O)$_3$** through cleavage of the $C_{cyclopropyl}$-Mg bond. The SIP species **3-33•(Et$_2$O)$_3$** was located at B3LYP/6-31G*. We also located the structure of the bond breaking transition state **3-32•(Et$_2$O)$_3$** involved in the formation of **3-33•(Et$_2$O)$_3$** from the trisolvate species **3-29•(Et$_2$O)$_3$-B**. The sole imaginary frequency of this transition structure corresponded to the breaking of the C_α-Mg bond. Figure 3-25 shows the optimized geometries for the ground state trisolvate **3-29•(Et$_2$O)$_3$-B**, the IPS transition state structure **3-32•(Et$_2$O)$_3$** and the separated ion pair (SIP) species **3-33•(Et$_2$O)**. Table 3-17 describes selected bond-lengths in these structures. Several bond-lengths change in

predictable ways as the contact ion-pair **3-29•$(Et_2O)_3$-B** undergoes ion-pair separation. First of all, a dramatic increase is seen in the lengths of the C_1-Mg_1 distances, as expected.

Figure 3-25: B3LYP/6-31G* Optimized geometries for the ground state trisolvate structure **3-29•$(Et_2O)_3$-B**, IPS transition structure **3-32•$(Et_2O)_3$** and SIP species **3-33•$(Et_2O)_3$**. NIMAG = number of imaginary frequencies calculated, signed quantities are the Mulliken charges.

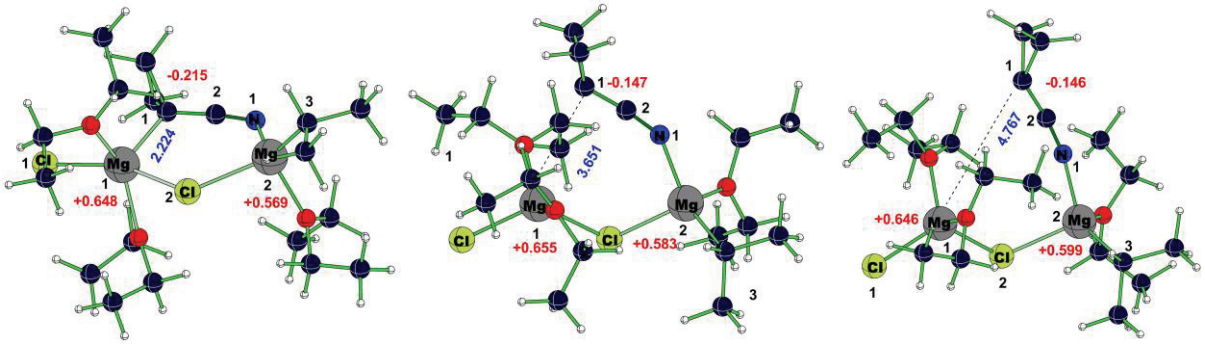

(μ = 5.331 D)
3-29•$(Et_2O)_3$-B

(μ = 4.988 D)
3-32•$(Et_2O)_3$
(NIMAG =1)

(μ = 4.640 D)
3-33•$(Et_2O)_3$

Table 3-17: Tabulation of the bond lengths of the significant bonds in B3LYP/6-31G* optimized structures of trisolvated heterodimers

Structure	C_1-Mg_1 Å	C_1-C_2 Å	C_2-N_1 Å	C_3-Mg_2 Å	N_1-Mg_2 Å	O_1-Mg_1 Å	O_2-Mg_1 Å
3-29•$(Et_2O)_3$-B	2.224	1.392	1.180	2.139	2.108	2.178	2.216
3-32•$(Et_2O)_3$ (TS)	3.651	1.358	1.193	2.147	2.040	2.079	2.069
3-33•$(Et_2O)_3$ (SIP)	4.767	1.355	1.193	2.145	2.035	2.056	2.050

Secondly, during this process, the C_1-C_2 and C_2-N_1 bond lengths shorten and lengthen respectively, to reflect the change from a *C*-metalated nitrile in **3-29•$(Et_2O)_3$-B** to a *N*-metalated keteniminate-like structure in **3-29•$(Et_2O)_3$**. Cleavage of the $C_{cyclopropyl}$-Mg bond is accompanied by a geometry change in the disolvated magnesium atom back to the tetrahedral geometry as observed for all 4-co-ordinate magnesium studied in this chapter. The lengths of the O-Mg_1 bonds decrease as the geometry changes to tetrahedral, reflecting additional electron donation by the ether ligands at the lower coordination number.

Interestingly, the separated ion pair **3-32•$(Et_2O)_3$** retains pyramidalization of the cyclopropyl carbanion. Nevertheless, the slight shortening of the C_1-C_2 bond and the slight elongation of the C_2-C_N bond compared to the trisolvate contact ion-pair species **3-29•$(Et_2O)_3$-B** suggest partial delocalization of the formal negative charge from the carbanion onto the nitrile nitrogen. The calculated Mulliken charges on both magnesium atoms and the cyclopropyl carbon atom along with the estimated dipole moments from these charges are listed in Figure 3-25. However, these calculated dipole moments are not what we anticipated since they do not depict the expected increased dipole in the SIP species **3-33•$(Et_2O)_3$**, based on the electrostriction argument presented for such processes in Chapter 2. Although these numbers do not match our expectation, it is well known that the concept of atomic charge is not unambiguously defined in quantum chemistry; Mulliken charges are simply one type of atomic charge, based on one type of population model.[56,57] Thus exploration of other population models (e.g. Natural Bond Order analysis) would be a logical next step.

The calculated reaction coordinate for the process of ion-pair separation is shown

in Figure 3-26. An activation energy $\Delta E_{IPS}^{\ddagger}$ of 14.9 kcal.mol^{-1} was found for the IPS process. The activation free energy ($\Delta G_{IPS}^{\ddagger}$) at 195 K was then determined from the calculated frequencies and found to be 14.3 kcal.mol^{-1}. This number is close to the experimentally determined activation free energy ($\Delta G_{enant}^{\ddagger}$) at 195 K for enantiomerization of related Grignard **2-40** (bearing two phenyl substituents, 15.5 ± 0.05 kcal.mol^{-1}). Yet it must be remembered that our calculated reaction path for ion-pair separation is based on calculations of a solvated Grignard heterodimer in-vacuo. In contrast, our experimental studies of **2-40** were performed in ether-toluene mixtures, and these studies indicated a key role for solvent reorganization during the rate-determining step of enantiomerization. In this case, the entropic cost of solvent reorganization is balanced by an enthalpic benefit. Thus the surprisingly close calculated vacuum $\Delta G_{IPS}^{\ddagger}$ and experimentally determined solution-phase $\Delta G_{enant}^{\ddagger}$ may either be a coincidence, or an example of enthalpy-entropy compensation.[58] To address these issues, one approach would be to reoptimize all the species in Table 3.17 with some form of continuum solvent model.[46] However, this approach is not expected to effectively reproduce the full enthalpic benefit of electrostriction. When economic methods for fully quantum molecular dynamics become available, perhaps the present system (in a box of Et_2O molecules) would provide a useful test case.

Figure 3-26: Reaction coordinate for ion-pair separation from **3-29•$(Et_2O)_3$** calculated at B3LYP/6-31G*. E= electronic energies of the calculated structures.

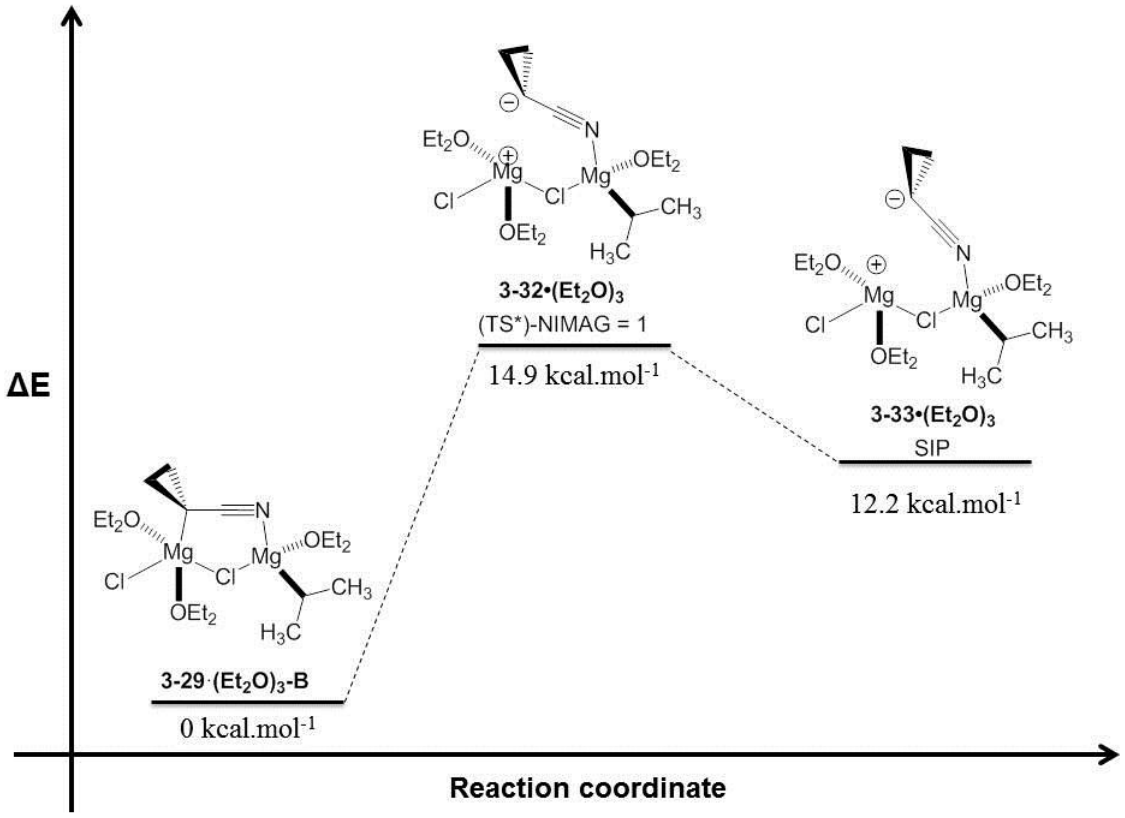

To address the possibility of a further solvated species to be involved in the process of ion-pair separation, we studied the corresponding tetrasolvated species. The species **3-29•$(Et_2O)_4$** was located at B3LYP/6-31G*. The optimized geometry of this tetrasolvate is shown in Figure 3-27. All the structural features of the trisolvate species **3-29•$(Et_2O)_3$** except the lengths of the O-Mg bond are maintained in **3-29•$(Et_2O)_4$**.

Figure 3-27: Optimized geometry for the tetrasolvated species **3-29•$(Et_2O)_4$** at B3LYP/6-31G* and thermodynamics of the fourth solvation of **3-29**

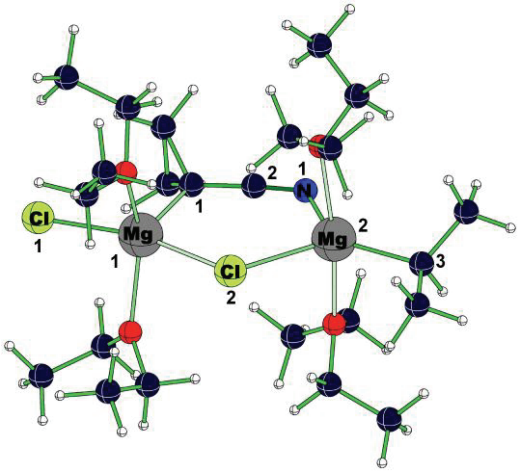

3-29•$(Et_2O)_4$

Entry	Method/Basis Set	Solvent	ΔE_{solv} [a] kcal.mol^{-1}	ΔG_{solv} (195 K)[b] kcal.mol^{-1}
1	B3LYP/6-31G*	Et_2O	1.2	11.0
2	MP2/6-31G* //B3LYP/6-31G*	Et_2O	-10.0	-0.2

The solvation energy ΔE_{solv} and the solvation free energy ΔG_{solv} for this additional solvation were also calculated. The fourth solvation was found to be endoenergetic and endergonic at B3LYP/6-31G* level and exoenergetic, but very slightly exergonic at MP2/6-31G*//B3LYP/6-31G*. However, considering the BSSE, these numbers suggest that this solvation step was unlikely to happen. Also, at the point of writing this dissertation, we were not able to find a separated ion pair species from this tetrasolvated species. Instead, a two unexpected structures were found during these attempts. In the next section we discuss these structures.

3.4.6 Two atypical structures observed in the process

In the course of locating the transition state structures for the ion-pair separation from the tetrasolvated species **3-29•$(Et_2O)_4$**, an unusual structure was found that requires a special mention in this section since it points towards the possibility of an unexplored alternate route for enantiomerization. The geometry optimization calculation for a tetrasolvated SIP species analogous to trisolvate SIP species **3-33•$(Et_2O)_3$** surprisingly yielded a distorted appearing structure **3-34•$(Et_2O)_4$** (Figure 3-28).

Figure 3-28: Two atypical heterodimeric structures observed at B3LYP/6-31G*

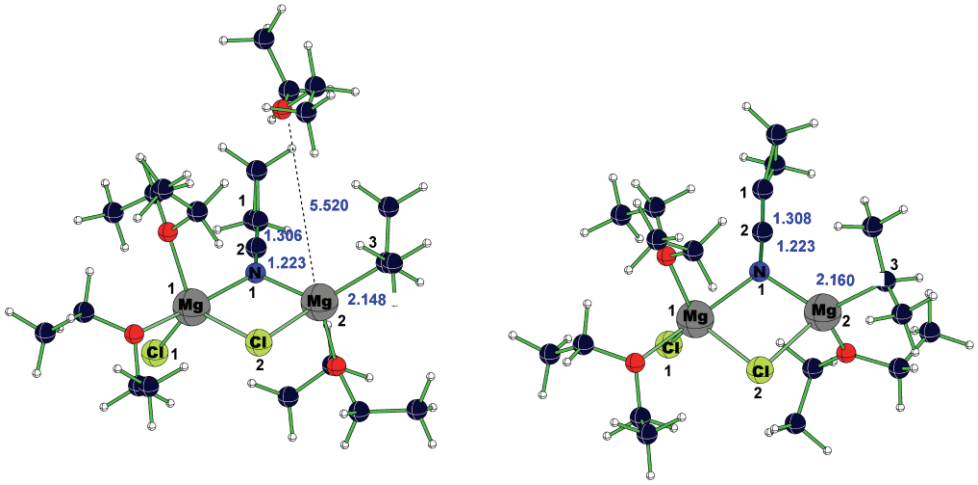

3-34•$(Et_2O)_4$
μ-Cl-μ(1,1)-cyclopropylnitrile

3-35•$(Et_2O)_3$
μ-Cl-μ(1,1)-cyclopropylnitrile

Observation of this structure revealed that one of the solvent ligands in the structure had moved away from the magnesium center (5.520 Å). Similarly, the nitrile nitrogen atom had moved closer to the other magnesium atom. This μ(1,1) bridging through the nitrile nitrogen between the two magnesium atoms leads to adoption of the keteniminate structure by the cyclopropyl nitrile fragment which is seen by the change in bond lengths of the $C_{cyclopropyl}$-CN (1.306 Å) and $C_{nitrile}$-$N_{nitrile}$ (1.223 Å) bonds in this new structure as compared to the earlier tetrakis solvated μ-Cl-μ(1,3)-cyclopropylnitrile

heterodimer structure **3-29•$(Et_2O)_4$** (1.350 Å and 1.194 Å respectively). As can be recalled from Chapter 1, this keteniminate structure can be on the inversion pathway of such cyclopropyl anions.[55,59,60] A similar trisolvated structure **3-35•$(Et_2O)_3$** was then located at B3LYP/6-31G* (Figure 3-28) by removing the distant Et_2O ligand and reoptimizing. As expected all above structural features were seen in this structure as well. The energies of all trisolvated structures located at B3LYP/6-31G* were then compared (Table 3-18). The new structure **3-35•$(Et_2O)_3$** was found to be ~2 kcal.mol^{-1} higher in energy as compared to the closed trisolvate structure **3-29•$(Et_2O)_3$** and ~8 kcal.mol^{-1} more stable as compared to the trisolvate SIP structure **3-33•$(Et_2O)_3$**.

Table 3-18: Comparison of the electronic energies of all trisolvate species calculated at B3LYP/6-31G*

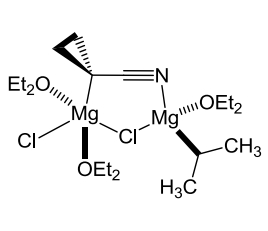

3-29·$(Et_2O)_3$-B

μ-Cl-μ(1,3)-cyclopropylnitrile

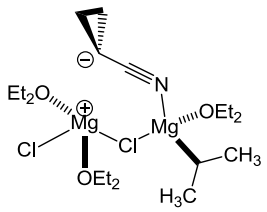

3-32•$(Et_2O)_3$

(TS*)-NIMAG = 1

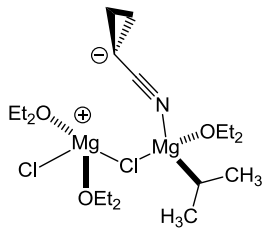

3-33•$(Et_2O)_3$

SIP

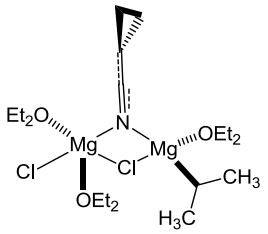

3-35•$(Et_2O)_3$

μ-Cl-μ(1,1)-cyclopropylnitrile

Entry	Method/Basis Set	Solvent	Structure	Rel E [a] kcal.mol^{-1}
1			**3-29•$(Et_2O)_3$-B**	0
2	B3LYP/6-31G*	Et_2O	**3-32•$(Et_2O)_3$**	14.9
3			**3-33•$(Et_2O)_3$**	12.2
4			**3-35•$(Et_2O)_3$**	2.0

[a] Electronic Energy ΔE in kcal.mol^{-1} at B3LYP/6-31G*

We believe that either a concerted or stepwise process of isomerization of μ-Cl-μ(1,3)-cyclopropylnitrile trisolvated structure **3-29•$(Et_2O)_3$-B** to the μ-Cl-μ(1,1)-cyclopropylnitrile structure **3-35•$(Et_2O)_3$** and inversion of the cyclopropylnitrile unit may

be involved in the enantiomerization. In Scheme 3-3, we show a possible scheme for this enantiomerization pathway. However, at the time of writing of this dissertation, we are not able to draw definite conclusions from these observations. Our initial attempts at finding the transition state for this isomerization were unsuccessful. Further computational studies have to be undertaken before any attempt to explain the inversion process is made.

Scheme 3-3: Possible ion-pair separation/ enantiomerization through μ-Cl-μ(1,1)-cyclopropylnitrile structure **3-35•$(Et_2O)_3$** and relative energies at B3LYP/6-31G*

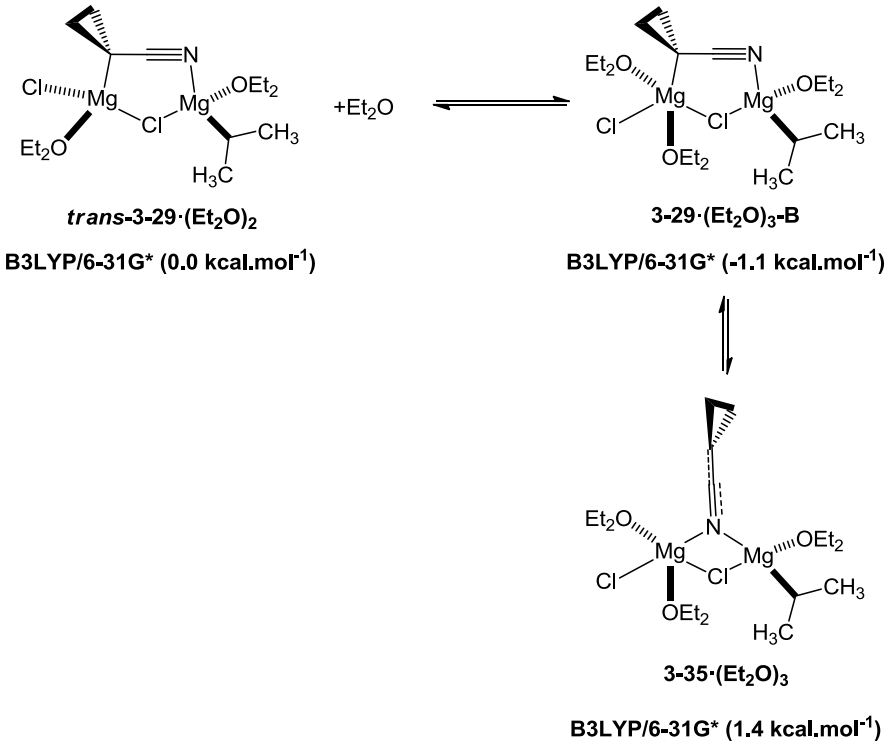

3.5 Conclusions

In the first part of this chapter, we demonstrated our computational studies towards estimating the solvation state of methylmagnesium chloride (MeMgCl) Grignard reagents. Our main intention in performing this study was computational modeling of the

solvation to duplicate the literature and we were able to show that the solvation of these Grignard reagents in solution was exoenergetic up to the disolvated level in case of both monomers and dimers. The trisolvated species in both monomers and dimers however showed the sensitivity of the calculated energies to the level of theory studied. To the best of our knowledge, the trisolvated closed dimer species **3-25•$(Et_2O)_3$** has been located for the first time, which revealed that Mori et al.'s [48] conclusion that the trisolvated species **3-25•$(Et_2O)_3$-open** is the resting solution structure of MeMgCl requires further scrutiny.

In the second part, we attempted a similar analysis on the magnesio cyclopropylcarbonitrile reagent **3-26** in order to model our observations in the kinetic experiments discussed in Chapter 2. Three types of hetero-dimeric structures were studied first, which showed that the μ-Cl-μ(1,3)-cyclopropylnitrile **3-29** was the most stable mixed-dimeric structure possible for the combination of **3-21** and reagent isopropylmagnesium chloride. The corresponding solvation studies were performed up to the trisolvated structures. Looking at the thermodynamics of these solvation steps we predicted that the disolvate species ***trans*-3-29•$(Me_2O)_2$** was the resting species in Et_2O solution. Further solvation of this species leads to the formation of trisolvated species **3-29•$(Me_2O)_3$** which is likely to be the higher solvated species inferred by our reaction order studies in Chapter 2. Ion-pair separation from **3-29•$(Me_2O)_3$** was then attempted, which predicted a free energy barrier of 14.3 kcal.mol^{-1} for the ion-pair separation process, via transition structure **3-32•$(Me_2O)_3$**.

3.6 References for Chapter 3

(1) Hutchison, D. A.; Beck, K. R.; Benkeser, R. A.; Grutzner, J. B. *J. Am. Chem. Soc.* **1973**, *95*, 7075.

(2) Nemukhin, A. V.; Topol, I. A.; Weinhold, F. *Inorg. Chem.* **1995**, *34*, 2980.

(3) Orchin, M. *J. Chem. Educ.* **1989**, *66*, 586.

(4) Spek, A. L.; Voorbergen, P.; Schat, G.; Blomberg, C.; Bickelhaupt, F. *J. Organomet. Chem.* **1974**, *77*, 147.

(5) Ashby, E. C. *J. Am. Chem. Soc.* **1965**, *87*, 2509.

(6) Seyferth, D. *Organometallics* **2009**, *28*, 1598.

(7) Silverman, G. S.; Rakita, P. E.; Editors *Handbook of Grignard Reagents* CRC-Press: New York, 1996.

(8) Schlenk, W.; Schlenk, W. *Berichte der deutschen chemischen Gesellschaft (A and B Series)* **1929**, *62*, 920.

(9) Tammiku-Taul, J.; Burk, P.; Tuulmets, A. *J. Phys. Chem. A* **2003**, *108*, 133.

(10) Patwardhan, N. N.; Gao, M.; Carlier, P. R. *Chem.--Eur. J.* **2011**, *17*, 12250.

(11) Richey, H. G. *Grignard reagents: new developments*; Wiley: Weinheim, 2000.

(12) Rappoport, Z.; Marek, I. *The Chemistry of Organomagnesium Compounds*; John Wiley & Sons: New York, 2008.

(13) Elschenbroich, C. *Organometallics*; Wiley-VCH: Weinheim, 2006.

(14) Morley, C. P.; Jutzi, P.; Krueger, C.; Wallis, J. M. *Organometallics* **1987**, *6*, 1084.

(15) Marsch, M.; Harms, K.; Massa, W.; Boche, G. *Angew. Chem.* **1987**, *99*, 706.

(16) Johnson, C.; Toney, J.; Stucky, G. D. *J. Organomet. Chem.* **1972**, *40*, C11.

(17) Toney, J.; Stucky, G. D. *Chem Commun.* **1967**, 1168.

(18) Markies, P. R.; Akkerman, O. S.; Bickelhaupt, F.; Smeets, W. J. J.; Spek, A. L. *J. Am. Chem. Soc.* **1988**, *110*, 4284.

(19) Stucky, G.; Rundle, R. E. *J. Am. Chem. Soc.* **1964**, *86*, 4825.

(20) Stucky, G. D.; Rundle, R. E. *J. Am. Chem. Soc.* **1963**, *85*, 1002.

(21) Guggenberger, L. J.; Rundle, R. E. *J. Am. Chem. Soc.* **1968**, *90*, 5375.

(22) Dohmeier, C.; Loos, D.; Robl, C.; Schnöckel, H.; Fenske, D. *J. Organomet. Chem.* **1993**, *448*, 5.

(23) E. Hibbs, D.; Jones, C.; F. Richards, A. *J. Chem. Soc., Dalton Trans.* **1999**, 3531.

(24) Vallino, M. *J. Organomet. Chem.* **1969**, *20*, 1.

(25) Toney, J.; Stucky, G. D. *J. Organomet. Chem.* **1971**, *28*, 5.

(26) Sakamoto, S.; Imamoto, T.; Yamaguchi, K. *Org. Lett.* **2001**, *3*, 1793.

(27) Smith, M. B.; Becker, W. E. *Tetrahedron Lett.* **1965**, *6*, 3843.

(28) Smith, M. B.; Becker, W. E. *Tetrahedron* **1967**, *23*, 4215.

(29) Smith, M. B.; Becker, W. E. *Tetrahedron* **1966**, *22*, 3027.

(30) Dessy, R. E.; Handler, G. S. *J. Am. Chem. Soc.* **1958**, *80*, 5824.

(31) Dessy, R. E.; Handler, G. S.; Wotiz, J. H.; Hollingsworth, C. A. *J. Am. Chem. Soc.* **1957**, *79*, 3476.

(32) Ashby, E. C.; Parris, G. E. *J. Am. Chem. Soc.* **1971**, *93*, 1206.

(33) Whitesides, G. M.; Roberts, J. D. *J. Am. Chem. Soc.* **1965**, *87*, 4878.

(34) Whitesides, G. M.; Witanowski, M.; Roberts, J. D. *J. Am. Chem. Soc.* **1965**, *87*, 2854.

(35) Benn, R.; Lehmkuhl, H.; Mehler, K.; Rufińska, A. *Angew. Chem. Int. Ed* **1984**, *23*, 534.

(36) Walker, F. W.; Ashby, E. C. *J. Am. Chem. Soc.* **1969**, *91*, 3845.

(37) Atkins, P. W.; De Paula, J. *Atkins' Physical chemistry*; Oxford University Press: Oxford; New York, 2006.

(38) Cundari, T. R. *Computational organometallic chemistry*; Marcel Dekker, 2001.

(39) Yamazaki, S.; Yamabe, S. *J. Org. Chem.* **2002**, *67*, 9346.

(40) Tuulmets, A.; Nguyen, B. T.; Panov, D. *J. Org. Chem.* **2004**, *69*, 5071.

(41) Tuulmets, A.; Tammiku-Taul, J.; Burk, P. *J. Mol. Struct. Theochem* **2004**, *674*, 233.

(42) Ivanova, N. M. *Int. J. Quantum Chem.* **2005**, *101*, 90.

(43) Henriques, A. M.; Barbosa, A. G. H. *J. Phys. Chem. A* **2011**, *115*, 12259.

(44) Jiménez-Halla, J. O. C.; Bickelhaupt, F. M.; Solà, M. *J. Organomet. Chem.* **2011**, *696*, 4104.

(45) Axten, J.; Troy, J.; Jiang, P.; Trachtman, M.; Bock, C. *Struct. Chem.* **1994**, *5*, 99.

(46) Deora, N.; Carlier, P. R. *J. Org. Chem.* **2010**, *75*, 1061.

(47) Ehlers, A. W.; van Klink, G. P. M.; van Eis, M. J.; Bickelhaupt, F.; Nederkoorn, P. H. J.; Lammertsma, K. *J. Mol. Mod* **2000**, *6*, 186.

(48) Mori, T.; Kato, S. *J. Phys. Chem. A* **2009**, *113*, 6158.

(49) Frisch, M. J.; Trucks, G. W.; Schlegel, H. B.; Scuseria, G. E.; Robb, M. A.; Cheeseman, J. R.; Scalmani, G.; Barone, V.; Mennucci, B.; Petersson, G. A.; Nakatsuji, H.; Caricato, M.; Li, X.; Hratchian, H. P.; Izmaylov, A. F.; Bloino, J.; Zheng, G.; Sonnenberg, J. L.; Hada, M.; Ehara, M.; Toyota, K.; Fukuda, R.; Hasegawa, J.; Ishida, M.; Nakajima, T.; Honda, Y.; Kitao, O.; Nakai, H.; Vreven, T.; Montgomery, J. A.; Peralta, J. E.; Ogliaro, F.; Bearpark, M.; Heyd, J. J.; Brothers, E.; Kudin, K. N.; Staroverov, V. N.; Kobayashi, R.; Normand, J.; Raghavachari, K.; Rendell, A.; Burant, J. C.; Iyengar, S. S.; Tomasi, J.; Cossi, M.; Rega, N.; Millam, J. M.; Klene, M.; Knox, J. E.; Cross, J. B.; Bakken, V.; Adamo, C.; Jaramillo, J.; Gomperts, R.; Stratmann, R. E.; Yazyev, O.; Austin, A. J.; Cammi, R.; Pomelli, C.; Ochterski, J. W.; Martin, R. L.; Morokuma, K.; Zakrzewski, V. G.; Voth, G. A.; Salvador, P.; Dannenberg, J. J.; Dapprich, S.; Daniels, A. D.; Farkas; Foresman, J. B.; Ortiz, J. V.; Cioslowski, J.; Fox, D. J. Wallingford CT, 2009.

(50) Dixon, D. D.; Tius, M. A.; Pratt, L. M. *J. Org. Chem.* **2009**, *74*, 5881.

(51) Pratt, L. M.; Jones, D.; Sease, A.; Busch, D.; Faluade, E.; Nguyen, S. C.; Thanh, B. T. *Int. J. Quantum Chem.* **2009**, *109*, 34.

(52) Erwin Weiss *Angew. Chem. Int. Ed* **1993**, *32*, 1501.

(53) Carlier, P. R. *Chirality* **2003**, *15*, 340.

(54) Zhang, Y.; University Libraries, Virginia Polytechnic Institute and State University: Blacksburg, Va., 2007.

(55) Boche, G.; Harms, K.; Marsch, M. *J. Am. Chem. Soc.* **1988**, *110*, 6925.

(56) Foresman, J. B.; Frisch, A. E.; Gaussian, I. *Exploring chemistry with electronic structure methods*; Gaussian, Inc., 1996.

(57) Koch, W.; Holthausen, M. C. *A chemist's guide to density functional theory*; Wiley-VCH, 2000.

(58) Dunitz, J. *Chem. Biol. (Cambridge, MA, U. S.)* **1995**, *2*, 709.

(59) Boche, G. *Angew. Chem. Int. Ed* **1989**, *28*, 277.

(60) Fleming, F. F.; Shook, B. C. *Tetrahedron* **2002**, *58*, 1.

Chapter 4: Experimental

General Info

NMR spectra were recorded on Bruker Avance II 500, JEOL Eclipse-plus 500 or Varian Inova 400 NMR Spectrometers. The corresponding ^{13}C NMR resonant frequencies were 126 MHz and 101 MHz respectively. Chemical shifts are reported in ppm using the known chemical shift of the indicated solvent as an internal reference. Deuterated solvents were purchased from Cambridge Isotope Laboratories Inc. and used as is. The following abbreviations are used to indicate coupling s (singlet), d (doublet), t (triplet), q (quartet), qt (quintet), bs (broad singlet), and br (broad). HRMS (TOF) was performed using a JEOL HX110 dual focusing mass spectrometer and (ESI) Agilent 6220 Accurate Mass TOF LC/MS. TLC was performed using 200 μm silica gel 60-F plates from EMD Chemicals Inc. Column chromatography was performed using 60A, 40-63 μm silica gel from SorbTech. Optical rotations were measured on a Jasco P-2000 polarimeter. Non-ethereal solvents (HPLC grade) were used as received from Fisher Scientific. Enantiomer ratios were determined by chiral stationary phase HPLC using Chiracel AD-H or OD-H columns on a Waters LC system using UV detector at 452 nm. Gas chromatography (GC) analyses were performed on a Hewlett Packard 6890 Series GC system coupled to a HP 5973 mass selective detector. The column was an Agilent DB-5MS with a length of 60 m, I.D. of 260 μm, and film thickness of 0.26 μm.

Tetrahydrofuran (THF), 2-methyl tetrahydrofuran (2-MeTHF) and diethyl ether (Et_2O) were distilled from sodium/benzophenone ketyl immediately prior to use in reactions. Toluene was dried by distilling over calcium hydride. Methylene chloride was dried by distilling from calcium hydride and storage over activated 4Å molecular sieves.

All starting materials were purchased from Sigma Aldrich and used without further purification unless otherwise noted. Grignard reagents were purchased as solutions in the desired solvent: *i*-PrMgCl (2.0 M in THF, Aldrich); *i*-PrMgCl (1.0 M in 2-MeTHF, Aldrich); *i*-PrMgCl (2.0 M in Et_2O, Aldrich); *i*-PrMgCl•LiCl (Turbo Grignard reagent, 1.3 M in THF, Aldrich). The concentrations of these commercial samples in Et_2O and THF were confirmed using the standard *sec*-butanol/phenanthroline titration procedure.[1] Organolithium reagents were purchased from Aldrich as solutions: *n*-BuLi (2.5 M in hexanes); *sec*-BuLi (1.4 M in cyclohexane); *t*-BuLi (1.7 M in pentane). Reactions at 175 K were performed using a methanol/liq N_2 slush bath; great care was taken to maintain homogeneity of the bath, and temperatures were checked regularly at different locations in the bath using an EtOH thermometer. Reactions at 195 K were maintained using the standard acetone/dry-ice bath. Temperatures of 212 K and 231 K were achieved using a Neslab Cryocool CC-100 immersion cooler.

4.1 Experimental section for Chapter 1

4.1.1: Synthetic procedures towards synthesis of 1-bromo cyclopropylcarbonitrile compounds (±) 1-76 [2].

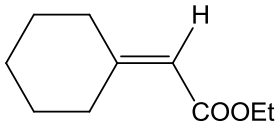

Ethyl 2-cyclohexylideneacetate (1-71) : Based on a literature procedure.[2] To a suspension of potassium tert-butoxide (KO^tBu) (2.29 g, 20.4 mmol) in 20 mL CH_2Cl_2 at 0 ^oC was added a solution of triethyl phosphonoacetate (4.58 g, 20.4 mmol) in 20 mL CH_2Cl_2 while maintaining the bath at 0 ^oC. The mixture was stirred at this temperature

for 30 minutes, after which the cyclohexanone (2.0 g, 20.4 mmol) was added to this solution. The reaction was warmed to room temperature and stirred overnight (18 h). The resulting pale yellow solution was then quenched by saturated solution of NH_4Cl (10 mL) at 0 ^oC, phases separated and the aqueous phase was extracted by 3×20 mL CH_2Cl_2. The organics were then combined, dried over anhydrous Na_2SO_4 and concentrated to yield a pale yellow colored oil, which was then purified by flash chromatography over silica gel with 9:1 Hexanes: EtOAc as the eluent to yield 3.2 g (93 %) of product **1-71** as a colorless oil. ^1H and ^{13}C NMR spectra were identical to the reported. **^{1}H NMR** (500 MHz, $CDCl_3$) δ 5.60 – 5.56 (s, 1H), 4.16 – 4.07 (q, 2H), 2.84 – 2.77 (m, 3H), 2.20 – 2.14 (m, 3H), 1.65 – 1.55 (m, 8H), 1.28 – 1.22 (t, 3H). **^{13}C NMR** (126 MHz, $CDCl_3$) δ 166.88, 163.44, 113.13, 59.47, 38.03, 29.90, 28.68, 27.86, 26.34, 14.37.

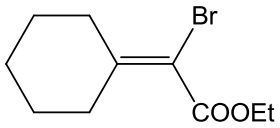

Ethyl 2-bromo-2-cyclohexylideneacetate (1-72) : Based on a literature procedure.[2] To a solution of Ethyl 2-cyclohexylideneacetate **1-71** (2 g, 11.9 mmol) in 20 mL CH_2Cl_2 at 0 ^oC was added a 10% solution of Bromine in CH_2Cl_2 (7.4 mL, 14.2 mmol) drop-wise using an addition funnel while maintaining the cooling bath at 0 ^oC. The mixture was stirred at this temperature for 120 minutes, after which the resulting dark orange colored solution was concentrated using a rotary evaporator and topped with Ethanol (10 mL). This solution was then added drop-wise to a suspension of NaOEt (0.97 g, 14.2 mmol) in Ethanol (15 mL) using an addition funnel. The reaction was warmed to room temperature and stirred overnight (18 h). The resulting pale yellow solution was then quenched by adding a 1N solution of HCl (10 mL) at 0 ^oC and diethyl ether (50 mL) was added. The

phases were separated and the aqueous phase was extracted with Et_2O (3×20 mL). The organics were then combined, dried over anhydrous Na_2SO_4 and concentrated under reduced pressure to yield a pale yellow colored oil, which was then purified by flash chromatography over silica gel with 9.5:0.5 Hexanes: EtOAc as the eluent to yield 2.4 g (81 %) of product **1-72** as a colorless oil. ^{1}H and ^{13}C NMR spectra were identical to the reported. **^{1}H NMR** (500 MHz, $CDCl_3$) δ 4.29 – 4.15 (q, 2H), 2.53 – 2.47 (m, 2H), 2.47 – 2.42 (m, 2H), 1.65 – 1.50 (m, 6H), 1.32 – 1.27 (t, 3H). **^{13}C NMR** (126 MHz, $CDCl_3$) δ 164.65, 151.58, 105.16, 61.76, 35.45, 33.04, 27.76, 27.18, 25.99, 14.10.

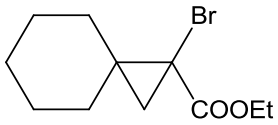

Ethyl 1-bromospiro[2.5]octane-1-carboxylate (1-73) : Based on a literature procedure.[2] Trimethyleuloxonium iodide (1.2 g, 5.4 mmol) was added portion wise to a slurry of sodium hydride (0.21 g, 5.4 mmol) in DMSO (15 mL). The mixture was stirred at room temperature until a completely clear solution was obtained (~2 h). Ethyl bromocyclohexylideneacetate (0.9 g, 3.6 mmol) was added drop-wise to this clear solution and the temperature was controlled by occasionally cooling the reaction flask in ice water. The reaction mixture was then stirred overnight (18h) at 80 ^{o}C and poured onto crushed ice. The oily product was extracted with diethyl ether (3×20 mL), and the ether solution was washed thoroughly with water (5×10 mL). The organic phase was dried over anhydrous magnesium sulfate, and the solvent was removed under reduced pressure. The resulting oily residue was purified by using flash chromatography with 1:1 Hexane: CH_2Cl_2 as an eluent to yield 0.61 g (64 %) of product **1-73** as a colorless oil. ^{1}H and ^{13}C NMR spectra were identical to the reported. **^{1}H NMR** (500 MHz, $CDCl_3$) δ 4.27 – 4.12

(m, 2H), 1.77 – 1.59 (m, 4H), 1.58 – 1.36 (m, 7H), 1.29 – 1.22 (t, 3H), 0.98 – 0.92 (d, J = 6.1 Hz, 1H). **^{13}C NMR** (126 MHz, $CDCl_3$) δ 175.03, 61.76, 38.87, 35.60, 34.50, 30.11, 29.03, 25.81, 25.34, 25.23, 14.10.

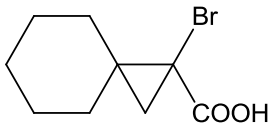

1-Bromospiro[2.5]octane-1-carboxylic acid (1-74) : Based on a literature procedure.[2] Potassium hydroxide (0.26 g, 4.6 mmol) was added to a solution of ethyl l-bromospiro[2,5]octanecarboxylate **1-73** (0.4 g, 1.5 mmol) in ethanol (7.5 mL) , and the reaction mixture was refluxed overnight in an oil bath. The solvent was evaporated under reduced pressure, and water (10 mL) was added to the residue. The aqueous phase was extracted with diethyl ether (3 × 10 mL). The aquaeous phase was then acidified with 6 N hydrochloric acid and again extracted with diethyl ether (3 × 10 mL). The ether phases were combined and dried over anhydrous magnesium sulfate and evaporated to dryness to leave a colorless oily product which solidified on standing to yield 0.28 g (80 %) of product **1-74**. This product was sufficiently pure for the next reaction and hence used as is. ^{1}H and ^{13}C NMR spectra were identical to the reported. **^{1}H NMR** (500 MHz, $CDCl_3$) δ 1.83 – 1.64 (m, 4H), 1.63 – 1.40 (m, 7H), 1.10 – 1.04 (d, J = 6.2 Hz, 1H). **^{13}C NMR** (126 MHz, $CDCl_3$) δ 175.03, 38.87, 35.60, 34.50, 30.11, 29.03, 25.81, 25.34, 25.23.

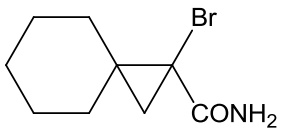

1-Bromospiro[2.5]octane-1-carboxamide (1-75): Thionyl Chloride ($SOCl_2$) (10 mL, excess) was added to a solution of 1-bromospiro[2.5]octane-1-carboxylic acid **1-74** (0.8

g, 0.35 mmol) in CH_2Cl_2 (10 mL), and the reaction mixture was refluxed for 3h in an oil bath. The solution was then concentrated using a rotary evaporator and fresh CH_2Cl_2 (20 mL) was added to the residual colorless oil. To this solution aqueous ammonia solution (NH_4OH, 20 mL, excess) was added drop-wise using an addition funnel to give a biphasic mixture, which was stirred overnight (18h) at room temp. The biphasic mixture was then separated and the aqueous phase was extracted with CH_2Cl_2 (3 × 15 mL). The organic phases were combined and dried over anhydrous sodium sulfate and evaporated to dryness to leave a light yellow powder, which was purified by flash chromatography over silica gel using 1:1 Hexane: CH_2Cl_2 as an eluent to yield 0.62 g (77 %) of product **1-75** as a white solid. **^{1}H NMR** (500 MHz, $CDCl_3$) δ 6.64 – 6.20 (bs, 1H), 5.84 – 5.60 (bs, 1H), 1.84 – 1.80 (dd, *J* = 6.0, 1.4 Hz, 1H), 1.74 – 1.69 (m, 2H), 1.57 – 1.46 (m, 8H), 0.96 – 0.93 (d, *J* = 6.0 Hz, 1H). **^{13}C NMR** (126 MHz, $CDCl_3$) δ 170.66, 43.26, 38.90, 36.08, 33.25, 29.60, 27.53, 25.98, 25.44. **HRMS** (ESI): Calculated for $C_9H_{15}BrNO$– 232.03370. [M+H] Found – 232.03330 (-0.65 ppm, -0.4 mmu)

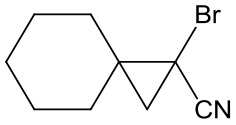

1-bromospiro[2.5]octane-1-carbonitrile (±)-1-76: Tosyl chloride (1.37 g, 0.72 mmol) was added portion-wise to a solution of 1-bromospiro[2.5]octane-1-carboxamide **1-75** (0.6 g, 0.24 mmol) in pyridine (10 mL) at room temperature and the reaction mixture was refluxed overnight in an oil bath. The resulting solution was then cooled to 0 ^oC in an ice bath and 1N HCl (8 mL) was added and this mixture was stirred at this temperature for 1h. CH_2Cl_2 (20 mL) was then added to this solution following which the phases were separated. The organic phase was then washed with water (3 × 15 mL), dried over

anhydrous sodium sulfate and concentrated under reduced pressure to yield an off-white solid. This solid was then purified by flash chromatography over silica gel using 1:1 Hexanes: CH_2Cl_2 as the eluent to yield 0.46 g (83 %) of product **(±)-1-76** as a white crystalline solid. **^{1}H NMR** (500 MHz, $CDCl_3$) δ 1.72 – 1.56 (m, 8H), 1.55 – 1.53 (d, *J* = 6.4 Hz, 1H), 1.51 – 1.40 (m, 2H), 1.23 – 1.17 (d, *J* = 6.4 Hz, 1H). **^{13}C NMR** (126 MHz, $CDCl_3$) δ 119.07, 38.81, 33.43, 33.33, 32.58, 30.74, 25.26, 24.86, 19.19. **HRMS** Calculated for $C_9H_{13}BrN$– 214.02314. [M+H] Found – 214.02210 (-2.31 ppm, +1.0 mmu).

4.1.2: Synthesis of (*S*)-1-bromo-2,2-diphenylcyclopropanecarbonitrile (*S*)-1-20. [3]

The synthesis of enantiopure bromonitrile (*S*)-**1-20** from racemic bromoacid (±)-**4-2** follows Carlier and Zhang's reported procedure.[3] Note that (*S*)-**1-20** was crystallized to constant rotation, and evidenced enantiopurity by CSP-HPLC (see Table 4-3 and Figure 4-4 below). However, for this work we report an improved synthesis of intermediate (±)-**4-2** itself (Scheme 4-1).

Scheme 4-1: Synthesis of *S*-(+)-1-bromo-2,2-diphenylcyclopropanecarbonitrile (*S*)-**1-20**

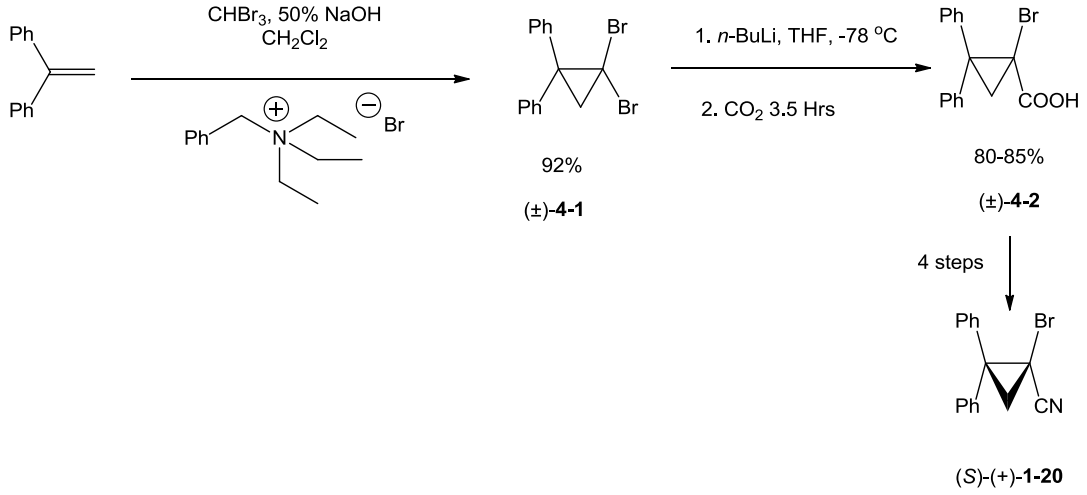

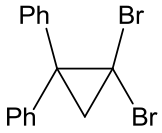

1,1 dibromo- 2,2 diphenyl cyclopropane (±)-4-1: Based on the literature procedure:[4] 50 mL of 50% NaOH solution was added dropwise to a solution of 1,1-diphenylethylene (8 g, 44 mmol), bromoform (9.7 mL, 111 mmol), and benzyl triethyl ammonium bromide (1.2g, 4.4 mmol) , in methylene chloride (50 mL). The resulting biphasic solution was stirred vigorously at room temperature for 14 hrs and then cooled to 0 ^{o}C using an ice-water bath. This cooled solution was diluted by adding 100mL CH_2Cl_2 and then neutralized by adding conc. HCl (~50 mL), until the pH of the aqueous phase was ~7 as checked by pH indicator strips. The phases were then separated and the organics were washed with water (3 x 50 mL) and brine (1 x 50 mL), dried over sodium sulfate, and concentrated in vacuo to give a deep orange colored semi-solid residue. This residue was purified using flash chromatography on silica gel (EtOAc: Hexanes = 2:98), affording 14.4g (90%) of the titled compound; ^{1}H and ^{13}C NMR spectra were identical to the reported. ^{1}H NMR (500 MHz, $CDCl_3$) δ 7.53 – 7.48 (m, 4H), 7.34 – 7.20 (m, 6H), 2.50 – 2.45 (dd, *J* = 4.2, 2.0 Hz, 2H). ^{13}C NMR (126 MHz, $CDCl_3$) δ 139.17, 138.87, 129.30, 129.10, 128.76, 128.69, 128.30, 128.13, 44.61, 30.06, 18.71.

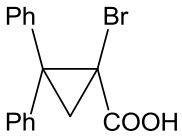

(±) 1-bromo-2,2-diphenylcyclopropanecarboxylic acid (±)-4-2: A solution of (±)-**4-1** (5g, 14.2 mmol)in THF (75 mL) was cooled to -61 °C using a chloroform-dry ice bath. To this solution *n*-butyllithium (2.5 M in hexanes, 6.8 mL, 17 mmol) was added and the resulting solution stirred for 30 min, maintaining the temperature at -61 °C. After 30 min,

CO_2 gas was bubbled into this solution via cannula from another flask containing chunks of dry ice, over the course of 3.5 hours. The reaction was then quenched with water (10 mL) and diluted with Et_2O (50 mL). The phases were then separated and the organic phase was extracted with satd $NaHCO_3$ solution (3 x 20 mL). The aqueous phases were combined and acidified using conc. HCl and extracted with Et_2O (3 x 30 mL). The ether phases were combined, dried over sodium sulfate, filtered and concentrated in vacuo to give an off-white colored solid. Flash chromatography on silica gel (AcOH: EtOAc: Hexanes = 1:49:50) afforded 3.7g (82%) of the titled compound; ^1H and ^{13}C NMR spectra were identical to the reported. ^1H NMR (500 MHz, $CDCl_3$) δ 7.55 – 7.48 (m, 4H), 7.36 – 7.27 (m, 4H), 7.27 – 7.20 (m, 2H), 2.47 (d, *J* = 1.1 Hz, 2H). ^{13}C NMR (126 MHz, $CDCl_3$) δ 173.65, 141.30, 140.09, 129.45, 129.03, 128.82, 128.38, 127.62, 125.51, 46.44, 37.87, 28.43.

4.1.3: Mg/Br exchange/ electrophilic trapping reactions of 1-bromo cyclopropylcarbonitrile 1-20 and 1-76.

Experimental procedures for the Mg/Br exchange and electrophilic trapping reactions of **1-20** and **1-76** are shown in this section. The five different types of exchange/trapping reactions shown include the elevated temperature, Lewis-base activation, and ate-complexes.

4.1.3.1 Typical procedure for Mg/Br exchange/ electrophilic quench reactions with 2.2 equiv *i*-PrMgCl.

A flame-dried 10 mL round bottom flask was charged with 1-bromo cyclopropylcarbonitrile (*S*)-**1-20** (8.5 mg, 0.0286mmol) and a magnetic stir-bar, capped

with rubber septa, and purged with nitrogen. Freshly distilled solvent (2 mL, Et_2O or THF) was then added and the flask was placed in a constant temperature bath set at the required temperature using appropriate cooling method. After allowing this reaction flask to cool to the correct temperature for 15 minutes, *i*-PrMgCl (2.2 equiv, 0.035 mL of 2.0 M commercial in Et_2O or THF) was added. Following a delay time of 5 minutes, the desired electrophile, MeI (0.0081 g, 4 μL, 0.572 mmol) or BnBr (0.0097g, 7 μL, 0.572 mmol), was added to the reaction flask and was allowed to stir for 30 min at the temperature. After 30 minutes, the reaction was quenched by a quick addition of D_2O (0.500 mL, excess) and, the reaction mixture was extracted with Et_2O (3 x 5 mL). The combined organic fractions were dried over magnesium sulfate, filtered and concentrated under reduced pressure to give an off-white solid (~7.0 mg , 95% wt recovery). This crude solid was analyzed by ^1H NMR spectroscopy ($CDCl_3$) to check for the ratio of the starting material (*S*)-**1-20** and alkylated product (**1-22**).

4.1.3.2 Typical procedure for Mg/Br exchange reactions with 2.2 equiv *i*-PrMgCl at 195 K and electrophilic quench reactions at elevated temperatures.

Follows a procedure similar to the one explained in 4.1.2.1 above. A flame-dried 10 mL round bottom flask was charged with 1-bromo cyclopropylcarbonitrile (*S*)-**1-20** (8.5 mg, 0.029 mmol) and a magnetic stir-bar, capped with rubber septa, and purged with nitrogen. Freshly distilled solvent (2 mL, Et_2O or THF) was then added and the flask was placed in a constant temperature bath set at 195 K. After allowing this reaction flask to cool to 195 K for 15 minutes, *i*-PrMgCl (2.2 equiv, 0.035 mL of 2.0 M commercial in Et_2O or THF) was added. At this point $[Mg]_{total}$ = 0.034 M and $[(S)\text{-}\mathbf{1\text{-}20}]_0$ = 0.014 M. Following a delay times of 5 minutes, the desired electrophile, MeI (0.0081 g, 4 μL,

0.572 mmol) or BnBr (0.0097g, 7 μL, 0.572 mmol), was added to the reaction flask. This reaction flask was then moved to another bath that was set at the desired temperature using an appropriate cooling mixture. After 30 minutes, the reaction was quenched by a quick addition of D_2O (0.500 mL, excess) and, the reaction mixture was extracted with Et_2O (3 x 5 mL). The combined organic fractions were dried over magnesium sulfate, filtered and concentrated under reduced pressure to give an off-white solid (~7.0 mg, 95% wt recovery). This crude solid was analyzed by ^1H NMR spectroscopy ($CDCl_3$) to check for the ratio of the starting material (*S*)-**1-20** and alkylated product (**1-22**). The alkylated product **1-22** was then isolated from the mixture using preparative thin layer chromatography on silica gel using 1:1 Hexanes: CH_2Cl_2 as an eluent. The purity of the resulting alkylated product was again analyzed by ^1H NMR spectroscopy. This purified product was then analyzed for enantiomeric excess using CSP-HPLC using ChiralPak OD column using 1% iPrOH – Hexanes as solvent at a flow rate of 0.8 mL/min.

4.1.3.3 Typical procedure for Mg/Br exchange reactions with 2.2 equiv *i*-PrMgCl and in-situ activation of the resulting Grignard species 1-20 using an appropriate Lewis base at 195 K.

A flame-dried 10 mL round bottom flask was charged 1-bromo cyclopropylcarbonitrile (*S*)-**1-20** (8.5 mg, 0.029 mmol) and a magnetic stir-bar, capped with rubber septa, and purged with nitrogen. Freshly distilled solvent (2 mL, Et_2O) was then added and the flask was placed in a constant temperature bath set at 195 K. After allowing this reaction flask to cool to 195 K for 15 minutes, *i*-PrMgCl (2.2 equiv, 0.035 mL of 2.0 M commercial in Et_2O) was added. Following a delay time of 5 minutes for formation of **1-21**, the desired electrophile (20 equiv) was added to the reaction flask and

allowed to stir for 10 minutes. After the 10 minutes, the appropriate Lewis-base (1 equiv, 10% solution in Et_2O) was added and the mixture was allowed to stir for 30 minutes to allow the complete formation of activated species **1-82** and its subsequent reaction to complete. After 30 minutes, the reaction was quenched by a quick addition of D_2O (0.500 mL, excess) and, the reaction mixture was extracted with Et_2O (3 x 5 mL). The combined organic fractions were dried over magnesium sulfate, filtered and concentrated under reduced pressure to give an off-white solid. This crude solid was analyzed by ^1H NMR spectroscopy ($CDCl_3$) to check for the ratio of the starting material (*S*)**-1-20** and alkylated product (**1-22**).

4.1.3.4 Typical procedure for Mg/Br exchange reactions with 1. 5 equiv of the ate-complex *i*-PrBu$_2$MgLi at 195 K.

To a flame-dried 10 mL round bottom flask was charged *i*-PrMgCl (1.5 equiv, 0.065 mL of 2.0 M commercial in THF), a magnetic stir-bar, capped with rubber septa, and purged with nitrogen. Freshly distilled solvent (5 mL, THF) was then added and the flask was placed in a constant temperature bath set at 195 K. After allowing this reaction flask to cool to 195 K for 15 minutes, *n*-BuLi (3 equiv, 0.103 mL of 2.5 M commercial in hexanes) was added. Following a delay times of 30 minutes to allow formation of the ate complex, the starting 1-bromo cyclopropylcarbonitrile (*S*)**-1-20** (25.5 mg, 0.86 mmol) was added to this flask and allowed to stir for 5 minutes for the Mg/Br exchange process to take place. A color change to dark yellow is observed at this point. After the 5-minute delay, the desired electrophile, MeI (0.054 mL, 8.6 mmol) was added to the reaction flask and allowed to stir at 195 K for additional 30 minutes. After 30 minutes, the reaction was quenched by a quick addition of D_2O (0.500 mL, excess) and, the reaction mixture was

extracted with Et_2O (3 x 5 mL). The combined organic fractions were dried over magnesium sulfate, filtered and concentrated under reduced pressure to give an off-white solid (~20 mg, 97% wt recovery). This crude solid was analyzed by ^1H NMR spectroscopy ($CDCl_3$) to check for the ratio of the starting material (*S*)-**1-20** and alkylated product (**1-22**). The methylated product **1-22** was then isolated from the mixture using preparative thin layer chromatography on silica gel using 1:1 Hexanes: CH_2Cl_2 as an eluent. The purity of the resulting alkylated product was again analyzed by ^1H NMR spectroscopy. This purified product was then analyzed for enantiomeric excess using CSP-HPLC using ChiralPak OD column using 1% iPrOH – Hexanes as solvent at a flow rate of 0.8 mL/min.

4.1.3.5 Typical procedure for Mg/Br exchange reactions with in situ formation of ate complex 1-87 at 195 K.

A flame-dried 10 mL round bottom flask was charged 1-bromo cyclopropylcarbonitrile (*S*)-**1-20** (25.5 mg, 0.86 mmol) and a magnetic stir-bar, capped with rubber septa, and purged with nitrogen. Freshly distilled solvent (5 mL, THF) was then added and the flask was placed in a constant temperature bath set at 195 K. After allowing this reaction flask to cool to 195 K for 15 minutes, *i*-PrMgCl (1.5 equiv, 0.065 mL of 2.0 M commercial in THF) was added. Following a delay time of 5 minutes, *n*-BuLi (3 equiv, 0.103 mL of 2.5 M commercial in hexanes) was added and the mixture was allowed to stir for 30 minutes to allow the complete formation of ate species **1-87**. After 30 minutes, the desired electrophile, MeI (0.054 mL, 8.6 mmol), was added to the reaction flask and allowed to stir for additional 30 minutes to allow the electrophilic quench reaction to complete. After 30 minutes, the reaction was quenched by a quick

addition of D_2O (0.500 mL, excess) and, the reaction mixture was extracted with Et_2O (3 x 5 mL). The combined organic fractions were dried over magnesium sulfate, filtered and concentrated under reduced pressure to give an off-white solid (~20.0 mg, 97% wt recovery). This crude solid was analyzed by ^{1}H NMR spectroscopy ($CDCl_3$) to check for the ratio of the starting material (*S*)-**1-20** and alkylated product (**1-22**). The alkylated product **1-22** was then isolated from the mixture using preparative thin layer chromatography on silica gel using 1:1 Hexanes: CH_2Cl_2 as an eluent. The purity of the resulting alkylated product was again analyzed by ^{1}H NMR spectroscopy. This purified product was then analyzed for enantiomeric excess using CSP-HPLC using ChiralPak OD column using 1% iPrOH – Hexanes as solvent at a flow rate of 0.8 mL/min.

4.1.3.6 Analytical Data for the electrophilic quench products –

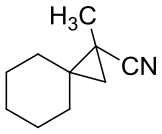

1-methylspiro[2.5]octane-1-carbonitrile 1-78:

^{1}H NMR (500 MHz, $CDCl_3$) δ 1.47-1.68 (m, 6H), 1.43 (m, 4H), 1.4 (s, 3H) 1.04 (d, *J* = 4.97 Hz, 1H), 0.59 (d, *J* = 4.97 Hz, 1H). **^{13}C NMR** (126 MHz, $CDCl_3$) δ ^{13}C NMR (126 MHz, CDCl3) δ 119.07, 36.34, 33.43, 33.33, 32.58, 30.74, 25.26, 24.86, 22.46, 19.19. **HRMS**: Calculated for $C_{10}H_{16}N$ - 150.12827. Found [M+H] – 150.12693 (-5.31 ppm, -1.3 mmu)

\

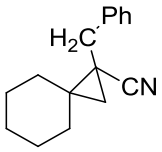

1-benzylspiro[2.5]octane-1-carbonitrile 1-79:

^{1}H NMR (500 MHz, $CDCl_3$) δ 7.45 – 7.19 (m, 5H), 3.05 – 2.99 (d, *J* = 15.3 Hz, 1H), 2.83 – 2.76 (d, *J* = 15.3 Hz, 1H), 1.79 – 1.44 (m, 10H), 1.11 – 1.08 (d, *J* = 5.1 Hz, 1H), 0.85 – 0.82 (d, *J* = 5.1 Hz, 1H). **^{13}C NMR** (126 MHz, $CDCl_3$) δ 137.96, 128.80, 128.73, 127.04, 122.73, 35.94, 34.92, 31.35, 31.03, 26.21, 25.87, 25.86, 25.85, 25.65, 25.30, 21.58. **HRMS**: Calculated for $C_{16}H_{19}NNa$ - 248.14152. Found [M+Na] – 248.14040 (-3.15 ppm, -1.1 mmu)

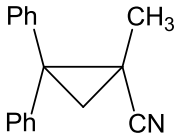

1-methyl-2,2-diphenylcyclopropanecarbonitrile (1-22): ^{1}H NMR (400 MHz, $CDCl_3$) δ 7.56 – 7.50 (m, 2H), 7.43 – 7.37 (m, 2H), 7.36 – 7.28 (m, 4H), 7.27 – 7.20 (m, 2H), 2.09 – 2.02 (d, *J* = 5.3 Hz, 1H), 1.68 – 1.61 (d, *J* = 5.3 Hz, 1H), 1.33 – 1.29 (s, 3H). **^{13}C NMR** (101 MHz, $CDCl_3$) δ 141.48, 139.36, 129.30, 129.13, 128.82, 128.76, 127.58, 127.45, 122.65, 42.81, 26.32, 19.82, 16.62.

4.1.4: Procedures for synthesis of various γ–hydroxyl group containing alkyl halides

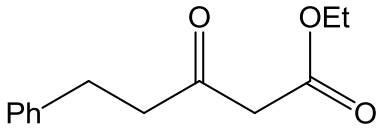

Ethyl 3-oxo-5-phenylpentanoate (1-89): Based on a literature procedure.[5] To a suspension of NaH (1.63 g 60% suspension in mineral oil, 4.23 mmol) in THF (30 mL), was added a solution of ethyl acetoacetate (5 g, 3.85 mmol) in THF (10 mL) at -78 ^{o}C

and stirred for 30 minutes. To this solution was added a solution of n-BuLi (16.9 mL, 2.5 M in hexanes commercial, 4.23 mmol). The solution turns to a deep yellow color at this point. This solution was stirred for additional 30 minutes to allow the dianion formation to complete. After 30 minutes, BnBr (7.23 g, 4.23 mmol) was added and the resulting solution was allowed to stir for 3h. The reaction was then quenched by addition of a saturated NH_4Cl solution at 0 ^oC. The phases were then separated and the aqueous phase was extracted by diethyl ether (3× 30 mL). The organics were then combined, dried over anhydrous sodium sulfate and concentrated under reduced pressure to yield a pale yellow oil. This pale yellow oil was then purified by flash chromatography over silica gel using 98:2 Hexanes: EtOAc as the eluent to yield 6.2 g (73%) of product **1-89** as a colorless oil. **^{1}H NMR** (500 MHz, CDCl3) δ 7.32 – 7.24 (m, 2H), 7.23 – 7.14 (m, 3H), 4.27 (q, 2H), 3.47 (s, 2H), 2.95 (m, 4H), 1.31 (t, 3H). **^{13}C NMR** (126 MHz, CDCl3) δ 201.98, 167.19, 140.64, 128.63, 128.42, 126.33, 61.49, 49.53, 44.58, 29.52, 14.18.

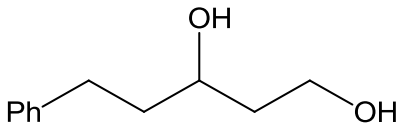

5-phenylpentane-1,3-diol (1-90): Based on a literature procedure.[6] Lithium aluminum hydride (LAH) (0.98 g, 2.59 mmol) was added portion-wise to a solution of ethyl 3-oxo-5-phenylpentanoate **1-89** (1.29 g, 0.59 mmol) in THF (30 mL) at 0 ^oC. The resulting solution was warmed to room temperature and stirred overnight. The reaction was then worked up by performing the Fieser workup.[7] The resulting aluminum complex was then filtered over celite, washed with Et_2O (20 mL) and the organics were combined and dried over anhydrous magnesium sulfate and concentrated under reduced pressure to give colorless oil. This was then purified by flash chromatography over silica gel using 1:1

Hexanes: EtOAc as an eluent to yield 0.78 g (74%) of product 5-phenylpentane-1,3-diol **1-90** as a colorless oil. **^{1}H NMR** (500 MHz, CDCl3) δ 7.32 – 7.23 (m, 2H), 7.23 – 7.15 (m, 3H), 3.93 – 3.77 (m, 2H), 2.83 – 2.73 (m, 2H), 2.73 – 2.63 (m, 2H), 1.89 – 1.65 (m, 2H). **^{13}C NMR** (126 MHz, CDCl3) δ 141.99, 128.55, 128.50, 125.99, 71.67, 61.87, 39.45, 38.40, 31.99.

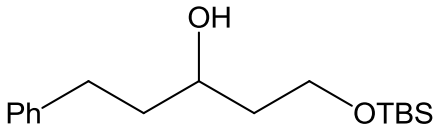

1-((*tert*-butyldimethylsilyl)oxy)-5-phenylpentan-3-ol (1-91): To a solution of 5-phenylpentane-1,3-diol **1-90** (0.76 g, 0.43 mmol) in THF (30 mL), imidazole (0.33 g, 0.48 mmol) was added. This solution was then stirred for 30 minutes at room temperature, following which *tert*-butyldimethylsilyl chloride (0.72 g, 0.48 mmol) was added in 3 portions with stirring. The resulting solution was stirred for 1h and quenched by addition of a saturated solution of NH_4Cl. The phases were separated and the organic phase was washed with water (3×15 mL). The organics were then combined, dried over anhydrous sodium sulfate and concentrated under reduced pressure to yield a colorless oil. This was then purified by flash chromatography over silica gel using 20:1 Hexanes: EtOAc as an eluent to yield 1.01 g (79 %) of 1-((*tert*-butyldimethylsilyl)oxy)-5-phenylpentan-3-ol **1-91** as a colorless oil. **^{1}H NMR** (500 MHz, CDCl3) δ 7.33 – 7.13 (m, 5H), 3.95 – 3.77 (m, 1H), 3.56 – 3.51 (m, 2H), 2.86 – 2.76 (m, 1H), 2.72 – 2.62 (m, 1H), 1.87 – 1.77 (m, 2H), 1.78 – 1.58 (m, 2H), 0.97 (s, 9H), 0.10 (s, 3H), 0.07(s, 3H). **^{13}C NMR** (126 MHz, CDCl3) δ 142.48, 128.56, 128.42, 125.78, 71.73, 63.01, 39.35, 38.34, 32.01, 25.95, 25.74, 18.20, -5.45, -5.48. **HRMS:** Calculated for $C_{17}H_{31}O_2Si$ - 295.20151; Found: [M+H] – 295.2089 (-0.44 ppm, -0.7 mmu)

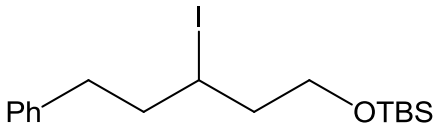

tert-*buty*l((3-iodo-5-phenylpentyl)oxy)dimethylsilane (1-92): To a solution of triphenyl phosphine (0.67 g, 0.255 mmol) and imidazole (0.18 g, 0.255 mmol) in toluene (5 mL) was added a solution of 1-((*tert*-butyldimethylsilyl)oxy)-5-phenylpentan-3-ol **1-91** (0.5 g, 0.17 mmol) in toluene (5 mL) and the resulting solution was stirred for 15 minutes till the solids completely dissolve. To this solution iodine crystals (0.65 g, 0.255 mmol) were added in three portions. The resulting deep purple colored reaction mixture was then refluxed overnight. The reaction was then quenched by addition of water (5 mL), the phases were separated and the organic phase was washed using saturated sodium thiosulfate solution (5 mL). The organics were combined, dried over anhydrous sodium sulfate and concentrated under reduced pressure to yield a pale yellow oil. This was then purified using flash chromatography over silica gel using 98:2 Hexanes: EtOAc as the eluent, to give 0.644g (94%) of tert-*buty*l((3-iodo-5-phenylpentyl)oxy)dimethylsilane **1-92** as a colorless oil. **^{1}H NMR** (500 MHz, CDCl3) δ 7.32 – 7.25 (m, 2H), 7.24 – 7.16 (m, 3H), 4.27 – 4.18 (m, 1H), 3.82 – 3.75 (ddd, *J* = 10.3, 8.2, 4.9 Hz, 1H), 3.75 – 3.66 (ddd, *J* = 10.3, 8.2, 4.9 Hz, 1H), 2.94 – 2.86 (ddd, *J* = 13.8, 9.2, 6.9 Hz, 1H), 2.79 – 2.69 (ddd, *J* = 13.8, 9.2, 6.9 Hz, 1H), 2.23 – 2.14 (m, 2H), 2.10 – 1.97 (m, 2H), 1.95 – 1.86 (m, 2H), 1.28 – 1.24 (s, 1H), 0.97 (s, 9H), 0.10 (s, 3H), 0.07(s, 3H). **^{13}C NMR** (126 MHz, CDCl3) δ 140.93, 128.65, 128.57, 126.18, 62.50, 43.42, 42.54, 35.68, 35.45, 26.03, 26.02, -5.19, -5.20. **HRMS:** Calculated for $C_{17}H_{30}IOSi$ - 405.1032; Found: [M+H] – 405.1029 (-1.1 ppm, -0.3 mmu)

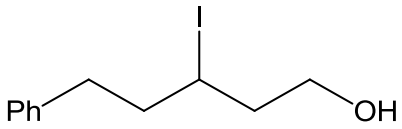

3-iodo-5-phenylpentan-1-ol (1-93): In a 100 mL HDPE bottle was added a solution of tert-*but*yl((3-iodo-5-phenylpentyl)oxy)dimethylsilane **1-92** (0.644 g, Y mmol) in THF (15 mL). To this, a solution of HF (70% in pyridine, 0.5 mL, excess) was added drop-wise. The resulting solution was stirred at room temperature for 6h. The reaction was then quenched by adding a 10% solution of $NaHCO_3$. Excessive effervescence is observed at this point, great care was taken to avoid spilling of the solution out of the bottle. The phases were then separated and the aqueous phase was extracted with Et_2O (3 × 10 mL). The organic layers were then combined and washed with water (3 × 10 mL), dried over anhydrous sodium sulfate and concentrated under reduced pressure to yield a pale yellow oil. This was then purified using flash chromatography over silica gel using 1:1 Hexanes: EtOAc as the eluent to yield 0.3921g (85%) 3-iodo-5-phenylpentan-1-ol **1-93** as a colorless oil. **^{1}H NMR** (500 MHz, CDCl3) δ 7.35 – 7.25 (m, 2H), 7.23 – 7.15 (m, 3H), 4.28 – 4.13 (m, 1H), 3.91 – 3.67 (m, 2H), 3.01 – 2.83 (m, 1H), 2.81 – 2.64 (m, 1H), 2.30 – 2.14 (m, 1H), 2.12 – 1.99 (m, 2H), 1.99 – 1.90 (m, 1H), 1.75 – 1.58 (s, 1H). **^{13}C NMR** (126 MHz, CDCl3) δ 140.84, 128.66, 128.64, 126.29, 62.53, 42.89, 42.60, 35.74, 34.85. **Elemental analysis:** Calculated for $C_{11}H_{15}IO$ - C, 45.54; H, 5.21; I, 43.74; Found - C, 46.42; H, 5.39; I, 42.18. Note this analysis is supportive of the proposed structure, but is not meet convention for a publishable match of elemental composition. Further confirmation of the structure is provided below.

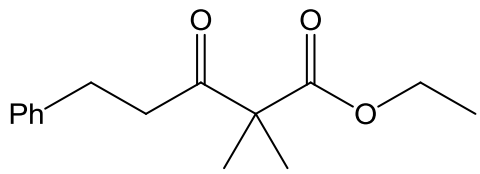

ethyl 2,2-dimethyl-3-oxo-5-phenylpentanoate (1-97): To a suspension of potassium tert-butoxide (KO^{t}Bu) (2.55 g, 23.4 mmol) in 20 mL THF at 0 ^{o}C was added a solution of ethyl 3-oxo-5-phenylpentanoate **1-89 (**2 g, 9.1 mmol) in 20 mL THF while maintaining the bath at 0 ^{o}C. The mixture was stirred at this temperature for 30 minutes, after which iodomethane (2.7 g, 18.2 mmol) was added to this solution. The reaction was warmed to room temperature and stirred for 3 h. The resulting pale yellow solution was then quenched by saturated solution of NH_4Cl (10 mL) at 0 ^{o}C, phases separated and the aqueous phase was extracted by Et_2O (3×20 mL). The organics were then combined, dried over anhydrous Na_2SO_4 and concentrated to yield a pale yellow colored oil, which was then purified by flash chromatography over silica gel with 9:1 Hexanes: EtOAc as the eluent to yield 2.02 g (89 %) of product **1-97** as a colorless oil. **^{1}H NMR** (500 MHz, CDCl3) δ 7.32 – 7.26 (m, 2H), 7.23 – 7.17 (m, 3H), 4.15 (q, *J* = 7.1 Hz, 2H), 3.85 – 3.81 (m, 2H), 2.12 -2.94(m, 2H), 1.32 (s, 6H), 1.22 (t, *J* = 7.1 Hz, 3H). **^{13}C NMR** (126 MHz, CDCl3) δ 205.99, 173.66, 140.96, 128.65, 128.61, 126.24, 61.36, 55.76, 41.57, 41.15, 25.76, 21.87, 14.06. **HRMS:** Calculated for $C_{15}H_{21}O_3$- 249.14124; Found: [M+H] – 249.1487 (+0.84 ppm, +0.7 mmu)

.

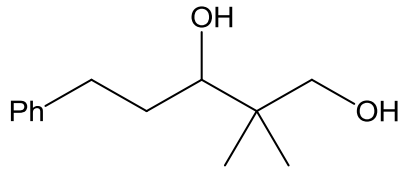

2,2-dimethyl-5-phenylpentane-1,3-diol (1-98): Based on a literature procedure.[8] Lithium aluminum hydride (LAH) (1.4 g, 3.6 mmol) was added portion-wise to a solution of ethyl 2,2-dimethyl-3-oxo-5-phenylpentanoate **1-97** (2.26 g, 0.9 mmol) in THF (50 mL) at 0 ^{o}C. The resulting solution was warmed to room temperature and stirred overnight. The reaction was then worked up by performing the Fieser workup.[7] The resulting aluminum complex was then filtered over celite, washed with Et_2O (50 mL) and the organics were combined and dried over anhydrous magnesium sulfate and concentrated under reduced pressure to give colorless oil. This was then purified by flash chromatography over silica gel using 1:1 Hexanes: EtOAc as an eluent to yield 1.72 g (91%) of product 2,2-dimethyl-5-phenylpentane-1,3-diol **1-98** as a colorless oil. **^{1}H NMR** (500 MHz, CDCl3) δ 7.32 – 7.26 (m, 2H), 7.24 – 7.16 (m, 3H), 3.66 – 3.40 (m, 3H), 3.01 – 2.83 (m, 1H), 2.71 – 2.57 (m, 2H), 2.56 – 2.40 (s, 1H), 1.93 – 1.76 (s, 3H), 1.73 – 1.65 (s, 3H). **^{13}C NMR** (126 MHz, CDCl3) δ 143.04, 128.65, 128.39, 125.71, 78.90, 38.31, 34.21, 33.10, 25.92, 22.56, 18.21.

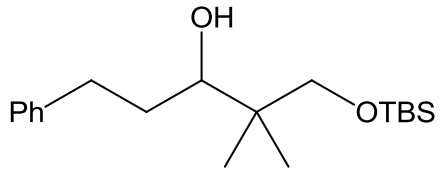

1-((*tert*-butyldimethylsilyl)oxy)-2,2-dimethyl-5-phenylpentan-3-ol (1-99): To a solution of 2,2-dimethyl-5-phenylpentane-1,3-diol **1-98** (1.97 g, 9.5 mmol) in THF (40 mL), imidazole (0.97 g, 14.2 mmol) was added. This solution was then stirred for 30

minutes at room temperature, following which *tert*-butyldimethylsilyl chloride (1.53 g, 10.4 mmol) was added in 3 portions with stirring. The resulting solution was stirred for 1h and quenched by addition of a saturated solution of NH_4Cl. The phases were separated and the organic phase was washed with water (3×25 mL). The organics were then combined, dried over anhydrous sodium sulfate and concentrated under reduced pressure to yield a colorless oil. This was then purified by flash chromatography over silica gel using 20:1 Hexanes: EtOAc as an eluent to yield 1.76 g (60 %) of 1-((*tert*-butyldimethylsilyl)oxy)-2,2-dimethyl-5-phenylpentan-3-ol **1-99** as a colorless oil. **^{1}H NMR** (500 MHz, CDCl3) δ 7.30 – 7.26 (m, 2H), 7.26 – 7.22 (m, 2H), 7.20 – 7.16 (m, 1H), 0.08 – 0.07 (m, 5H), 3.86 – 3.71 (m, 1H), 3.57 – 3.39 (m, 3H), 3.12 – 2.88 (m, 1H), 2.72 – 2.51 (ddd, *J* = 13.6, 10.3, 6.4 Hz, 1H), 1.86 – 1.57 (m, 2H), 0.92 – 0.91 (m, 9H), 0.87 – 0.87 (m, 3H), 0.82 – 0.82 (d, *J* = 1.1 Hz, 3H), 0.12 (s, 6H). **^{13}C NMR** (126 MHz, CDCl3) δ 143.04, 128.65, 128.39, 125.71, 78.90, 38.31, 34.21, 33.10, 25.92, 22.56, 19.04, 18.21, -5.59, -5.61. **HRMS:** Calculated for $C_{19}H_{35}O_2Si$ - 323.24063; Found: [M+H] – 323.2408 (+0.53 ppm, +0.4 mmu)

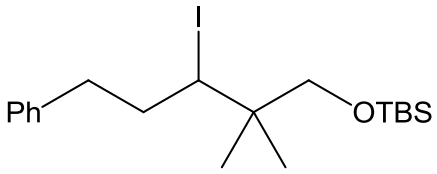

***tert*-Butyl((3-iodo-2,2-dimethyl-5-phenylpentyl)oxy)dimethylsilane (1-100):** To a solution of triphenyl phosphine (0.61 g, 0.233 mmol) and imidazole (0.16 g, 0.233 mmol) in toluene (5 mL) was added a solution of 1-((*tert*-butyldimethylsilyl)oxy)-2,2-dimethyl-5-phenylpentan-3-ol **1-99** (0.5 g, 0.15 mmol) in toluene (5 mL) and the resulting solution was stirred for 15 minutes till the solids completely dissolve. To this solution iodine

crystals (0.59 g, 0.233 mmol) were added in three portions. The resulting deep purple colored reaction mixture was then refluxed overnight. The reaction was then quenched by addition of water (5 mL), the phases were separated and the organic phase was washed using saturated sodium thiosulfate solution (5 mL). The organics were combined, dried over anhydrous sodium sulfate and concentrated under reduced pressure to yield a pale yellow oil. This was then purified using flash chromatography over silica gel using 98:2 Hexanes: EtOAc as the eluent, to give 0.485g (72%) of *tert*-Butyl((3-iodo-2,2-dimethyl-5-phenylpentyl)oxy)dimethylsilane **1-100** as a colorless oil. **^{1}H NMR** (500 MHz, CDCl3) δ 7.31 – 7.26 (m, 3H), 7.25 – 7.17 (m, 3H), 4.27 – 4.19 (dd, *J* = 11.6, 2.0 Hz, 1H), 3.49 – 3.37 (m, 2H), 3.12 – 3.03 (m, 1H), 2.70 – 2.60 (m, 1H), 2.09 – 1.99 (m, 1H), 1.99 – 1.89 (m, 1H), 1.01 – 0.97 (m, 6H), 0.08 – -0.03 (m, 5H), 0.88 – 0.84 (m, 9H), 0.04 (s, 6H). **^{13}C NMR** (126 MHz, CDCl3) δ 141.26, 128.71, 128.52, 126.12, 71.80, 53.28, 40.43, 37.12, 25.95, 24.09, 21.95, 18.27, -5.36, -5.49. **HRMS:** Calculated for $C_{19}H_{33}INaOSi$- 455.12340; Found: [M+Na] – 455.1236 (-1.2 ppm, -0.2 mmu)

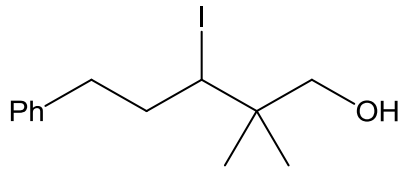

3-iodo-2,2-dimethyl-5-phenylpentan-1-ol (1-101): In a 100 mL HDPE bottle was added a solution of *tert*-Butyl((3-iodo-2,2-dimethyl-5-phenylpentyl)oxy)dimethylsilane **1-100** (1.0 g, 2.3 mmol) in THF (15 mL). To this, a solution of HF (70% in pyridine, 1.0 mL, excess) was added drop-wise. The resulting solution was stirred at room temperature for 12h. The reaction was then quenched by adding a 10% solution of $NaHCO_3$. Excessive effervescence is observed at this point, great care was taken to avoid spilling of the

solution out of the bottle. The phases were then separated and the aqueous phase was extracted with Et_2O (3 × 20 mL). The organic layers were then combined and washed with water (3 × 10 mL), dried over anhydrous sodium sulfate and concentrated under reduced pressure to yield a pale yellow oil. This was then purified using flash chromatography over silica gel using 1:1 Hexanes: EtOAc as the eluent to yield 0.63g (86%) 3-iodo-2,2-dimethyl-5-phenylpentan-1-ol **101** as a colorless oil. **^{1}H NMR** (500 MHz, CDCl3) δ 7.35 – 7.27 (m, 2H), 7.26 – 7.17 (m, 3H), 4.22 – 4.10 (dd, *J* = 11.5, 1.8 Hz, 1H), 3.65 – 3.51 (m, 1H), 3.50 – 3.37 (m, 1H), 3.15 – 2.97 (m, 1H), 2.74 – 2.54 (m, 1H), 2.16 – 1.85 (m, 2H), 1.58 – 1.48 (bs, 1H), 1.08 – 1.05 (s, 3H), 0.99 – 0.96 (s, 3H). **^{13}C NMR** (126 MHz, CDCl3) δ 141.05, 128.68, 128.62, 126.27, 72.59, 52.21, 40.21, 37.12, 36.83, 22.91, 21.70. **Elemental analysis:** Calculated for $C_{13}H_{19}IO$ - C, 49.07; H, 6.02; I, 39.88; Found – C, 49.95; H, 6.36; I, 38.20. Note this analysis is supportive of the proposed structure, but is not meet convention for a publishable match of elemental composition. Further confirmation of the structure is provided below.

COSY: The alkyl region in the COSY spectrum below confirms the structure of **1-101**.

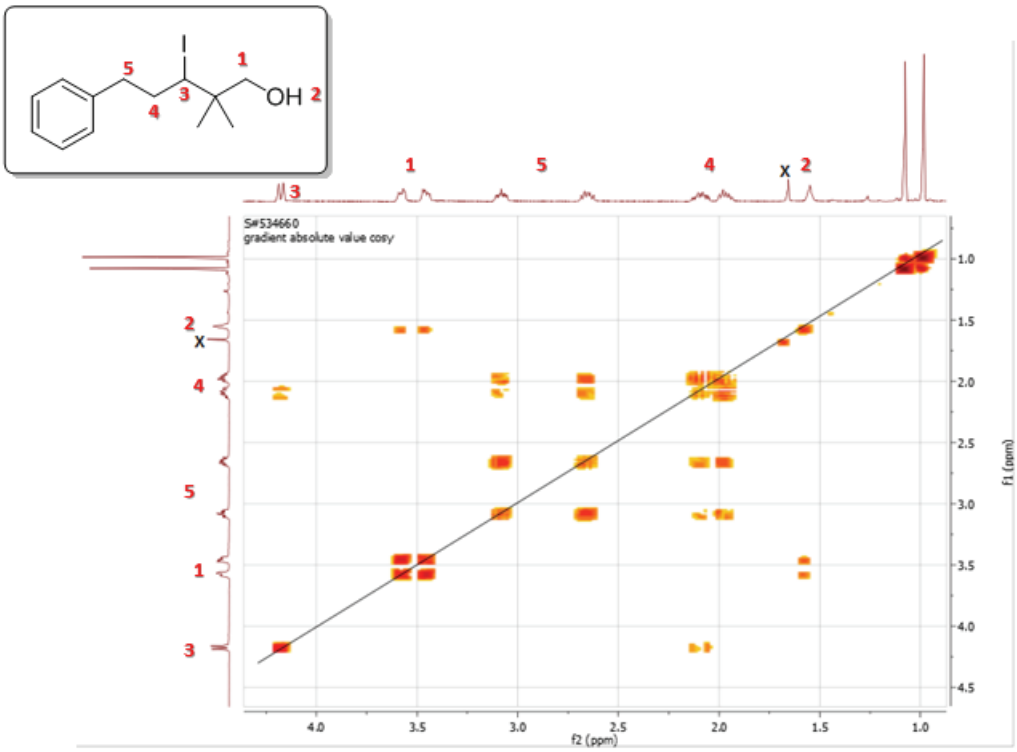

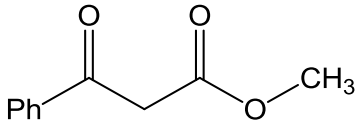

Methyl 3-oxo-3-phenylpropanoate (1-108): Based on a literature procedure.[9] To a suspension of NaH (2.016 g 60% suspension in mineral oil, 8.4 mmol) in THF (100 mL), was added a solution of acetophenone (5 g, 4.2 mmol) in THF (10 mL) at -78 ^{o}C and stirred for 30 minutes. To this solution was added dimethyl carbonate (18.9 mL, 21.0 mmol). This solution was stirred for additional 18h, after which quenched by addition of a saturated NH_4Cl solution at 0 ^{o}C. The phases were then separated and the aqueous phase was extracted by diethyl ether (3× 50 mL). The organics were then combined, dried over anhydrous sodium sulfate and concentrated under reduced pressure to yield a pale yellow oil. This pale yellow oil was then purified by flash chromatography over silica gel

using 98:2 Hexanes: EtOAc as the eluent to yield 7.4 g (94%) of product **1-105** as a colorless oil. **^{1}H NMR** (500 MHz, CDCl3) δ 4.02 – 3.98 (s, 2H), 3.75 – 3.71 (s, 3H), 7.96 – 7.90 (m, 2H), 7.62 – 7.54 (m, 1H), 7.51 – 7.36 (m, 2H). **^{13}C NMR** (126 MHz, CDCl3) δ 192.49, 168.08, 129.58, 129.14, 128.24, 128.07, 46.04, 45.77.

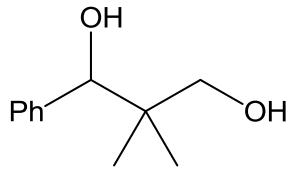

2,2-dimethyl-1-phenylpropane-1,3-diol (1-109): Based on literature procedure.[10] To a suspension of potassium tert-butoxide (KO^{t}Bu) (11.8 g, 105.4 mmol) in 100 mL THF at 0 ^{o}C was added a solution of methyl 3-oxo-3-phenylpropanoate **1-108** (7.5 g, 42.2 mmol) in 50 mL THF while maintaining the bath at 0 ^{o}C. The mixture was stirred at this temperature for 30 minutes, after which iodomethane (12.6 g, 89 mmol) was added to this solution. The reaction was warmed to room temperature and stirred for 3 h. The resulting pale yellow solution was then quenched by saturated solution of NH_4Cl (10 mL) at 0 ^{o}C, phases separated and the aqueous phase was extracted by Et_2O (3×60 mL). The organics were then combined, dried over anhydrous Na_2SO_4 and concentrated to yield 8.0 g (92 %) of product as a pale yellow colored oil, which was used as is in the next reaction. To a solution of this product in THF (100 mL), was added LAH (5.47 g, 144 mmol) in 3 portions. The resulting solution was warmed to room temperature and stirred overnight. The reaction was then worked up by performing the Fieser workup.[7] The resulting aluminum complex was then filtered over celite, washed with Et_2O (50 mL) and the organics were combined and dried over anhydrous magnesium sulfate and concentrated under reduced pressure to give colorless oil. This was then purified by flash

chromatography over silica gel using 1:1 Hexanes: EtOAc as an eluent to yield 5.7 g (75 %) of product 2,2-dimethyl-1-phenylpropane-1,3-diol **1-106** as a colorless oil. **^{1}H NMR** (500 MHz, CDCl3) δ 7.43 – 7.12 (m, 5H), 4.71 – 4.51 (s, 2H), 3.73 – 3.29 (m, 2H), 0.82 – 0.79 (s, 3H), 0.92 – 0.72 (s, 3H). **^{13}C NMR** (126 MHz, CDCl3) δ 141.53, 127.82, 127.68, 127.60, 82.29, 72.15, 39.12, 22.86, 19.06.

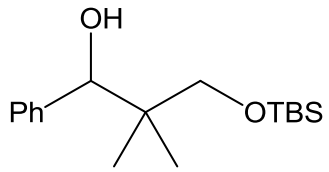

3-((*tert*-butyldimethylsilyl)oxy)-2,2-dimethyl-1-phenylpropan-1-ol (1-110): Based on a literature procedure.[11] To a solution of 2,2-dimethyl-1-phenylpropane-1,3-diol **1-109** (5.7 g, 32.0 mmol) in THF (40 mL), imidazole (3.09 g, 4.7 mmol) was added. This solution was then stirred for 30 minutes at room temperature, following which *tert*-butyldimethylsilyl chloride (5.22 g, 35.0 mmol) was added in 3 portions with stirring. The resulting solution was stirred for 1h and quenched by addition of a saturated solution of NH_4Cl. The phases were separated and the organic phase was washed with water (3×50 mL). The organics were then combined, dried over anhydrous sodium sulfate and concentrated under reduced pressure to yield a colorless oil. This was then purified by flash chromatography over silica gel using 20:1 Hexanes: EtOAc as an eluent to yield 8.05 g (87 %) of 3-((*tert*-butyldimethylsilyl)oxy)-2,2-dimethyl-1-phenylpropan-1-ol **1-107** as a colorless oil. **^{1}H NMR** (500 MHz, CDCl3) δ 7.50 – 7.03 (m, 5H), 4.63 – 4.56 (d, *J* = 3.7 Hz, 1H), 4.41 – 4.35 (d, *J* = 3.8 Hz, 1H), 3.57 – 3.43 (m, 2H), 0.99 – 0.92 (s, 9H), 0.87 – 0.79 (d, *J* = 7.5 Hz, 6H), 0.15 – 0.07 (d, *J* = 1.5 Hz, 6H). **^{13}C NMR** (126 MHz,

CDCl3) δ 141.86, 127.83, 127.57, 127.19, 82.17, 73.00, 39.09, 25.95, 25.94, 25.92, 22.87, 19.40, 18.27, -5.55.

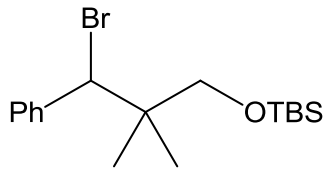

(3-bromo-2,2-dimethyl-3-phenylpropoxy)(*tert*-butyl)dimethylsilane (1-111): To a solution of triphenyl phosphine (3.67 g, 14.02 mmol) and imidazole (0.96 g, 14.02 mmol) in toluene (30 mL) was added a solution of 3-((*tert*-butyldimethylsilyl)oxy)-2,2-dimethyl-1-phenylpropan-1-ol **1-110** (2.75 g, 9.3 mmol) in toluene (20 mL) and the resulting solution was stirred for 15 minutes till the solids completely dissolve. To this solution carbon tetrabromide (CBr_4) (4.65 g, 14.02 mmol) was added in three portions. The resulting yellow colored reaction mixture was then refluxed overnight. The reaction was then quenched by addition of water (25 mL), the phases were separated and the organic phase was washed using saturated sodium thiosulfate solution (25 mL). The organics were combined, dried over anhydrous sodium sulfate and concentrated under reduced pressure to yield a pale yellow oil. This was then purified using flash chromatography over silica gel using 98:2 Hexanes: EtOAc as the eluent, to give 3.33 g (93%) of (3-bromo-2,2-dimethyl-3-phenylpropoxy)(*tert*-butyl)dimethylsilane **1-108** as a colorless oil. **^{1}H NMR** (500 MHz, CDCl3) δ 7.50 – 7.16 (m, 5H), 5.26 – 5.20 (s, 1H), 3.55 – 3.47 (d, *J* = 9.5 Hz, 1H), 3.21 – 3.14 (dd, *J* = 9.5, 0.9 Hz, 1H), 1.14 – 1.09 (s, 3H), 0.97 – 0.92 (m, 9H), 0.89 – 0.85 (s, 3H), 0.09 – 0.07 (d, *J* = 0.9 Hz, 3H), 0.06 – 0.05 (d, *J* = 0.9 Hz, 3H). **^{13}C NMR** (126 MHz, CDCl3) δ 139.84, 129.52, 127.84, 127.75, 70.18,

64.05, 41.78, 26.03, 25.94, 22.22, 21.45, -5.40. **HRMS:** Calculated for $C_{17}H_{30}BrOSi$- 357.12493; Found: [M+H] – 357.1253 (+1.7 ppm, 0.4 mmu)

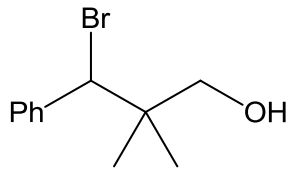

3-bromo-2,2-dimethyl-3-phenylpropan-1-ol (1-112): To a solution of (3-bromo-2,2-dimethyl-3-phenylpropoxy)(*tert*-butyl)dimethylsilane **1-111** (3.3 g, 9.3 mmol) in THF (25 mL). To this, a solution of HCl (6 mL 1N solution, excess) was added dropwise. The resulting solution was stirred at room temperature for 6h. The reaction was then quenched by adding a 10% solution of $NaHCO_3$. The phases were then separated and the aqueous phase was extracted with Et_2O (3 × 20 mL). The organic layers were then combined and washed with water (3 × 20 mL), dried over anhydrous sodium sulfate and concentrated under reduced pressure to yield a pale yellow oil. This was then purified using flash chromatography over silica gel using 1:1 Hexanes: EtOAc as the eluent to yield 1.76 g (78%) 3-bromo-2,2-dimethyl-3-phenylpropan-1-ol **1-109** as a colorless oil that solidified on standing. **^{1}H NMR** (500 MHz, CDCl3) δ 7.45 – 7.35 (m, 2H), 7.34 – 7.21 (m, 2H), 5.21 – 5.14 (s, 1H), 3.70 – 3.61 (d, *J* = 10.9 Hz, 1H), 3.36 – 3.28 (d, *J* = 10.9 Hz, 1H), 1.11 – 1.07 (s, 3H), 0.95 – 0.91 (s, 3H). **^{13}C NMR** (126 MHz, $CDCl_3$) δ 139.41, 129.45, 128.08, 127.95, 70.57, 63.83, 41.53, 21.77, 21.53. **Elemental analysis:** Calculated for $C_{11}H_{15}BrO$ - C, 54.34; H, 6.22; Br, 32.86; Found – C, 54.20; H, 6.26; Br, 32.65.

NMR data as additional proof for structure for compounds 1-93, 1-101 and 1-112

Elemental analysis on bromoalcohol **1-112** matched theory. Elemental analyses of iodoalcohols **1-93** and **1-101** confirmed nearly the expected weight percentage of iodine, but did not meet the convention of ≤ 0.4% difference between theory and actual for %C, %H, and %I. Since we were successful in getting good quality mass spectroscopy data on the TBS protected precursors **1-92**, **1-100** and **1-111**, we propose that comparison of the ^{1}H and ^{13}C NMR spectra of the protected and the unprotected alcohols in each case would provide additional support for the proposed structures of **1-93** and **1-101.**

In Figures 4-1 and 4-2, we compare the ^{1}H and the ^{13}C spectra respectively for **1-92** and **1-93**.

Figure 4-1: Comparison of the chemical shifts of alkyl protons in the ^{1}H NMR spectra of compounds **1-92** and **1-93**.

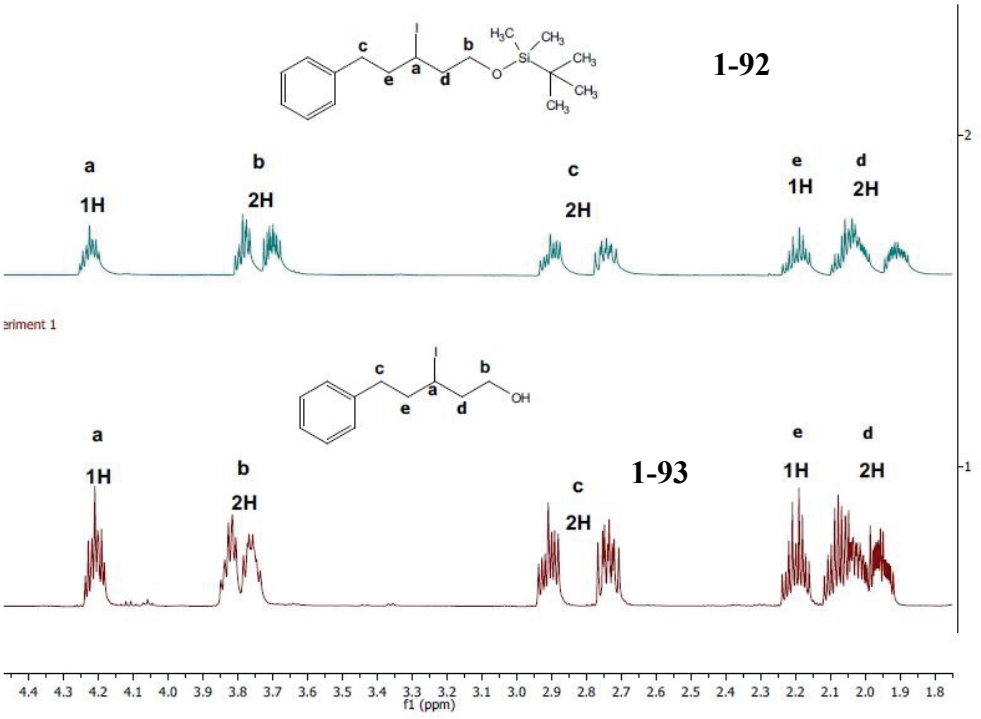

Figure 4-2: Comparison of the chemical shifts of alkyl carbons in the ^{13}C spectra of compounds **1-92** and **1-93**.

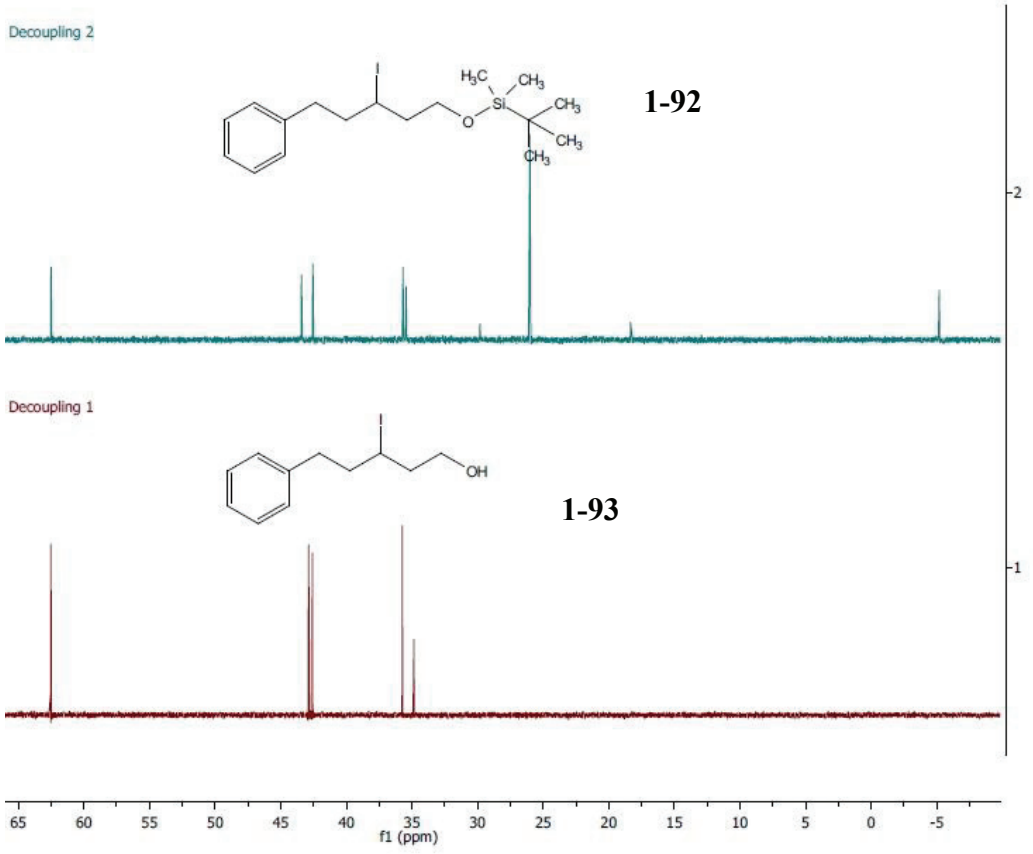

As seen from the proton spectrum in Figure 4-1, the chemical shifts of the alkyl protons in **1-92** and **1-93** match well with each other. Similarly, the chemical shifts of the peaks of the backbone carbons in **1-92** and **1-93** in Figure 4-2 match well. The absence of the TBS carbon peaks is clearly observed. Furthermore, the absence of a 19F-coupled carbon rules out the possibility of fluoride substitution of the iodide during silyl removal, consistent with the 42.18% iodide found by elemental analysis (43.74% theory).

A similar analysis for establishing the structure of compound **1-101** is shown in Figures 4-3 and 4-4.

Figure 4-3: Comparison of the chemical shifts of alkyl protons in the ^{1}H NMR spectra of compounds **1-100** and **1-101**.

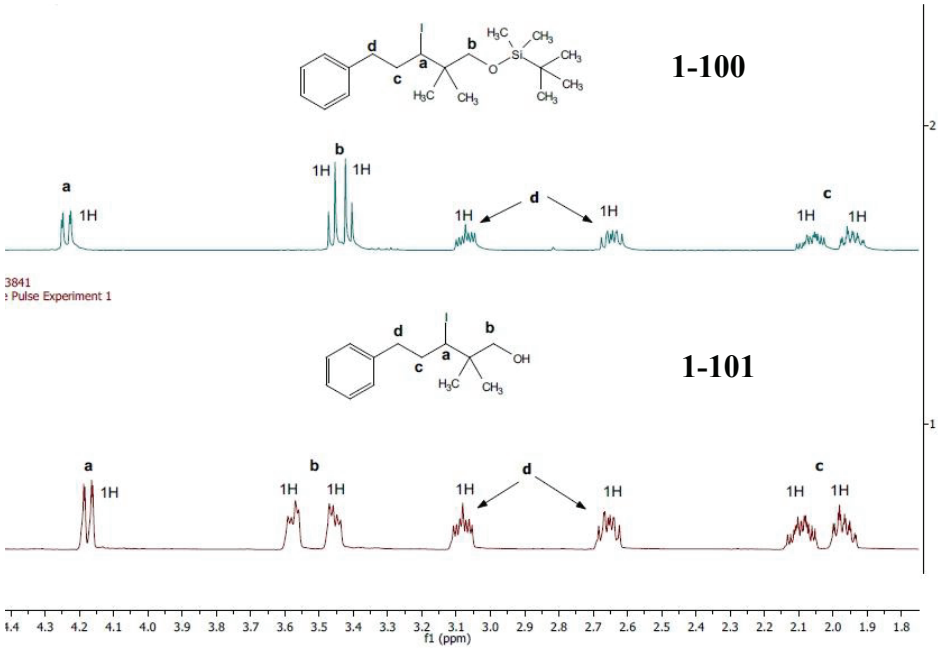

Figure 4-4: Comparison of the chemical shifts of alkyl carbons in the ^{13}C spectra of compounds **1-100** and **1-101**.

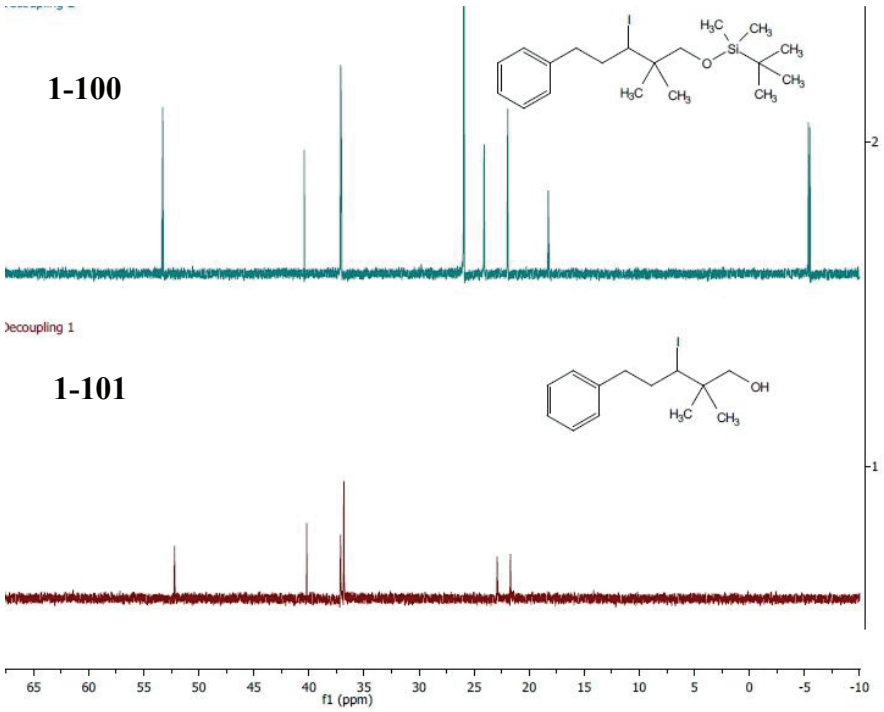

Finally, although the elemental analysis of bromoalcohol **1-112** was a match, for completeness and for the sake of comparison, we provide the same comparison of NMR spectra of silyl precursor **1-111** and alcohol **1-112** in Figures 4-5 and 4-6 respectively

Figure 4-5: Comparison of the chemical shifts of alkyl protons in the ^{1}H NMR spectra of compounds **1-111** and **1-112**.

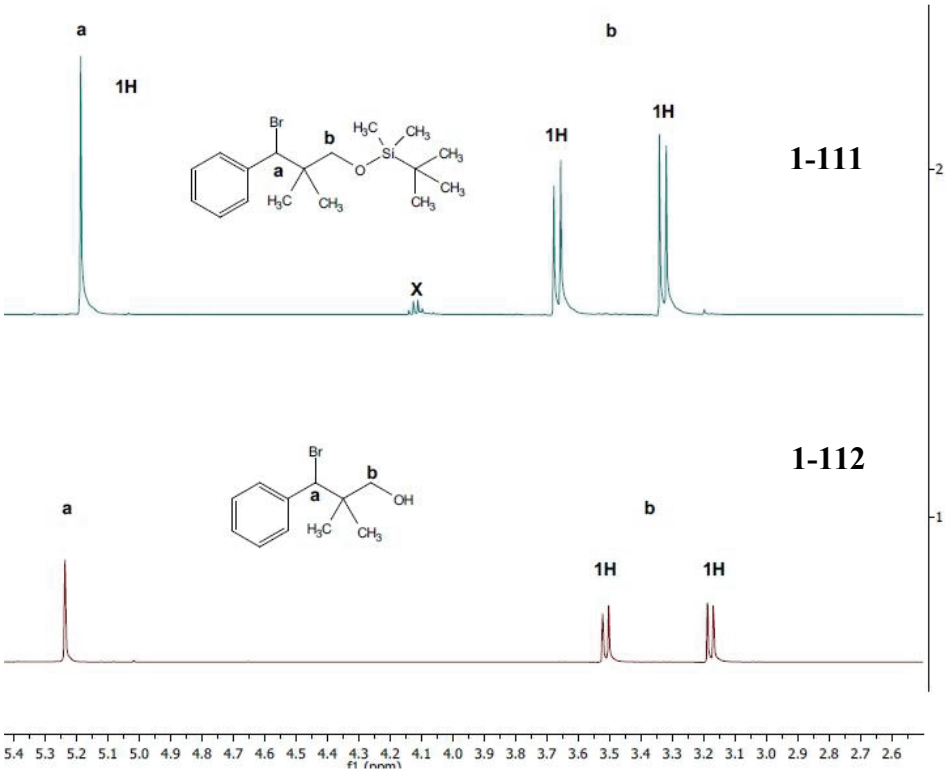

Figure 4-6: Comparison of the chemical shifts of alkyl protons in the ^{13}C NMR spectra of compounds **1-111** and **1-112**.

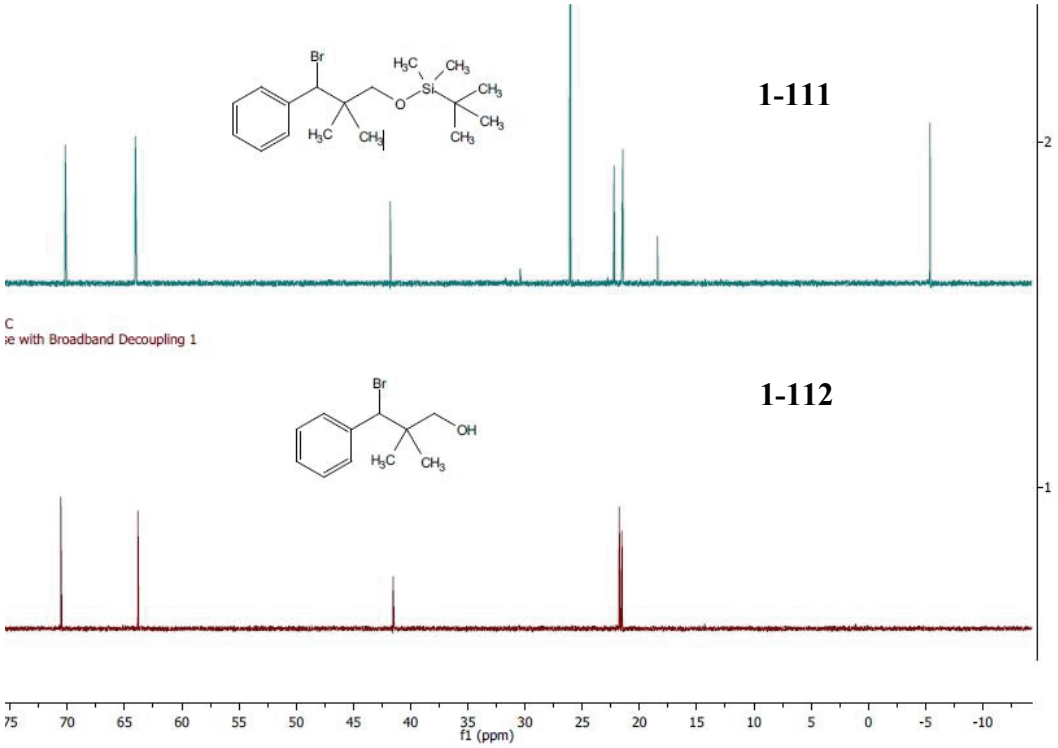

4.1.5: Mg/X exchange/ electrophilic trapping reactions of γ–hydroxyl group containing alkyl halides

These reactions were performed in 3 different ways, first with only *i*-PrMgCl, with using organolithium reagents to generate the intermediate ate complexes and then with these two methods at elevated temperatures.

4.1.5.1 Mg/X exchange reactions with 3.0 equiv of Grignard reagent (*i*-PrMgCl) in Et_2O at 195 K.

A flame-dried 10 mL round bottom flask was charged with 3-iodo-5-phenylpentan-1-ol **1-94** (30.0 mg, 0.135 mmol) and a magnetic stir-bar, capped with rubber septa, and purged with argon. Freshly distilled solvent (5 mL, Et_2O) was then added and the flask was placed in a constant temperature bath set at 195 K using dry-ice acetone bath. After allowing this reaction flask to cool for 15 minutes, *i*-PrMgCl (3 equiv, 0.16 mL of 2.0 M commercial in Et_2O) was added. Following a delay time of 5 minutes, MeI (0.127 mL, 2.7 mmol) was added to the reaction flask and was allowed to stir for 30 min at the temperature. After 30 minutes, the reaction was quenched by addition of sat NH_4Cl (0.500 mL, excess) and, the reaction mixture was extracted with Et_2O (3 x 5 mL). The combined organic fractions were dried over magnesium sulfate, filtered and concentrated under reduced pressure to give a colorless oil, which was purified by flash chromatography to isolate the individual components, which were analyzed individually by ^1H NMR spectroscopy ($CDCl_3$).

4.1.5.2 Mg/X exchange reactions with in-situ formation of ate complex.

A flame-dried 10 mL round bottom flask was charged 3-iodo-5-phenylpentan-1-ol **1-94** (30.0 mg, 0.1035 mmol) and a magnetic stir-bar, capped with rubber septa, and purged

with argon. Freshly distilled solvent (5 mL, Et_20) was then added and the flask was placed in a constant temperature bath set at 195 K. After allowing this reaction flask to cool for 15 minutes, *i*-PrMgCl (1.1 equiv, 0.058 mL of 2.0 M commercial in Et_2O) was added. Following a delay time of 5 minutes, *n*-BuLi (2.1 equiv, 0.087 mL of 2.5 M commercial in hexanes) [or *sec*-BuLi (2.1 equiv, 0.16 mL of 1.4 M commercial in cyclohexanes) or t-BuLi (2.1 equiv, 0.13 mL of 1.7 M commercial in hexanes)] was added and the mixture was allowed to stir for 30 minutes to allow the complete formation of ate species. A deep yellow color is observed for the solution at this point. After 30 minutes, the electrophile PhCHO (0.03 mL, 0.3 mmol, 2.5 equiv), was added to the reaction flask and allowed to stir for additional 30 minutes to allow the electrophilic quench reaction to complete. After 30 minutes, the reaction was quenched by addition of sat. NH_4Cl (0.500 mL, excess) and, the reaction mixture was extracted with Et_2O (3 x 5 mL). The combined organic fractions were dried over magnesium sulfate, filtered and concentrated under reduced pressure to give a pale yellow oil. This was purified by flash chromatography to isolate the individual components, which were analyzed individually by ^1H NMR spectroscopy ($CDCl_3$).

4.1.5.3 Mg/X exchange reactions with above protocols at elevated temperatures.

The initial steps of these reactions were similar to that shown in 4.1.4.1 and 4.1.4.2. After the addition of the electrophile, the reaction flask was transferred to a flask maintained at the desired temperature using an appropriate method. The reaction was then quenched at this new temperature.

4.1.5.4 Analytical data for the new products obtained after Mg/X exchange/ electrophilic trapping reactions of γ–hydroxyl group containing alkyl halides

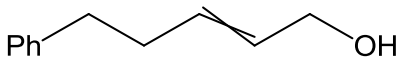

5-phenylpent-2-en-1-ol (1-97):

^{1}H NMR (500 MHz, CDCl3) δ 7.47 – 6.88 (m, 5H), 5.90 – 5.55 (m, 2H), 4.11 – 4.03 (d, *J* = 4.3 Hz, 2H), 2.73 – 2.67 (m, 2H), 2.41 – 2.33 (m, 2H).

4.2 Experimental procedures for Chapter 2

4.2.1 Procedures for Mg/Br exchange/D-OCH_3 trapping experiments

4.2.1.1 General Procedure for Mg/Br exchange/D-OCH_3 trapping experiments at $[Mg]_{total}$ = 0.034 M:

Five flame-dried 10 mL long neck round bottom flasks (custom built: necks 7.5 cm long) were each charged with bromonitrile (*S*)-**2-39** (8.5 mg, 0.0286 mmol) and a magnetic stir-bar, capped with rubber septa, and purged with nitrogen. Freshly distilled solvent (2 mL) was then added and the flasks were all placed in the same constant temperature bath set at the required temperature using appropriate cooling method. After allowing these reaction flasks to cool to the correct temperature for 15 minutes, *i*-PrMgCl (2.2 equiv, 0.035 mL of 2.0 M commercial or 0.070 mL of commercial 1.0 M commercial solution (2-MeTHF)) was added. At this point $[Mg]_{total}$ = 0.034 M and $[$(S)-**2-39**$]_0$ = 0.014 M. Following delay times *t* of 1, 5, 10, 30 and 60 minutes (or 15 and 20 minutes in some cases- see tables 4-6, 4-8, 4-9, 4-10 below), the reactions were quenched by a quick addition of CH_3OD (99.98% d, 0.020 mL, 20 equiv) from a flask that had been pre-cooled to the reaction temperature for 15 min, using a syringe. This operation was performed rapidly in order to avoid warm-up of the CH_3OD before addition to the reaction flask. After removing each flask from the cooling bath, water (1 mL) was added and, the reaction mixture was extracted with Et_2O (3 x 5 mL). The combined organic fractions were dried over magnesium sulfate, filtered and concentrated in vacuo to give ~6.0 mg of a white solid (95% wt recovery). This solid was analyzed by ^1H NMR spectroscopy ($CDCl_3$) in each case to demonstrate >99 % conversion of starting material and >95% deuterium incorporation in **[D_1]-2-41**.

4.2.1.2 Mg/Br exchange/D-OCH_3 trapping experiments at varying $[Mg]_{total}$ in Et_2O

Reactions at $[Mg]_{total}$ of 0.0625 M were performed in Et_2O similarly to the general procedure above. Reactions at $[Mg]_{total}$ = 0.00625 M and 0.0025 M were performed in 25 mL and 50 mL round bottom flasks respectively. In both these cases, 0.100 mL or 100 equiv of CH_3OD was added to ensure rapid and complete quench of the organomagnesium species in these solutions of significantly larger volume.

4.2.1.3 Mg/Br exchange/D-OCH_3 trapping experiments at varying $[Et_2O]$

Part A: Preparation of 0.25 M stock solutions of *i*-PrMgCl in Et_2O and Et_2O-Toluene mixtures

In order to perform measurements of k_{enant} at various $[Et_2O]$ we adopted the following procedure. Three different 0.25 M stock solutions of *i*-PrMgCl A-C were prepared by diluting the commercially available 2.0 M Et_2O solution of *i*-PrMgCl using Et_2O and Et_2O-toluene mixtures. The volumes of solvents used are listed in Table 4-1 below. The solutions were prepared as follows: In a 10 mL flame dried pear shaped flask, equipped with magnetic stir-bar and rubber septa and purged with nitrogen, was charged 1 mL of 2.0 M *i*-PrMgCl solution, ***x*** mL (Table 4-1) of Et_2O and ***y*** mL (Table 4-1) of toluene. Based on the density of the stated 2.0 M commercial solution of *i*-PrMgCl in Et_2O (0.834 g/mL – Sigma Aldrich), 1 mL of this solution contains 0.89 mL of Et_2O. The v/v% of Et_2O in the stock solution was calculated from the total volume of Et_2O in the solution (***x*** mL + 0.89 mL)/ Total volume of the stock solution (8 mL).

Table 4-1: Preparation of 0.25 M stock solutions of *i*-PrMgCl.

Stock Solution	Volume of 2.0M iPrMgCl used (mL)	Volume of added Et_2O *x* (mL)	Volume of added toluene *y* (mL)	Total Volume (mL)	Final [*i*-PrMgCl] M	v/v % Et_2O in stock
A	1	7	0	8	0.25	98.64
B	1	4	3	8	0.25	15.29
C	1	1	6	8	0.25	5.91

Part B: Mg/Br exchange/D-OCH_3 trapping experiments at varying [Et_2O]

Similar to the general procedure above, five flame-dried 10 mL long neck round bottom flasks (custom built: necks 7.5 cm long) were each charged with bromonitrile (*S*)-**1**(8.5 mg, 0.0286mmol) and a magnetic stir-bar, capped with rubber septa, and purged with nitrogen. Freshly distilled Et_2O, ***a*** mL (Table 4-2) and, toluene ***b*** mL (Table 4-2) was then added and the flasks were all placed in the same constant temperature bath set at the required temperature using appropriate cooling method. Along with these reaction flasks the pear shaped flask containing the appropriate stock solution required for this set of experiments (A, B or C- see Part A above) was placed in this bath. After allowing these flasks to cool to the correct temperature for 15 minutes, *i*-PrMgCl (0.25 M from the pre-cooled stock solution, 0.25 mL, 2.2 equiv) was added into these flasks using a syringe. This operation was performed rapidly to avoid significant warm up of the stock solution before addition. At this point, the total volume of the reaction is 10 mL and $[Mg]_{total}$ = 0.006 M. Following delay times *t* of 1, 5, 10, 20 minutes, the reactions were quenched, worked-up and analyzed as explained in the general procedure above. The volumes of solvents used and the appropriate final [Et_2O] achieved are listed in Table 4-2 below. The final [Et_2O] was calculated from the molarity of pure Et_2O at room temp (9.5 M)* (Total volume of Et_2O/ Total volume of reaction solution)

Table 4-2: Volumes of added solvent and final [Et_2O]

Entry	Volume of Et_2O added *a* (mL)	Volume of Toluene added *b* (mL)	Volume of *i*-PrMgCl Stock solution added (mL)	Volume of Et_2O in 0.25 mL Stock (mL)	Total Volume of Et_2O (mL)	Final [Et_2O] M
1	9.75	0	0.25 (A)	0.246	9.996	9.52
2	0.75	9	0.25 (A)	0.246	0.996	0.95
3	0	9.75	0.25 (A)	0.246	0.246	0.23
4	0	9.75	0.25 (B)	0.153	0.153	0.15
5	0	9.75	0.25 (C)	0.059	0.059	0.06

4.2.2 Analysis of Deuterio product [D_1]-2-41 using ^{1}HNMR and HPLC

4.2.2.1 Determination of %Conversion and %Deuterium incorporation by ^{1}H NMR Spectroscopy.

As seen in Figure 4-1 below, the chemical shifts for the diastereotopic H_A and H_B protons of the product deuterionitrile **[D_1]-2-41** (top) can be clearly distinguished from the corresponding protons in the starting material (*S*)**-2-39** (bottom). Furthermore, protonated product **2-41** (middle) differs from **[D_1]-2-41** (top) in the multiplicity of H_A and H_B as well as in the distinct proton H_C. According to the integration, the ratio of **[D_1]-2-41** to **2-41** is 98:2. No signal for residual **2-39** is seen at δ 2.56, allowing us to estimate >99% conversion of **2-39**. Even for the shortest time points in all three solvents, >95% conversion of **2-39** to deuterionitrile **[D_1]-2-41** is observed.

Figure 4-7: Overlay of the alkyl regions of the ^{1}H NMR spectra of pure samples of **[D$_1$]-2-41**, **2-41**, and (*S*)**-2-39**

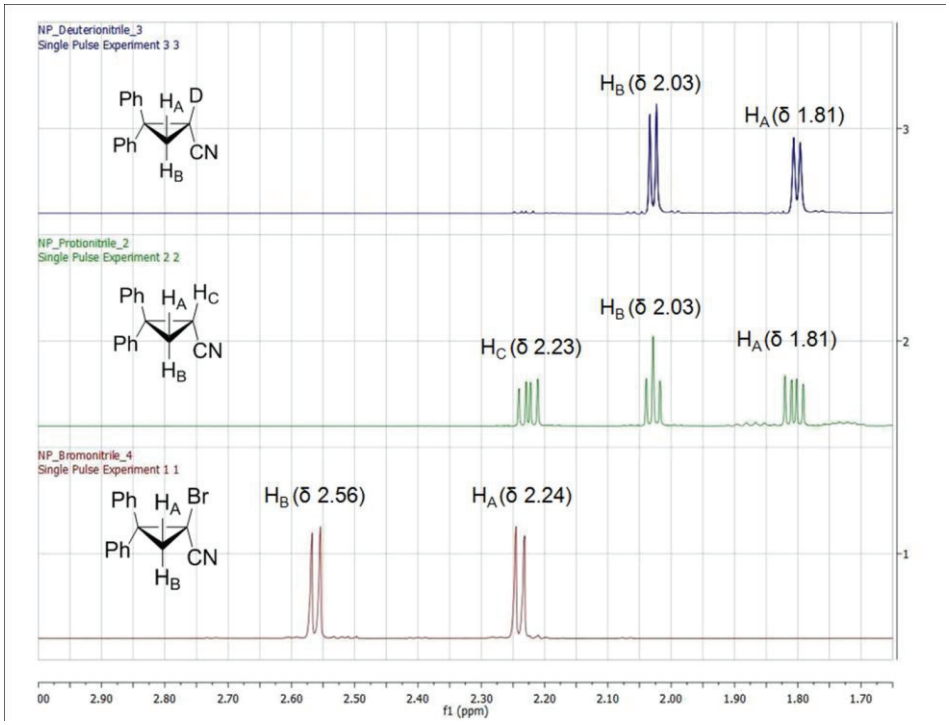

Figure 4-8. ^{1}H NMR Spectrum of a typical Mg/Br exchange/trapping reaction mixture (Et_2O, 195 K, t = 5 min)

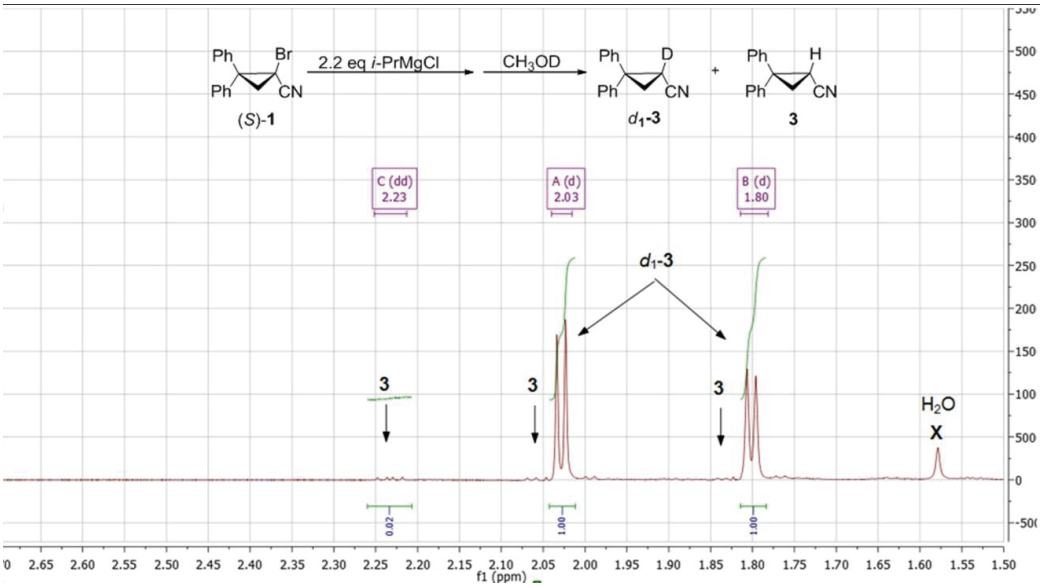

4.2.2.1 Determination of enantiomer ratio using CSP-HPLC analysis

To remove any highly polar materials before HPLC analysis, the crude product mixture in the NMR tube was passed through short plug of silica gel, and concentrated in vacuo. The resulting white solid was analyzed by HPLC by dissolving 1 mg in 1 mL of the mobile phase (99:1 hexanes:*i*-PrOH) by vigorous shaking and sonication. This solution was filtered through a 0.45μ Teflon syringe filter injected into the HPLC (10 uL). The HPLC conditions and retention times are given in Table 4-3 below.

Table 4-3: HPLC analysis conditions and retention times

Sample	Column	solvent, flow rate	fast enantiomer retention time (config)	slow enantiomer retention time (config)
(±)-**2-39**	OD-H	1% isopropanol-hexane, 0.8 mL/min	25.1 min (R)	26.9 min (S)
(±)-**[D_1]-2-41**	AD-H	1% isopropanol-hexane, 0.8 mL/min	16.6 min (S)	18.5 min (R)

Figure 4-9: HPLC Chromatogram (OD-H) of mixture of (*S*)- and (*R*)-**2-39** (72:28 er)

Virginia Tech
Project Name: Neeraj
Reported by User: System

Breeze

SAMPLE INFORMATION

Sample Name:	Rac-Std	Acquired By:	System
Sample Type:	Unknown	Date Acquired:	10/5/2010 7:53:00 PM
Vial:	1	Acq. Method:	1%B@80%flow
Injection #:	1	Processed By:	System
Injection Volume:	10.00 ul	Date Processed:	5/12/2011 5:16:07 PM
Run Time:	60.00 Minutes	Channel Name:	2487Channel 1
Sampling Rate:	1.00 per sec	Sample Set Name:	NP_10_05_2010

Sample Values
Used in Calculations:

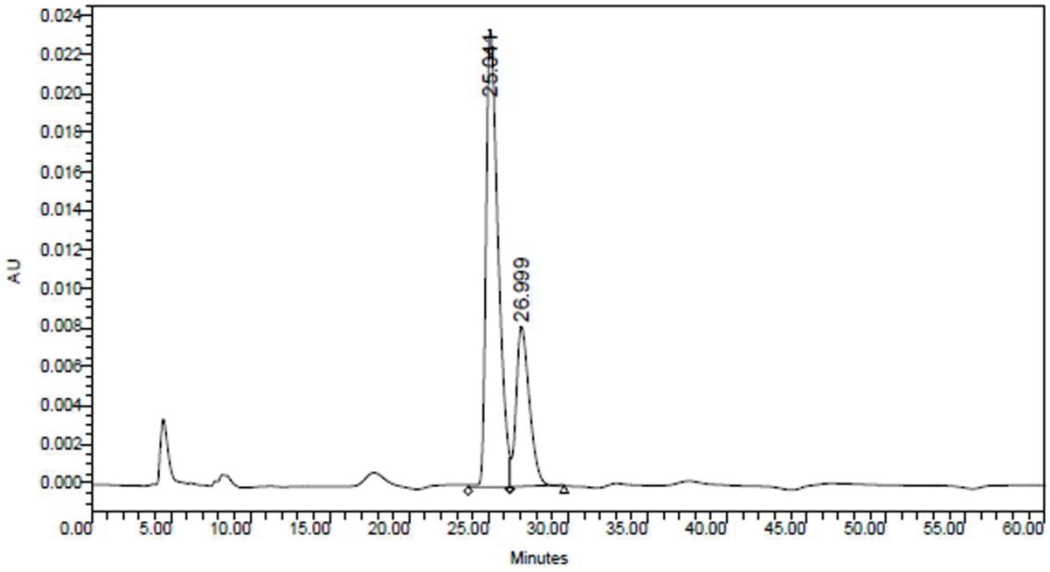

	RT (min)	Peak Type	Area (µV*sec)	% Area	Height (µV)	% Height	Integration Type	Points Across Peak	Start Time (min)	End Time (min)
1	25.041	Unknown	1247269	72.27	23508	74.05	VV	157	23.717	26.350
2	26.999	Unknown	478672	27.73	8236	25.95	VB	206	26.350	29.783

Figure 4-10: HPLC Chromatogram (OD-H) of enantiopure (*S*)-**2-39**

Virginia Tech
Project Name: Neeraj
Reported by User: System

Breeze

SAMPLE INFORMATION

Sample Name:	NP-IV-95E	Acquired By:	System
Sample Type:	Unknown	Date Acquired:	10/5/2010 9:42:30 PM
Vial:	2	Acq. Method:	1%B@80%flow
Injection #:	1	Processed By:	System
Injection Volume:	10.00 ul	Date Processed:	5/12/2011 5:14:58 PM
Run Time:	60.00 Minutes	Channel Name:	2487Channel 1
Sampling Rate:	1.00 per sec	Sample Set Name:	NP_10_05_2010

Sample Values
Used in Calculations:

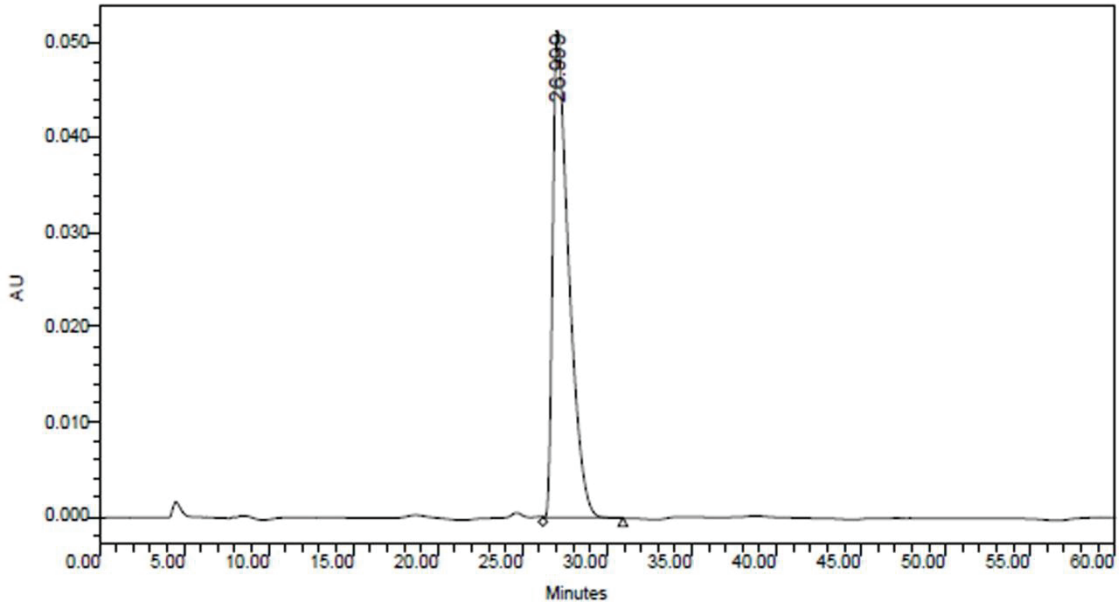

	RT (min)	Peak Type	Area (μV*sec)	% Area	Height (μV)	% Height	Integration Type	Points Across Peak	Start Time (min)	End Time (min)
1	26.999	Unknown	3390304	100.00	51419	100.00	VB	285	26.217	30.967

Figure 4-11: HPLC Chromatogram (AD-H) of (±)-**[D_1]-2-41**

Virginia Tech
Project Name: Neeraj
Reported by User: System

Breeze

SAMPLE INFORMATION

Sample Name:	NP-IV-031	Acquired By:	System
Sample Type:	Unknown	Date Acquired:	4/8/2010 1:05:07 AM
Vial:	4	Acq. Method:	1%B@80%flow
Injection #:	1	Processed By:	System
Injection Volume:	10.00 ul	Date Processed:	4/8/2010 9:59:00 AM
Run Time:	40.00 Minutes	Channel Name:	2487Channel 1
Sampling Rate:	1.00 per sec	Sample Set Name:	NP_04_08_10_THF_78

Sample Values
Used in Calculations:

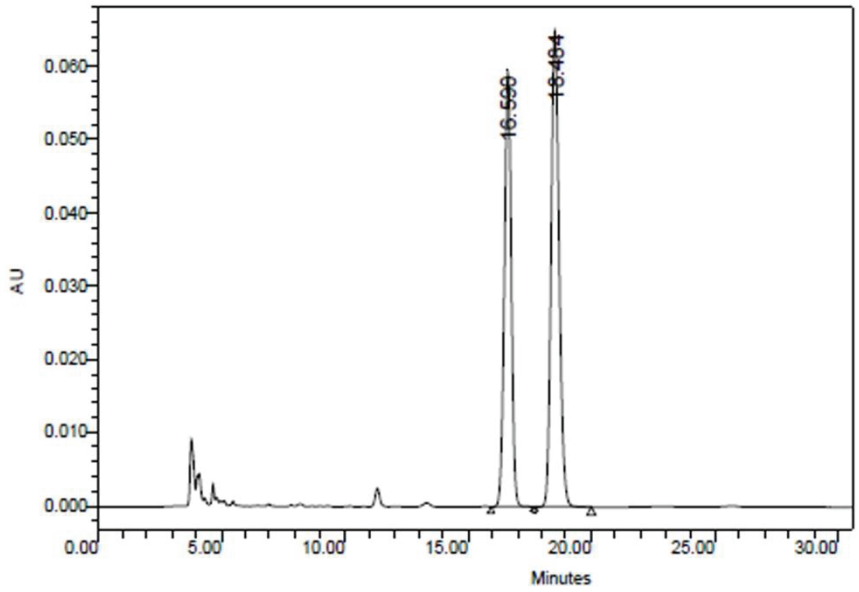

	RT (min)	Peak Type	Area (μV*sec)	% Area	Height (μV)	% Height	Integration Type	Points Across Peak	Start Time (min)	End Time (min)
1	16.590	Unknown	1158215	44.07	59484	47.81	BV	104	15.950	17.700
2	18.484	Unknown	1469913	55.93	64943	52.19	VB	136	17.700	19.983

Figure 4-12: HPLC Chromatogram (AD-H) of enantioenriched **[D_1]-2-41** ((*R*) : (*S*) = 90 : 10)

Virginia Tech
Project Name: Neeraj
Reported by User: System

Breeze

SAMPLE INFORMATION

Sample Name:	NP-IV-037	Acquired By:	System
Sample Type:	Unknown	Date Acquired:	4/18/2010 8:46:50 PM
Vial:	2	Acq. Method:	1%B@80%flow
Injection #:	1	Processed By:	System
Injection Volume:	10.00 ul	Date Processed:	4/19/2010 10:11:51 AM
Run Time:	40.00 Minutes	Channel Name:	2487Channel 1
Sampling Rate:	1.00 per sec	Sample Set Name:	NP_04_18_10

Sample Values
Used in Calculations:

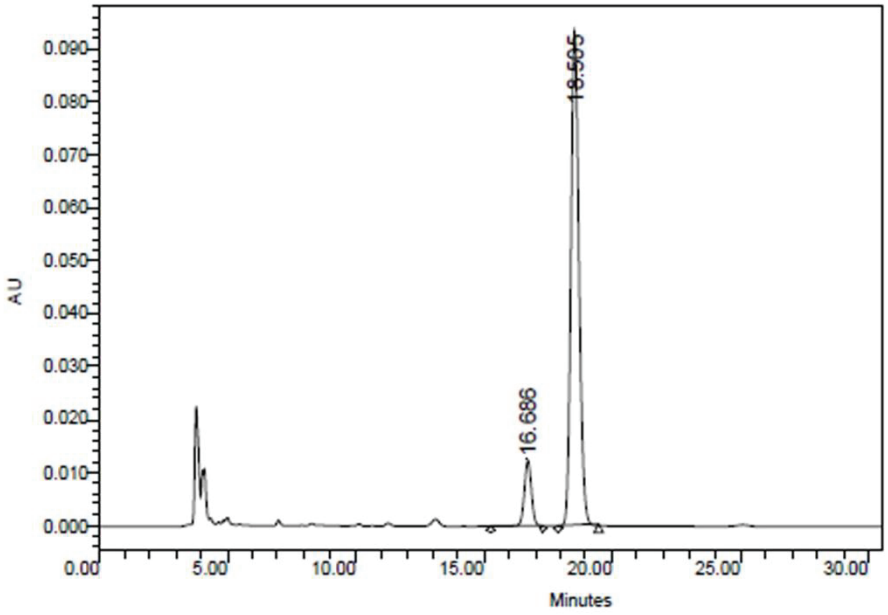

	RT (min)	Peak Type	Area (µV*sec)	% Area	Height (µV)	% Height	Integration Type	Points Across Peak	Start Time (min)	End Time (min)
1	16.686	Unknown	240250	10.56	12429	11.74	VV	121	15.300	17.333
2	18.505	Unknown	2034572	89.44	93427	88.26	VB	94	17.900	19.483

4.2.3 Kinetic data and plots

4.2.3.1 – Error estimation method

As described in Chapter 2 section 2.4, first order enantiomerization rate constants were determined by plotting ln(|2X_R(**[D$_1$]-2-41**)-1|) vs delay time t; the slope of this line is -2k_{enant}. The "Data Analysis Add-In" tool of Excel 2007 (PC) was used to calculate the standard error in the slope; the error in k_{enant} is half of this quantity. Errors in logarithmic functions of k_{enant} such as $\Delta G^{\ddagger}$ and ln($t_{1/2}$(rac))were calculated using the standard formula for propagation: if f = a*ln(b*A), error(f) = a*error(A)/A.[12] Errors in calculated $\Delta H^{\ddagger}$ and $\Delta S^{\ddagger}$ from Eyring plots were determined from the standard errors in slope and intercept, according to the graphing method employed.

4.2.3.2 – Raw data for determination of k_{enant} in 3 solvents

Table 4-4: Enantiomer ratios in diethyl ether (Et_2O) at $[Mg]_{total}$ = 0.0342 M.

Entry	**Temp T (K)**	**Delay Time t (s)**	er (**[D$_1$]-2-41**: *ent*-**[D$_1$]-2-41**)	2X_R(**[D$_1$]-2-41**)-1	ln (|2X_R(**[D$_1$]-2-41**)-1|)
1	175	60	95:5	0.9006	-0.104694071
2		300	94:6	0.883	-0.124430078
3		600	93:7	0.863	-0.147340588
4		1800	93:7	0.8548	-0.156887756
5		3600	92:8	0.8442	-0.169365846
6	195	60	95:5	0.89	-0.116533816
7		300	94:6	0.8874	-0.11945944
8		600	92:8	0.8442	-0.169365846
9		1800	91:9	0.8096	-0.21121498
10		3600	88:12	0.7678	-0.264225996
11	212	60	93:7	0.8616	-0.148964153
12		300	88:12	0.767	-0.265268478
13		600	84:16	0.6792	-0.386839644
14		1800	79:21	0.5684	-0.564929883
15		3600	65:35	0.2914	-1.233058385
16	231	60	73:27	0.4748	-0.744972248
17		300	69:31	0.3794	-0.969164221
18		600	66:34	0.3214	-1.135068826
19		900	63:37	0.2502	-1.385494681
20		1200	58:42	0.165	-1.801809805

Table 4-5: Enantiomer ratios in diethyl ether (2-MeTHF) at $[Mg]_{total}$ = 0.0342 M.

Entry	**Temp *T* (K)**	**Delay Time *t* (s)**	er (**[D_1]-2-41**: *ent*-**[D_1]-2-41**)	$2X_R$(**[D_1]-2-41**)-1	ln (|$2X_R$(**[D_1]-2-41**)-1|)
1	175	60	84:16	0.6776	-0.389198136
2		300	88:12	0.757	-0.278392026
3		600	84: 16	0.686	-0.376877651
4		1800	80:20	0.6096	-0.494952275
5		3600	75:25	0.4902	-0.712941808
6	195	60	78:22	0.5698	-0.562469857
7		300	77:23	0.5308	-0.633369977
8		600	73:27	0.4698	-0.755448207
9		1800	66:34	0.3214	-1.135068826
10		3600	60:40	0.1974	-1.622523152
11	212	60	69:31	0.373	-0.986176859
12		300	64:36	0.2718	-1.302688777
13		600	62:38	0.2334	-1.455001559
14		1800	57:43	0.1472	-1.915963073
15		3600	54:46	0.0792	-2.53577898

Table 4-6: Enantiomer ratios in diethyl ether (THF) at $[Mg]_{total}$ = 0.0342 M.

Entry	**Temp *T* (K)**	**Delay Time *t* (s)**	er (**[D_1]-2-41**: *ent*- **[D_1]-2-41**)	$2X_R$(**[D_1]-2-41**)-1	ln (|$2X_R$(**[D_1]-2-41**)-1|)
1	175	60	69:31	0.373	-0.986176859
2		300	63:37	0.267	-1.320506621
3		600	62:38	0.2334	-1.455001559
4		1800	57:43	0.1472	-1.915963073
5		3600	56:44	0.119	-2.128631786
6	195	60	61:39	0.2154	-1.535258514
7		300	56:44	0.1274	-2.060423536
8		600	56:44	0.1186	-2.131998792
9		1800	53:47	0.0618	-2.783851915
10		3600	51:49	0.017	-4.074541935
11	212	60	54:46	0.0838	-2.479322271
12		300	53:47	0.0528	-2.941244088
13		600	52:48	0.031545427	-3.456326632
14		900	51:49	0.0268	-3.619353391
15		1200	51:49	0.01309869	-4.335243044

Rate constants and plots of ln(|$2X_R$(**[D_1]-2-41**)-1|) vs delay time *t* in these three solvents are reported in Table 2-1, 2-2 and 2-3 and Figures 2-2, 2-3 and 2-4 of Chapter 2.

4.2.3.2 Determination of activation parameters using standard Eyring analysis

Figure 2-5 of chapter 2 shows the calculations of the activation parameters $\Delta H^{\ddagger}$ and $\Delta S^{\ddagger}$ from the plot of $\Delta G^{\ddagger}$ vs T. This calculation can also be performed by plotting the Eyring equation ($\Delta G^{\ddagger}$ =-RT*ln((h/k_BT)*k_{enant}) Equation 12 Chapter 2). The straight line plot of ln((h*k_{enant} /k_BT) vs 1/T is used for this purpose. The enthalpy of activation $\Delta H^{\ddagger}$ is calculated from the slope of this line using Equation 1 and the entropy of activation $\Delta S^{\ddagger}$ is calculated from the intercept of this line on the Y axis using Equation 2.

$$\Delta H^{\ddagger} = -(\text{slope}*R) \text{ (kcal/mol)} \quad (1)$$

$$\Delta S^{\ddagger} = (\text{Intercept})*R \text{ eu} \quad (2)$$

Figure 4-13: Traditional Eyring Plot to determine the activation parameters of the enantiomerization process in 3 solvents at $[Mg]_{total}$ = 0.0342 M.

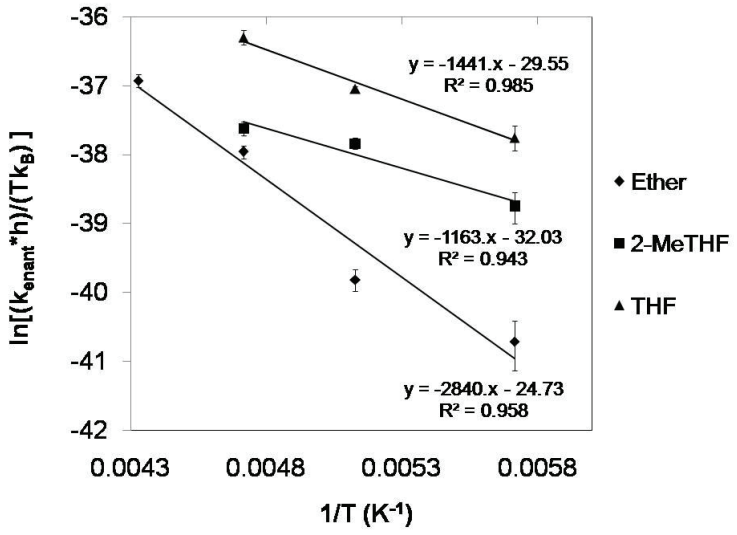

Table 4-7: Activation parameters from the Eyring analysis

Solvent	$\Delta H^{\ddagger}$=-(slope*R) (kcal/mol)	$\Delta S^{\ddagger}$=(Intercept)*R eu
Diethyl Ether	5.3 ± 0.2	-51± 1
Me-THF	2.3 ± 0.6	-66 ± 3
THF	2.6 ± 0.4	-60 ± 2

Note that the $\Delta G^{\ddagger} = \Delta H^{\ddagger} - T\Delta S^{\ddagger}$ plotting method gave values of $\Delta H^{\ddagger}$ and $\Delta S^{\ddagger}$ that are indistinguishable within error (see Figure 2-5 of Chapter 2).

4.2.3.3 Kinetic plots and rate constants as $[Mg]_{total}$ is varied in Et_2O at 195 K

Table 4-8: Enantiomer ratios at four different $[Mg]_{total}$ at a constant temp of 195 K

Note that data at 0.0342 M is reproduced from Table 4-4.

Entry	**$[Mg]_{total}$ M**	**Delay Time *t* (s)**	er (**[D_1]-2-41**: *ent*- **[D_1]-2-41**)	$2X_R$(**[D_1]-2-41**)-1	ln ($\|2X_R$(**[D_1]-2-41**)-1$\|$)
1	0.0625	60	94:6	0.8768	-0.1314764
2		300	93:7	0.8604	-0.1503579
3		600	92:8	0.848	-0.1648746
4		1200	92:8	0.8396	-0.1748297
5		1800	90:10	0.8085	-0.2125562
6	0.0342	60	95:5	0.89	-0.116533816
7		300	94:6	0.8874	-0.11945944
8		600	92:8	0.8442	-0.169365846
9		1800	91:9	0.8096	-0.21121498
10		3600	88:12	0.7678	-0.264225996
11	0.00625	60	92:8	0.8342	-0.1812821
12		300	92.8	0.8416	-0.1724504
13		600	92:8	0.8358	-0.1793659
14		1200	90:10	0.809	-0.2119564
15		1800	88:12	0.7678	-0.264226
16	0.00250	60	91:9	0.8266	-0.1904344
17		300	89:11	0.7886	-0.2374961
18		600	89:11	0.7812	-0.2469241
19		1200	88:12	0.7702	-0.2611051
20		1800	87:13	0.7466	-0.2922257

Rate constants and plots of ln($|2X_R$(**[D_1]-2-41**)-1$|$) vs delay time *t* in these concentrations are reported in Table 2-4 and Figures 2-7 of Chapter 2.

4.2.3.4 Kinetic plots and rate constants as [Et_2O] is varied in toluene at two temperatures

Table 4-9: Enantiomer ratios at varying concentrations of Et_2O solvent at 195 K.

Entry	[Et_2O] M	Delay Time *t* (s)	er ([**D_1]-2-41**: *ent*-[**D_1]-2-41**)	$2X_R$([**D_1]-2-41**)-1	ln ($\|2X_R$([**D_1]-2-41**)-1$\|$)
1	9.5	60	92:8	0.8342	-0.18128
2		300	92.:8	0.8416	-0.17245
3		600	91:9	0.8358	-0.17937
4		1200	90:10	0.809	-0.21196
5		1800	88:12	0.7678	-0.26423
6	0.95	60	97:3	0.9388	-0.06315
7		300	96:4	0.914	-0.08992
8		600	96:4	0.9164	-0.0873
9		1200	94:6	0.883	-0.12443
10	0.23	60	97:3	0.9368	-0.06529
11		300	96:4	0.9108	-0.09343
12		600	96:4	0.914	-0.08992
13		1200	94:6	0.8842	-0.12307
14	0.15	60	98:2	0.9592	-0.04166
15		300	97:3	0.944	-0.05763
16		600	96:4	0.9396	-0.0623
17		1200	96:4	0.911	-0.09321
18	0.056	300	98:2	0.9604	-0.04041
19		600	98:2	0.959	-0.04186
20		900	97:3	0.951	-0.05024
21		1200	97:3	0.9386	-0.06337

Table 4-10: Enantiomer ratios at varying concentrations of Et_2O solvent at 212 K.

Entry	[Et_2O] M	Time t min	er ([**D_1]-2-41**: *ent*-[**D_1]-2-41**)	$2X_R$([**D_1]-2-41**)-1	ln ($\|2X_R$([**D_1]-2-41**)-1$\|$)
1	9.53	60	93:7	0.8616	-0.14896
2		300	88:12	0.767	-0.26527
3		600	84:16	0.6792	-0.38684
4		1200	78:22	0.5684	-0.56493
5	0.953	60	97:3	0.939	-0.06294
6		300	89:11	0.7716	-0.25929
7		600	88:12	0.7576	-0.2776
8		1200	83:17	0.6472	-0.4351
9	0.23	60	93:7	0.8516	-0.16064
10		300	93:7	0.8542	-0.15759
11		600	91:9	0.8288	-0.18778
12		1200	83:17	0.664	-0.40947
13	0.15	60	97:3	0.9398	-0.06209
14		300	93:7	0.856	-0.15548
15		600	93:7	0.8522	-0.15993
16		1200	89:11	0.7842	-0.24309
17	0.056	120	97:3	0.9312	-0.07128
18		300	96:4	0.926	-0.07688
19		600	96:4	0.9152	-0.08861
20		1200	95:5	0.9066	-0.09805

Rate constants and plots of ln(|2X_R(**[D_1]-2-41**)-1|) vs delay time *t* in these concentrations of [Et_2O] at 195 K and 212 K are reported in Tables 2-6 and 2-7 and Figures 2-8 and 2-9 of Chapter 2.

For the experimental details on reaction stoichiometry studies, please see the supporting information from our communication on this topic.[13]

4.3 Experimental Data for Chapter 3

4.3.1: Tabulation of energies of all structures studied in chapter 3

Table 4-11: Electronic Energies, ZPVE at 298.15 K and 1 atm, all at B3LYP/6-31G* for MeMgCl monomers (**3-24**) and dimers (**3-25**)

Structure	ε_0 (hartrees)[a,b]	ZPVE[c]	ΔE_{solv}[d] (kcal/mol)	$\Delta E_{Z,solv}$[e] (kcal/mol)
Me_2O	-155.025044198	0.078733	-	-
Et_2O	-233.663459329	0.134809	-	-
3-24	-700.26603120	0.035527	0	0
3-24•Me_2O	-855.32596680	0.116565	-21.9	-20.4
3-24• $(Me_2O)_2$	-1010.37769466	0.197103	-16.7	-15.6
3-24• $(Me_2O)_3$-A	-1165.41119918	0.278374	-5.3	-3.7
3-24• $(Me_2O)_3$-B	-1165.40624183	0.278334	-2.2	-0.6
3-24•Et_2O	-933.95973515	0.171997	-19.0	-17.9
3-24• $(Et_2O)_2$	-1167.64543592	0.309474	-14.0	-12.3
3-24• $(Et_2O)_3$-A_1	-1401.31442830	0.446214	-3.5	-2.3
3-24• $(Et_2O)_3$-A_2	-1401.31222529	0.446063	-2.1	-1.0
3-25	-1400.58618906	0.072033	0	0
3-25•Me_2O	-1555.64301535	0.152813	-19.9	-18.7
cis-**3-25• $(Me_2O)_2$**	-1710.69562865	0.233558	-17.3	-16.0
trans- **3-25• $(Me_2O)_2$**	-1710.69895933	0.233529	-19.4	-18.1
3-25• $(Me_2O)_3$-A	-1865.73504995	0.314217	-6.9	-5.7
3-25• $(Me_2O)_3$-B	-1865.73414297	0.314217	-6.4	-5.1
3-25• $(Me_2O)_3$-C	-1865.73039970	0.314346	-4.0	-2.7
3-25• $(Me_2O)_3$-open	-1865.72812638	0.314504	-2.6	-1.2

3-25•Et_2O	-1634.27792510	0.208828	-17.7	-16.5
cis-**3-25• $(Et_2O)_2$**	-1867.96543856	0.345491	-15.1	-13.9
trans- **3-25• $(Et_2O)_2$**	-1867.96770763	0.345400	-16.5	-15.4
3-25• $(Et_2O)_3$-A	-2101.63814907	0.482257	-4.4	-3.1
3-25• $(Et_2O)_3$-B	-2101.63731748	0.482360	-3.9	-2.5
3-25• $(Et_2O)_3$-C	-2101.63096893	0.481680	0.1	1.0
3-25• $(Et_2O)_3$-open	-2101.63249772	0.482231	-0.8	0.4

[a] Electronic energies in hartrees, [b] All B3LYP/6-31G* stationary points are characterized by zero imaginary frequencies. [c] Zero-point vibrational energies based on frequencies corrected by a factor of 0.9815 at 298.15 K and 1 atm. [d]Incremental energy of solvation: change in energy from $(Me_2O/Et_2O)_n$ solvate to $(Me_2O/Et_2O)_{n+1}$ solvate. [e] Incremental energy of solvation, based on ZPVE-corrected energies.

Table 4-12: MP2/6-31G* Single-point electronic energies on B3LYP/6-31G* optimized geometries of selected (lowest energy conformer) solvates of MeMgCl monomers (**3-24**) and dimers (**3-25**).

Structure	**ε_0** [a]	**ΔE_{solv}** [b] **(kcal/mol)**
Me_2O	-154.50331080	-
Et_2O	-232.84538940	-
3-24	-699.05435360	0
3-24•Me_2O	-853.59862180	-25.7
3-24• $(Me_2O)_2$	-1008.13549420	-21.0
3-24• $(Me_2O)_3$-A	-1162.65680370	-11.3
3-24□Et_2O	-931.93799790	-24.0
3-24• $(Et_2O)_2$	-1164.81446350	-19.5
3-24• $(Et_2O)_3$-A_1	-1397.67865920	-11.8
3-25	-1398.17060030	0
3-25•Me_2O	-1552.71329600	-24.7
trans- **3-25• $(Me_2O)_2$**	-1707.25600890	-24.7

3-25• $(Me_2O)_3$-A	-1861.77865960	-12.1
3-25• $(Me_2O)_3$-open	-1861.76705310	-4.8
3-25•Et_2O	-1631.05381970	-23.7
trans- **3-25• $(Et_2O)_2$**	-1863.93581520	-23.0
3-25• $(Et_2O)_3$-A	-2096.80034580	-12.0
3-25• $(Et_2O)_3$-open	-2096.78980210	-5.4

[a] All energies in hartrees. [b]Incremental energy of solvation: change in energy from $(Me_2O/Et_2O)_n$ solvate to $(Me_2O/Et_2O)_{n+1}$ solvate.

Table 4-13: Free energies at 195 K calculated at B3LYP/6-31G* for selected (lowest energy conformer) solvates of MeMgCl monomers (**3-24**) and dimers (**3-25**)

Structure	ε_0 [a]	G_{corr} [b] (195 K)	G (195 K)	ΔG_{solv} [c]
Me_2O	-155.025044198	0.063924	-154.961120198	-
Et_2O	-233.663459329	0.117043	-233.546416329	-
3-24	-700.26603120	0.018876	-700.247155203	0
3-24•Me_2O	-855.32596680	0.095238	-855.230728796	-14.1
3-24• $(Me_2O)_2$	-1010.37769466	0.171664	-1010.206030660	-8.9
3-24• $(Me_2O)_3$-A	-1165.41119918	0.250680	-1165.160519180	4.2
3-24•Et_2O	-933.95973515	0.147764	-933.81197115	-11.5
3-24• $(Et_2O)_2$	-1167.64543592	0.280422	-1167.36501392	-4.2
3-24• $(Et_2O)_3$-A_1	-1401.31442830	0.413054	-1400.90137430	6.3
3-25	-1400.58618906	0.047532	-1400.53865706	0
3-25•Me_2O	-1555.64301535	0.126421	-1555.51659435	-10.6
trans- **3-25• $(Me_2O)_2$**	-1710.69895933	0.202009	-1710.49695033	-12.1
3-25• $(Me_2O)_3$-A	-1865.73504995	0.281283	-1865.45285997	3.3
3-25• $(Me_2O)_3$-open	-1865.72812638	0.279197	-1865.44892938	5.7
3-25•Et_2O	-1634.27792510	0.179394	-1634.09853110	-8.4
trans- **3-25• $(Et_2O)_2$**	-1867.96770763	0.309974	-1867.65773363	-8.0
3-25• $(Et_2O)_3$-A	-2101.63814907	0.442502	-2101.19564707	5.3

3-25• $(Et_2O)_3$-open	-2101.63249772	0.441833	-2101.19066472	8.5

[a] All energies in hartrees, [b] Calculated from the free energy corrections (at 195 K) to the absolute energies ε_0, determined from B3LYP/6-31G* frequencies, scaled by 0.9804. [c] Incremental free energy of solvation: change in free energy from $(Me_2O/Et_2O)_n$ solvate to $(Me_2O/Et_2O)_{n+1}$ solvate.

Table 4-14: Free energies at 195 K calculated at MP2/6-31G*//B3LYP/6-31G* using G_{corr} values obtained at B3LYP/6-31G* for selected (lowest energy conformers) solvates of MeMgCl monomers (**3-24**) and dimers (**3-25**)

Structure	ε_0 [a]	G_{corr} [b] (195 K)	G (195 K)	ΔG_{solv} [c]
Me_2O	-154.50331080	0.063924	-154.961120198	-
Et_2O	-232.84538940	0.117043	-233.546416329	-
3-24	-699.05435360	0.018876	-699.035477600	0
3-24•Me_2O	-853.59862180	0.095238	-853.503383800	-17.9
3-24• $(Me_2O)_2$	-1008.13549420	0.171664	-1007.963830200	-13.2
3-24• $(Me_2O)_3$-A	-1162.65680370	0.250680	-1162.406123700	-1.8
3-24•Et_2O	-931.93799790	0.147764	-931.790233900	-16.6
3-24• $(Et_2O)_2$	-1164.81446350	0.280422	-1164.534041500	-9.7
3-24• $(Et_2O)_3$-A_1	-1397.67865920	0.413054	-1397.265605200	-2.0
3-25	-1398.17060030	0.047532	-1398.123068300	0.0
3-25•Me_2O	-1552.71329600	0.126421	-1552.586875000	-15.3
trans- **3-25• $(Me_2O)_2$**	-1707.25600890	0.202009	-1707.053999900	-17.4
3-25• $(Me_2O)_3$-A	-1861.77865960	0.281283	-1861.497376600	-2.5
3-25• $(Me_2O)_3$-open	-1861.76705310	0.279197	-1861.487856100	3.5
3-25•Et_2O	-1631.05381970	0.179394	-1630.874425700	-14.4
trans- **3-25• $(Et_2O)_2$**	-1863.93581520	0.309974	-1863.625841200	-14.5
3-25• $(Et_2O)_3$-A	-2096.80034580	0.442502	-2096.357843800	-2.3
3-25• $(Et_2O)_3$-open	-2096.78980210	0.441833	-2096.347969100	3.9

[a] All energies in hartrees, [b] Calculated from the free energy corrections (at 195 K) to the absolute energies ε_0, determined from B3LYP/6-31G* frequencies, scaled by 0.9804. [c] Incremental free energy of solvation: change in free energy from $(Me_2O/Et_2O)_n$ solvate to $(Me_2O/Et_2O)_{n+1}$ solvate.

Table 4-15: Electronic Energies, ZPVE at 298.15 K and 1 atm, all at B3LYP/6-31G* for heterodimers **3-27**, **3-28**, and **3-29** of magnesiated cyclopropylnitrile/*i*-PrMgCl.

Structure	ε_0 (hartrees)[a,b]	ZPVE[c]	ΔE_{solv}[d] (kcal/mol)	$\Delta E_{Z,solv}$[e] (kcal/mol)
Me_2O	-155.025044198	0.078733	-	-
Et_2O	-233.663459329	0.134809	-	-
3-27	-1648.83164588	0.162751	0	0
3-28	-1648.84079825	0.163258	0	0
3-29	-1648.85345327	0.163676	0	0
3-27•Me_2O	-1803.91376614	0.243927	-35.8	-34.3
3-28•Me_2O	-1803.91387646	0.244100	-30.1	-28.8
3-29•Me_2O	-1803.91356118	0.244359	-22.0	-20.8
trans-**3-27• (Me_2O)$_2$**	-1958.95725944	0.324735	-11.6	-10.3
cis-**3-27• (Me_2O)$_2$**	-1958.94543086	0.324224	-4.1	-3.2
trans-**3-29• (Me_2O)$_2$**	-1958.96956462	0.324831	-19.2	-18.0
cis-**3-29• (Me_2O)$_2$**	-1958.96666783	0.324892	-17.6	-16.5
3-29• (Me_2O)$_3$ - A	-2114.00660138	0.406062	-7.5	-6.0
3-29• (Me_2O)$_3$ - B	-2114.00802702	0.406345	-8.4	-6.7
3-27•Et_2O	-1882.55265600	0.298784	-36.1	-35.3
3-28•Et_2O	-1882.55217269	0.300227	-30.1	-28.7
3-29•Et_2O	-1882.54850661	0.300420	-19.8	-18.6
trans-**3-27• (Et_2O)$_2$**	-2116.22783160	0.436706	-7.3	-5.4
cis-**3-27• (Et_2O)$_2$**	-2116.21014264	0.441653	3.7	8.8
trans-**3-29• (Et_2O)$_2$**	-2116.24036925	0.437005	-17.8	-16.7
cis-**3-29• (Et_2O)$_2$**	-2116.23709858	0.437249	-15.7	-14.5
3-29• (Et_2O)$_3$ - A	-2349.90579200	0.573987	-1.2	0.1
3-29• (Et_2O)$_3$ - B	-2349.90655181	0.574138	-1.7	-0.2
3-29• (Et_2O)$_4$	-2583.56811392	0.710872	1.2	2.4
3-32• (Et_2O)$_3$ (TS)	-2349.88277238	0.573042	13.2	14.0
3-33• (Et_2O)$_3$ (SIP)	-2349.88712484	0.573351	10.5	11.4
3-34• (Et_2O)$_4$	-2583.56609801	0.708803	2.5	2.4

3-35• $(Et_2O)_3$	-2349.90351402	0.573360	0.2	1.2

[a] Electronic energies in hartrees, [b] All B3LYP/6-31G* stationary points are characterized by zero imaginary frequencies. [c] Zero-point vibrational energies based on frequencies corrected by a factor of 0.9815 at 298.15 K and 1 atm. [d]Incremental energy of solvation: change in energy from $(Me_2O/Et_2O)_n$ solvate to $(Me_2O/Et_2O)_{n+1}$ solvate. [e] Incremental energy of solvation, based on ZPVE-corrected energies.

Table 4-16: MP2/6-31G* Single-point electronic energies on B3LYP/6-31G* optimized geometries of selected (lowest energy conformer) solvates of heterodimer **3-29** of magnesiated cyclopropylnitrile/*i*-PrMgCl.

Structure	**ε_0 [a]**	**ΔE_{solv} [b] (kcal/mol)**
3-29	-1645.64938778	0
3-29•Me_2O	-1800.19635270	-27.4
trans- **3-29• $(Me_2O)_2$**	-1954.74032960	-25.5
3-29• $(Me_2O)_3$-B	-2109.26671980	-14.5
3-29•Et_2O	-1878.53707360	-26.5
trans- **3-29• $(Et_2O)_2$**	-2111.42240210	-25.1
3-29• $(Et_2O)_3$-B	-2344.28516900	-10.9
3-29• $(Et_2O)_4$	-2577.14647360	-11.0

[a] All energies in hartrees. [b]Incremental energy of solvation: change in energy from $(Me_2O/Et_2O)_n$ solvate to $(Me_2O/Et_2O)_{n+1}$ solvate.

Table 4-17: Free energies at 195 K calculated at B3LYP/6-31G* for selected (lowest energy conformer) solvates of heterodimer **3-29** of magnesiated cyclopropylnitrile/*i*-PrMgCl.

Structure	**ε_0 [a]**	**G_{corr} [b] (195 K)**	**G (195 K)**	**ΔG_{solv} [c]**
3-29	-1648.85345327	0.136899	-1648.71670205	0
3-29•Me_2O	-1803.91356118	0.212621	-1803.70094018	-14.6
trans- **3-29• $(Me_2O)_2$**	-1958.96956462	0.288504	-1958.68106062	-11.9
3-29• $(Me_2O)_3$-B	-2114.00802702	0.372922	-2113.63510523	4.4
3-29•Et_2O	-1882.54850661	0.267389	-1882.28111761	-11.4

trans- **3-29• $(Et_2O)_2$**	-2116.24036925	0.39846	-2115.84190925	-9.0
3-29• $(Et_2O)_3$-B	-2349.90655181	0.531653	-2349.37489881	8.4
3-29• $(Et_2O)_4$	-2583.56811392	0.664321	-2582.90379292	11.0

[a] All energies in hartrees, [b] Calculated from the free energy corrections (at 195 K) to the absolute energies ε_0, determined from B3LYP/6-31G* frequencies, scaled by 0.9804. [c] Incremental free energy of solvation: change in free energy from $(Me_2O/Et_2O)_n$ solvate to $(Me_2O/Et_2O)_{n+1}$ solvate.

Table 4-18: Free energies at 195 K calculated at MP2/6-31G*//B3LYP/6-31G* using G_{corr} values obtained at B3LYP/6-31G* for selected (lowest energy conformer) solvates of heterodimer **3-29** of magnesiated cyclopropylnitrile/*i*-PrMgCl.

Structure	**ε_0 [a]**	**G_{corr} [b] (195 K)**	**G (195 K)**	**ΔG_{solv} [c]**
3-29	-1645.64938778	0.136899	-1645.512488780	0.0
3-29•Me_2O	-1800.19635270	0.212621	-1799.983731700	-20.0
trans- **3-29• $(Me_2O)_2$**	-1954.74032960	0.288504	-1954.451825600	-18.0
3-29• $(Me_2O)_3$-B	-2109.26671980	0.372922	-2108.893797800	-1.6
3-29•Et_2O	-1878.53707360	0.267389	-1878.269684600	-18.1
trans- **3-29• $(Et_2O)_2$**	-2111.42240210	0.39846	-2111.023942100	-16.3
3-29• $(Et_2O)_3$-B	-2344.28516900	0.531653	-2343.753516000	-0.8
3-29• $(Et_2O)_4$	-2577.14647360	0.664321	-2576.482152600	-0.2

[a] All energies in hartrees, [b] Calculated from the free energy corrections (at 195 K) to the absolute energies ε_0, determined from B3LYP/6-31G* frequencies, scaled by 0.9804. [c] Incremental free energy of solvation: change in free energy from $(Me_2O/Et_2O)_n$ solvate to $(Me_2O/Et_2O)_{n+1}$ solvate.

4.3.2: XYZ Coordinates for all B3LYP/6-31G* optimized structures studied in Chapter 3.

Me_2O

C	-1.170811000000	0.000000000000	-0.195281000000
H	-1.232397000000	-0.892927000000	-0.839757000000
H	-1.232397000000	0.892927000000	-0.839757000000
H	-2.021657000000	0.000000000000	0.491395000000
O	0.000000000000	0.000000000000	0.589950000000
C	1.170811000000	0.000000000000	-0.195281000000
H	1.232397000000	-0.892927000000	-0.839757000000
H	2.021657000000	0.000000000000	0.491395000000
H	1.232397000000	0.892927000000	-0.839757000000

Et_2O

C	0.000024000000	0.521920000000	-1.182683000000
H	0.887401000000	1.178742000000	-1.206210000000
H	-0.886862000000	1.179335000000	-1.207075000000
O	-0.000686000000	-0.256992000000	0.000000000000
C	0.000024000000	0.521920000000	1.182683000000
H	0.887401000000	1.178742000000	1.206210000000
H	-0.886862000000	1.179335000000	1.207075000000
C	0.000212000000	-0.416540000000	-2.378840000000
H	-0.887451000000	-1.057257000000	-2.363584000000
H	0.886529000000	-1.059059000000	-2.361801000000
H	0.001710000000	0.153927000000	-3.314296000000
C	0.000212000000	-0.416540000000	2.378840000000
H	0.001710000000	0.153927000000	3.314296000000
H	0.886529000000	-1.059059000000	2.361801000000
H	-0.887451000000	-1.057257000000	2.363584000000

3-24

Mg	0.469170145249	0.000551326296	0.000000000000
C	2.549336772387	0.003553933789	0.000000000000
H	2.947116000246	1.025484384893	-0.000000000002
H	2.950862793677	-0.505852100775	-0.884147308236
H	2.950862793677	-0.505852100771	0.884147308238
Cl	-1.750116021939	-0.002569171294	0.000000000000

3-24•Me_2O

C	-0.194679711535	2.735986384565	-0.015177563799
H	-0.764074145368	2.967454430381	0.896815936849
H	-0.845598995536	2.990313442985	-0.864379967358
H	0.640632916480	3.448083372847	-0.044609498666
Mg	0.489586178751	0.753268618381	-0.072430530616
Cl	2.259212912461	-0.654690010054	-0.171601882034
O	-1.140796126317	-0.555084748425	-0.014589166683

C	-1.051098376009	-1.991220366393	-0.038944729530
H	-1.577166825656	-2.379128576094	-0.918932607935
H	-1.497807729798	-2.404493079477	0.872782443287
H	0.009120100397	-2.238598733486	-0.089439587785
C	-2.491457642545	-0.076113469174	0.052680554889
H	-3.053988616860	-0.418305915458	-0.823987148617
H	-2.445252055482	1.013210330853	0.065596985035
H	-2.973491882984	-0.442956681452	0.966542762963

3-24•Et_2O

C	1.254546578412	1.468187905912	1.860509877969
H	1.751900561171	0.649274283027	2.399866393357
H	0.518008189885	1.893733232997	2.557062958072
H	2.016172794435	2.242214939739	1.696422459611
Mg	0.389506085651	0.828501503764	0.065459203333
Cl	0.485642285333	1.013750469133	-2.198449255637
O	-1.226247535550	-0.547427711111	0.185513012323
C	-0.977107803873	-1.888489888197	-0.296729943519
H	-1.013286749497	-1.876979366151	-1.392808437970
H	-1.783421732144	-2.531398673963	0.078735680256
C	-2.526455967395	-0.053985333043	-0.213718212059
H	-2.579505697302	-0.054915026013	-1.309206198224
H	-3.279952555391	-0.748675005495	0.178901123923
C	0.373662964362	-2.368366267715	0.203018104012
H	0.524479342684	-3.409026068055	-0.102854910077
H	0.434464259022	-2.318097441348	1.294657287215
H	1.197454660439	-1.788038694325	-0.230996732861
C	-2.735335023784	1.342597131576	0.343553594420
H	-3.748274747209	1.681796449508	0.102355770992
H	-2.043966426492	2.066471114265	-0.106003879257
H	-2.617438482755	1.358571445494	1.431593104120

3-24•$(Me_2O)_2$

Mg	0.001774451513	0.008488126424	-0.794874918523
Cl	0.100516681098	-2.302099920153	-0.786154127440
O	1.640904947621	0.438403199358	0.511278835496
O	-1.643214664598	0.298048247216	0.542216780932
C	2.280236137639	1.717478488138	0.502709657212
H	1.712530334576	2.352878018018	-0.177383316133
H	3.312266337781	1.622062654015	0.142863483610
H	2.283585420699	2.147430401679	1.512602356925
C	2.326274264908	-0.527232300466	1.319660383788
H	2.312682517515	-0.213447790385	2.371226198525
H	3.364157686927	-0.629733700352	0.979999716563
H	1.802384266519	-1.473931533705	1.188967741579
C	-0.077607715236	1.580957091504	-2.213188954249
H	-0.954985945082	1.485795497579	-2.871416206901
H	0.794532283276	1.560533575164	-2.884861808260
H	-0.118407818056	2.608219939126	-1.814416336082

C	-2.229824581511	-0.722162453210	1.361177576704
H	-1.629209982940	-1.620685245343	1.220844890441
H	-3.260738872923	-0.913195386216	1.038994333956
H	-2.225327090210	-0.407748666626	2.412632102174
C	-2.389212681788	1.517993240569	0.545916859698
H	-3.415323407587	1.334970249990	0.203437423954
H	-1.889297001611	2.199233190181	-0.142963407634
H	-2.412058568533	1.946397077495	1.556213733665

3-24•(Et_2O)$_2$

Mg	-0.039680451143	0.253171575221	1.108702273451
O	1.791959488198	0.166004249363	-0.008440807987
O	-1.378994110898	-0.429075978461	-0.418928732348
Cl	-0.488689281077	2.526844399414	1.057779775234
C	0.125104165214	-1.190308106218	2.650153227111
H	0.880741193316	-0.917811683387	3.403881463772
H	0.382873997715	-2.210772376916	2.322065690776
H	-0.816435776763	-1.286700979300	3.213198966720
C	2.929179506758	-0.483334994994	0.605051941613
H	2.520928771330	-0.980579552229	1.486982876204
H	3.629820361015	0.291885984409	0.941854221036
C	2.098319177243	1.150592265867	-1.031331409349
H	3.164255359419	1.395758927465	-0.964805586170
H	1.523782477885	2.042955467858	-0.769386326378
C	1.728192739350	0.646195329305	-2.418401216197
H	2.309652786503	-0.236819387833	-2.701273587378
H	1.913439418988	1.433314020249	-3.158678111201
H	0.665842320060	0.385852821135	-2.459367799848
C	3.615757662069	-1.485834175577	-0.311928313967
H	4.420905199731	-1.987471335338	0.237299581314
H	4.061098853351	-1.005878443523	-1.189680224662
H	2.908124258218	-2.248686964140	-0.653365382410
C	-2.214980782620	0.455221716472	-1.208017244210
H	-2.055196320998	0.212905452170	-2.267422731911
H	-1.817425925393	1.451249376616	-1.007241516283
C	-3.690852166370	0.394567549471	-0.843330850870
H	-3.830735253420	0.596349324391	0.223161718575
H	-4.144530101802	-0.571981306806	-1.084944387410
H	-4.228245604643	1.165496721396	-1.407887847818
C	-1.462033774438	-1.841133784429	-0.727268736585
H	-1.810446375133	-1.941690065184	-1.762406844371
H	-0.434574078876	-2.216393322750	-0.683564731873
C	-2.345120739800	-2.617216509931	0.240384607156
H	-2.309836493336	-3.683323358480	-0.015005870529
H	-3.387498570269	-2.290451501047	0.195181722708
H	-1.984846929385	-2.498436354259	1.265582194085

3-24•$(Me_2O)_3$-A

Cl	0.132784217035	0.091829074883	1.782217690018
Cl	0.184296110942	0.076574647930	-1.799130416401
C	2.671662957767	2.760876619003	0.010476477707
H	3.315285956025	2.884138214425	0.895415377874
H	2.001668412162	3.633088160610	0.005725173844
H	3.322573863456	2.880031991131	-0.869666397330
Mg	1.610723452375	0.941215429689	0.010439353827
O	3.009550692781	-0.642232121682	0.038860606659
C	4.418021001665	-0.392424511791	0.029856507204
H	4.873618035065	-0.828038048719	-0.868147657967
H	4.883535420477	-0.822670501746	0.925304458588
H	4.546828430355	0.690136421342	0.025868620804
C	2.676783357078	-2.034337166826	0.044555267495
H	1.589399258636	-2.107004124972	0.051532591602
H	3.090044382963	-2.513439593840	0.940667335192
H	3.079108590427	-2.518621715566	-0.853745115663
Mg	-1.572200229266	-0.115022722445	-0.033781832184
C	-3.679628853060	-0.355920800356	-0.039198695961
H	-4.059504078777	-0.743040307671	0.920449504663
H	-4.028697280518	-1.066939451871	-0.805232702718
H	-4.238553270852	0.574383026398	-0.223610790175
O	-1.525342544809	2.161238708300	-0.040291949177
O	-1.124735324108	-2.356107302053	-0.015286199517
C	-2.031100384314	2.805655412042	1.133880033993
H	-1.718335405311	3.857190740352	1.143635522568
H	-1.600877581052	2.288997559028	1.991784178626
H	-3.126363231306	2.745349562799	1.165296424282
C	-1.967125689093	2.814456978878	-1.235037812364
H	-1.500579320827	2.296719140746	-2.073030234305
H	-1.644670242900	3.863069452114	-1.225043737197
H	-3.060128224517	2.765319964509	-1.320445559151
C	-1.558201585309	-3.042288787409	1.162664035914
H	-1.114993398494	-4.046356835523	1.194252863909
H	-2.651861933693	-3.122242653348	1.185544624870
H	-1.207593522268	-2.460879503029	2.016246592952
C	-1.470753441138	-3.066004967437	-1.207655982571
H	-1.065327666518	-2.496942305973	-2.044976049022
H	-2.559708519522	-3.155053419401	-1.305716184359
H	-1.020872411556	-4.067486262519	-1.189823926526

3-24•$(Me_2O)_3$-B

Cl	0.285531315885	-0.809163112082	1.456998423485
Cl	0.849093020895	1.300753735697	-1.217387944713
C	3.394311377551	1.723808665197	1.916429102172
H	3.987183237659	1.116588015220	2.618211549522
H	2.811863630020	2.416171406080	2.542466469180
H	4.110092585677	2.352040425598	1.363901553877

Mg	2.158228734465	0.569172447140	0.658764338006
O	3.336629507058	-0.906120467281	-0.291332116593
C	4.758945498873	-0.751297215770	-0.344202341042
H	5.065565444128	-0.379214672803	-1.329842783680
H	5.245914784295	-1.713758553871	-0.145503322060
H	5.028649805367	-0.029314978257	0.427074506321
C	2.834559094394	-1.826824753028	-1.268232290205
H	1.757884964771	-1.902426931438	-1.119447750233
H	3.300335967227	-2.808851259605	-1.122468820990
H	3.041691878252	-1.458764269249	-2.279607219461
Mg	-1.182913371323	-0.260308105797	-0.474912964489
O	-2.195433540997	1.603476168090	-0.167442619852
O	-2.934339652107	-1.020091070351	0.802971745903
C	-1.637349231581	-1.400211732198	-2.200077341585
H	-1.964681823108	-2.427633643985	-1.971629106862
H	-0.781790343671	-1.498244911888	-2.883969001352
H	-2.447270336869	-0.960882322434	-2.806623663343
C	-2.367493340268	2.465588249590	-1.302687911386
H	-2.536382584648	1.822005658910	-2.167471228408
H	-1.467930795673	3.066982006809	-1.464723337661
H	-3.238419389737	3.112295593767	-1.140095158298
C	-1.939692178208	2.331460939625	1.042157900664
H	-1.012653956803	2.908074205208	0.948265572908
H	-1.841439075750	1.597185991089	1.842544021878
H	-2.780602319386	3.003311384596	1.252780475716
C	-2.827532630746	-2.308465277550	1.417098759079
H	-1.845361455717	-2.361589155444	1.884326727318
H	-2.929446251009	-3.103278853926	0.666739151925
H	-3.609197536812	-2.423748473756	2.179273316764
C	-4.213162016459	-0.841836557960	0.190264174829
H	-4.240361607852	0.174225845285	-0.201889932715
H	-5.007071595701	-0.968489361921	0.938119144412
H	-4.357106812091	-1.560242057306	-0.625999079030

3-24•$(Et_2O)_3$-A_1

C	0.013938839208	0.662903438116	-2.464073464216
H	0.053321876632	-0.278421126393	-3.039514446182
H	0.887221978378	1.242421259476	-2.803821306729
H	-0.863633321748	1.202214597806	-2.854208986348
Mg	-0.028689512131	0.525003225180	-0.328856840540
Cl	-0.204287210949	1.798639442989	1.644046549240
O	-2.483519895641	0.347026951361	-0.291169337558
O	-0.030818764872	-1.512992259170	0.372941680641
O	2.292858472670	0.569671521722	-0.096197176419
C	-3.129523128733	-0.273509182858	-1.412270763781
H	-2.321319349606	-0.619628886952	-2.059827969000
H	-3.696420953271	0.477473923612	-1.978000805535
C	-4.035174571512	-1.432378722832	-1.003436844215
H	-4.465195245805	-1.902585258354	-1.895924746390
H	-4.864934276035	-1.103788457839	-0.368722980325

H	-3.470824843958	-2.192575520974	-0.452744831736
C	-3.311933511128	1.293541474831	0.417977455049
H	-4.325871900553	0.882618172421	0.510001011972
H	-2.873418671148	1.366520729891	1.413346760616
C	-3.331321339019	2.665183020621	-0.244496750382
H	-3.717897451270	2.627287923505	-1.269046079675
H	-2.322124365147	3.085692730575	-0.262433943535
H	-3.974143591692	3.342300127282	0.330796158248
C	-0.361145402695	-1.782745163445	1.762655092160
H	-0.941406006452	-2.712026659561	1.802468170954
H	-0.999387911996	-0.958861370973	2.089168237645
C	0.886011956693	-1.855828291382	2.628377160091
H	0.595839039382	-2.006749305417	3.674995929081
H	1.440697067963	-0.916282752360	2.561199609548
H	1.543677426884	-2.679084544378	2.330642327005
C	-0.244599509109	-2.599587035598	-0.547396722954
H	-0.147738346334	-2.147271406521	-1.537305825067
H	-1.276939160689	-2.957523323512	-0.436636991653
C	0.742424344321	-3.747705796464	-0.380151610259
H	0.542519422656	-4.511615389330	-1.140775696177
H	0.654202042152	-4.224816069094	0.601396410990
H	1.772626632761	-3.400977850649	-0.505507595376
C	3.070570818205	-0.107152653942	-1.096547909525
H	2.342836644834	-0.580634691491	-1.759371978330
H	3.622616478389	0.627951026940	-1.696485751383
C	2.993857021004	1.636737546397	0.582082896022
H	4.025342104904	1.315752382175	0.774159590206
H	2.479939306805	1.751842507094	1.536444517990
C	2.959919052605	2.945330006655	-0.196938679560
H	3.407475894011	2.847576164584	-1.192249752722
H	3.521811092693	3.712295448963	0.349584623599
H	1.929262913043	3.294205828818	-0.308370472704
C	4.018842836679	-1.142469045645	-0.499869773548
H	4.547574789733	-1.669167783362	-1.303403716901
H	3.464748556872	-1.877681056601	0.092218604813
H	4.773389632016	-0.685462845915	0.148976962857

3-24•$(Et_2O)_3$-A_2

Mg	0.086168715753	0.465421769709	-0.211612959630
C	0.255688423780	1.966959109270	1.301686120377
H	1.288737799133	2.324925545613	1.430809042971
H	-0.072169817075	1.653137993517	2.308623297811
H	-0.329487067629	2.872676349177	1.077556188774
O	-2.281638367575	0.442146989924	-0.145151435509
O	-0.025711766443	-1.543017383469	0.538769884541
C	-2.972950445244	1.537964132167	0.488222789348
H	-2.410437556870	1.745644065202	1.399497685114
H	-3.979432414124	1.205829426933	0.775760835920
C	-3.082806892801	-0.287157685338	-1.098087905558
H	-3.698570943307	0.418072720801	-1.668768173403

H	-2.371301310363	-0.729467868470	-1.796268137377
C	0.607134119003	-2.664952691756	-0.122112463877
H	1.446438668030	-2.234243781157	-0.669088564453
H	1.007583627305	-3.337128199174	0.647179227793
C	-0.751758096350	-1.864333534145	1.743771742999
H	-1.237765940008	-2.838521162725	1.610970226059
H	-1.535313479064	-1.108296164172	1.821164504365
O	2.462387898573	0.047187719974	-0.277126056456
Cl	0.044538032624	0.199654016069	-2.548880601175
C	3.182788321141	0.114009312028	0.963692823437
H	2.426179122297	0.280340063510	1.732778158560
H	3.840922298803	0.992326885237	0.961951746858
C	3.258455761715	0.355290713916	-1.443907690202
H	4.245290381386	-0.112661214977	-1.333026917246
H	2.737375469820	-0.118379495318	-2.276288424319
C	-3.952569034753	-1.349162534183	-0.434149693934
H	-3.337725378776	-2.084955140706	0.094000435439
H	-4.535107051357	-1.878529070058	-1.197536779828
H	-4.660389288611	-0.916860210275	0.282087147604
C	-3.038991121441	2.783145993696	-0.388146210476
H	-2.031577321497	3.126591904121	-0.638736351486
H	-3.554825777912	3.586081074967	0.152138173084
H	-3.583626757870	2.604067636118	-1.320921292545
C	0.142208301583	-1.855472356214	2.976198048344
H	0.576736716962	-0.862725624223	3.126458206538
H	0.955260659820	-2.585309559045	2.895159592787
H	-0.448706302285	-2.109995672679	3.864040769065
C	-0.341872741654	-3.390001882424	-1.064186711764
H	-1.219120935229	-3.785710814067	-0.539810496995
H	0.178887042377	-4.236166154303	-1.528149465772
H	-0.671262641421	-2.711391341622	-1.855716639652
C	3.977645848265	-1.155977627982	1.253566303019
H	4.494157212051	-1.058500747537	2.215967721946
H	4.736248298341	-1.350883417030	0.488095948678
H	3.316237265250	-2.026762431611	1.307530498537
C	3.384538445016	1.853110626792	-1.690201996167
H	4.010632412725	2.027211110264	-2.573627256783
H	3.845100190212	2.375721085061	-0.844611945197
H	2.399726417694	2.289190520591	-1.879482950164

3-25

Mg	1.696997919409	0.004945039864	0.014657990843
Cl	0.000000370987	1.725187975832	0.013742825344
Cl	-0.000039227192	-1.715865667657	0.013530790611
Mg	-1.697043094465	0.004584459007	0.012469886627
C	3.776780645621	-0.002148997038	0.013978146562
H	4.188545284047	1.014614315722	0.031432169229
H	4.177490790376	-0.501969272424	-0.877377243312
H	4.178511537057	-0.533017318531	0.886694688339
C	-3.776829543497	-0.000575805803	0.011688013108

H	-4.187187924272	1.016270233056	-0.024834686305
H	-4.179152730058	-0.483251159140	0.911717555776
H	-4.178419028013	-0.546877802886	-0.851504136823

3-25•Me_2O

Mg	-2.363932999652	0.048885938924	-0.071486193752
Cl	-0.662346765383	-0.500712408211	-1.661501081367
Cl	-0.801212261685	0.026381688090	1.754870456871
C	-4.396486506453	0.489681698101	-0.203797882531
H	-4.850760776936	0.629797495007	0.785415863604
H	-4.953284351950	-0.312040400098	-0.706618434014
H	-4.577708918877	1.408978904406	-0.776716535229
C	2.182443428710	-2.480431595065	0.454069125070
H	2.941793369614	-2.334404487881	1.236971018831
H	2.722511614143	-2.758631806990	-0.463242781029
H	1.611158442630	-3.371974676073	0.748887845578
Mg	0.941789860410	-0.807826769413	0.209410768573
O	2.102604784727	0.932035518601	0.002094208412
C	3.420709950110	0.808616314953	-0.554165070077
H	4.127458634648	1.403413174198	0.035609698665
H	3.425230894382	1.149431206936	-1.596363391476
H	3.689357648661	-0.246995898051	-0.501758919795
C	1.625628315142	2.283865458050	0.021719767756
H	0.660608167073	2.275568091486	0.528819909200
H	1.514565333118	2.663168261303	-1.000786372151
H	2.327640137568	2.914376291730	0.579367998862

3-25•Et_2O

Mg	-3.316949880359	-0.702212979271	-0.869677279194
Cl	-1.280231402980	-1.655741781837	-1.678516032250
Cl	-2.298769968769	0.017997474328	1.183390024032
C	-5.228873594144	-0.473106982647	-1.668368264761
H	-5.647794935446	-1.431846861192	-2.001654187924
H	-5.226216307924	0.191878509753	-2.542581016721
H	-5.931427993669	-0.047045217234	-0.940653471280
C	0.878409183938	-2.424057823702	1.663887250672
H	1.205175002689	-3.314175150308	1.106075739591
H	0.265126450311	-2.795893870334	2.497073150310
H	1.783311991825	-1.993454632861	2.120222607672
Mg	-0.171322149299	-1.058614349072	0.465321670112
O	0.935967230560	0.665059770265	-0.097540623852
C	2.299542215901	0.555225091516	-0.579277679412
H	2.986257799920	0.617039271141	0.272288251793
H	2.483095874277	1.415135750515	-1.235785346715
C	0.578006454196	1.995496633646	0.359030616938
H	-0.511635595282	1.991335875832	0.414311693084
H	0.882604692500	2.705327479232	-0.420172847769
C	1.185484869182	2.351237341710	1.708697154138

H	2.279344227371	2.376937596260	1.678519210365
H	0.874130106377	1.637158161156	2.478110391588
H	0.836904710986	3.345725669816	2.009164930520
C	2.487600384084	-0.747534261270	-1.335344749022
H	3.509837351653	-0.786986760931	-1.727595337331
H	1.792706187999	-0.819915550587	-2.177542020644
H	2.349709094102	-1.614967403925	-0.681383833941

cis-**3-25•(Me_2O)$_2$**

Cl	0.017592204001	-0.787693820257	-1.745019140322
Cl	0.040808555911	-0.726681723694	1.751827385994
C	3.480779708236	-2.056362437690	0.020472551210
H	4.095351182085	-1.914366895030	0.922635174567
H	4.143818362066	-1.892103193427	-0.842778169566
H	3.221018074929	-3.124404648568	0.000039826084
Mg	1.762324121770	-0.847891477275	-0.009361136189
O	2.358215968978	1.172311753286	-0.046430624152
C	3.743181722451	1.526092525864	0.057636046372
H	3.919115462105	2.088599009395	0.982693754712
H	4.040657683365	2.132006773177	-0.806714276204
H	4.307398128506	0.593559496847	0.073128098438
C	1.486673608744	2.306474104698	-0.081638383502
H	0.466773289985	1.930695600715	-0.163970318329
H	1.724208411848	2.933210420000	-0.949856587696
H	1.595801628748	2.892548095094	0.839088921374
Mg	-1.672393945518	-0.914175320736	0.019048228257
C	-3.412903281978	-2.087212436227	0.043180041255
H	-4.068466854773	-1.870214561905	0.900157458219
H	-3.178205656568	-3.159383262471	0.105221794321
H	-4.028454481759	-1.963269262296	-0.860590858762
O	-2.180529985592	1.180528055448	-0.020128856310
C	-2.862032538932	1.640483942903	-1.196870944173
H	-2.357487644578	1.188708734138	-2.052358295849
H	-2.790336279570	2.732694476187	-1.260989699996
H	-3.915434943390	1.337437197695	-1.176846057137
C	-2.702133311676	1.754642482014	1.187298626102
H	-2.627546583335	2.847448613903	1.137483740316
H	-2.086704712532	1.378960099754	2.005975582783
H	-3.748431893528	1.461494658457	1.334422118183

trans- **3-25•(Me_2O)$_2$**

Cl	-0.142530559279	-0.079972390247	1.734521052678
Cl	0.140940502974	0.099037397252	-1.735845374517
C	-2.355284682164	-2.781116147783	-0.276751628545
H	-3.121590775005	-2.854247344260	-1.063721401835
H	-2.840271622888	-3.084865061194	0.663285945319
H	-1.619425248439	-3.566917679562	-0.502060333202
Mg	-1.477864236627	-0.872913702488	-0.183780056753

O	-2.973185575594	0.609829610705	-0.217501008233
C	-4.227731700244	0.314555162229	0.411305989788
H	-5.048291898268	0.721259345519	-0.191137911552
H	-4.258523919059	0.743812732954	1.420116871628
H	-4.308387262532	-0.772003963654	0.462986169146
C	-2.737228182980	2.016504940974	-0.370668264472
H	-1.797252534118	2.124792305843	-0.912075643987
H	-2.666679683858	2.499830792147	0.610686337222
H	-3.552242467392	2.464577493718	-0.950936110286
Mg	1.481205763892	0.884423760209	0.182587135377
O	2.966396931906	-0.609460499264	0.211132918034
C	2.720007805481	-2.014191671342	0.365819568000
H	1.785645819661	-2.114737128346	0.918309962251
H	3.538006037892	-2.469924500411	0.935827838880
H	2.633405446592	-2.495878729964	-0.615061292640
C	4.215923070487	-0.324956546777	-0.432558074105
H	4.305905591168	0.760884348988	-0.484190344652
H	4.230604109020	-0.753378862530	-1.442074229202
H	5.039935403420	-0.739719599029	0.159580925590
C	2.371705490142	2.786427595223	0.275712366357
H	1.641949748919	3.576682380833	0.505177817017
H	2.855084363594	3.088432561567	-0.665707330470
H	3.141548263301	2.852956398691	1.059797107160

cis-**3-25•(Et_2O)$_2$**

Cl	0.418274455159	-0.491605843767	-1.643181034749
Cl	-0.117442131253	0.045730709173	1.766407939053
C	2.990456461367	-2.356371791323	0.936064462676
H	3.416618837417	-2.246115527868	1.945293627431
H	3.840119647989	-2.509343803831	0.253296507744
H	2.434514825020	-3.304808506266	0.946548003146
Mg	1.775138757104	-0.734766928099	0.380101057567
O	2.897453113696	1.054097849598	0.240787645865
C	3.644752281198	1.485308205566	1.404828901868
H	3.081279214498	1.113116495308	2.265111834703
H	3.623138991539	2.580440383096	1.444698481805
C	3.086910082975	1.850947911082	-0.953289231347
H	2.870413644473	1.181937696661	-1.788679479728
H	4.141650373471	2.142073122109	-1.012582149740
Mg	-1.563968524096	-0.162528870119	-0.210955287165
C	-3.292939350167	-1.355467540326	-0.320702402244
H	-4.229161394683	-0.788198538162	-0.196270021115
H	-3.301572101744	-2.127489896123	0.462314544873
H	-3.381868549524	-1.893553265306	-1.276313509131
O	-2.041763168021	1.902211437937	-0.518699916596
C	-1.886869053586	2.873218262462	0.545860366995
H	-1.754112201325	3.857860692977	0.078575811155
H	-0.956712399053	2.594526002778	1.043713874914
C	-3.060719090667	2.241586746693	-1.491742482496
H	-4.047530961722	2.013709496769	-1.074060084882

H	-2.998337640387	3.323057025855	-1.668044917319
C	-2.824053104694	1.472196314952	-2.779153565949
H	-2.928446319679	0.393701883068	-2.623784722128
H	-1.828179297084	1.677463868174	-3.183109590143
H	-3.571408338487	1.774984950810	-3.521147137965
C	-3.044746880070	2.879626491777	1.534363975519
H	-3.990744500303	3.165410783911	1.063327567210
H	-2.835634189713	3.603910601046	2.329876599696
H	-3.167514834025	1.895311125173	1.997359407701
C	5.067023084572	0.944630175855	1.408260130958
H	5.059554101351	-0.148711092178	1.383361841492
H	5.580396057036	1.270193593852	2.320461518903
H	5.643962292660	1.310101251571	0.551963148641
C	2.165549932100	3.061292377127	-0.984624298951
H	2.337437319807	3.727883463784	-0.132512075928
H	1.119302049349	2.742211215982	-0.977884943360
H	2.345821507502	3.635094468223	-1.901154398978

trans- **3-25•(Et_2O)$_2$**

Cl	-0.455203282295	-0.821518891033	1.473408250495
Cl	0.454161444983	0.824766941993	-1.471501146901
C	-2.163671635299	-2.196671256153	-1.901247840512
H	-3.066874448060	-1.955122975069	-2.483809156868
H	-2.420939292969	-3.070489501816	-1.283354734746
H	-1.421526899629	-2.550790656244	-2.631905404656
Mg	-1.441981986663	-0.571127129518	-0.775156804704
O	-2.904191973614	0.935303957772	-0.419447085977
C	-4.280965057607	0.584935489697	-0.136676750411
H	-4.808948409277	0.410562088887	-1.081252319594
H	-4.741612925210	1.446139955957	0.363354730831
C	-2.711832657699	2.314248889037	-0.824916718786
H	-1.636864460261	2.483775490901	-0.750910415928
H	-3.216363377237	2.949663600383	-0.086095735716
Mg	1.441690624055	0.573183184727	0.776560808920
O	2.902664215335	-0.934958668356	0.420586506049
C	2.710255069911	-2.313474936941	0.827489108890
H	3.210375909570	-2.949844473077	0.086484076106
H	1.634714746301	-2.481465463522	0.758549647448
C	4.278869144922	-0.586390957999	0.133051387952
H	4.736519247630	-1.447906696531	-0.369224410486
H	4.810482257672	-0.413420009823	1.075845299584
C	2.165774841088	2.196889343780	1.903749119424
H	1.421145701026	2.556828971581	2.629015150608
H	2.432535163428	3.068094650686	1.286198989448
H	3.063627475791	1.950563638024	2.492550549330
C	3.210411623024	-2.597116808311	2.236781339727
H	4.290956761974	-2.447947897211	2.331774507590
H	2.993307998983	-3.640190844385	2.493395172408
H	2.702856043100	-1.956795632521	2.965544960481

C	4.333694984834	0.641583953103	-0.758629924120
H	5.379599873942	0.862155234625	-1.000262741321
H	3.915262893461	1.519836266000	-0.256726158254
H	3.788744786250	0.472444056253	-1.692220159434
C	-4.337121539614	-0.642469746826	0.755722311059
H	-3.795535244832	-0.471817577723	1.690999342973
H	-3.915760095870	-1.520515846828	0.255920997405
H	-5.383524104280	-0.864303662759	0.994024649238
C	-3.205853678929	2.597513585394	-2.236443766426
H	-2.693392932333	1.958711956577	-2.963093269679
H	-2.989877153759	3.641196122926	-2.491542018519
H	-4.285607651842	2.445945254342	-2.336590342930

3-25•(Me_2O)$_3$-A

Cl	0.132784217035	0.091829074883	1.782217690018
Cl	0.184296110942	0.076574647930	-1.799130416401
C	2.671662957767	2.760876619003	0.010476477707
H	3.315285956025	2.884138214425	0.895415377874
H	2.001668412162	3.633088160610	0.005725173844
H	3.322573863456	2.880031991131	-0.869666397330
Mg	1.610723452375	0.941215429689	0.010439353827
O	3.009550692781	-0.642232121682	0.038860606659
C	4.418021001665	-0.392424511791	0.029856507204
H	4.873618035065	-0.828038048719	-0.868147657967
H	4.883535420477	-0.822670501746	0.925304458588
H	4.546828430355	0.690136421342	0.025868620804
C	2.676783357078	-2.034337166826	0.044555267495
H	1.589399258636	-2.107004124972	0.051532591602
H	3.090044382963	-2.513439593840	0.940667335192
H	3.079108590427	-2.518621715566	-0.853745115663
Mg	-1.572200229266	-0.115022722445	-0.033781832184
C	-3.679628853060	-0.355920800356	-0.039198695961
H	-4.059504078777	-0.743040307671	0.920449504663
H	-4.028697280518	-1.066939451871	-0.805232702718
H	-4.238553270852	0.574383026398	-0.223610790175
O	-1.525342544809	2.161238708300	-0.040291949177
O	-1.124735324108	-2.356107302053	-0.015286199517
C	-2.031100384314	2.805655412042	1.133880033993
H	-1.718335405311	3.857190740352	1.143635522568
H	-1.600877581052	2.288997559028	1.991784178626
H	-3.126363231306	2.745349562799	1.165296424282
C	-1.967125689093	2.814456978878	-1.235037812364
H	-1.500579320827	2.296719140746	-2.073030234305
H	-1.644670242900	3.863069452114	-1.225043737197
H	-3.060128224517	2.765319964509	-1.320445559151
C	-1.558201585309	-3.042288787409	1.162664035914
H	-1.114993398494	-4.046356835523	1.194252863909
H	-2.651861933693	-3.122242653348	1.185544624870
H	-1.207593522268	-2.460879503029	2.016246592952
C	-1.470753441138	-3.066004967437	-1.207655982571

H	-1.065327666518	-2.496942305973	-2.044976049022
H	-2.559708519522	-3.155053419401	-1.305716184359
H	-1.020872411556	-4.067486262519	-1.189823926526

3-25•$(Me_2O)_3$-B

Cl	0.285531315885	-0.809163112082	1.456998423485
Cl	0.849093020895	1.300753735697	-1.217387944713
C	3.394311377551	1.723808665197	1.916429102172
H	3.987183237659	1.116588015220	2.618211549522
H	2.811863630020	2.416171406080	2.542466469180
H	4.110092585677	2.352040425598	1.363901553877
Mg	2.158228734465	0.569172447140	0.658764338006
O	3.336629507058	-0.906120467281	-0.291332116593
C	4.758945498873	-0.751297215770	-0.344202341042
H	5.065565444128	-0.379214672803	-1.329842783680
H	5.245914784295	-1.713758553871	-0.145503322060
H	5.028649805367	-0.029314978257	0.427074506321
C	2.834559094394	-1.826824753028	-1.268232290205
H	1.757884964771	-1.902426931438	-1.119447750233
H	3.300335967227	-2.808851259605	-1.122468820990
H	3.041691878252	-1.458764269249	-2.279607219461
Mg	-1.182913371323	-0.260308105797	-0.474912964489
O	-2.195433540997	1.603476168090	-0.167442619852
O	-2.934339652107	-1.020091070351	0.802971745903
C	-1.637349231581	-1.400211732198	-2.200077341585
H	-1.964681823108	-2.427633643985	-1.971629106862
H	-0.781790343671	-1.498244911888	-2.883969001352
H	-2.447270336869	-0.960882322434	-2.806623663343
C	-2.367493340268	2.465588249590	-1.302687911386
H	-2.536382584648	1.822005658910	-2.167471228408
H	-1.467930795673	3.066982006809	-1.464723337661
H	-3.238419389737	3.112295593767	-1.140095158298
C	-1.939692178208	2.331460939625	1.042157900664
H	-1.012653956803	2.908074205208	0.948265572908
H	-1.841439075750	1.597185991089	1.842544021878
H	-2.780602319386	3.003311384596	1.252780475716
C	-2.827532630746	-2.308465277550	1.417098759079
H	-1.845361455717	-2.361589155444	1.884326727318
H	-2.929446251009	-3.103278853926	0.666739151925
H	-3.609197536812	-2.423748473756	2.179273316764
C	-4.213162016459	-0.841836557960	0.190264174829
H	-4.240361607852	0.174225845285	-0.201889932715
H	-5.007071595701	-0.968489361921	0.938119144412
H	-4.357106812091	-1.560242057306	-0.625999079030

3-25•$(Me_2O)_3$-C

Cl	-0.348059573541	-1.283095114906	0.932574584213
Cl	-0.800325665901	1.008652596408	-1.583620546357

C	-3.473033863656	-2.120622305299	-1.446101756541
H	-3.798127594689	-2.895732369169	-0.734714864794
H	-2.982957018208	-2.659973985587	-2.269655412140
H	-4.388879848807	-1.685233556421	-1.875429112626
Mg	-2.194458051732	-0.676550529448	-0.598589964331
O	-3.395471464963	0.505981388983	0.693184307050
C	-4.540196683596	-0.081993451233	1.321083862066
H	-5.408494300382	0.578470476870	1.208162157019
H	-4.342382242336	-0.254769701064	2.386419717832
H	-4.726340747327	-1.028919467880	0.813765183095
C	-3.048669724210	1.783143572631	1.232857340244
H	-2.193708155044	2.143659203418	0.660466143322
H	-2.786211986621	1.691448720531	2.294413821764
H	-3.891118145320	2.476931306240	1.120488357995
Mg	1.356521470324	-0.295132377338	-0.579234165586
O	1.929103312112	1.662686310196	0.087858987202
C	1.404922474437	2.202418763350	1.304021123539
H	0.431823972792	2.673742723234	1.122892657838
H	2.104057313506	2.941177482072	1.715375799859
H	1.290833349051	1.370824445381	2.000473817090
C	2.144743810807	2.662079544010	-0.920197902100
H	2.536811341816	2.144967060790	-1.796897227846
H	2.874447895399	3.395876504234	-0.556371575539
H	1.201522217890	3.154157697036	-1.177168368186
C	2.395641420880	-0.988372354162	-2.284276630521
H	2.841897925175	-1.986216462067	-2.145772415597
H	3.229245508357	-0.331393358458	-2.585423343713
H	1.744954969947	-1.067094141086	-3.166303442083
O	2.909990751621	-0.937982888629	0.974853145812
C	2.914020685981	-2.298462341231	1.422219588827
H	1.882302164689	-2.568546763009	1.641930664579
H	3.525786729277	-2.389263665741	2.329255386286
H	3.316512843584	-2.958195611260	0.642764757051
C	4.236037592077	-0.480432703819	0.699338581619
H	4.159141638358	0.565710460270	0.405284387294
H	4.688235458826	-1.061770818680	-0.113294996516
H	4.855026219427	-0.565858289168	1.602386352880

3-25•$(Et_2O)_3$-A

Cl	0.420926883816	-0.897282624752	1.178704837736
Cl	0.869572122274	1.341376514392	-1.418304184705
C	3.514626671200	1.570255768005	1.665768289527
H	3.986085337375	0.927964049899	2.426102747558
H	2.957212197896	2.334175809595	2.228523401492
H	4.332762368893	2.108696892959	1.162459992678
Mg	2.274631640823	0.508560263189	0.329709337698
O	3.437846007473	-0.882504329863	-0.738742637917
C	4.843518592792	-1.035755932765	-0.431101412016
H	5.105582148705	-2.096639906924	-0.516342275109
H	4.942238429614	-0.742408822401	0.616280219203

C	2.943543493968	-1.680958284658	-1.843635491306
H	2.070325653037	-1.140500781565	-2.214904367018
H	3.700943281766	-1.683390763353	-2.635745759106
Mg	-1.178885580328	-0.238989822837	-0.598208510045
O	-2.180496650038	1.581901979227	-0.118830535733
O	-2.829721531329	-1.178379544973	0.696692392477
C	-1.707174754572	-1.130926620659	-2.448711767910
H	-2.137572166611	-2.140931280742	-2.358694679241
H	-0.829348775052	-1.228977881394	-3.104893657505
H	-2.437650351947	-0.546153360596	-3.033447674127
C	-2.376623551941	2.522806117888	-1.203457666861
H	-2.235074088921	1.922081104660	-2.104477077510
H	-1.579192348492	3.270676607428	-1.177807795308
C	-2.201204874064	2.117478011574	1.225597278091
H	-2.052655499691	1.241786759369	1.860807576582
H	-3.204609207641	2.510140345431	1.429955353683
C	-2.676291920783	-2.104363759150	1.795121425575
H	-1.901361082075	-1.675235305740	2.431861322842
H	-3.612909275979	-2.129539246191	2.365869800783
C	-4.109313728863	-1.255010512168	0.034191560255
H	-3.936942222365	-0.873451382675	-0.973923651689
H	-4.403245632194	-2.307264191114	-0.061316711707
C	-5.184485772824	-0.448138396985	0.751809453621
H	-4.904270761638	0.608201758731	0.801562495870
H	-5.358170074020	-0.807267850547	1.772024985164
H	-6.132080332485	-0.528168758737	0.205954346278
C	-2.273754806159	-3.499987833208	1.336459519750
H	-1.310853371448	-3.468214248341	0.819325493972
H	-3.016882749503	-3.943235514726	0.664957527201
H	-2.174536997587	-4.157769752075	2.208082630857
C	-3.758290439361	3.162429583284	-1.197483003860
H	-3.915449288819	3.817509463930	-0.334105986000
H	-4.545217146195	2.400746275573	-1.204661050430
H	-3.870197624609	3.775766441276	-2.098655984164
C	-1.133509951652	3.168358477683	1.497887925103
H	-0.139650960904	2.795800481774	1.235487586101
H	-1.142329268136	3.412132979469	2.566331525372
H	-1.310909069060	4.097031757991	0.946076322467
C	5.722261032255	-0.164816528835	-1.317685508410
H	6.773941851914	-0.300144639241	-1.039389689213
H	5.465904919970	0.891268514143	-1.190129164633
H	5.619917944995	-0.422404148015	-2.377199999920
C	2.577673578803	-3.091816865304	-1.407098648762
H	3.445293437953	-3.643257879441	-1.027980436615
H	2.176139184437	-3.646020375585	-2.263380699740
H	1.814057077327	-3.061732811912	-0.624436321376

3-25•$(Et_2O)_3$-B

Cl	0.020419568879	0.018591527017	1.729717286333
Cl	0.081685825342	0.011362265816	-1.844205050016

C	2.598765916795	2.649013708751	0.020868298385
H	3.174534941599	2.777273115863	0.950954797449
H	1.942485146969	3.528635756195	-0.047880201502
H	3.319626838896	2.749127523381	-0.806001402284
Mg	1.534994556108	0.830643990615	-0.045279987896
O	2.939294890010	-0.735202872408	-0.000845390263
C	4.282247910311	-0.482401115350	0.478112332235
H	4.973613880585	-1.136489709796	-0.065042133180
H	4.495818792959	0.550422159516	0.195273400882
C	2.613903579374	-2.121155100238	-0.261522988578
H	1.526250470709	-2.179578058965	-0.185690346343
H	3.046784235817	-2.738048724849	0.534694174303
Mg	-1.693784606300	-0.154988498094	-0.076208145771
C	-3.804099694355	-0.319717709792	-0.221867834744
H	-4.262132710094	-0.416324333671	0.776642126849
H	-4.155106736855	-1.193311882399	-0.791961757686
H	-4.281773052529	0.558536172235	-0.681381146896
O	-1.641701161617	2.150170245819	-0.079480017820
O	-1.327079945084	-2.440626528335	-0.059829045434
C	-1.819279373641	2.956031162047	1.106214640501
H	-1.527879713168	3.987809950888	0.876302677395
H	-1.104346220560	2.558837290655	1.828624353027
C	-2.106735437047	2.770089081565	-1.298634373579
H	-2.294390617347	1.947283711805	-1.992251092569
H	-3.066045623156	3.265517815796	-1.107106859181
C	-1.278432634918	-3.237236294838	1.141307766244
H	-0.887131326952	-4.231850534193	0.890272016190
H	-0.548717609092	-2.737576135286	1.781623510554
C	-1.831059457348	-3.131544754778	-1.221471430797
H	-2.236435420500	-2.354272400195	-1.873101389922
H	-2.666053738435	-3.778015306924	-0.926157460510
C	-1.085944523785	3.735972103888	-1.885063440634
H	-0.152324821736	3.214012757415	-2.111549537239
H	-0.863606367545	4.564319542629	-1.203926526009
H	-1.479497418574	4.164722711790	-2.814524615652
C	-3.236529939824	2.896500396049	1.664928672860
H	-3.515039399043	1.868734398007	1.914964710877
H	-3.977413985739	3.284440003429	0.958053610441
H	-3.293125402290	3.504056861755	2.576113605321
C	-0.743683492894	-3.919119199179	-1.940200375622
H	0.048627175024	-3.246707287099	-2.281132989931
H	-1.169474565863	-4.423328729774	-2.815785506452
H	-0.301721977282	-4.688050509806	-1.296261886161
C	-2.626587313958	-3.342373520396	1.844887284205
H	-3.379911715244	-3.834438601534	1.221035106387
H	-3.003761132086	-2.350928029143	2.111159924927
H	-2.514805019833	-3.930654205491	2.763515918827
C	4.398307159366	-0.668784909559	1.984405368389
H	5.425563554192	-0.456134717337	2.302505652594
H	4.156976641724	-1.692256685016	2.290435196272
H	3.726368316283	0.015586997048	2.511449592522

C	3.086578288198	-2.561652097351	-1.639345862934
H	4.174273976869	-2.486352712614	-1.744311219467
H	2.616410132924	-1.948613797957	-2.413889549292
H	2.807476355763	-3.608298287611	-1.807657459602

3-25•$(Et_2O)_3$-C

Cl	-0.932401272506	0.056529298215	-1.193038730887
Cl	-1.376546269918	2.863185557106	0.820332972079
C	-4.400077688783	2.112286959806	-1.774888129289
H	-5.109814547876	1.320064736321	-2.059618100786
H	-4.001251736930	2.513060717137	-2.717980919335
H	-4.997158647835	2.924709111555	-1.333119702357
Mg	-2.859653094070	1.423821730288	-0.519514646431
O	-3.699141712490	0.267813813159	1.031703736071
C	-5.023045101339	0.651444887348	1.477153650030
H	-4.931931601716	1.097123952496	2.476068797047
H	-5.331461856972	1.432156952846	0.778049749355
C	-2.929213749527	-0.561882061142	1.937039194336
H	-3.370089768714	-0.476654680730	2.937036314119
H	-1.928409451323	-0.122609836735	1.971927599616
Mg	0.566319903085	1.789512846943	-0.264716601034
C	2.022401548272	2.895325966943	-1.302524388366
H	3.047508951937	2.563185346846	-1.076900786828
H	1.984013900733	3.968656291201	-1.064351095731
H	1.904497859721	2.819296624215	-2.393184019916
O	2.944348802596	-1.170007276657	-1.903776698223
O	1.307293871180	0.759559636912	1.430393492542
C	2.128052381099	-2.002100913285	-2.731118682206
H	2.312273517857	-1.784896260712	-3.792673668275
H	1.095585288042	-1.712801838510	-2.514508862828
C	4.260291144038	-0.925733311491	-2.399485633987
H	4.861135236197	-0.665862027519	-1.520624898516
H	4.686130037654	-1.848319852761	-2.822505896531
C	2.109400496128	-0.441978502143	1.272179811143
H	3.065475757086	-0.289636484863	1.785832165991
H	2.314358225493	-0.539978824576	0.202737777054
C	1.415733811804	1.411621812911	2.719317564957
H	0.484950195504	1.971557668828	2.835639458112
H	1.447134951264	0.637537527618	3.494922787247
C	2.339905633716	-3.486782007313	-2.442865266411
H	2.125717246751	-3.707210635854	-1.391407913914
H	3.369433248732	-3.798437021888	-2.653172621199
H	1.671987314659	-4.094922245086	-3.064636410614
C	4.309011102055	0.208599898387	-3.419578220540
H	3.913148767002	1.131550155497	-2.985111336234
H	3.721235224315	-0.027258105496	-4.313631462152
H	5.343799745566	0.385862691465	-3.737672978828
C	1.382646795951	-1.672546114437	1.793891280671
H	1.154827132322	-1.595939474202	2.863202498612

H	2.013895651576	-2.556977833848	1.648941809599
H	0.448641147826	-1.823365860937	1.244345221624
C	2.623663639387	2.335206663406	2.800311366191
H	2.646020097738	2.824522266412	3.781007744126
H	2.572361761622	3.109943607014	2.029011282733
H	3.564683527134	1.789124715188	2.675500660489
C	-6.022403386797	-0.495594878661	1.466115762993
H	-7.014548993805	-0.109911223757	1.727604702879
H	-5.767612608010	-1.275197950905	2.191475905436
H	-6.081474806905	-0.946818395811	0.470740557333
C	-2.865510812794	-2.008001206137	1.467892938636
H	-2.420791604495	-2.064004006788	0.470026299107
H	-3.856652688765	-2.469623520496	1.436341559606
H	-2.238690514467	-2.588209083323	2.155863011682

3-25•(Me_2O)$_3$-open

Cl	-0.128261296988	-1.151156861440	0.135666975791
Mg	-2.103751329894	0.282385792067	0.971459816757
O	-3.543492870893	-0.887606936951	-0.048466913400
C	-3.775914128785	-0.819493951903	-1.459467299623
H	-4.851450689084	-0.894002762835	-1.661750529672
H	-3.245557390404	-1.632614934574	-1.970998226956
H	-3.397350297472	0.147546051548	-1.791620129874
C	-4.013554031103	-2.099318712356	0.548554949493
H	-5.094246199619	-2.199064508479	0.389398542173
H	-3.800090405370	-2.029252626329	1.615827146765
H	-3.493547760617	-2.964226081081	0.117850261215
Mg	1.912753327390	-0.064072188733	0.732111346735
C	2.854075028088	0.268941999236	2.586404347169
H	2.166099266763	0.691847986470	3.332879303983
H	3.713477267716	0.957251430851	2.544262179128
H	3.232820812530	-0.663885154148	3.031639228701
O	1.851067334362	1.685670097429	-0.405883315747
O	3.211056554119	-1.176050001324	-0.526535815742
C	1.656245742688	2.943676961207	0.273466570005
H	2.006925516294	2.805558947813	1.297368434418
H	0.595229286690	3.210789643765	0.261300377350
H	2.254562233137	3.717340381231	-0.221993805526
C	1.413937632601	1.733528051849	-1.776059822319
H	1.609816275063	0.750842124990	-2.208295127552
H	1.993979375547	2.493194881495	-2.313899131013
H	0.344338091111	1.957122064025	-1.818210190356
C	2.871004920432	-2.130620782295	-1.540460492686
H	3.357563022897	-1.862351331967	-2.486435061257
H	1.786966853127	-2.109553195282	-1.650137663962
H	3.192204779307	-3.133248471898	-1.233887099852
C	4.617613984602	-1.131219365915	-0.249880398748
H	4.758975733437	-0.428730503599	0.571937575102
H	5.164961079013	-0.794515162458	-1.138646809668
H	4.973075996469	-2.124056409126	0.050262035098

Cl	-1.978313162638	2.157847772734	-0.420548401490
C	-2.391279522557	0.094887444648	3.053745937315
H	-3.379651366380	0.454519229377	3.379325908992
H	-1.656984335256	0.686031852699	3.621676905451
H	-2.294912326324	-0.935639770743	3.429657393800

3-25•$(Et_2O)_3$-open

Cl	-0.021032616503	-1.451458841213	-0.143747053540
Mg	-1.993634579562	0.106019199802	0.351590501731
O	-3.488406685980	-1.210405026131	-0.337160089434
C	-3.999216271523	-1.233993500767	-1.692765205999
H	-5.080378435971	-1.411640222285	-1.652135147488
H	-3.826528323335	-0.226559578176	-2.076286629081
C	-4.055718430434	-2.186485217303	0.566065073738
H	-3.288234528423	-2.366390459220	1.322681338175
H	-4.214310862698	-3.121421671433	0.016283835896
Mg	1.969747369003	-0.477665041970	0.775112920581
C	2.736850588214	-0.631107548852	2.731182225293
H	2.032045867109	-0.260478314444	3.490044400975
H	3.672874870858	-0.071371226842	2.888820708532
H	2.953341798084	-1.672765462533	3.014199694885
O	1.866731165460	1.502701746436	0.103195777384
O	3.330166532741	-1.183549404795	-0.695968597654
C	1.238922624373	2.449742326557	1.021748598169
H	0.601364381211	1.863366854598	1.690727780688
H	0.582857748816	3.101140203853	0.438116678307
C	1.755314564291	1.838982315660	-1.308533365384
H	2.098180255249	0.941588399598	-1.828431483913
H	0.696686133628	1.987875250530	-1.542742351259
C	3.090279124233	-2.307087546694	-1.584974220884
H	2.218691689502	-2.819684049776	-1.174985376108
H	3.949566484228	-2.983541240566	-1.525148819472
C	4.701572442404	-0.717330322878	-0.645787856799
H	4.639390880797	0.316220011899	-0.293621743033
H	5.097301511268	-0.698897349976	-1.667854610838
Cl	-1.937947274613	1.708807701593	-1.347704900309
C	-2.164154947979	0.397839382508	2.441915571807
H	-3.054172071102	0.989111316733	2.709449898636
H	-1.312152165619	0.938660474825	2.883764056748
H	-2.236014551141	-0.542194505848	3.011535123491
C	-5.339767659158	-1.683244889513	1.209441036432
H	-5.734096293032	-2.444020800818	1.893306428671
H	-6.112047539531	-1.469477032242	0.462562134717
H	-5.144679663945	-0.771355545473	1.781503722730
C	-3.287932600245	-2.272077953580	-2.548754940320
H	-2.213870627899	-2.066767325719	-2.580913806976
H	-3.680358024231	-2.234571879510	-3.571862220058
H	-3.434780087168	-3.289641156288	-2.169993145066
C	2.823674102729	-1.856912621970	-3.012879723848
H	3.666161933034	-1.295641617399	-3.432089133527

H	1.925500021288	-1.233837888700	-3.056880881298
H	2.659757265936	-2.735360017615	-3.647609590327
C	5.571159115491	-1.553133231994	0.282294416709
H	6.583739486349	-1.133885125824	0.307808773780
H	5.650130219095	-2.591691437295	-0.055859853772
H	5.164793768931	-1.545227914508	1.297459450672
C	2.606520516703	3.038625851903	-1.697211653295
H	3.658678636392	2.885425988069	-1.432437917361
H	2.259110110431	3.960345744389	-1.219677157218
H	2.541466963570	3.187293525112	-2.781277725919
C	2.276963540027	3.225309526954	1.815937484038
H	2.910870263629	3.838313974323	1.167599199441
H	2.914086958955	2.542900483657	2.386907106085
H	1.768510306065	3.888842691154	2.525231261865

3-27

H	-3.680062017038	-1.662354135804	1.777412893050
C	-4.202677908274	-1.033254819916	1.060550740451
C	-4.262342297853	0.441629696168	1.295156035615
C	-3.363768858772	-0.101352557904	0.175477652540
H	-5.070373163538	-1.507731884487	0.609502025312
H	-3.781427913489	0.857028417163	2.177745103179
H	-5.170465831681	0.962578485041	1.002869110179
C	-3.815470186382	0.095803925768	-1.171775511347
N	-4.066804936712	0.267729337711	-2.300096709693
Mg	-1.278584081872	0.006791929368	0.090357520506
Cl	0.279558080862	1.779948053476	0.417201682496
Cl	0.447962967359	-1.580747979284	-0.319167187810
Mg	2.081878395425	0.205189468519	-0.036759891867
C	4.194541919773	0.297769392840	-0.083097138421
H	4.443391182474	1.359139004746	-0.241168153123
C	4.800284110978	-0.502318072845	-1.250675496525
H	5.900837813077	-0.427612557960	-1.261137040797
H	4.447159314220	-0.150604300147	-2.229012193738
H	4.562228367256	-1.572909546387	-1.185412027505
C	4.826214077970	-0.129931540366	1.255440805966
H	4.599679791262	-1.176298226829	1.503659252909
H	4.485377771888	0.486574049915	2.097921363445
H	5.926034403067	-0.049717138786	1.224847165177

3-28

Cl	0.130893880559	-0.878148959032	-1.744278899294
Cl	0.327841282172	-0.628713188184	1.730926096829
Mg	1.930838164145	0.213936607330	-0.173390695874
C	4.018342233997	-0.144417694872	-0.251450010614
H	4.342319947146	0.202140755156	-1.247710029897
C	4.390305382649	-1.633626693887	-0.143139321311
H	5.481113331730	-1.791887462208	-0.215201074939
H	3.926067710233	-2.238055340619	-0.933698397901

H	4.077549528685	-2.065714359742	0.818041234658
C	4.791555118579	0.683495671657	0.791267672318
H	4.514210748957	0.410501906750	1.819625661322
H	4.614415074082	1.762405441055	0.684672884961
H	5.882479816386	0.528616816043	0.713732869172
Mg	-1.162038577035	-0.114934119511	0.026989900477
C	-1.679173297066	1.976052662358	-0.093171381104
C	-2.705474507220	2.819701289383	-0.845394721604
C	-2.620855011561	2.924755062115	0.644558329372
H	-3.544856934058	2.291564189847	-1.289861297287
H	-2.346527673687	3.658932753198	-1.435239282692
H	-3.400759576482	2.470897660597	1.250223931030
H	-2.204269749554	3.835287566894	1.066998050675
C	-0.297562021987	2.234351411679	-0.189813464147
N	0.873840129331	2.126600023992	-0.248644054153

3-29

H	-2.710408720174	-2.663066776877	-1.876955528855
C	-2.080182834893	-2.020731576279	-2.486317639387
C	-2.621205113982	-0.708171326840	-2.940986534169
C	-1.569144457763	-0.732793072424	-1.821017726806
H	-1.406738855039	-2.552943374057	-3.153055765224
H	-3.630891584064	-0.430292625397	-2.650521896015
H	-2.317993204212	-0.343156527394	-3.918821334298
C	-0.272768703912	-0.283133307662	-2.063102991812
N	0.819505882401	0.159955777808	-2.080090603521
Cl	-0.061925458337	0.892406744171	1.124810120185
Cl	-3.886345809374	-0.583161985559	1.353260169373
C	3.679484051106	1.964626184689	-0.170560201585
H	3.487991818514	3.028192153911	0.048254974702
C	4.569763584192	1.907241718124	-1.425143402364
H	4.792565274840	0.873688487692	-1.725703060511
H	5.543388046062	2.398700664755	-1.256441496067
H	4.108353891252	2.401226904517	-2.290594737914
C	4.415786611828	1.377634837293	1.048486134769
H	4.640724561512	0.309214101361	0.919355353601
H	3.836556794950	1.476653672997	1.975672271673
H	5.383783510552	1.879453713482	1.218494757588
Mg	1.776482887591	1.091507893993	-0.486269076215
Mg	-1.999037173050	-0.199488282307	0.237451212851

3-27•Me_2O

Cl	0.421411372744	0.947112637798	1.821352257391
Cl	0.646388426281	0.793296432984	-1.671644590804
Mg	1.750451018942	-0.598589405447	0.212089884637
C	3.840712846480	-0.942004008437	0.357688853425
H	4.000276904963	-1.413169458161	1.343306120368
C	4.682274762720	0.346162499259	0.331350827981
H	5.763084948053	0.139990791013	0.436930694764

H	4.408624876968	1.039004065202	1.138620002217
H	4.563494661663	0.893491399250	-0.615024713016
C	4.348793296777	-1.935292425360	-0.703448039708
H	4.213510043106	-1.549153329073	-1.724451083945
H	3.828617961928	-2.901786403083	-0.654212123389
H	5.428198943166	-2.146568683404	-0.594057767135
Mg	-1.055213750404	0.933850853439	-0.029149777305
C	-2.128023229051	-0.967031876490	-0.021442988187
C	-3.407635064973	-1.435170202878	0.668610872965
C	-3.312703689388	-1.500119201337	-0.824416064635
H	-4.032520499614	-0.670471628075	1.123982939737
H	-3.388545244915	-2.373522248448	1.217235725947
H	-3.871528364310	-0.781620712054	-1.419584159162
H	-3.229559904616	-2.482153720305	-1.283291410439
C	-0.940408596039	-1.710717534108	0.087035976121
N	0.172326245868	-2.086746190916	0.175848343660
O	-1.979600890877	2.761096997867	-0.177784629619
C	-2.118296191847	3.426360172504	-1.447797316496
H	-1.998489778610	2.671456713842	-2.226043779791
H	-1.339931986979	4.188659956107	-1.556561470410
H	-3.111265082257	3.883263096874	-1.514697198292
C	-2.069405153890	3.660636659356	0.944690858058
H	-1.894271408512	3.072948349316	1.846466380092
H	-3.066950000453	4.111572476453	0.971665610759
H	-1.302802472925	4.437926926311	0.860785764212

3-28•Me_2O

Cl	0.197789765329	-0.664274259757	-1.960893655770
Cl	0.127454016225	-0.659450555981	1.529334167738
Mg	1.915682918461	0.098123260241	-0.163972945276
C	3.940454530830	-0.541114812917	-0.133976902037
H	4.381657521708	-0.190286480840	-1.083239677876
C	4.101502230804	-2.071285324249	-0.099735750756
H	5.163078619011	-2.378924830108	-0.113824449204
H	3.615617180525	-2.560445314543	-0.954903335973
H	3.665562900248	-2.508589832669	0.810233985931
C	4.748454994592	0.107646439846	1.004798706717
H	4.363067873709	-0.177070331090	1.994901686592
H	4.730843068841	1.205129953036	0.956874061987
H	5.810910278014	-0.196768149794	0.988194131997
Mg	-1.290324580605	0.015560136926	-0.251201008735
O	-2.965389838564	-1.172044139560	-0.257805705393
C	-1.389138707935	2.195992162046	-0.243083137883
C	-2.231640107625	3.191426299624	-1.039003863898
C	-2.277185874882	3.221394029395	0.457468034184
H	-3.082856752846	2.792099348126	-1.585386004162
H	-1.727776778384	4.010972119401	-1.545244005546
H	-3.163424434035	2.848009773147	0.965890828606
H	-1.804316334547	4.060684653570	0.961311645038
C	0.011533614401	2.314670671638	-0.208369350894

N	1.175945297857	2.140383336391	-0.182827370170
C	-3.931985317708	-1.072618430900	0.802779310184
H	-3.667027158619	-1.750695177843	1.621151156754
H	-4.926802864375	-1.316241616703	0.415484458404
C	-2.907976494908	-2.488870761288	-0.848053953291
H	-2.143548593581	-2.456171632697	-1.624885337213
H	-3.883031202155	-2.730271171600	-1.283441039782
H	-3.920470926548	-0.040110352774	1.157296062090
H	-2.636660843235	-3.226859008074	-0.085871742361

3-29•Me_2O

H	2.600758655804	2.723249688626	1.156367006802
C	1.804175576688	2.991285398148	0.467162705248
C	1.993290974728	2.738414503010	-0.992385929686
C	1.062385152526	1.820170366944	-0.191492358180
H	1.230918354675	3.867922274336	0.758391719805
H	2.931884819012	2.305993206958	-1.331359226493
H	1.550016335533	3.444403706800	-1.690710832771
C	-0.315544111762	1.875976103186	-0.364018267628
N	-1.483892196111	1.740183444674	-0.466096793922
Cl	-0.601867987264	-1.432538931686	0.402634927184
Cl	3.064349770264	-0.629177561871	2.037635070225
C	-4.565506022581	-0.545682001873	-0.059207022995
H	-4.633064153119	-1.478552465434	-0.643593766795
C	-5.448657240732	0.500845301884	-0.762599884949
H	-5.416010101487	1.475440459378	-0.255293930203
H	-6.509644183513	0.195832390996	-0.781771551117
H	-5.147111720972	0.672269839613	-1.804883506199
C	-5.111876153750	-0.855752133764	1.347654200108
H	-5.072272173965	0.022465762085	2.008235539598
H	-4.554480824531	-1.660062428738	1.845614493617
H	-6.169749817811	-1.170091731751	1.315504979161
Mg	-2.513247510137	-0.014303091498	-0.047760825499
Mg	1.555217176433	-0.245574957136	0.389719559676
O	2.385651320490	-1.157712959072	-1.292766128258
C	3.291526859162	-2.270365072374	-1.167391816282
H	3.704606888144	-2.224318773442	-0.159596871001
H	4.089828623470	-2.173714221028	-1.911752072789
C	1.773973345577	-1.074404382505	-2.585055960311
H	2.548750305075	-0.994917499001	-3.356353327410
H	1.157219604520	-0.174182757502	-2.594427558634
H	2.750722578005	-3.211974194639	-1.317422334670
H	1.150874857628	-1.956629283324	-2.771871235632

3-27•Et_2O

Cl	0.468404127365	-0.694346693533	-1.801200522369
Cl	0.497887803446	-0.355849635248	1.673396485144
Mg	2.237051164178	0.212997532185	-0.148141294482
C	4.252306347844	-0.457009382578	-0.096008588311

H	4.667322888719	-0.248745926078	-1.097670810610
C	4.388883250483	-1.971227602159	0.142728238314
H	5.443960303414	-2.301022103573	0.138889149711
H	3.866964969013	-2.561979143989	-0.622423131115
H	3.975408889744	-2.271003741853	1.116644210930
C	5.109208763362	0.323856886430	0.917147531746
H	4.751606786109	0.187072595345	1.948365431155
H	5.109217492753	1.404384452017	0.718344995174
H	6.165151723263	-0.003204539096	0.911084276969
Mg	-0.993344081247	0.134664248352	-0.112713321918
O	-2.661169419199	-1.066631665910	-0.080790154885
C	-1.037857014908	2.307259410678	-0.347273211157
C	-1.901048769054	3.220220088572	-1.216258263537
C	-1.901057518155	3.404680967990	0.269886684680
H	-2.770665803625	2.772495844011	-1.691854527531
H	-1.411471462153	3.980379847369	-1.819966548480
H	-2.771558568400	3.088614840984	0.840366598712
H	-1.411084809670	4.289145079336	0.669376991072
C	0.362593550015	2.421526287289	-0.363658992111
N	1.528072461552	2.252399104719	-0.348783149398
C	-3.399025428138	-1.355218920482	1.137032998480
H	-2.927787484250	-2.203709597357	1.642969027469
H	-4.415414875940	-1.640610887948	0.840733666983
C	-2.864069909349	-2.031256342962	-1.158188788752
H	-2.418824835123	-1.562858805910	-2.038663481375
H	-3.946363272493	-2.111443340301	-1.315163141965
C	-2.223543354375	-3.382225197142	-0.886267227035
H	-1.145377722669	-3.276543519587	-0.734079728221
H	-2.380858977853	-4.028675019013	-1.756890329774
H	-2.661573757564	-3.883272650940	-0.017416356178
C	-3.416616416308	-0.128192913584	2.029955579667
H	-2.410120176665	0.143314981020	2.367376303133
H	-4.009664321583	-0.345515547281	2.924781464674
H	-3.872452542540	0.726806010228	1.519625935190

3-29•Et_2O

H	-1.949574477937	3.491360959521	-0.900144187081
C	-1.199061448360	3.529929936242	-0.114920701481
C	-1.551666934106	3.036113233765	1.249746878405
C	-0.651187850277	2.175649372782	0.356698847982
H	-0.511619614669	4.369150873660	-0.186559431735
H	-2.558850532979	2.666368582204	1.428076831349
H	-1.105937815401	3.542019313341	2.102987120540
C	0.702587974908	2.033110912055	0.633826758592
N	1.837575917675	1.745445890655	0.786920636550
Cl	0.735525403212	-1.027704755971	-0.851343673661
Cl	-2.723148159971	0.541752912682	-2.429272557201
C	4.696168692926	-0.749520826517	0.175050654122
H	4.747845208400	-1.270591419139	1.147068332940
C	5.759908538703	0.363700766492	0.205919843090

H	5.776952483252	0.941680544577	-0.729202035092
H	6.777384754156	-0.044519312267	0.335982836422
H	5.595468884324	1.078933737597	1.022917760799
C	5.027247353901	-1.788393083759	-0.911533333346
H	4.994091504657	-1.352157696702	-1.919852803353
H	4.329875679508	-2.636187479276	-0.906898493685
H	6.042201600213	-2.204128799196	-0.785596527816
Mg	2.721726235264	0.014616110996	0.060330439723
Mg	-1.311996520513	0.334359330099	-0.663080029661
O	-2.371340756615	-0.800788535499	0.719163601009
C	-3.627859366635	-1.463226585471	0.382042850356
H	-4.212132218358	-0.723800842566	-0.169896094583
H	-4.140757673380	-1.689348785999	1.323305146988
C	-1.913498097615	-0.944874846538	2.083260549664
H	-2.743729094642	-0.678677158646	2.749466236072
H	-1.137784795626	-0.182873893615	2.200854382278
C	-1.364683397953	-2.328504046556	2.398506575588
H	-2.141218835596	-3.098029603947	2.346085431678
H	-0.960122772565	-2.333232887219	3.417369814367
H	-0.561665513751	-2.592375913438	1.703694487622
C	-3.413177389119	-2.707611412296	-0.463283783258
H	-2.931457863916	-2.447752626552	-1.410397263353
H	-4.387058367527	-3.154313340640	-0.695900305658
H	-2.805036733587	-3.456018624860	0.052998204829

trans-**3-27•(Me_2O)$_2$**

Cl	0.229792508199	0.482565273781	1.796621167709
Cl	0.240072244485	0.659512003070	-1.718145040643
C	3.864732985232	1.149127218149	0.074479124827
H	4.377290166187	0.803646702458	0.989810966751
C	3.751451127558	2.681229517249	0.179474543001
H	4.739824548134	3.174097167212	0.224129082421
H	3.197901248032	2.996570167357	1.074837606906
H	3.232231697157	3.113289578354	-0.688958997944
C	4.766160020398	0.765066060182	-1.113875279898
H	4.322521161504	1.057424638715	-2.077235601657
H	4.954841602887	-0.316831731480	-1.162994398269
H	5.754415075353	1.257969911809	-1.068454943811
Mg	-1.389151851547	0.378362948961	0.019074300669
O	-2.298165947720	2.246118612756	0.198456444369
C	-2.801424184659	-1.213993322267	-0.085135262748
C	-4.232966613953	-1.246467328279	0.463864386779
C	-4.023358978967	-1.223713554513	-1.016509400686
H	-4.613691029720	-0.353764454881	0.957016656531
H	-4.593434472603	-2.172522041848	0.905620676733
H	-4.244013765689	-0.312492126287	-1.568915805201
H	-4.244305282928	-2.134428114190	-1.568220445779
C	-2.065634619351	-2.436686386150	-0.006634393392
N	-1.370662681784	-3.375888855306	0.060568157611
C	-3.026800099401	2.518881214067	1.407240890464

H	-3.873749414367	3.177167907142	1.184963795041
H	-2.369018065977	2.984797060249	2.149070324645
C	-1.782681477937	3.439997032750	-0.420081624757
H	-1.234763593545	3.129442714483	-1.309488295383
H	-1.108534300058	3.959835951750	0.269731583519
H	-3.394297624831	1.564038572991	1.786966101378
H	-2.617285632001	4.093867980389	-0.695622415277
Mg	1.967994535073	0.184612426356	0.036185565903
O	1.894943139090	-1.896394215142	-0.070091100263
C	1.857784339893	-2.743079984325	1.096124955303
H	1.940827551440	-2.094715091817	1.969710833942
H	2.704256814067	-3.439214666783	1.067274230786
H	0.907982750866	-3.284508409512	1.119889075168
C	1.758991336712	-2.647987821093	-1.291629814299
H	1.750369760208	-1.930688782261	-2.113285462206
H	0.818715105958	-3.206024584583	-1.270736307565
H	2.611972918603	-3.328491189510	-1.397793880682

cis-**3-27•(Me_2O)$_2$**

H	-3.006184383138	3.452957783664	1.311600404006
C	-2.179402153809	3.083088483805	1.912434656024
C	-2.374919173458	1.849239358776	2.732487659955
C	-1.541357145688	1.768338762755	1.448178897078
H	-1.532632287217	3.858991869859	2.314942277861
H	-3.345663440682	1.358796592161	2.718114900728
H	-1.862564690813	1.792887969298	3.690393259632
C	-0.158148786257	1.610783753037	1.513767208661
N	0.995516171965	1.388250217896	1.410283478998
Cl	-0.241099112757	-0.161324237163	-1.431534418445
Cl	-3.859770549000	1.764901667784	-1.655528420464
Mg	1.850592393736	0.630934168482	-0.370797776255
Mg	-2.237692035292	0.791800449188	-0.395712345131
O	-3.127327308168	-1.002898359408	0.228893396372
C	-2.422302059967	-1.913547141349	1.077785709048
H	-1.704545587423	-1.327706780938	1.654102725259
H	-1.893322839469	-2.664387864905	0.479263078546
C	-4.165783150046	-1.634482373701	-0.540188826073
H	-4.628944698619	-0.851014813534	-1.140173592962
H	-4.900638062744	-2.081657829618	0.139137689368
C	3.406507414345	1.571805947421	-1.486870584116
H	3.039101499004	2.586237631111	-1.720562532623
C	3.717341198133	0.895248745830	-2.834466978127
H	4.088328841719	-0.134205858516	-2.705329326708
H	4.499876519092	1.428675546158	-3.404704035708
H	2.833408899503	0.835609645538	-3.483165060770
C	4.702860361541	1.750444699987	-0.674335912746
H	5.144267487141	0.783804781275	-0.381454588439
H	4.541565280421	2.321127594746	0.251049624997
H	5.489629431588	2.279989749379	-1.242429282798
O	2.473667165090	-1.222176858344	0.475934795818

C	3.224332984658	-1.219763778680	1.698103938979
H	4.293254494596	-1.088335592454	1.492392813061
H	3.061998801563	-2.163629687489	2.232063402170
C	2.824301978397	-2.303948823026	-0.397223134700
H	2.163268114001	-2.244474347567	-1.263163106589
H	2.669337552546	-3.259212411562	0.118215718255
H	-3.126381052946	-2.406133015641	1.758936865600
H	-3.736515717110	-2.407807447183	-1.188326369552
H	3.869555052215	-2.218437055894	-0.716365360069
H	2.851478593348	-0.387495141181	2.296142151859

trans-**3-29•(Me_2O)$_2$**

H	-3.206641944126	-2.258447422759	-1.921419199827
C	-2.377880308846	-1.806974738539	-2.460714061655
C	-2.500884692599	-0.393323669053	-2.930721846753
C	-1.609501197885	-0.703559218612	-1.723915724954
H	-1.819259978427	-2.498460967081	-3.087169499702
H	-3.424282362990	0.146221432668	-2.732361486221
H	-2.027467600326	-0.131187366620	-3.874221247938
C	-0.220667056634	-0.630946651309	-1.835943189487
N	0.949310942047	-0.520851280692	-1.748723259949
Cl	0.010879612996	0.374857798775	1.426704642953
Cl	-3.597531677596	-1.474106415323	1.511035315003
C	3.467462303916	1.734549625578	-0.137300915999
H	2.878892018147	2.666936414746	-0.212585936777
C	4.373301025030	1.693480073067	-1.381745671118
H	5.010019267717	0.794535760069	-1.405138920770
H	5.066481743669	2.553220262826	-1.429634547294
H	3.797474962879	1.693703275874	-2.317184072632
C	4.320137530352	1.862255272529	1.138560597010
H	4.939198212714	0.968763414622	1.314898861593
H	3.704358484905	2.001744070377	2.037661848806
H	5.022849463989	2.714538074147	1.095880153519
Mg	1.997200463301	0.186473914265	-0.052057139594
Mg	-2.107702139481	-0.200231161810	0.355826392927
O	2.755931636510	-1.638453824121	0.681964065359
O	-2.958565479554	1.708417526537	0.322148159946
C	-3.884218745536	2.127212396613	1.340934831902
H	-4.648603495238	2.773300415312	0.894349880288
H	-3.352571444739	2.668368281914	2.132384666641
H	-4.338084347104	1.220625817936	1.741760061765
C	-2.267955790504	2.801865795367	-0.295392331450
H	-2.993598657267	3.493340376097	-0.739111087127
H	-1.635577386276	2.382690774405	-1.079582889151
H	-1.648421233179	3.326997899114	0.440201640060
C	4.063918574112	-2.048127774480	0.262199221156
H	4.633586200219	-2.413920317779	1.124313398410
H	4.557877564457	-1.170327997345	-0.156850178027
H	3.990398790509	-2.836439966494	-0.496790714155
C	2.006301608909	-2.696616950479	1.296259231000

H	1.058335057461	-2.269885828508	1.623221704466
H	2.556966434674	-3.082604068499	2.161913476319
H	1.831650639794	-3.505144053335	0.576402771457

cis-**3-29•(Me_2O)$_2$**

H	-3.006184383138	3.452957783664	1.311600404006
C	-2.179402153809	3.083088483805	1.912434656024
C	-2.374919173458	1.849239358776	2.732487659955
C	-1.541357145688	1.768338762755	1.448178897078
H	-1.532632287217	3.858991869859	2.314942277861
H	-3.345663440682	1.358796592161	2.718114900728
H	-1.862564690813	1.792887969298	3.690393259632
C	-0.158148786257	1.610783753037	1.513767208661
N	0.995516171965	1.388250217896	1.410283478998
Cl	-0.241099112757	-0.161324237163	-1.431534418445
Cl	-3.859770549000	1.764901667784	-1.655528420464
Mg	1.850592393736	0.630934168482	-0.370797776255
Mg	-2.237692035292	0.791800449188	-0.395712345131
O	-3.127327308168	-1.002898359408	0.228893396372
C	-2.422302059967	-1.913547141349	1.077785709048
H	-1.704545587423	-1.327706780938	1.654102725259
H	-1.893322839469	-2.664387864905	0.479263078546
C	-4.165783150046	-1.634482373701	-0.540188826073
H	-4.628944698619	-0.851014813534	-1.140173592962
H	-4.900638062744	-2.081657829618	0.139137689368
C	3.406507414345	1.571805947421	-1.486870584116
H	3.039101499004	2.586237631111	-1.720562532623
C	3.717341198133	0.895248745830	-2.834466978127
H	4.088328841719	-0.134205858516	-2.705329326708
H	4.499876519092	1.428675546158	-3.404704035708
H	2.833408899503	0.835609645538	-3.483165060770
C	4.702860361541	1.750444699987	-0.674335912746
H	5.144267487141	0.783804781275	-0.381454588439
H	4.541565280421	2.321127594746	0.251049624997
H	5.489629431588	2.279989749379	-1.242429282798
O	2.473667165090	-1.222176858344	0.475934795818
C	3.224332984658	-1.219763778680	1.698103938979
H	4.293254494596	-1.088335592454	1.492392813061
H	3.061998801563	-2.163629687489	2.232063402170
C	2.824301978397	-2.303948823026	-0.397223134700
H	2.163268114001	-2.244474347567	-1.263163106589
H	2.669337552546	-3.259212411562	0.118215718255
H	-3.126381052946	-2.406133015641	1.758936865600
H	-3.736515717110	-2.407807447183	-1.188326369552
H	3.869555052215	-2.218437055894	-0.716365360069
H	2.851478593348	-0.387495141181	2.296142151859

trans-**3-27•(Et_2O)$_2$**

Cl	0.023627326002	-0.502124396036	-1.809899021268
Cl	0.020029165820	-0.575637182018	1.696164937085
C	3.000873167338	-2.631234200807	-0.208970948797
H	3.422921834271	-2.612288078277	-1.230154431078
C	2.167949594571	-3.922263011932	-0.098905730681
H	2.780239238361	-4.832163703855	-0.238009960303
H	1.363341114840	-3.963121678559	-0.846404368942
H	1.692973269200	-4.018982527981	0.888664955007
C	4.193050846655	-2.688651305536	0.761910838364
H	3.868136806548	-2.691869236563	1.813069805309
H	4.871736352282	-1.832735538272	0.639465431943
H	4.803194097198	-3.600278522321	0.625960648293
Mg	-1.406810650139	0.267043347287	-0.038272312987
O	-3.003325001274	-1.057393088457	-0.035637512803
C	-1.998639956459	2.316520600684	-0.011249888830
C	-3.174548501256	2.931270860780	-0.781142796439
C	-3.232396399341	2.871899889058	0.712392586628
H	-3.808007842154	2.264317339987	-1.363585227360
H	-3.037350265453	3.908394917150	-1.238604153032
H	-3.904146010991	2.158990010949	1.186961554492
H	-3.135604218242	3.809111579371	1.255655243664
C	-0.811313722934	3.108313918861	0.066153509897
N	0.218480122902	3.660652976220	0.130360632860
C	-3.776189149329	-1.282962993834	-1.246062548201
H	-4.836413899443	-1.322406601821	-0.972283944089
C	-3.410221906546	-1.838482305490	1.122273748514
H	-2.506345936223	-1.955556980968	1.723768880228
H	-3.716294272543	-2.829994739453	0.774377492270
H	-3.623445072149	-0.387342512575	-1.855576419165
Mg	1.794157515340	-0.881456551569	-0.060684753496
O	2.720575290256	1.000776446601	-0.057295584792
C	2.772079813365	1.796049518964	-1.280673006612
H	2.124157086313	1.280632589525	-1.992585091633
H	2.319138754535	2.767969202172	-1.064640894387
C	3.025051610474	1.778955486818	1.136852698519
H	2.140230781077	2.374688237537	1.379797637566
H	3.843019986015	2.461225665619	0.883936091982
C	-3.331590757334	-2.529289380518	-1.995544251329
H	-2.275280237968	-2.457489500959	-2.268783053202
H	-3.923562948409	-2.628941697201	-2.912570513342
H	-3.480177572017	-3.438130090679	-1.403436950377
C	-4.515334946541	-1.149556175754	1.907714880693
H	-4.788886869790	-1.766638561171	2.771108655796
H	-5.416468969656	-1.001420700387	1.302964689596
H	-4.182017479310	-0.174954025919	2.278769601419
C	3.443250847484	0.865932711741	2.274785321706
H	4.316257586627	0.263962097025	2.003277357265
H	2.632510003374	0.199045218528	2.584051964710
H	3.706641132669	1.481105159797	3.142749658686

C	4.191024817002	1.905165917170	-1.818272544377
H	4.603284032940	0.915486999231	-2.041272486587
H	4.862836313273	2.408409113709	-1.114901285331
H	4.182851078767	2.490599484127	-2.744996143051

cis-**3-27•(Et_2O)$_2$**

Cl	0.179191528314	0.140589296928	-1.656193722265
Cl	0.012955884926	0.309841339458	1.812757890590
Mg	-1.575011476869	0.399390767055	-0.008639885842
O	-2.447770217114	-1.501426595979	0.096504086833
C	-3.107769021695	1.857205665307	-0.201258913375
C	-4.575533292965	1.554136534008	-0.537413846073
C	-4.228542706899	2.042526537586	0.832537800195
H	-4.870255976507	0.513625035292	-0.664853838046
H	-5.103553219439	2.239676246182	-1.196204978609
H	-4.273571762724	1.348433783859	1.670263227906
H	-4.521873264338	3.056650961073	1.093449572796
C	-2.586239087616	3.070660945832	-0.760234089894
N	-2.087009132237	4.027379655588	-1.218719078339
C	-3.143955756429	-2.018886394205	-1.069166848731
H	-4.097351665162	-2.447118629970	-0.740631066390
C	-2.528970190226	-2.322209420697	1.290847807623
H	-1.641589149418	-2.066003443877	1.873569778199
H	-2.451572059986	-3.372792855336	0.990485278210
H	-3.369429368546	-1.143037746207	-1.684101652781
Mg	1.815529199250	0.691834564247	0.123041707399
C	-2.302292511156	-3.024339573136	-1.839174072022
H	-1.367040368060	-2.564989507491	-2.171383597949
H	-2.856385200837	-3.362318325147	-2.722206218133
H	-2.066734503991	-3.907372819609	-1.235365770149
C	-3.799447615439	-2.056165502878	2.084031607614
H	-3.812528435165	-2.691181543197	2.977164266112
H	-4.700606661032	-2.277143463305	1.502630153092
H	-3.844818707117	-1.011824578662	2.408498075460
O	2.891458209112	-1.112137038218	0.281456535097
C	4.293076468372	-1.021361795558	0.648965375185
H	4.415953025940	-1.497485964962	1.630109325322
H	4.477767416392	0.048497870328	0.762147619194
C	2.283317189579	-2.425823467301	0.374473821479
H	2.877590360609	-3.024999947701	1.074273273385
H	1.300039335655	-2.262582329238	0.824948269059
C	2.148883290294	-3.104078919323	-0.981257733192
H	3.121731716831	-3.314862756280	-1.433625203669
H	1.575258624188	-2.473262783800	-1.665977393662
H	1.617217883336	-4.055640297578	-0.859041936075
C	5.235997281432	-1.619240934484	-0.383669983135
H	6.269822510979	-1.418659177216	-0.079797852035
H	5.074831986284	-1.164001450921	-1.365829390947

H	5.121081502649	-2.704009858828	-0.473537675156
C	3.039023805509	2.437778508758	0.109369329943
H	2.296588030689	3.233039745126	-0.077669815025
C	3.726282005890	2.795919776590	1.439657595215
H	4.488268501056	2.056475732084	1.734379523847
H	3.011951929004	2.861757955133	2.271106183910
H	4.252722316736	3.765849175402	1.389732761298
C	4.047485141493	2.504853392814	-1.052289901678
H	4.830312319059	1.733667014834	-0.972084008388
H	4.579674705224	3.472249675221	-1.090287997525
H	3.565449472843	2.368338855181	-2.029730755459

trans-**3-29•$(Et_2O)_2$**

H	-2.536429365889	3.476647251294	1.247100342445
C	-1.839918393022	3.010124468166	1.939103575590
C	-2.305022619588	1.864566478953	2.779870925629
C	-1.386309875204	1.588235623970	1.586794409219
H	-1.115650535932	3.693245451796	2.376894826777
H	-3.337921282899	1.535004593322	2.691202975370
H	-1.896636547013	1.776262263178	3.784153681218
C	-0.056977926250	1.218532813893	1.789496220334
N	1.052422770803	0.820021534444	1.802021898308
Cl	-0.139843924422	-0.625924930820	-1.105796798531
Cl	-3.189872621995	1.987380610774	-1.782031460377
C	2.912039032698	-2.276009280935	0.891661335232
H	2.177293541832	-2.881590605736	1.452833189329
C	4.100982323105	-2.042136919201	1.842199069600
H	4.896752592450	-1.445934263494	1.367592874604
H	4.582916088571	-2.984782868511	2.161269046095
H	3.806263014162	-1.510838497078	2.758063986834
C	3.358306028586	-3.128352738281	-0.310126986466
H	4.091050199314	-2.599242382022	-0.939220772112
H	2.517143061275	-3.401483936073	-0.962258338281
H	3.846232292779	-4.072403050952	-0.004542048625
Mg	1.869856747189	-0.492599231333	0.351043320571
Mg	-2.044639739251	0.679668309914	-0.308285478902
O	2.974871926747	0.913453974936	-0.765357721171
O	-3.375263627654	-0.846623414120	0.178072034733
C	-4.650765669350	-1.023692553724	-0.503736566472
H	-5.081428904670	-0.023197837773	-0.585075866628
H	-5.289473816463	-1.631206603311	0.147390861523
C	-3.064846331069	-1.791557965134	1.229038405790
H	-3.928173758147	-1.840023489083	1.904846840958
H	-2.237085353094	-1.335573031719	1.779108383318
C	4.094850114542	1.572971652987	-0.122782821309
H	4.938069925129	1.584980958547	-0.822267005895
H	4.373415543414	0.929402583835	0.716763178403
C	2.808891927444	1.206516789810	-2.177868480670
H	1.746793726992	1.057931933234	-2.380740749365
H	3.042339396267	2.264809589937	-2.337717492715

C	-2.674970294555	-3.169825796489	0.716900615735
H	-3.509945080043	-3.672868592286	0.219086972344
H	-2.365972759087	-3.794194958872	1.563302135717
H	-1.837196319577	-3.095837518917	0.017312163701
C	-4.491879269233	-1.641463772290	-1.883700360913
H	-3.868954269640	-1.002804601854	-2.516454331181
H	-5.478597413250	-1.720260490326	-2.355434529005
H	-4.050013138821	-2.641059826567	-1.840786389703
C	3.665562357526	0.301295939308	-3.050465214694
H	3.489421232359	0.538468233308	-4.105941746225
H	3.409101883382	-0.750249073868	-2.888003920989
H	4.734888909452	0.430731192030	-2.851258157528
C	3.734104066479	2.971050704911	0.356587453780
H	3.444476310244	3.623423307181	-0.474089304742
H	4.600544319461	3.423924727671	0.852410146397
H	2.907229503915	2.927253243367	1.071055672944

cis-**3-29•$(Et_2O)_2$**

H	-2.921069068199	3.459202688248	0.911963011287
C	-2.146299524103	3.138592582744	1.603551388119
C	-2.428948045714	2.001704774231	2.532032979540
C	-1.517402217030	1.768337900938	1.323475282667
H	-1.505730438563	3.938706648987	1.966842881459
H	-3.410431297532	1.533736943764	2.503410182886
H	-1.982830782484	2.036672248563	3.523650905228
C	-0.144451487524	1.596483949809	1.490020094612
N	1.008952505725	1.352960777493	1.471993886682
Cl	-0.006105618021	-0.264609123070	-1.356464747982
Cl	-3.668642268790	1.589795021321	-1.838329555387
Mg	2.055942775507	0.570471325704	-0.194139114291
Mg	-2.102190056408	0.646563999444	-0.479097864457
O	-3.013370408679	-1.145549121761	0.102550590384
C	-2.326125485019	-2.142977493199	0.893396567905
H	-1.260248107893	-1.947660520076	0.751197891848
H	-2.541185835554	-3.130500297657	0.470074226542
C	-4.323809898900	-1.546078522042	-0.391840266261
H	-4.871766199597	-0.614553963981	-0.539236576977
H	-4.816688188647	-2.126952145803	0.395958047198
C	-4.223077168029	-2.320697817261	-1.695767307569
H	-3.778227687092	-1.694979706006	-2.474787602018
H	-5.227615233072	-2.612130614560	-2.023644497204
H	-3.626402694827	-3.233235588041	-1.588708765253
C	-2.711940406685	-2.066139708042	2.363777542660
H	-2.463624423273	-1.083821690448	2.776665100729
H	-2.164385117589	-2.828460627970	2.930275804363
H	-3.782468550820	-2.243806167216	2.511738795714
C	3.421436787409	1.725397832777	-1.363368363020
H	2.832322604043	2.618621903820	-1.638826092248
C	3.843171499597	1.057026792471	-2.684277395178
H	4.441902612866	0.148439411057	-2.511281765039

H	4.471082985506	1.716225268212	-3.311577416255
H	2.980422769025	0.761981460277	-3.296619839788
C	4.664680858347	2.235642599091	-0.614660523549
H	5.325445372337	1.409858316086	-0.305611709027
H	4.406463954814	2.798450289069	0.293513146362
H	5.290061679851	2.903271562889	-1.235477630725
O	2.779351038322	-1.308999196354	0.548862928964
C	3.653355894114	-1.501338781075	1.687701145615
H	4.580578461267	-1.970867621177	1.340620849699
H	3.152639224390	-2.197501112693	2.373976556987
C	2.538869612082	-2.531515790309	-0.197507029837
H	1.614907969428	-2.353377777216	-0.750574896638
H	2.353754134171	-3.334162740520	0.528157038731
C	3.951372065732	-0.182232822334	2.374970607135
H	4.593849076702	-0.375112230380	3.241504856189
H	3.037629694052	0.303976253813	2.726827858559
H	4.485259492304	0.504488342354	1.710311606724
C	3.676719885183	-2.883623951485	-1.145627048774
H	3.847559605688	-2.075419926933	-1.863326310150
H	3.411047385784	-3.787467612437	-1.705891063065
H	4.614496265796	-3.084257223115	-0.617706394097

3-29•$(Me_2O)_3$ – A

H	-2.462421099991	2.039434136177	3.164072228350
C	-1.824155206108	1.192105121890	3.401883385198
C	-2.352961859060	-0.195546273712	3.216226591780
C	-1.331734279422	0.353952570993	2.219398404707
H	-1.149326973164	1.364327228595	4.237390803134
H	-3.372558217299	-0.322865793036	2.858883747334
H	-2.035253815956	-0.955537944005	3.926732848718
C	-0.018475412244	-0.122293191596	2.210257183026
N	1.092419115815	-0.463402103105	2.014638623166
Cl	-0.390870253347	-0.554725458218	-1.259702594447
Cl	-2.025986698453	3.129481515459	-0.401298523392
C	3.838938964673	-0.571579763344	-0.827931437085
H	4.233410210764	-1.565932454996	-0.542593632038
C	4.801352949619	0.461501787126	-0.215312863368
H	4.485313510016	1.493371350548	-0.432268225974
H	5.833127833978	0.372843774732	-0.604769870823
H	4.867183010696	0.375465310708	0.879049135395
C	3.922351730644	-0.502435530313	-2.364515960390
H	3.548724278076	0.456730199921	-2.752925307970
H	3.330006091456	-1.288648430864	-2.854572766350
H	4.957404856900	-0.600847948617	-2.743018934329
Mg	-1.727728661677	0.919110097395	0.127148959304
O	1.471230869640	1.739003437407	-0.024205418639
O	-3.602596524982	0.076620411418	-0.316282355517
C	-4.539129441161	0.718368660952	-1.198653489900
H	-4.440659620227	0.310250390504	-2.211680043840
H	-4.295172814751	1.780583251866	-1.195498668604

C	-3.793875739607	-1.341077677194	-0.235766247238
H	-4.809149028455	-1.556623087503	0.118091546362
H	-3.063578438742	-1.726782381985	0.476508541974
C	1.841688586726	2.622018878536	1.041220417212
H	2.863509753656	2.992468890895	0.891432434705
H	1.791943683443	2.050265542909	1.967277026792
C	1.531875902651	2.406537635599	-1.296169353772
H	1.244951971375	1.679837730959	-2.055634520682
H	0.823062824196	3.240794500217	-1.306322190558
Mg	1.839425276625	-0.506871428708	-0.015465368647
O	1.625056144683	-2.751750693679	0.188039415130
C	2.392962704501	-3.362955625713	1.226568186918
H	1.993281809657	-4.361216550974	1.448510331596
H	2.300489046489	-2.726154981788	2.106503633120
C	1.639700450006	-3.522518140419	-1.014930909131
H	2.656680862050	-3.589458696035	-1.421765918045
H	0.985197037831	-3.018205993909	-1.726503889143
H	-5.558407012580	0.556120927912	-0.829092460397
H	-3.631979828966	-1.804502225543	-1.215525587251
H	1.256361498314	-4.532079523422	-0.816795122535
H	3.447299549450	-3.447867905837	0.933183794053
H	2.552001983891	2.761849552980	-1.484901615739
H	1.141485418370	3.464407898818	1.082582037830

3-29•$(Me_2O)_3$ – B

H	-2.794273924561	-1.107154126154	-3.185988480248
C	-1.975278819003	-0.436218430680	-3.434360210783
C	-2.162290877608	1.028951177460	-3.203293274351
C	-1.258780412207	0.231357498638	-2.257997198217
H	-1.393993577117	-0.738611231459	-4.303023493946
H	-3.107083472866	1.375510668379	-2.791652857699
H	-1.704044706693	1.712180906022	-3.915161664635
C	0.117147307483	0.443891388864	-2.277866003839
N	1.270661809495	0.621224739186	-2.102375955230
Cl	0.255824122090	0.625890974633	1.218484628906
C	3.418058046135	2.761187897599	0.131387634959
H	2.737417936150	3.625892071150	0.027741310979
C	4.532640606753	2.951931717917	-0.914318714509
H	5.261337363571	2.126855022244	-0.893161144760
H	5.114725651970	3.877700144943	-0.750344391550
H	4.138867532054	3.001132669075	-1.939047663514
C	4.008736783149	2.843386977622	1.550753575884
H	4.721625106555	2.026570693464	1.748017148023
H	3.235561258371	2.790157060837	2.329631299992
H	4.573217306669	3.778482288436	1.722661577627
Mg	2.197562476384	1.051299799247	-0.252115970973
O	3.201872107046	-0.797591000787	-0.022083332095
C	3.028114238053	-1.935960603573	-0.874455137521
H	3.993277337393	-2.433975716089	-1.025665576093
H	2.643336790328	-1.565111665819	-1.823895624683

C	3.742738515274	-1.135432807191	1.261104064446
H	3.869582087456	-0.203854111721	1.814064001786
H	3.057026443422	-1.799216098909	1.800800790939
Mg	-1.753583160875	-0.137681318902	-0.115709369315
O	-0.753912555328	-2.179983156406	-0.028840790079
O	-2.552691930489	1.879798834819	0.248088332817
Cl	-3.747560267351	-1.173070055605	0.502012246731
C	-3.362283190004	2.138926259673	1.404270882387
H	-3.920024293534	1.226025258952	1.608652735636
H	-4.053893886766	2.963281869484	1.190376618130
C	-1.819527601075	3.039662161827	-0.153380984487
H	-1.270669858896	2.781532316160	-1.059088732866
H	-1.117685641969	3.344085495792	0.631414586859
C	-0.691915282600	-2.760804893894	1.281586431818
H	-0.027040544439	-3.634913186572	1.266334254550
H	-0.284477139744	-1.998386548692	1.945764862120
C	-1.229773463263	-3.128192521738	-0.991939111716
H	-0.571972309079	-4.007397166930	-1.002127063179
H	-1.200068655933	-2.637194777825	-1.964498640586
H	4.716640819110	-1.623342528651	1.136977312673
H	2.310086589373	-2.636335913927	-0.431604635667
H	-2.256667615484	-3.429371310115	-0.757498220546
H	-1.692727001986	-3.056032455991	1.614533255410
H	-2.727101484720	2.403109368658	2.259364536785
H	-2.515768560695	3.859664366549	-0.370352846373

3-29•$(Et_2O)_3$ – B

H	-2.542908497658	-1.166001956501	-3.350928323764
C	-1.681672888278	-0.545346700988	-3.583981305168
C	-1.843093595226	0.934873023010	-3.472770026770
C	-1.034091892472	0.190823328521	-2.403082818106
H	-1.041158961481	-0.927166715019	-4.376168279982
H	-2.812577598798	1.317355481856	-3.163682411532
H	-1.313960471239	1.559666935623	-4.189125811259
C	0.348542946965	0.345409051654	-2.372135610157
N	1.507301151218	0.471327848785	-2.186379267747
Cl	0.337814592721	0.543943257581	1.043902111252
C	3.534901478414	2.681881723790	0.037170299315
H	2.921637613390	3.517644387175	-0.347145647568
C	4.845625396229	2.696968674085	-0.770666836125
H	5.523127686176	1.880871442768	-0.473901137508
H	5.419801812316	3.632562628211	-0.635343654870
H	4.670398752074	2.586338537652	-1.850208822028
C	3.821084631679	2.999333626589	1.515743189003
H	4.429091127714	2.217260998421	1.997861696246
H	2.899957573224	3.090803556366	2.107193943991
H	4.384108736367	3.942140392540	1.647746282979
Mg	2.349579583673	0.935659709057	-0.310558625102
O	3.363262813304	-0.906287727913	-0.027043645842
C	3.724224671556	-1.791442480425	-1.114861259499

H	4.744088981370	-2.154568564896	-0.946008394746
H	3.730320009570	-1.162152468315	-2.006961152090
C	3.764530692137	-1.335801875750	1.295566311436
H	3.093615936809	-0.810857037815	1.981052778302
H	3.562326833620	-2.408992513287	1.390691536184
C	5.220160165547	-1.010772398811	1.599099226232
H	5.457072146389	-1.322583095350	2.622951383381
H	5.402239080917	0.064647734819	1.515047481524
H	5.907172091429	-1.533431874335	0.925148307219
C	2.737640227094	-2.938588338959	-1.277328397683
H	2.699281096063	-3.577735990875	-0.388577294745
H	3.041915462259	-3.564079539340	-2.124532859977
H	1.733950568052	-2.552042098333	-1.475822187929
Mg	-1.840576574431	-0.057085410096	-0.344856770096
O	-1.322043658634	-2.135199403523	0.226439755382
O	-2.474208872085	1.909746405547	0.345139524447
Cl	-4.087569116853	-0.694815845610	-0.690213614662
C	-3.605131951985	2.092423508498	1.233676436319
H	-4.324463778203	1.327031038502	0.939774606446
H	-4.046982060855	3.074463749669	1.032389643134
C	-3.206235831973	1.956715576426	2.696783907762
H	-2.810064445426	0.956786838041	2.902488051852
H	-4.085994564065	2.110752369461	3.332706158661
H	-2.444967818607	2.688603210293	2.986780423789
C	-1.717288623866	3.115309375983	0.091584895211
H	-0.724695451313	2.782121051642	-0.213190684130
H	-1.599967189409	3.662996391786	1.033991159101
C	-2.356113839995	3.982229239659	-0.985148271127
H	-2.438621635772	3.429965701390	-1.925622112343
H	-1.732328249447	4.867262056827	-1.157412849422
H	-3.355331532744	4.328166104684	-0.700076495170
C	-0.668537259473	-2.615516417930	1.424575062741
H	-0.470957627935	-3.685900957581	1.301252884990
H	0.286756705307	-2.092018752413	1.493236134358
C	-1.511488622919	-2.357779119474	2.664113496054
H	-2.487155827892	-2.847543803384	2.594204951598
H	-1.669524853692	-1.283513172010	2.804691328961
H	-0.991323754264	-2.736057099686	3.552461071524
C	-1.724274205199	-3.175924811990	-0.698060027536
H	-0.828362982693	-3.757093203511	-0.958043685000
H	-2.060662995300	-2.646008223342	-1.588982496707
C	-2.837302367884	-4.071910939046	-0.174460559387
H	-3.098725188098	-4.804171084648	-0.947824051109
H	-3.723518684859	-3.473743919454	0.050991831675
H	-2.536378092561	-4.629784416302	0.719119515817

3-29•$(Et_2O)_4$

H	-2.901244800841	-1.086240019459	-3.039178717400
C	-1.962028607159	-0.610702116024	-3.308393632416

C	-1.897256198012	0.879823462564	-3.245054175021
C	-1.175939736682	0.053610240939	-2.169971795007
H	-1.411227218821	-1.108783984426	-4.103517260584
H	-2.789835076246	1.410324825144	-2.924498281798
H	-1.303991926429	1.392277933492	-3.999849453912
C	0.218481171051	-0.003252123579	-2.203201584521
N	1.390232792221	-0.050942473501	-2.087409748040
Cl	0.267983967208	-0.110433884331	1.252291262800
Mg	-1.955977336273	0.022544865047	-0.083643342592
O	-2.282719048033	-2.049843120558	0.624559132621
O	-1.949936928275	2.083458510443	0.686926840393
Cl	-4.296351646897	0.235094684046	-0.469292479660
C	-2.593704260567	2.292660637656	1.960769300908
H	-2.520510687964	1.325913962794	2.467004539993
H	-3.656757585943	2.497171574317	1.798123558163
C	-1.928789604793	3.367573173791	2.810546418948
H	-0.866567841423	3.147316915187	2.956485384746
H	-2.411238103540	3.396027324001	3.794187934671
H	-2.023467465788	4.365644554292	2.370234480055
C	-1.935384453783	3.208041846127	-0.221307460968
H	-1.476153446815	2.807790038265	-1.127791236277
H	-1.260210894032	3.971300233105	0.185360414876
C	-3.306036245341	3.797495221458	-0.532399838430
H	-3.994955765599	3.016495375027	-0.865047633689
H	-3.195924833191	4.542285009641	-1.329536125526
H	-3.745476804517	4.306747443155	0.332068220872
C	-1.764098043054	-2.685470260954	1.817672457850
H	-1.974513140644	-3.758569311515	1.752130979447
H	-0.683267876888	-2.541765234043	1.804599768758
C	-2.368341909432	-2.088660046407	3.079598002157
H	-3.457971323177	-2.185879732466	3.088944242285
H	-2.110348366352	-1.027951279528	3.162963372062
H	-1.962689752906	-2.598359824876	3.961832409174
C	-3.114719431234	-2.907512370580	-0.196260059427
H	-2.525726277786	-3.798839912494	-0.452404388293
H	-3.296947669468	-2.337072676875	-1.106663586712
C	-4.440821716872	-3.277891687532	0.450956961419
H	-5.019087034551	-3.894051960132	-0.247951945933
H	-5.013216918097	-2.372999538370	0.669610791467
H	-4.307898853024	-3.858388794061	1.370498567058
Mg	2.338894695190	-0.145230886972	-0.166925410886
O	2.255836061822	2.171178643598	-0.285465600020
O	2.064285818815	-2.480043604498	-0.415385168080
C	4.390172975272	-0.385539352165	0.496736572501
H	4.690402963252	-1.357610732197	0.065699885737
C	4.540533053543	-0.519252082546	2.024622431645
H	5.580761086638	-0.731712394620	2.338128234348
H	3.913802550560	-1.318672390492	2.445774800141
H	4.252462579137	0.404829775265	2.548554166173
C	5.410981585379	0.641864581862	-0.019484439012
H	6.440869491355	0.432878491770	0.327531789132

H	5.176526746455	1.660571874115	0.322164359070
H	5.451227196195	0.675371550911	-1.117968141682
C	2.957645294088	2.808481085189	-1.369700921540
H	3.499417083161	2.006229170378	-1.874877461441
H	3.704095467164	3.501726158139	-0.962622834914
C	2.025525961564	3.512780409970	-2.348702875174
H	1.462745211405	4.324325795389	-1.874661817373
H	1.316964040235	2.800491674155	-2.780172861833
H	2.614507863328	3.951731747202	-3.162833160716
C	1.834891281118	3.053695395786	0.771834605903
H	1.440439747097	3.977195284865	0.328794692522
H	1.007866990295	2.532506642518	1.257454950705
C	2.943927036894	3.362397981552	1.770262344332
H	3.788184180347	3.881593837743	1.304206189479
H	3.319106871564	2.442767939842	2.227921196485
H	2.552149062937	4.009882438945	2.564267737566
C	2.060722241426	-3.328598833667	0.745262155541
H	1.205652236468	-4.015720588614	0.691538679122
H	1.880948305943	-2.647047793433	1.579906651195
C	3.359427739250	-4.099176908967	0.962205952990
H	4.211816447062	-3.415778664458	1.001005447882
H	3.542583792244	-4.843235052737	0.179905415365
H	3.302334205947	-4.635971051500	1.916588077008
C	2.073890371603	-3.153864293018	-1.685486607508
H	2.871503161685	-3.906564966008	-1.697355373261
H	2.332823223332	-2.379477440170	-2.409251105672
C	0.728959441190	-3.777125829735	-2.045205272623
H	-0.060156083842	-3.018739921700	-2.037052324898
H	0.445029999812	-4.581499546533	-1.357816719971
H	0.783090923038	-4.209238623942	-3.051503532759

3-32•$(Et_2O)_3$ (IPS-TS)

Cl	0.174916744035	0.086934441845	-1.413058938764
C	1.850285106887	-0.971994011694	1.997297199917
H	0.958414516679	-1.028019690509	2.648514411489
C	3.044676342764	-0.705701041848	2.933945625804
H	3.991557802341	-0.614338445949	2.378935963603
H	3.201017661251	-1.516887167033	3.669008632073
H	2.923804477110	0.223074879308	3.509881616770
C	1.999173664574	-2.356616549723	1.341292381692
H	2.877831611480	-2.407098408483	0.678714438038
H	1.130518709467	-2.623464121545	0.724215797179
H	2.133208903722	-3.168166119208	2.080381561977
Mg	1.495301627050	0.669922690008	0.659920552833
O	3.280148571309	1.372381654085	-0.210495988456
C	3.758086908059	2.732712270738	-0.070723610858
H	2.856317962735	3.337599381275	0.040853927264
H	4.259204459940	3.022493791766	-1.001526944423
C	4.187958209307	0.447943784826	-0.858653305556
H	5.206653251995	0.658586317846	-0.514658302761

H	3.909048305748	-0.540084520964	-0.482606376474
C	4.079823780915	0.506694729874	-2.375507535558
H	4.766524024422	-0.223190105212	-2.819587777135
H	4.346644023389	1.495220216422	-2.764845615287
H	3.062768037512	0.267189880319	-2.699619249227
C	4.670587365017	2.900678370089	1.135839588161
H	4.146369538625	2.626376510144	2.056269204940
H	4.980976611039	3.948976071155	1.215581576103
H	5.575837447506	2.289391204613	1.057759797522
Mg	-2.033672172855	0.989457953985	-1.275237669611
O	-1.810338593174	2.838353778875	-2.176829773738
O	-2.560786849222	0.361617550758	0.635161284508
Cl	-3.795612717331	0.210047153438	-2.516796057016
C	-3.633746918961	1.040994868366	1.342765980846
H	-3.624611414160	2.056222642651	0.939563742689
H	-3.335853674704	1.115475570386	2.395178575873
C	-4.988120358026	0.368854211206	1.180420971401
H	-5.246952953086	0.269813925230	0.122233142850
H	-5.751079137927	0.981510323431	1.675668541616
H	-5.011039914627	-0.624041074081	1.641848281565
C	-2.124033619948	-0.901327397463	1.216719713469
H	-2.501095212714	-0.932703550984	2.244278149977
H	-1.033221591995	-0.858086646816	1.262634919772
C	-2.582402963628	-2.110341891445	0.416179098911
H	-3.672168599842	-2.171163652657	0.355884441744
H	-2.205615750170	-3.018699617833	0.901379995473
H	-2.186197222784	-2.084403794799	-0.603180901808
C	-0.549234592658	3.533577565583	-2.367375994878
H	-0.746620511113	4.608487666953	-2.302851549706
H	0.081561188418	3.258469269813	-1.520189291703
C	0.110116757915	3.153887333410	-3.684700133704
H	-0.505737233611	3.431266378511	-4.544818641747
H	0.296664351582	2.076804017398	-3.722226541802
H	1.073754986455	3.671078344118	-3.770779287289
C	-3.006851506578	3.644645524639	-2.348496154867
H	-2.911650978480	4.519897228810	-1.697299193759
H	-3.821887574290	3.018721865097	-1.979859100013
C	-3.269488267013	4.022066068107	-3.797153561205
H	-4.219388776984	4.566116350497	-3.857150685369
H	-3.348528344663	3.122625113340	-4.414548368967
H	-2.488840041968	4.671928806591	-4.206155606545
N	0.613958203511	2.452379541273	1.117520042507
C	-0.386173845213	3.102928499004	1.147610378637
C	-1.577419697417	3.750154415249	1.070660149943
C	-2.285561607682	4.424098613823	2.218916561680
C	-1.770015465750	5.247269923392	1.064574382617
H	-1.782558130576	4.539772635238	3.179236106856
H	-3.363120668627	4.277707333002	2.310631193866
H	-0.925878558612	5.909290702720	1.260946572066
H	-2.495308686366	5.670206439042	0.367491653997

3-33•$(Et_2O)_3$ (SIP)

Cl	0.385532002123	-0.745918516399	-1.956829205533
C	1.953369631592	-2.122563991064	1.416153509499
H	1.079459896562	-2.011503889690	2.084900223346
C	3.196874224273	-2.084824200004	2.324865536713
H	4.130518426856	-2.173472954283	1.747571325738
H	3.215455414372	-2.910980686586	3.060243634667
H	3.265763115750	-1.149383919300	2.898775761296
C	1.822706665840	-3.509862112109	0.762882246606
H	2.653022277186	-3.720428329316	0.070421412364
H	0.897930214326	-3.609376824794	0.178650374660
H	1.830352108169	-4.332850671820	1.501942161091
Mg	1.867123285187	-0.462144174648	0.061411013735
O	3.657734234447	-0.078483909241	-1.005715157122
C	4.591551663828	0.916617979545	-0.519055617552
H	5.603207102879	0.498299694573	-0.566698561394
H	4.335749597039	1.066573005013	0.532220673678
C	4.105346387530	-0.845341698828	-2.149898614078
H	3.191795278445	-1.200880335049	-2.632324365563
H	4.606984522856	-0.164721933820	-2.847465339722
C	5.006550910410	-2.006381508788	-1.754676943613
H	5.289646050737	-2.569885890988	-2.651280043443
H	4.488019223085	-2.684921745616	-1.070617573797
H	5.927716291413	-1.664630471174	-1.270619446858
C	4.482433421284	2.225820580451	-1.285893208171
H	4.696594463585	2.095608329984	-2.352252268427
H	5.204366427820	2.947096493853	-0.885421592326
H	3.478182311981	2.643399859033	-1.173719870742
Mg	-1.719123344027	0.341643681477	-1.714237010676
O	-1.362685238117	2.352806753938	-1.890675548696
O	-2.312794656555	-0.056970175107	0.213532675330
Cl	-3.373918139532	-0.383643284720	-3.090265805030
C	-3.051539870460	-1.299373423772	0.408393791211
H	-2.572451108205	-1.855944646166	1.218692479941
H	-2.906024283342	-1.853923055583	-0.521110993347
C	-4.534710068122	-1.079857393959	0.658901050653
H	-4.727212583886	-0.543140871212	1.593560317073
H	-5.028044117963	-2.055641127075	0.731178568367
H	-4.986972831369	-0.532146634206	-0.173226391790
C	-2.207391675714	0.830519561560	1.366747455754
H	-3.215164886479	1.176430366249	1.623436780009
H	-1.630651522606	1.689747970378	1.014028400167
C	-1.522388358928	0.195639133887	2.566292863094
H	-2.123577843146	-0.591665039430	3.032196870078
H	-1.358230440027	0.975782624715	3.317682876696
H	-0.547309140057	-0.216752342447	2.291822787778
C	-0.067572225566	2.834288808928	-2.360793494813
H	0.194473560590	3.705223684473	-1.753534903391
H	0.642953363725	2.040164421115	-2.131237850618

C	-0.095239508187	3.138678129709	-3.850310443235
H	-0.822603081562	3.918685245049	-4.098811472148
H	-0.340906123097	2.241911242586	-4.428242030759
H	0.893424492860	3.490479393794	-4.167494844976
C	-2.251744690613	3.440465737548	-1.498351752901
H	-2.184495505725	4.213108515008	-2.271600359492
H	-1.858075955051	3.835330983277	-0.554440739756
C	-3.683404659547	2.955392104898	-1.374402920653
H	-4.318437590791	3.807118432275	-1.105210691451
H	-3.795927386936	2.202522803659	-0.587862900743
H	-4.048944432107	2.528907926386	-2.312707589142
N	1.449585995258	1.449239350357	0.623320330227
C	0.934511141781	2.480732729516	0.929065484375
C	0.208078959093	3.594955353498	1.187829151167
C	0.167717252875	4.383741040705	2.468853725424
C	0.689648146263	5.022955456191	1.203914402993
H	0.891920953140	4.183247011416	3.259402269093
H	-0.807131332305	4.697597738101	2.845165681777
H	1.757494945049	5.242847355722	1.162525644460
H	0.075392639816	5.778749258327	0.711270072895

3-34•$(Et_2O)_4$

C	0.522889564311	-0.930715247550	-1.899179431052
N	-0.092694410508	-0.709605404067	-0.865828018196
Cl	-1.749392714205	-0.318077685998	1.780780595757
Mg	-0.201024089390	-1.972741671726	0.810580913996
O	4.176528348502	0.937536010632	0.660432382029
O	-1.616546911059	-3.390669527430	0.120411623218
C	1.397715065132	-2.840514841947	1.952230424996
H	1.225918963723	-3.932389716023	1.984114787356
C	1.442822329311	-2.359716709209	3.414266951470
H	2.267497692345	-2.821706553675	3.989507424632
H	0.512745147136	-2.579588027914	3.957066153682
H	1.592417526170	-1.271297350000	3.482710538203
C	2.775968642774	-2.634349689741	1.294836021793
H	3.597524427118	-3.093507138189	1.877802207864
H	3.023659508932	-1.567343443165	1.195243404018
H	2.824531421474	-3.065355747081	0.284525159234
C	4.683738476471	0.396694479149	-0.556626453321
H	3.811567253548	0.271530389758	-1.206765366334
H	5.100287344036	-0.605919187649	-0.374405104291
C	5.717984137117	1.295029788677	-1.234264300787
H	6.626838030078	1.403007270108	-0.632665270868
H	5.302930030866	2.293992629435	-1.407624717795
H	6.009253924197	0.870358812031	-2.202250447438
C	5.045581337026	0.786654325136	1.777651291072
H	5.293978010611	-0.278203051845	1.910272275705
H	5.989208625182	1.329429273197	1.611629494026
C	4.343691114563	1.324535096464	3.013490110938
H	3.420562710187	0.767932183766	3.205146105660

H	4.094108359821	2.383589307333	2.885206699685
H	4.992632419257	1.228495030698	3.890955544956
C	-2.514396505607	-4.045998132280	1.046157551245
H	-3.465812735464	-4.232482939904	0.536966164993
H	-2.701616871616	-3.310031960870	1.832938778764
C	-1.923428434855	-5.327111111077	1.619838948847
H	-0.981722804218	-5.121699099303	2.137815005122
H	-1.733412538690	-6.073474588947	0.841128498184
H	-2.626643233162	-5.765379413818	2.337657947818
C	-1.638505993645	-3.890679667560	-1.241743023308
H	-1.607032809787	-4.986374809907	-1.207853927375
H	-0.702936910702	-3.542397800417	-1.686654531756
C	-2.829623156820	-3.379149025813	-2.037286352601
H	-2.836515544753	-2.285814384275	-2.078438285357
H	-3.782158159519	-3.720789512527	-1.617950554255
H	-2.765207529942	-3.763232516876	-3.062397785543
C	1.185592662083	-1.192846602224	-2.993963502985
C	2.406249365476	-1.017875966735	-3.811865606378
C	1.168620398191	-1.697289446626	-4.384056561896
H	3.277664036980	-1.639533699662	-3.599396130624
H	2.657996214943	-0.024525974570	-4.188310348402
H	1.215096787524	-2.774049250551	-4.555090888810
H	0.588790170517	-1.157492106828	-5.133602617736
Mg	-1.523144537394	0.868977841246	-0.405584415269
Cl	-2.998203781239	0.586372415548	-2.176145219191
O	0.104022756187	2.284884443775	-0.385281831485
O	-2.707907538832	2.527105834759	0.475510752617
C	0.884170553467	2.256649343379	0.847998145147
H	0.299669181398	1.660485722110	1.552928802817
H	1.827017155833	1.733756763858	0.656320971358
C	0.923938388163	2.498139977542	-1.562098030856
H	1.642413971022	3.292582511131	-1.332020587680
H	1.479782444781	1.576248493165	-1.764833074373
C	-2.641642785605	3.894259783076	0.010791654161
H	-1.588770715861	4.053574690721	-0.223796819442
H	-2.903904899980	4.557727182093	0.844728975521
C	-3.927088369761	2.204570499043	1.191236702062
H	-4.056815663826	1.127185046855	1.083204444383
H	-4.769384059657	2.692784622355	0.690747035558
C	-3.513218081192	4.172367133061	-1.209068093812
H	-3.282750975322	3.473943156290	-2.017555688450
H	-3.329335608484	5.197734086560	-1.552908615647
H	-4.581370850958	4.087145444049	-0.985593806715
C	1.120965959549	3.654351860982	1.401616601269
H	1.703728530345	3.579300123388	2.326586016428
H	0.174529590099	4.152630886303	1.633997147959
H	1.685986220053	4.284128802732	0.705989389501
C	0.056846685623	2.887538875130	-2.745106183324
H	-0.457789947229	3.837036207658	-2.564479607178
H	-0.692594993681	2.122118919652	-2.971442659201
H	0.693353249776	3.008751507517	-3.628957640730

C	-3.843514113094	2.592307839885	2.660844242514
H	-3.023596571187	2.058456218432	3.149124244694
H	-4.779541225615	2.322145011969	3.163876103485
H	-3.694000659043	3.669498163330	2.794744265721

3-35•$(Et_2O)_3$

C	0.291446766773	-0.324245922593	-2.300487606110
N	0.048599162326	-0.517369108880	-1.119231963652
Cl	-0.564745125480	-1.018547359182	1.906337190436
Mg	1.275531252571	-1.435113348321	0.336570075257
O	1.095715605533	-3.476487618770	-0.116127288034
C	3.276727998381	-0.814074637219	0.801884589704
H	3.155815981397	0.274018693747	0.963750429420
C	4.314515404629	-0.965129142935	-0.325269105009
H	5.295656338684	-0.525803133801	-0.064953876099
H	3.989912850131	-0.485271268963	-1.259632540536
H	4.514401921903	-2.021176509128	-0.565458788936
C	3.843331555657	-1.378920465378	2.117618463686
H	4.826565981137	-0.945912195287	2.380857959715
H	3.999833848678	-2.468577923321	2.069068346373
H	3.175054623583	-1.195623958551	2.970065640764
C	-0.174504379199	-4.151101705349	-0.341902152251
H	-0.043922374826	-4.855794786372	-1.170702548906
H	-0.869812546974	-3.375101858149	-0.668196722572
C	-0.683151460179	-4.841309563041	0.914035055492
H	-0.817320855601	-4.113429795402	1.719356336197
H	-0.004100834557	-5.629351444958	1.258680655543
H	-1.654263042826	-5.302595496883	0.701715827883
C	2.269352133955	-4.318971533055	-0.199048144777
H	2.043578721806	-5.278572981543	0.279214473085
H	3.032294925973	-3.814345725971	0.398057419463
C	2.742023207015	-4.505528295778	-1.634024734103
H	3.005088531034	-3.542276967033	-2.082037486668
H	1.978555416439	-4.982290465112	-2.257595646586
H	3.633195457786	-5.143773300550	-1.647209632299
C	0.478980949004	-0.057318031151	-3.569945119345
C	1.378291384919	0.626491438934	-4.535268562697
C	0.670240187681	-0.665496408312	-4.908954254632
H	2.455960768809	0.590205863110	-4.372707575015
H	1.036168595815	1.549757327152	-5.005700096927
H	1.273926952140	-1.569034907915	-4.999003825182
H	-0.150505939766	-0.611731559904	-5.625106210520
Mg	-1.820359675251	-0.185803401048	-0.088420503758
O	-3.302159318426	0.604329822022	1.312976828324
O	-2.070588242112	1.721623018432	-1.099688993995
C	-4.144212288322	-0.360604236947	2.000662695470
H	-4.065761748469	-0.183041174883	3.078867231027
H	-3.708536467127	-1.336186251468	1.784155658552
C	-3.322848403786	1.925469911777	1.891666875246
H	-3.018623722851	2.593288154940	1.083845824156

H	-4.357922166151	2.173375060866	2.156045690860
C	-2.400045540286	2.064598591685	3.096728819621
H	-2.425825052142	3.099655121925	3.458436676016
H	-1.370082462604	1.806818189915	2.834785706824
H	-2.704984815237	1.414391272816	3.922667402288
C	-5.584044414448	-0.299330978760	1.515218175096
H	-6.035305961099	0.685767321061	1.680509296223
H	-6.184265381916	-1.035831719392	2.062487639167
H	-5.629614907703	-0.541145499579	0.449962192689
C	-3.053194473654	1.671603026854	-2.175084989543
H	-3.526538753820	0.690759718730	-2.093882241201
H	-2.510950504595	1.704348354529	-3.127280748862
C	-4.084323642820	2.785323122117	-2.063949374977
H	-3.635667743050	3.782276813054	-2.133197942631
H	-4.630831701938	2.713877789874	-1.118291556454
H	-4.807619881008	2.690186053109	-2.881947215420
C	-0.990601958055	2.647742764930	-1.374691113144
H	-1.433296021071	3.598504376942	-1.693384685852
H	-0.398200186759	2.244591285854	-2.203142503319
C	-0.138473019594	2.856909472812	-0.136810396784
H	0.674194439482	3.551832601306	-0.375561491938
H	0.319145144575	1.921855765336	0.200027954437
H	-0.718961354976	3.287469401594	0.685366553925
Cl	-3.225175739135	-1.780048654536	-1.035937044207

4.4 References for Chapter 4

(1) Watson, S. C.; Eastham, J. F. *J. Organomet. Chem.* **1967**, *9*, 165.

(2) Hamdouchi, C.; Topolski, M.; Goedken, V.; Walborsky, H. M. *J. Org. Chem.* **1993**, *58*, 3148.

(3) Carlier, P. R.; Zhang, Y. Q. *Org. Lett.* **2007**, *9*, 1319.

(4) Bloodworth, A. J.; Chan, K. H.; Cooksey, C. J. *J. Org. Chem.* **1986**, *51*, 2110.

(5) Bowman, R. K.; Johnson, J. S. *Org. Lett.* **2006**, *8*, 573.

(6) Harada, T.; Kurokawa, H.; Kagamihara, Y.; Tanaka, S.; Inoue, A.; Oku, A. *J.Org.Chem* **1992**, *57*, 1412.

(7) Fieser, L. F. F., M *Reagents for Organic Synthesis* **1967**, 581.

(8) Matsuda, F.; Kawatsura, M.; Hosaka, K.-i.; Shirahama, H. *Chem. Eur. J.* **1999**, *5*, 3252.

(9) Yu, W.; Du, Y.; Zhao, K. *Org. Lett.* **2009**, *11*, 2417.

(10) Ten Hoeve, W.; Wynberg, H. *J.Org.Chem* **1985**, *50*, 4508.

(11) Soltani, O.; De Brabander, J. K. *Angew. Chem., Int. Ed. Engl.* **2005**, *44*, 1696.

(12) Andraos, J. *J. Chem. Educ.* **1996**, *73*, 150.

(13) Patwardhan, N. N.; Gao, M.; Carlier, P. R. *Chem.--Eur. J.* **2011**, *17*, 12250.